Dynamical Climatology

Modelling of land surface processes and their influence on European climate.

by

D.A. Warrilow, A.B. Sangster and A. Slingo

DCTN 38

May 1986

Meteorological Office (Met. O. 20)
London Road
Bracknell
Berkshire RG12 2SZ

DYNAMICAL CLIMATOLOGY TECHNICAL NOTE NO. 38

MODELLING OF LAND SURFACE PROCESSES AND THEIR INFLUENCE ON EUROPEAN CLIMATE

by

D. A. WARRILOW, A.B. SANGSTER and A. SLINGO

Report prepared for CEC contract CL.113.UK(H)

Met O 20 (Dynamical
Climatology Branch)
Meteorological Office
London Road
Bracknell
Berkshire RG12 2SZ
England

May 1986

Note: This paper has not been published. Permission to quote from it should be obtained from the Assistant Director of the above Meteorological Office Branch.

Contents

1. Introduction

2. Climate modelling and land surface processes

3. Hydrology and soil moisture

4. Evaporation and interception

5. Land surface data

6. Soil temperatures

7. Sensitivity of European climate to land surface variations.

8. Conclusions and Summary.

Symbols

$a, a_x, a_{i,i+1}$	constants in section 2.
A	Ratio of model surface temperature to exact solution of diffusion equation.
A_x	Amplitude of some variable x over an annual cycle (s^{-1})
A_1	Coefficient of soil heat flux in multilayer temperature model (m^2KJ^{-1}).
A_r, A_m	Coefficients in multilayer soil temperature model (s^{-1}).
b	Exponent in a $K(\theta)$ relationship.
b_x	constant in section 2.
B_x	Mean of some variable x over an annual cycle (s^{-1})
B_1, B_r, B_n	Coefficients in multilayer soil temperature model (s^{-1})
c	Exponent in a $K(\theta)$ relationship.
c_{i+1}	constant in section 2.
C	Volumetric heat capacity of soil ($Jm^{-3}K^{-1}$)
C_E	Bulk transfer coefficient
C_p	Specific heat of air at constant pressure ($Jkg^{-1}K^{-1}$)
d	time in days
d_o	time of maximum daily surface temperature in annual cycle.
d_a	number of days in a year
D	Root zone depth (m)
D_d	Dew point depression (K)
D_{dR}	Reference dew point depression (K)
D_r	Drip rate from canopy (ms^{-1})
E_a, E_c, E_d, E_p, E_s	Evapotranspiration (ms^{-1}); actual, wet canopy, dry canopy, potential and soil respectively.
f	probability distribution of grid box rainfall.

F, F_v, F_s	Infiltration capacity (ms^{-1}); general, vegetation and bare soil.
G, $\underline{G}$	Soil heat flux (Wm^{-2}); vertically downwards at surface and in general.
h, h_o, h_d	Local time in hours; general, maximum daily surface temperature and hours in a day.
H	Sensible heat flux (Wm^{-2}).
H_θ	Total soil water potential (m)
i	$\sqrt{-1}$
I_f	Infiltration rate (ms^{-1})
I_s	Interception rate (ms^{-1})
k	constant in gas equation
K, K_s	Soil moisture conductivity (ms^{-1}); in general and at saturation.
L	Latent heat of evaporation of water (Jm^{-3}).
LAI, LAI_1, LAI_2	Leaf area index; in general, single sided and double sided.
$\underline{n}$	Unit vector in direction of atmospheric gradient of T or q in ODM.
p, p_i	Atmospheric pressure; in general and at model level i (mb).
P, P_1	Period of soil temperature forcing flux (s) and characteristic period of multilayer or MO soil model.
q_i, q_{Ri}, q_{11}, q_*	Specific humidity (kg/kg); in general, at model level i, reference value at level i, at lowest model level and at surface.
$\underline{Q}$	Soil moisture flux vector (ms^{-1})
r_a, r_s, r_{ss}, r_{sc}	Resistance to evaporation (sm^{-1}); aerodynamic, surface, soil, and crop canopy.
$r_{i,i+1}$	correlation between ODM levels.
R	Rainfall rate (ms^{-1})
R_g	Gas constant ($J\ kg^{-1}\ K^{-1}$)
S, S_m	Canopy storage (m), general and maximum capacity.

SAI	Stem area index
SM	Snowmelt rate (ms^{-1})
S_n, S_d	Snowfall rate (ms^{-1}), Snowdepth (m)
SMC, SMC_c, SMC_f	Available soil moisture content (cm), in general, at the critical point and at field capacity.
t	time (s)
T, T_i, T_{Ri}	Air temperature (K), in general; at model level i and reference value in ODM at level i.
$T, T_o, T_m, T_k, T_1, T_r, T_n, \bar{T}, T^*$	Soil temperatures (K); in general; in force restore models for surface, daily mean and a deep layer; in multilayer models; long term mean and at surface in general.
T_f	Throughfall rate (ms^{-1})
u, $\bar{u}$	Component of wind velocity in x-direction, general and mean (ms^{-1}).
v, $\bar{v}$	Component of wind velocity in y-direction, general and mean (ms^{-1})
$\underline{v}$, $\bar{\underline{v}}$, $\underline{v}'$	3 dimensional wind vector, general, mean and transient component (ms^{-1}).
VAI	Vegetation area index
v_n, $\bar{v}_n$, v_{ni}	Horizontal advection velocity, general, mean, and at level i (ms^{-1}).
v_p	Horizontal wind velocity component perpendicular to v_n (ms^{-1}).
v_{11}	Horizontal wind at lowest atmospheric level (ms^{-1})
w	Vertical component of wind velocity (mbs^{-1})
$W_{i,i+1}$	Weights used to calculate vertical fluxes in ODM
$x_i, \bar{x}_i$	Random variables at level i in ODM, general and mean
x_1 x_7	Locally defined variable to denote annual minimum or maximum.
Y, Y_g, Y_s	Runoff, total, gravitational drainage and surface runoff (ms^{-1}).
z	vertical cartesian coordinate in soil (positive downwards) (m)

z_o	Aerodynamic roughness (m)
z, z_r, z_n	Soil temperature model depths (m)
α	Exponent in gas equation
α_r, α_o	Ratio of thickness of r_{th} soil temperature layer to top layer and constant ratio between the depths of adjacent layers.
β	Soil moisture function limiting evaporation.
β_v	Factor to enhance infiltration rates in the presence of vegetation.
γ	Thermal inertia of soil ($Jm^{-2}\ K^{-1}s^{-1/2}$)
Γ	Dry adiabatic lapse rate (K/km)
$\delta, \delta_j, \delta_o, \delta_d, \delta_m, \delta_a, \delta_k$	e-folding depths of surface temperature waves; general, jth wave, diurnal wave (o and d), annual wave (m and a), long period (k).
ΔG	amplitude of surface heat flux (Wm^{-2})
Δn	radius of ODM area (m)
$\Delta T, \Delta T_j, \Delta T_a, \Delta T_d$	Amplitude of surface temperature wave; general, jth wave, annual and diurnal (K).
$\Delta T', \Delta T_o', \Delta T_m', \Delta T_k', \Delta T_1' \ldots \Delta T_r', \Delta T_n'$	Amplitude of surface temperature waves in soil temp models; general, diurnal, annual and deep in force restore models, at levels, 1, r, n in multilayer model. (K).
Δz_1 Δz_r	Thickness of layers in soil temperature multilayer model (m).
ε	Proportion of rainfall area to grid box area.
ξ_{dr} ξ_{ar}	Normalised soil temperature model depth for diurnal cycle and annual cycle.
ζ	Normalised frequency in multilayer soil temperature model.
$\theta, \hat{\theta}, \theta_D, \theta_w, \theta_s, \theta_f, \theta_c$	Volumetric soil moisture concentration, in general, locally defined mean through layer, value at depth D, value at wilting point, saturation, field capacity and critical point.
$\tilde{\theta}$	Potential temperature (K)
κ	Thermal diffusivity of soil (m^2s^{-1})

λ	Thermal conductivity of soil ($J\ m^{-1}K^{-1}s^{-1}$)
Λ	Probability of canopy interception of rainfall.
μ	Ratio of standard deviations of dewpoint depression to temperature.
ν	Proportion of surface covered by vegetation.
$\xi, \hat{\xi}, \xi', \xi_R, \xi_i$	General conservative atmospheric variable, general, mean, transient component, reference value, value at level i.
ρ, ρ^*, ρ_w	Density; general, air at surface, water (kgm^{-3})
σ_T, σ_{Dd}	Standard deviation of atmospheric temperature and dew point depression (K).
σ_{xi}, σ_{ci+1}	Standard deviation of random variables x_i and c_{i+1}
σ_u, σ_v, σ_{vn}, σ_{vp}	Standard deviation of velocity components u,v,v_n, v_p (ms^{-1})
ϕ	Direction of vector $\underline{n}$ relative to x-axis.
χ, χ'	Phase angle of surface temperature wave in exact solution of diffusion equation and in soil temperature parametrization.
ψ, ψ_s	Soil moisture matrix potential, general and at saturation (m).
$\omega, \omega_y, \omega_1, \omega_o, \omega_m, \omega_a, \omega_d$	Angular frequency of soil heat flux at surface; in general, jth wave, characteristic of MO or multilayer model, force restore models, annual.
Ω_r	Ratio of amplitudes of soil temperatures at levels r and r-1 in multilayer model.

1. Introduction

The nature of the land surface plays an important part in determining the micro-climate of a local area (Geiger (1961)) through variations in surface albedo, roughness, shelter, transpiration and evaporation and underlying soil types, as well as its general situation and aspect. Since the surface 'drives' the atmosphere by being a source of heat and moisture, any attempts to model climate require that land surface processes be modelled adequately. Over a continental area, the surface albedo determines the amount of energy available to evaporate moisture at the surface and the nature of the surface determines how the available energy is divided between latent and sensible heat. As interest in the effect of the land surface on climate has grown so also has the need to model land surface processes with greater realism.

In this report a number of aspects of land surface processes have been considered and some parametrizations have been proposed.

It is demonstrated that it is necessary to take into account the control that vegetation exerts on evaporation, the interception of rainfall by a vegetation canopy and the ability of vegetation to tap moisture from varying levels in the soil. Hydrological processes have been considered in detail and a simple but physically realistic scheme is proposed and compared with a 'bucket' model. The effect of a deep soil heat flux on surface temperatures is investigated and a 4 layer soil temperature model is proposed. The relationship between vegetation and soil parameters and types is investigated as a first step in determining large scale variations in the land surface.

To aid the study of land surface processes an existing one dimensional atmospheric model (ODM) was developed further by allowing for horizontal advection of heat and moisture. Long term stable climate integrations for a local area could then be carried out easily and cheaply. Atmospheric general circulation model (AGCM) integrations were carried out to assess the impact of the new hydrology and soil temperature parametrizations and inclusion of surface resistance to evaporation. The impact of land surface processes on European climate has been assessed largely using the ODM in simulations of the climate of Southern England.

The report has been written in fairly self contained sections, each section having its own bibliography tables and figures.

Reference

Geiger, R 1961 The Climate near the ground. Translation from the fourth (1961) German edition. Harvard University Press.

2. Climate modelling and land surface processes.

2.1 Introduction

2.2 The Meteorological Office atmospheric general circulation model.

2.3 A one dimensional atmospheric model.

2.4 Summary

2.5 References

Appendix 2 Development of a one dimensional model

2. Climate modelling and land surface processes

2.1 Introduction

Global atmospheric general circulation models (AGCMs) have been developed and used over the last ten to twenty years to study the complex processes of climate and climatic change. Land surfaces processes play an important part in climate and because these processes occur on a small scale it is necessary to develop parametrizations to treat them in an AGCM. Development and assessment of any parametrization of physical processes is usually carried out in the AGCM for which they are intended. However this can be expensive in computing time and so it is convenient to test them initially in a one dimensional representation of the AGCM. Such a model is cheaper to run, simpler to program and tests can be made quickly. For most locations on earth's surface, however, a single atmospheric column is not in radiative equilibrium so that one dimensional model (ODM) climates become unrealistic in anything other than short integrations. As land surface processes often change slowly, long integrations are required. For this reason an ODM has been developed to include the compensating effects on the energy balance of large scale advection and this was used to test the land surface parametrizations discussed in this report. The hydrology and soil temperature parametrizations were also tested in AGCM integrations. An outline of both models is given in the following sections. Details concerning the development of the ODM are given in an appendix, hereafter referred to as Appendix 2.

2.2 The Meteorological Office atmospheric general circulation model

AGCMs are powerful tools for the study of climate and climatic change. They comprise mathematical descriptions of physical processes and are able to simulate the global circulation of the atmosphere, taking into account a large number of complex atmospheric interactions, the effects of which are often difficult to isolate in observational studies of the real atmosphere. They allow experiments to be carried out which would be impossible with the real atmosphere, such as investigations into the effect of doubling CO_2, changes to the land surface etc. The development of the Meteorological Office AGCMs and their current status are discussed in detail by Slingo (1985).

The model used in this report is a global primitive-equation finite-difference AGCM with sigma (pressure divided by its surface value) as the vertical coordinate and 11 unevenly-spaced layers, to provide enhanced resolution near the surface and in the upper troposphere (Rowntree (1971)). The climatology of the model is discussed by Wilson and Slingo (1983) and Wilson (1984). The model used in this report had a horizontal resolution of 2.5 degrees of latitude by 3.75 degrees of longitude. Sub-grid scale physical processes are modelled in four subroutines, which deal with radiative processes, boundary layer and surface exchanges, large scale precipitation and finally convection. In our experiments interactive diurnally varying radiation was used but with climatological fixed cloud, and boundary layer processes were modelled using the so-called 'Clarke' boundary layer scheme, based on Method 1 of Clarke (1970). The convection scheme which treats both saturated and unsaturated convection was developed by Lyne and Rowntree (1976).

For convenience, a 360 day year is used in the AGCM made up of twelve months each of 30 days. This leads to considerable simplification of the logic required to run the model. The small error thus introduced into the incoming solar radiation is minimised by a slight adjustment to the date of perihelion (Slingo (1982)).

2.3 A one dimensional model

A one dimensional model of the atmosphere (ODM), having largely the same parametrization routines as the AGCM has been developed to include statistical treatment of the heat and moisture changes due to large scale dynamic processes. The main difference between model parametrizations was that climatological cloud was replaced with variable cloud, diagnosed in the model.

Figure 2.1 gives a schematic view of the ODM. Within the column radiative, convective, precipitation, boundary layer, and land surface processes are treated explicitly. Since an imbalance of heat and moisture within the column generally arises, horizontal convergence of heat and moisture, resulting from larger scale motion in the real atmosphere, is included. The means of taking this large scale forcing into account is derived in Appendix 2, Section 2.1 so that a practical ODM for use in developing surface parametrizations and local climate studies can be developed.

Practical problems relating to treatment of random sampling in the statistical processes, correlation between levels and horizontal velocities are dealt with in Appendix 2, Section 2.2. Suitable climate statistics are discussed in Appendix 2, Section 2.3.

The model has been developed as a practical tool and so there are some aspects which are somewhat heuristic and more work would be needed to produce a rigorous treatment of correlations for example. Although some effort is required in deriving climate statistics, it is in principle likely that successful long simulations can be made for any location on the earth. Although not attempted here, it would also be possible to undertake simple anomaly experiments providing the deviation from present climate is not too large.

Two examples are given of climate simulations over a duration of one year for two quite different climates: Southern England and the Sahel. These are shown for a variety of variables in figures 2.2 to 2.9. Both climates are quite well simulated and show the potential for testing parametrizations in different climatic contexts. Particular studies are dealt with in later sections.

2.4 Summary

The AGCM and ODM used for testing the new land surface parametrizations described later in this report have been briefly summarised here. More details of the ODM will be found in Appendix 2. The ODM was developed to make parametrization studies initially easier to run and appraise. However the AGCM needs to be used for a full assessment of a parametrization scheme, as it also includes the effects of large scale feedback.

2.5 References

Clarke, R.H. 1970 Recommended methods for the treatment of the boundary layer in numerical models. Austr. Met. Mag., 18, 51-73.

Lyne, W.H. and Rowntree, P.R. 1976 Development of a convective parametrization using GATE data. Met O 20 Technical Note II/70, Meteorological Office, Bracknell.

Oort, A.H. 1983 Global atmospheric circulation statistics, 1958-1973, NOAA Professional Paper. 14, Washington, National Oceanic and Atmospheric Administration.

Rowntree, P.R. 1971 Proposed vertical resolution in the new Met O 20 model. Met O 20 Technical Note No. 1, Meteorological Office, Bracknell.

Slingo, A. 1982 Insolation calculations for a 360-day year. Met O 20 Technical Note II/184, Meteorological Office, Bracknell.

Slingo, A. (Ed) 1985 Handbook of the Meteorological Office 11-layer atmospheric general circulation model, Volume 1: Model description. Met O 20 DCTN 29, Meteorological Office, Bracknell.

Wilson, H. 1984 A study of the July climatology of the 11-layer model over the European area. Met O 20 Technical Note II/222, Meteorological Office, Bracknell.

Wilson, H. and Slingo, A. 1983 A study of the January climatology of the 11-layer model over the European area. Met O 20 Technical Note II/214, Meteorological Office, Bracknell.

Appendix 2. Development of a one dimensional model

A2.1 Large scale heat and moisture convergence

A2.1.1 Introduction
A2.1.2 Stable treatment of large scale dynamics
A2.1.3 Vertical motion

A2.2 A practical one dimensional model

A2.2.1 Introduction
A2.2.2 Heat and moisture convergence
A2.2.3 Random processes
A2.2.4 Vertical correlation
A2.2.5 Treatment of horizontal velocity

A2.3 Climate data

A2.1 Large scale heat and moisture convergence

A2.1.1 Introduction

Consider some conservative atmospheric variable, ξ, whose local time evolution is due to both local physical and large scale dynamical processes. Denoting these processes by subscripts P and D respectively, then the time evolution of ξ is given in Eq. 2.1

$$\frac{\partial \xi}{\partial t} = \frac{\partial \xi}{\partial t}_P + \frac{\partial \xi}{\partial t}_D \qquad (2.1)$$

Over a long period of time the climate can be considered to be constant, and so $(\partial\xi/\partial t) \sim 0$. Then local physical and large-scale dynamical processes are balanced. Thus

$$\frac{\partial \xi}{\partial t}_D \sim - \frac{\partial \xi}{\partial t}_P \qquad (2.2)$$

A simple procedure would be to replace $(\partial\xi/\partial t)_D$ in Eq. 2.1 by a constant. Thus:

$$\frac{\partial \xi}{\partial t} = \frac{\partial \xi}{\partial t}_P + \text{Constant} \qquad (2.3)$$

Such a procedure is non-interactive, does not take non-linear processes into account and neglects time dependent forcing. It might be possible to let the constant vary seasonally but the same disadvantages still exist. In the following section an interactive treatment of dynamical processes is proposed.

A2.1.2 Stable treatment of large scale dynamics

The local rate of change of ξ due to large scale dynamics is given by:

$$\frac{\partial \xi}{\partial t}_D = - \nabla . \xi \underline{v} \qquad (2.4)$$

where $\underline{v}$ is a three dimensional velocity vector and ∇ is the usual differential operator.
Eq. 2.4 can be expanded on the right hand side to give

$$\frac{\partial \xi}{\partial t}_D = - \xi \nabla . \underline{v} - \underline{v} . \nabla \xi \qquad (2.5)$$

The first term on the right hand side can be set to zero by making the assumption of incompressibility.

Taking time means of Eq. 2.5 with $\nabla . \underline{v} = 0$ and denoting $\underline{v} = \bar{\underline{v}} + \underline{v}'$ and $\xi = \bar{\xi} + \xi'$ where the bar denotes the time mean and the dash the transient component, leads to

$$\frac{\partial \xi}{\partial t}_D = - \bar{\underline{v}} . \nabla \bar{\xi} - \overline{\underline{v}' . \nabla \xi'} \qquad (2.6)$$

Thus local changes in ξ due to dynamical processes involve both mean and transient components of the advection term.

Separating into horizontal advection and vertical motion, where v_n is the component of horizontal velocity in the direction of positive gradient (n), Eq. 2.5 becomes

$$\left(\frac{\partial \xi}{\partial t}\right)_D = - v_n \frac{\partial \xi}{\partial n} - w \frac{\partial \xi}{\partial p} \qquad (2.7)$$

The second term on the right hand side can be computed within a vertical column where w is vertical velocity and p is pressure. The first term on the right hand side can be simplified as follows. We assume a circular area of radius Δn (see figure 2.10) and a constant gradient of ξ across the area. Then we can make a finite difference approximation such that:

$$- v_n \frac{\partial \xi}{\partial n} = |v_n| \frac{(\xi_R - \xi)}{\Delta n} \qquad (2.8)$$

where ξ_R is a reference value of ξ on the edge of the area in the upwind direction along n. Combining Eqs. 2.7 and 2.8 and making a finite difference approximation gives

$$\left(\frac{\Delta \xi}{\Delta t}\right)_D = |v_n| \frac{(\xi_R - \xi)}{\Delta n} - w \frac{\Delta \xi}{\Delta p} \qquad (2.9)$$

To solve Eq. 2.9 it is necessary to specify v_n, w and ξ_R. Since these are not calculated within a vertical column but are a result of large scale motion, it is possible to treat them as random variables drawn from populations appropriate to the climatic situation being simulated. It has been noted that transient components need to be taken into account and random sampling at convenient intervals will do this. Vertical motion is treated in detail in section A2.1.3 and random sampling in section A2.2.3.

A2.1.3 Vertical Motion

The vertical component of $\left(\Delta \xi / \Delta t\right)_D$ is given by $-w \Delta \xi / \Delta p$ from equation (2.9).

Within the ODM w is specified for each level, i, but a mean $\Delta \xi / \Delta p$ has to be computed.

If it is assumed that ξ is an approximately linear function of the logarithm of p between two levels, then we can write:

$$\left(\frac{\Delta \xi}{\Delta p}\right)_{i,i+1} = \frac{\xi_{i+1} - \xi_i}{p_i \ln(p_{i+1}/p_i)} \qquad (2.10)$$

or

$$\left(\frac{\Delta \xi}{\Delta p}\right)_{i,i-1} = \frac{\xi_i - \xi_{i-1}}{p_i \ln(p_i/p_{i-1})} \qquad (2.11)$$

Then the average gradient is given by averaging the above estimates as follows

$$\left(\frac{\Delta \xi}{\Delta p}\right)_i = W_{i,i-1} \left(\frac{\Delta \xi}{\Delta p}\right)_{i,i-1} + W_{i,i+1} \left(\frac{\Delta \xi}{\Delta p}\right)_{i,i+1} \qquad (2.12)$$

where $W_{i,i-1}$ and $W_{i,i+1}$ are weights related to the depths of the layers, ie in this case $\ln p_i/p_{i-1}$ etc.

$$W_{i,i-1} + W_{i,i+1} = 1 = \frac{X}{\ln(p_i/p_{i-1})} + \frac{X}{\ln(p_{i+1}/p_i)} \qquad (2.13)$$

$$\text{so that } X = \frac{\{\ln(p_i/p_{i-1})\}\ \{\ln(p_{i+1}/p_i)\}}{\ln(p_{i+1}/p_{i-1})} \qquad (2.14)$$

$$\text{Then } W_{i,i-1} = \frac{\ln(p_{i+1}/p_i)}{\ln(p_{i+1}/p_{i-1})} \qquad (2.15)$$

$$W_{i+1,i} = \frac{\ln(p_i/p_{i-1})}{\ln(p_{i+1}/p_{i-1})} \qquad (2.16)$$

Then from Eqs. 2.10, 2.11, 2.12, 2.15 and 2.16 we have:

$$\left(\frac{\Delta\xi}{\Delta p}\right)_i = \frac{1}{p_i}\left[\frac{\xi_{i+1} - \xi_i}{\ln(p_{i+1}/p_i)} + \frac{(\xi_i - \xi_{i-1})}{\ln(p_i/p_{i-1})} - \frac{\xi_{i+1} - \xi_{i-1}}{\ln(p_{i+1}/p_{i-1})}\right] \qquad (2.17)$$

A2.2 A practical ODM

A2.2.1 Introduction

The framework for dealing with the effects of large scale dynamic motions has been developed and it remains to form a practical series of equations which can be used in an ODM. Details of random sampling need to be worked out and various questions on correlation between variables need to be considered. The dependence on areal size of assumptions made regarding uniformity of the gradient of ξ also needs to be looked at.

A2.2.2 Heat and moisture convergence

The general equation for changes due to dynamical processes is Eq. 2.9. To deal with heat and moisture convergence, we replace ξ with potential temperature $\tilde{\theta}$ and specific humidity q. Convergence of moisture is given simply as in Eq. 2.18 for level i.

$$\left(\frac{\Delta q_i}{\Delta t}\right)_D = \frac{|v_{ni}|}{\Delta n}(q_{Ri} - q_i) - \frac{w_i}{p_i}\left[\frac{(q_{i+1}-q_i)}{\ln(p_{i+1}/p_i)} + \frac{(q_i-q_{i-1})}{\ln(p_i/p_{i-1})} - \frac{(q_{i+1}-q_{i-1})}{\ln(p_{i+1}/p_{i-1})}\right] \qquad (2.18)$$

For heat convergence it is noted that

$$\tilde{\theta} = k\, Tp^{-\alpha} \qquad (2.19)$$

where $k = (1000)^{\alpha}$ and $\alpha = R_g/C_p$

R_g is the gas constant and C_p the specific heat of air at constant pressure, giving $\alpha = 0.2856$.

$$\text{It is noted that } \frac{\partial\tilde{\theta}}{\partial p} = k\, p^{-\alpha}\left[\frac{\partial T}{\partial p} - \frac{\alpha T}{p}\right] \qquad (2.20)$$

Making finite difference approximations and substituting for θ in Eq 2.9 leads to

$$\left(\frac{\Delta T_i}{\Delta t}\right)_D = \frac{|v_{ni}|}{\Delta n}(T_{Ri} - T_i) - \frac{w_i}{p_i}\left[\frac{(T_{i+1}-T_i)}{\ln(p_{i+1}/p_i)} + \frac{(T_i-T_{i-1})}{\ln(p_i/p_{i-1})} - \frac{(T_{i+1}-T_{i-1})}{\ln(p_{i+1}/p_{i-1})} - \alpha T_i\right]$$

where T_i is in degrees K. (2.21)

In practice the first terms in Eqs. 2.18 and 2.21 are applied at all atmospheric levels but the second terms only cover the lowest 8 levels, thus mainly confining vertical motion to the troposphere.

A2.2.3 Random processes

It was noted in section A2.1.2 that it is necessary to include both mean and transient advection terms. In practice this means that the unknown variables in Eqs. 2.18 and 2.21 are treated as random variables drawn from a suitable population with known mean and standard deviation. Gaussian distributions are assumed and as will be seen this means using a measure of humidity other than q. The random variables are T_R, q_R, v_n and w. A fifth variable, v_p, is included, where v_p is the horizontal component of wind velocity normal to v_n. This is needed for calculations in the boundary layer. Each variable is treated as being independent although arguably warm advection should be correlated with vertical ascent. However it is recognised that there is likely to be vertical correlation between variables at different levels. This is included and dealt with more fully in the next sub-section.

For T_R, v_n, v_p and w it is possible to use published atmospheric statistical values directly, as means and variances are readily available, and it is reasonable to assume that the parent distributions are Gaussian. For humidity there is some difficulty. q is a highly skewed variable and its statistical properties are not so easily dealt with. Because of this, dewpoint depression (D_d) is used as a random variable to predict the reference value of q. D_d was assumed to be independent of T and so cross correlation between D_d and T was neglected. The variance of humidity is more difficult to define, since we require to take into account the advection of cloud liquid water in the absence of an explicit cloud liquid water variable. This can be done by allowing D_d to become negative at times, thus generating supersaturation which is immediately removed in the large scale rain parametrization routines in the model. In practice it was found best to let the variance of D_d be related to the variance of T, thus

$$\sigma_D = \mu\sigma_T \qquad (2.22)$$

where μ is an experimentally derived constant, determined by ensuring that the model generated the correct rainfall in both summer and winter. This is the only instance of 'tuning' in the parametrization of large-scale forcing. On occasion D_d is negative, thereby generating large-scale rainfall.

Means and standard deviations of the random variables generally pertain to the centre of the location being studied. However, strictly speaking, the mean of T_R and q_R (or D_{dR}) should be that found on the edge of the area in the upwind direction of the mean advection velocity. This means that a small correction (about $^1/_2$°C for AGCM grid size areas) to the mean of T_R and D_{dR} is required if those are taken from the centre of the area. This correction was derived from the gradient in the climate statistics for each location studied.

A number of fairly arbitrary choices had to be made and further work is needed to study the dependence on areal size of vertical correlation, the μ factor and the variances and the frequency with which random sampling takes place. In practice sampling was carried out daily, largely as climate statistics deal with daily variances. For sub-synoptic scale areas (such as those comparable in size to an AGCM grid square) the assumption of a uniform gradient holds quite well and so taking point values for means and variances is probably realistic. However, if the area becomes very large these assumptions break down. For smaller areas it would probably be necessary to take account of the diurnal cycle of the reference variables, especially near the surface.

A2.2.4 Vertical Correlation

It is necessary to account for vertical correlation between random variables. Although the degree of correlation is likely to vary from location to location and depend on inter-level spacing, in this model it is assumed to be constant. The temperature and dewpoint correlation coefficients $r_{i,i+1}$ were set to 0.9 and the horizontal and vertical velocity coefficients to 0.5. These values were based on a few experimental integrations and further work is needed to ascertain their true values and variability. No serial correlation was included between random numbers.

Let x_i be a random variable at level i, drawn from a population with mean $\bar{x}_i$ and standard deviation σ_{xi}. Then for the subsequent level we can write:

$$x_{i+1} = a_{i,i+1}\, x_i + c_{i+1} \qquad (2.23)$$

where $a_{i,i+1}$ is some measure of inter-level correlation and c_{i+1} is a random variable drawn from a population with mean $\bar{c}_{i+1}$ and standard deviation σ_{ci+1}.

We define the covariance of x_i and c_{i+1} to be zero. The correlation between x_i, and x_{i+1} is given by

$$r_{i,i+1} = \mathrm{COV}\,(x_i, x_{i+1})/\sigma_{xi}\,\sigma_{xi+1} \qquad (2.24)$$

From Eq. 2.23 the variance of x_{i+1} is given by

$$\sigma^2_{xi+1} = a^2_{i,i+1}\,\sigma^2_{xi} + \sigma^2_{ci+1} \qquad (2.25)$$

By rearranging Eq. 2.23 in terms of c_{i+1} we can give an expression for the variance of c_{i+1} as

$$\sigma^2_{ci+1} = \sigma^2_{xi+1} + a^2_{i,i+1}\,\sigma^2_{xi} - 2\, a_{i,i+1}\,\sigma_{xi+1}\sigma_{xi}\, r_{i,i+1} \qquad (2.26)$$

Solving Eqs. 2.25 and 2.26 simultaneously for $a_{i,i+1}$ gives

$$a_{i,i+1} = r_{i,i+1}\,\sigma_{xi+1}/\sigma_{xi} \qquad (2.27)$$

Then from Eqs. 2.23 and 2.27 the mean and variance of c_{i+1} can be found.

$$\bar{c}_{i+1} = \bar{x}_{i+1} - \frac{r_{i,i+1}\ \sigma_{xi+1}\ \bar{x}_i}{\sigma_{xi}} \qquad (2.28)$$

and $$\sigma^2_{ci+1} = (1 - r^2_{i,i+1})\ \sigma^2_{x_{i+1}} \qquad (2.29)$$

Thus for each variable it is necessary to calculate means and variances of a random variable c_i for each level i. The practical procedure is to sample randomly for each variable for the first level and then compute each subsequent level using Eq. 2.23 sampling randomly from the appropriate distribution of c_i.

A2.2.5 Treatment of horizontal velocity

Climate statistics give means and standard deviations of the two horizontal velocity components. These are referred to as u, σ_u, v, σ_v respectively. To solve Eqs. 2.18 and 2.21 we need to know v_n which is defined as:

$$v_n = u\cos\phi + v\sin\phi \qquad (2.30)$$

where ϕ is the angle relative to the x-axis of the vector n parallel to the gradient of the field of T or q. It is necessary to estimate v_n and σ_{vn}.

Let E(x) denote the expectation of x. Then

$$\bar{v}_n = E(v_n),\ \sigma^2_{vn} = E(v_n^2) - (E(v_n))^2 \qquad (2.31)$$

It is assumed that u, v and ϕ are independent.

$$\text{So } E(v_n) = E(u)\,E(\cos\phi) + E(v)\,E(\sin\phi) \qquad (2.32)$$

$$E(v_n^2) = E(u^2)\,E(\cos^2\phi) + E(v^2)\,E(\sin^2\phi) + 2E(uv)\,E(\sin\phi\cos\phi) \qquad (2.33)$$

If we set $\phi = \bar{\phi} + \phi'$ then it can be shown that

$$E(\cos\phi) = E(\cos\phi')\cos\bar{\phi} \qquad (2.34)$$

$$E(\sin\phi) = E(\cos\phi')\sin\bar{\phi} \qquad (2.35)$$

$$E(\cos^2\phi) = E(\cos^2\phi')\cos^2\bar{\phi} + E(\sin^2\phi')\sin^2\bar{\phi} \qquad (2.36)$$

$$E(\sin^2\phi) = E(\cos^2\phi')\sin^2\bar{\phi} + E(\sin^2\phi')\cos^2\bar{\phi} \qquad (2.37)$$

$$E(\sin\phi\cos\phi) = \cos\bar{\phi}\sin\bar{\phi} \qquad (2.38)$$

It remains to estimate $E(\cos\phi')$ etc. This is not trivial as the distribution of ϕ' is not known. We make a grossly simplifying assumption that the variance of ϕ' is small so that

$$E(\cos\phi') \sim 1 \qquad E(\cos^2\phi') \sim 1 \text{ and } E(\sin^2\phi') \sim 0$$

Then we can write

$$\bar{v}_n = E(v_n) = \bar{u}\cos\bar{\phi} + \bar{v}\sin\bar{\phi} \qquad (2.39)$$

$$\sigma^2_{vn} = \sigma_u^2\cos^2\bar{\phi} + \sigma_v^2\sin^2\bar{\phi} \qquad (2.40)$$

Figure 2.1 Schematic side view of the one dimensional model. T_i, q_i, u_i, v_i, w_i are atmospheric quantities of temperature, specific humidity and wind components at model level i. Advection is given by $\underset{\sim}{v}.\nabla T$ and $\underset{\sim}{v}.\nabla q$. C_H, C_M, C_L and C_C denote amounts of high, medium, low and convective cloud. Net radiation at the top and the bottom of the atmosphere is given by R_{TN} and R_{BN} respectively. Other variables are: surface temperature, T*, canopy moisture, S, snowdepth, S_d, soil moisture concentration, θ, root depth, D, surface and gravitational drainage, Y_s and Y_g, rainfall, R, snowfall, S_n, evaporation, E and sensible heat flux, H.

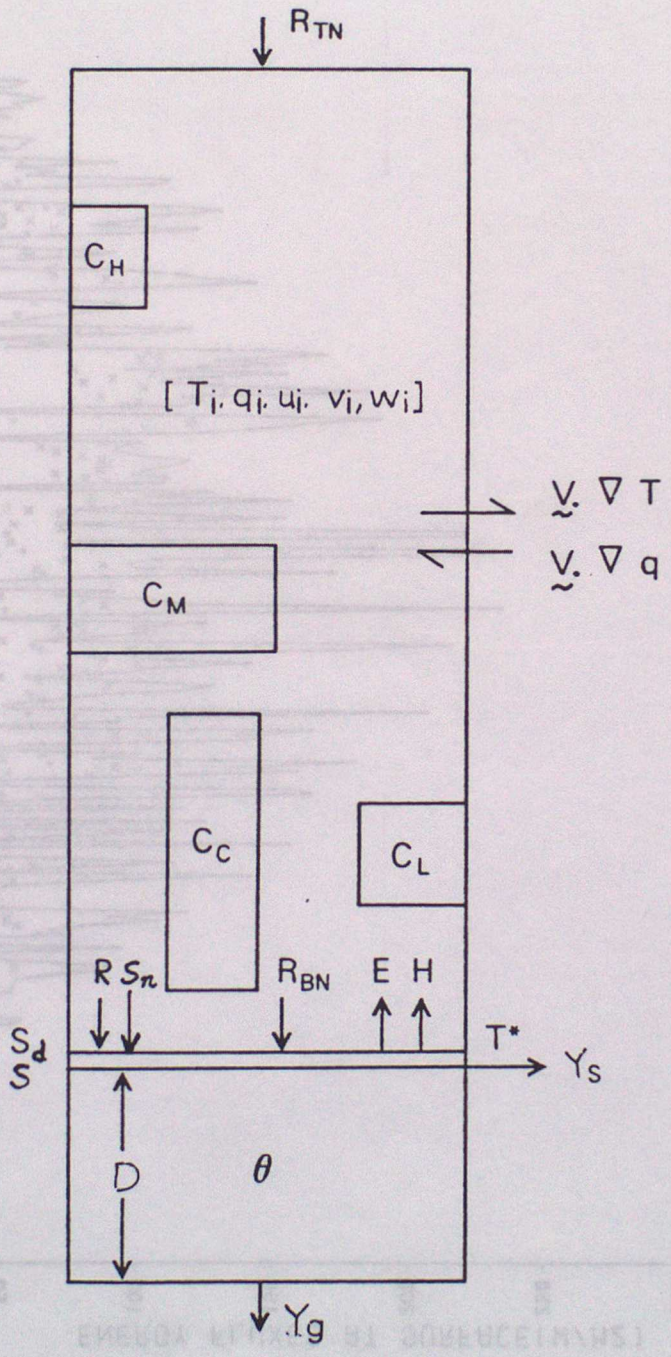

FIGURE 2.2 ANNUAL CYCLE SOUTHERN ENGLAND
TEST SOIL. LONG GRASS

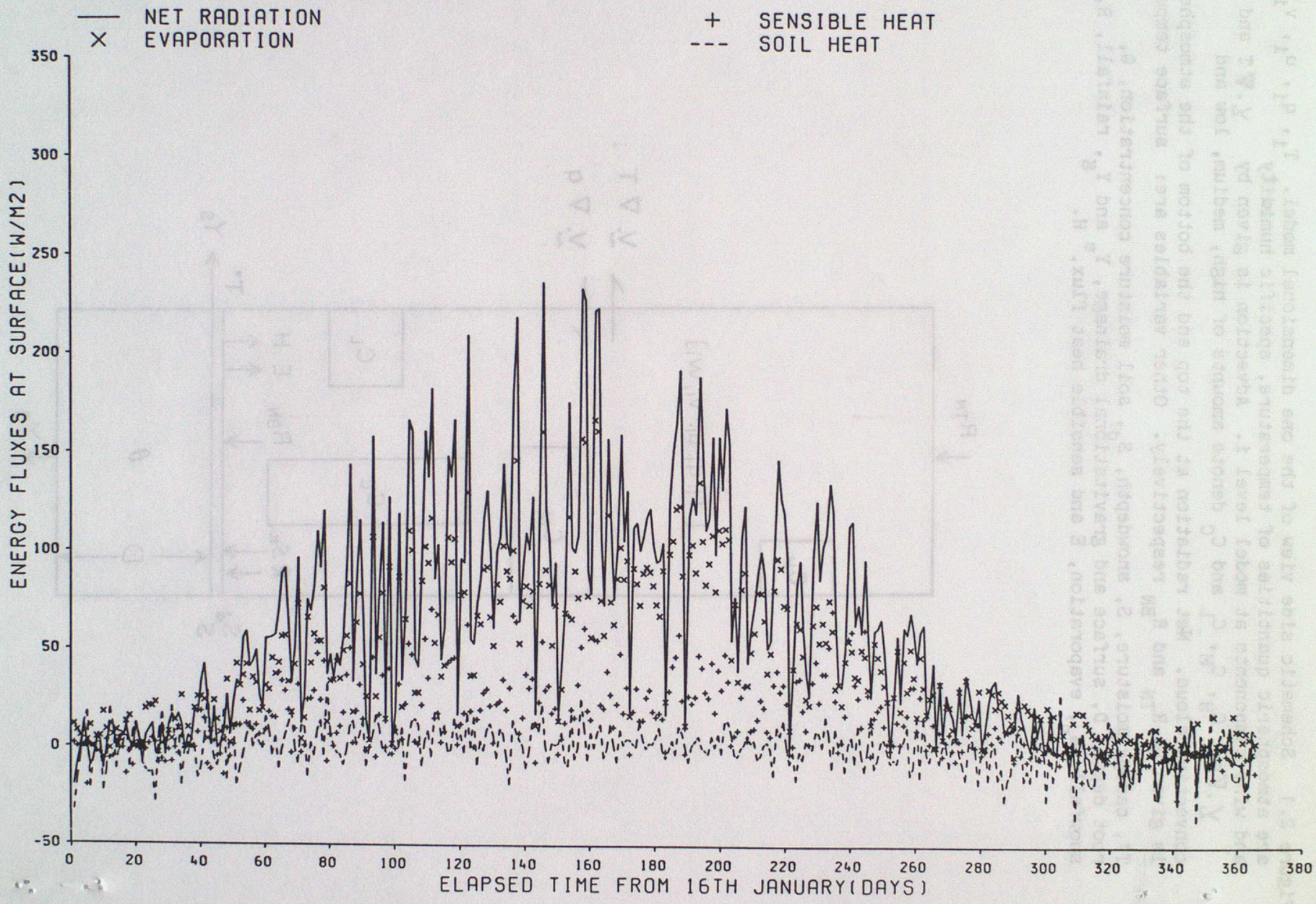

It was noticed that further simplification could be made as $\sigma_u^2 \sim \sigma_v^2$ so that:

$$\sigma_{vn} = \sigma_u$$

Then $\sigma_{vp} = \sigma_u$ by implication.

Finally we note that

$$\bar{v}_p^2 = \bar{u}^2 + \bar{v}^2 - \bar{v}_n^2 \qquad (2.41)$$

A2.3 Climate data

The following information is required at the centre of the region: $\bar{v}_n$, σ_{vn}, $\bar{v}_p$, $\bar{w}$, σ_w, $\bar{T}$, σ_T, $\bar{D}_d$, σ_{Dd} and a correction to T and D which is expressed as a gradient of T and D_d in order to get edge values. Data were derived from information given by Oort (1983). As discussed earlier σ_{Dd} was defined as $\sigma_{Dd} = \mu\sigma_T$ where μ was found experimentally, for each location, such that the correct precipitation was produced. The data are summarised in tables 2.1 to 2.4 for southern England and Sahel climates. Data for the approximate extremes of the seasonal cycle were derived, viz January and July and a sinusoidal variation between these extremes was assumed.

Let x_1 and x_7 be the mean or standard deviations of the reference variables for minimum and maximum of annual cycle respectively. Let d_1 and d_7 be the associated time in days relative to the winter solstice. The amplitude of the seasonal variation of x is given by

$$A_x = (x_7 - x_1)/2 \qquad (2.42)$$

The mean is given by

$$B_x = (x_7 + x_1)/2 \qquad (2.43)$$

Then the appropriate mean or standard deviation at d days from the winter solstice is given by:

$$x_d = A_x \sin(2\pi(d-d_7)/d_a + \pi/2) + B_x$$

where d_a is the number of days in a model year.

x_d is fixed for a constant solstice integration or varies seasonally for annual cycle integrations (in these all x_d are updated every 10 model days).

FIGURE 2.3 ANNUAL CYCLE SOUTHERN ENGLAND
TEST SOIL. LONG GRASS

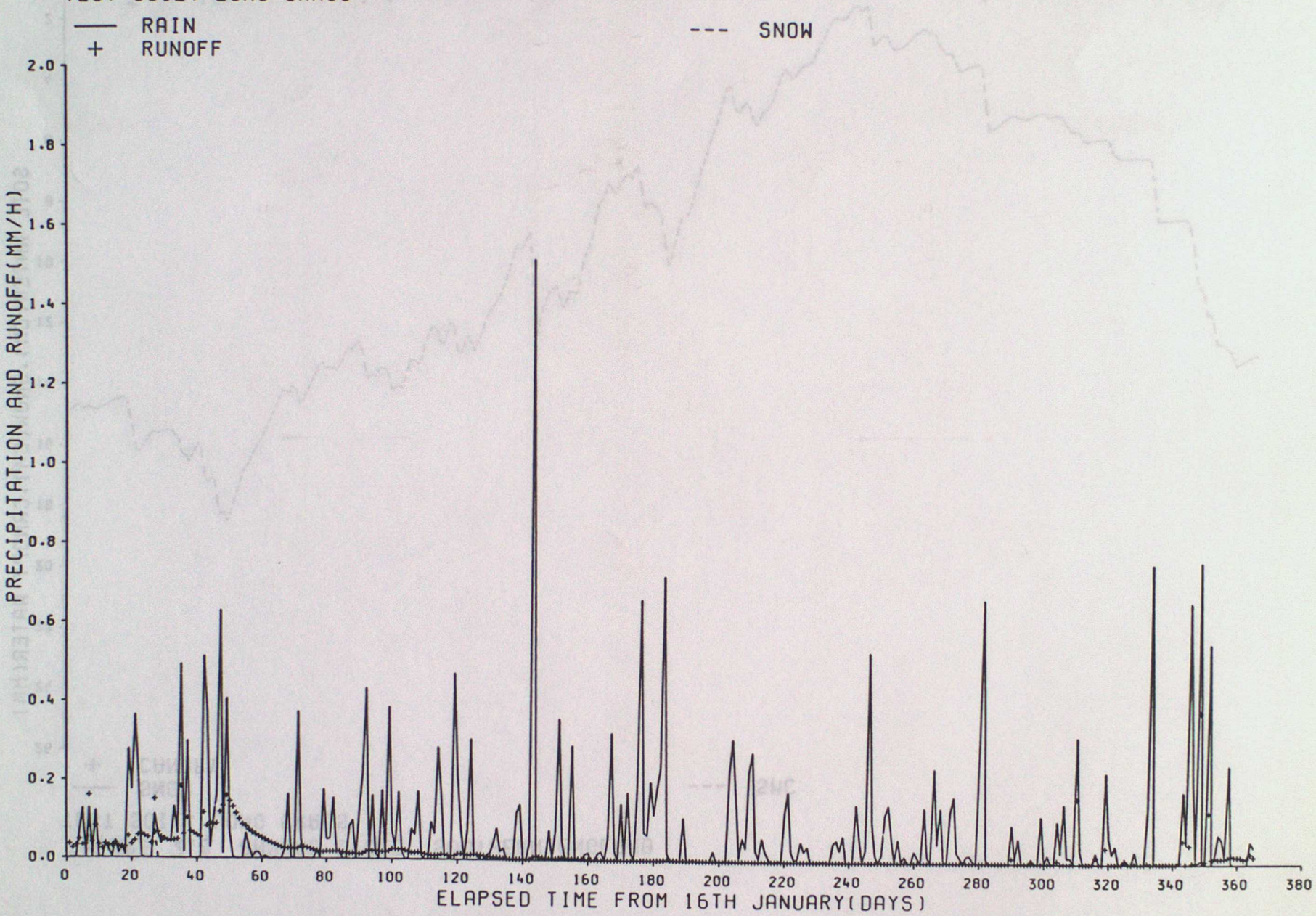

FIGURE 2.4 ANNUAL CYCLE SOUTHERN ENGLAND
TEST SOIL. LONG GRASS

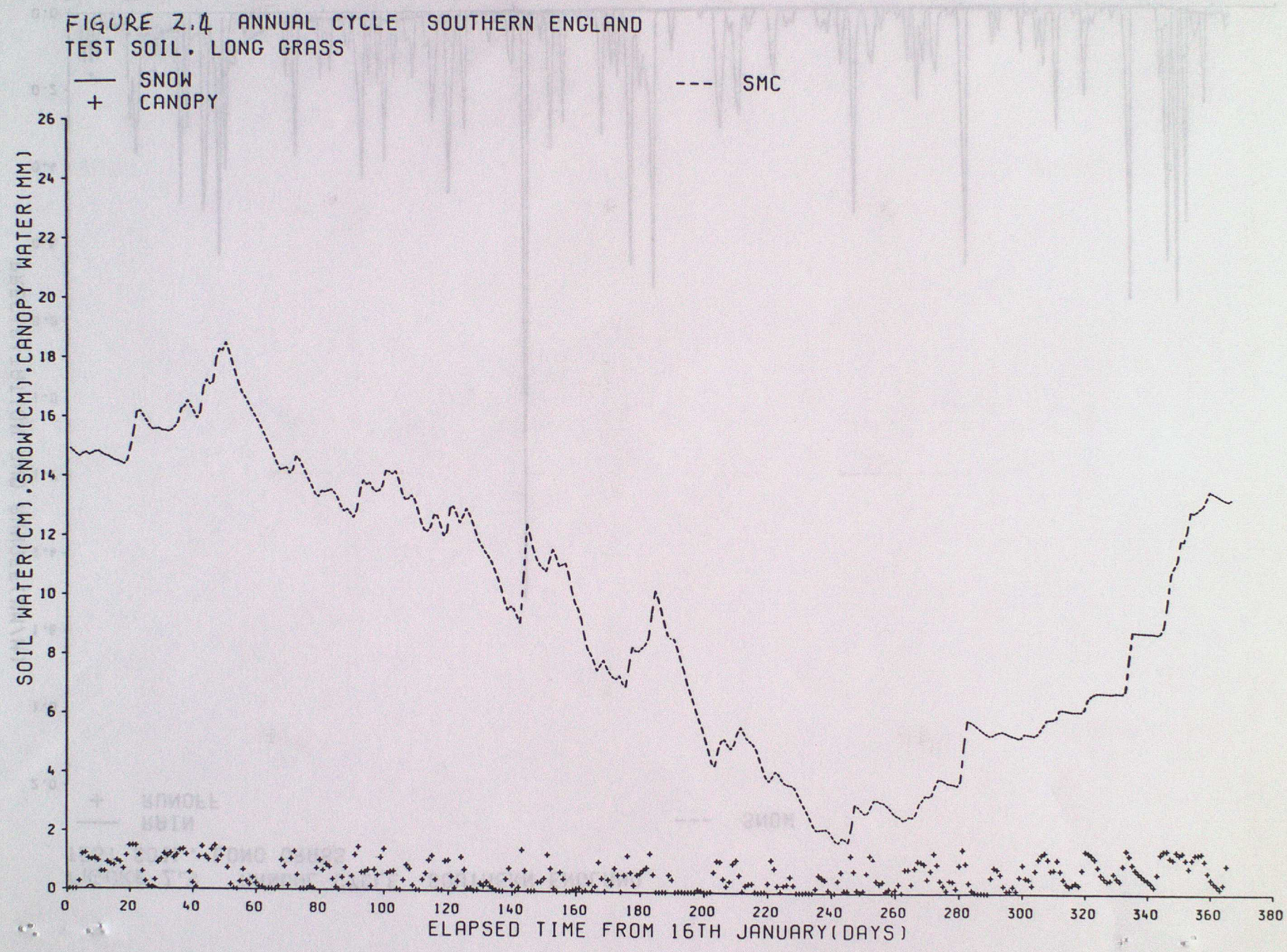

FIGURE 2.5 ANNUAL CYCLE SOUTHERN ENGLAND
TEST SOIL. LONG GRASS

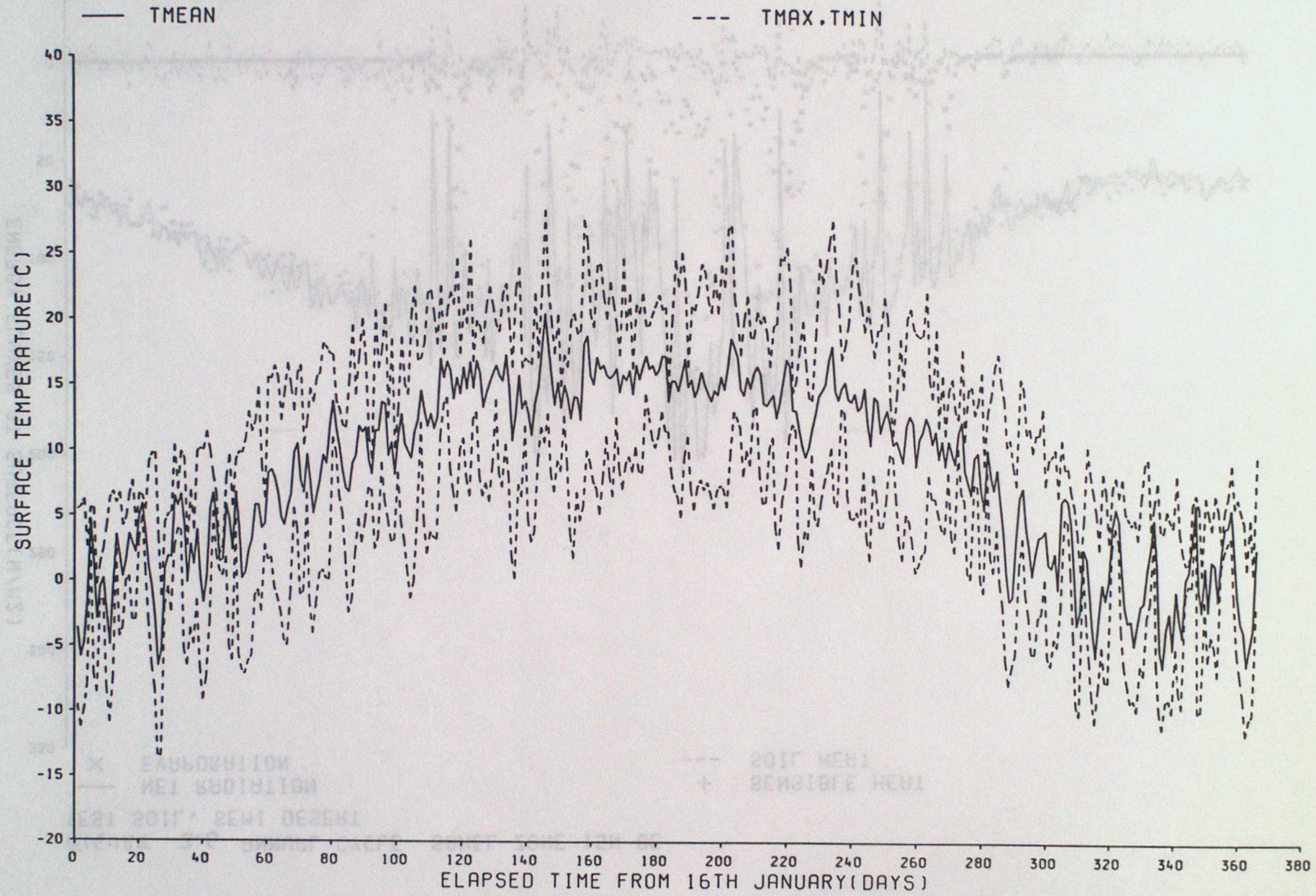

FIGURE 2.6 ANNUAL CYCLE SAHEL ZONE 15N 0E
TEST SOIL. SEMI DESERT

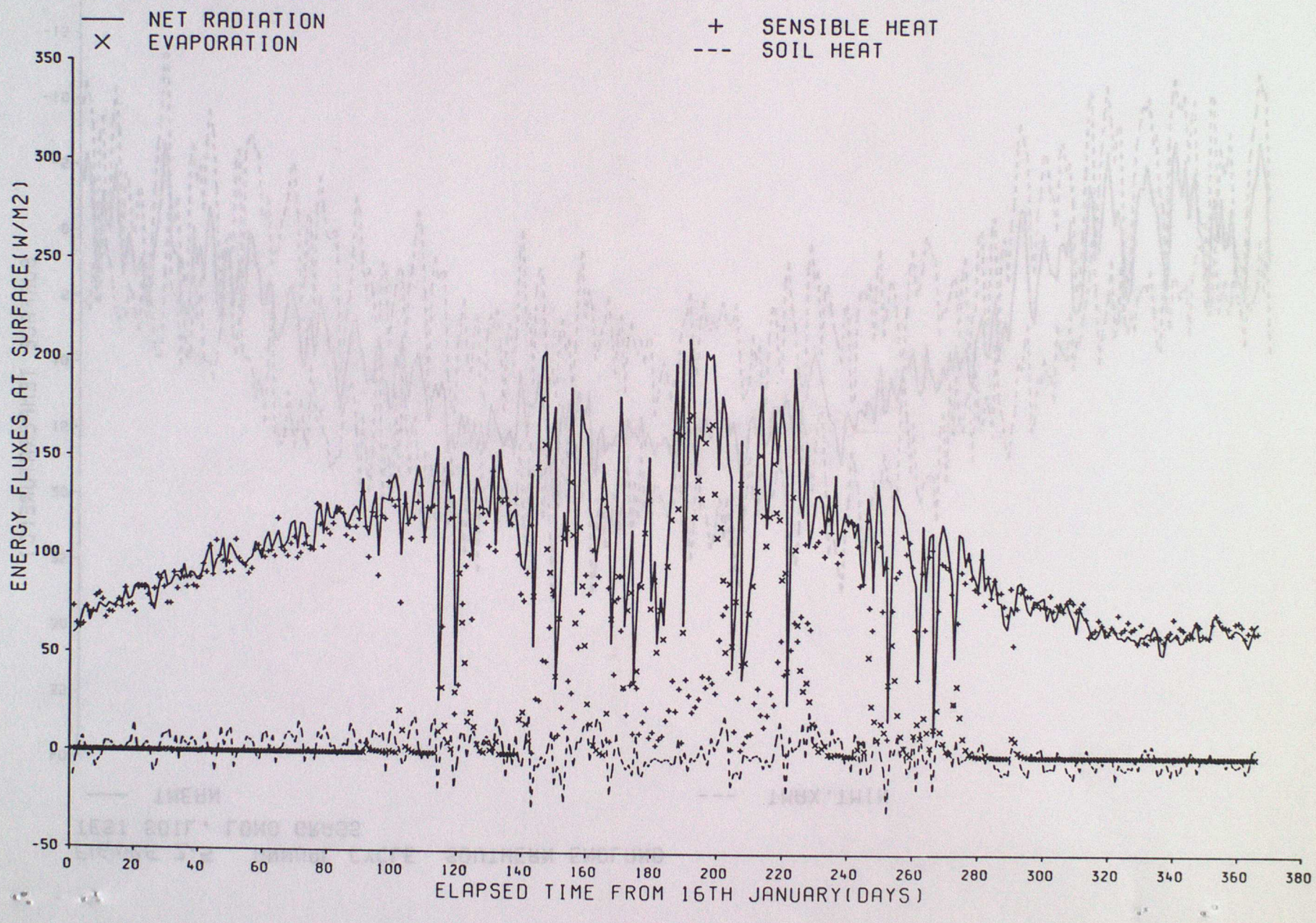

FIGURE 2.7 ANNUAL CYCLE SAHEL ZONE 15N 0E
TEST SOIL. SEMI DESERT

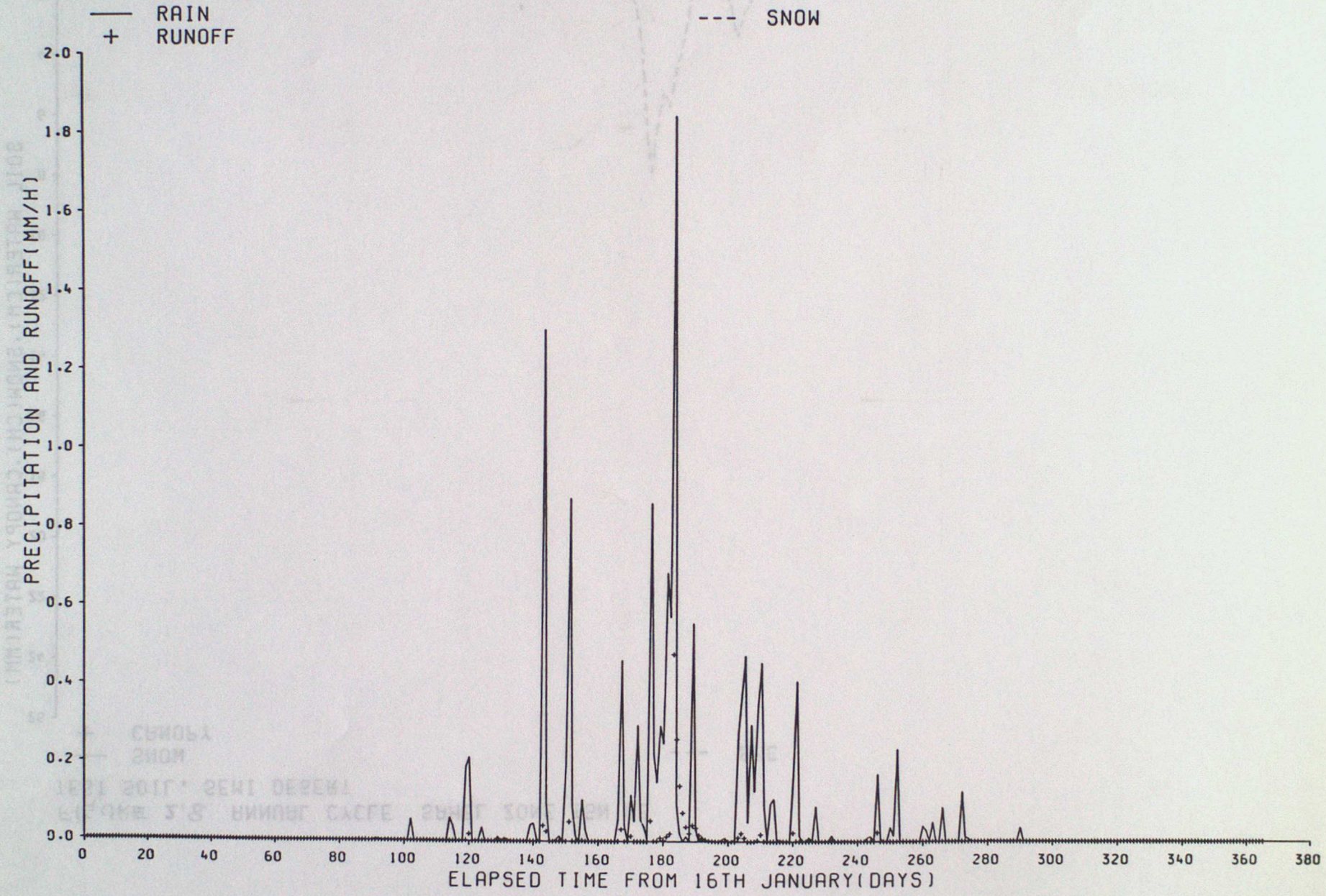

FIGURE 2.8 ANNUAL CYCLE SAHEL ZONE 15N 0E
TEST SOIL. SEMI DESERT

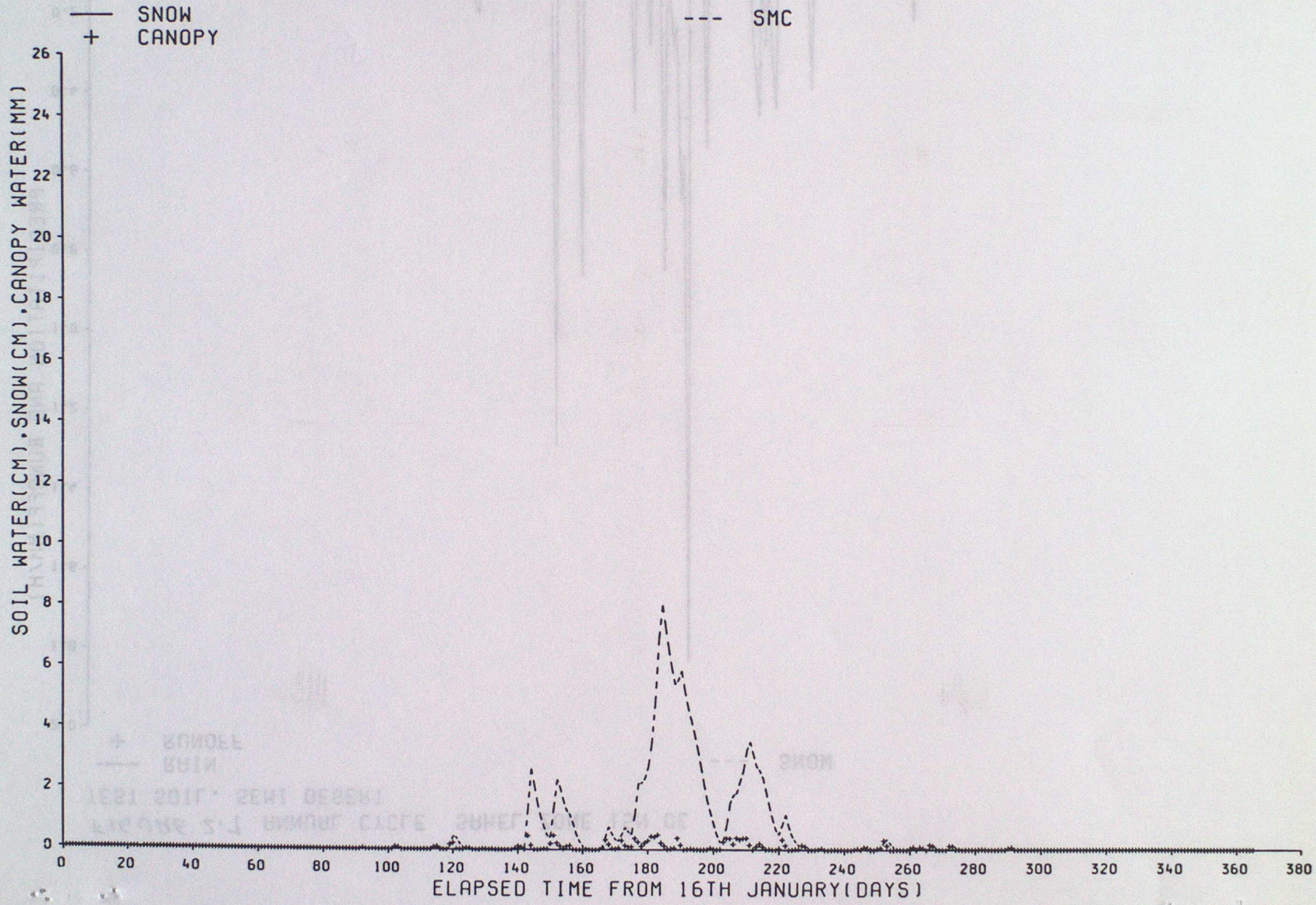

FIGURE 2.9 ANNUAL CYCLE SAHEL ZONE 15N 0E
TEST SOIL. SEMI DESERT

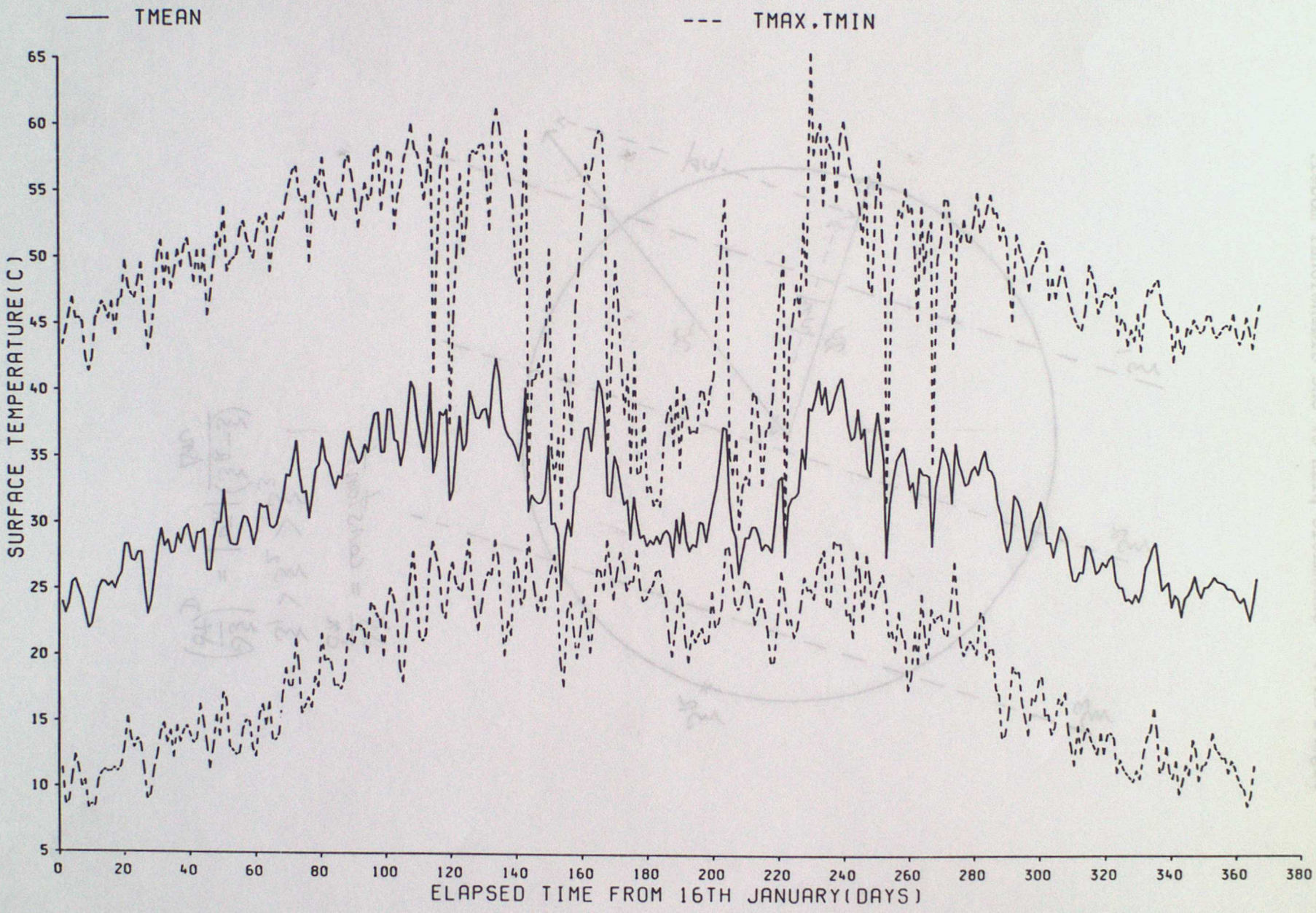

Figure 2.10 Schematic plan of one dimensional model.

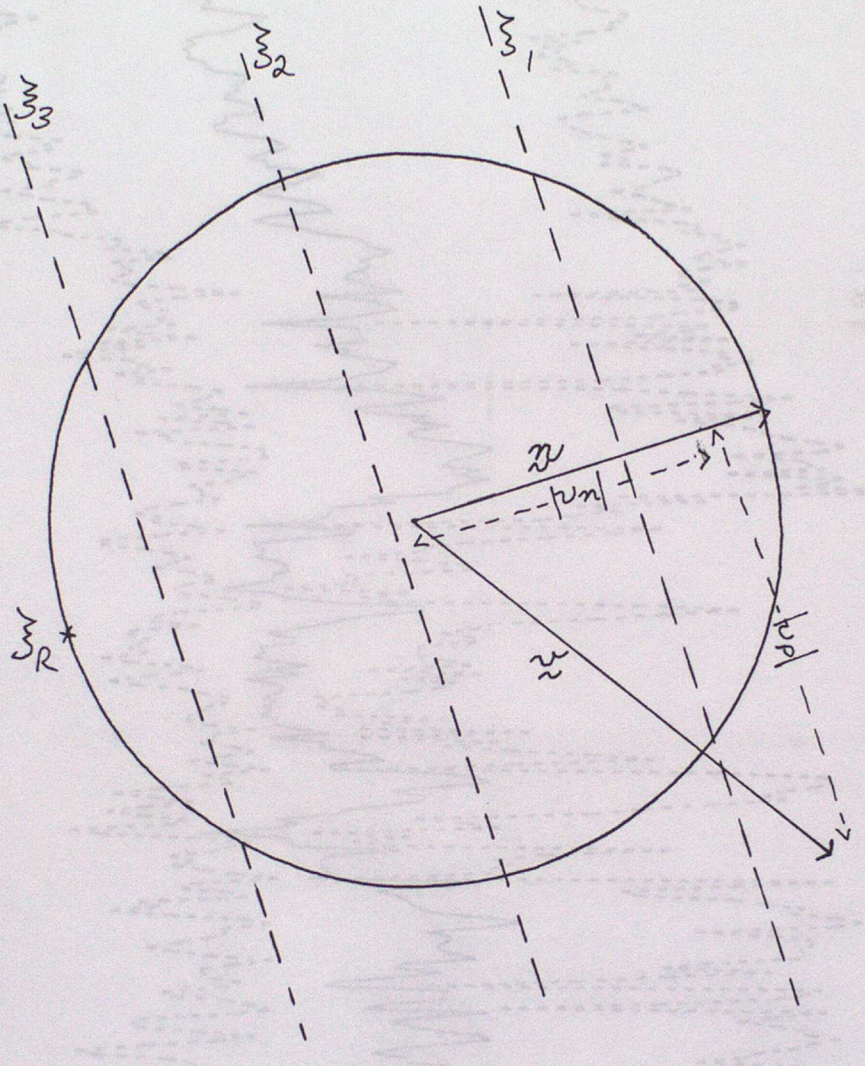

$$\frac{\partial \xi}{\partial x} = \text{constant}$$

$$\xi_1 > \xi_2 > \xi_3$$

$$\left(\frac{\partial \xi}{\partial t}\right)_D = |v_n| \frac{(\xi_R - \xi)}{\Delta x}$$

TABLE 2.1 SOUTHERN ENGLAND JANUARY

LATITUDE 52.0N LONGITUDE 0.0E

MEAN PRESSURE 1014.0 MEAN TEMPERATURE 275.0 MU 1.3

ATMOSPHERIC LEVEL	11	10	9	8	7	6	5	4	3	2	1
MEAN TEMPERATURE(K)	277.00	275.00	271.40	266.00	256.00	241.00	226.00	214.00	214.00	210.00	210.00
SD OF TEMPERATURE(K)	3.00	3.00	4.00	4.50	4.50	4.50	4.50	4.50	4.50	4.50	4.50
DEW PT DEPRESSION(K)	3.60	3.30	3.90	7.20	7.70	6.10	6.00	9.80	34.00	30.00	30.00
GRADIENT OF T(K/KM)	0.00533	0.00400	0.00400	0.00400	0.00400	0.00400	0.00267	0.00000	0.00000	0.00000	0.00000
GRADIENT OF D(K/KM)	0.00200	0.00067	0.00067	0.00067	0.00067	0.00133	0.00267	0.00000	0.00000	0.00000	0.00000
MEAN VN(M/S)	-1.70	-2.60	-3.80	-3.20	-2.10	-1.05	-0.35	-0.05	0.00	0.00	0.00
MEAN VP(M/S)	-0.60	-1.30	-2.60	-4.20	-6.00	-7.90	-10.00	-11.60	-13.00	-14.00	-14.00
SD OF VELOCITY(M/S)	5.50	6.00	7.00	8.70	10.90	13.70	16.70	15.10	10.90	7.00	5.00
MEAN W(MB/S)	-0.00003	-0.00004	-0.00005	-0.00005	-0.00004	0.00000	0.00000	0.00000			
SD OF W(MB/S)	0.00006	0.00008	0.00010	0.00010	0.00008	0.00004	0.00002	0.00001			

TABLE 2.2 SOUTHERN ENGLAND JULY

LATITUDE 52.0N LONGITUDE 0.0E

MEAN PRESSURE 1018.0 MEAN TEMPERATURE 285.0 MU 1.5

ATMOSPHERIC LEVEL	11	10	9	8	7	6	5	4	3	2	1
MEAN TEMPERATURE(K)	267.70	285.60	281.60	275.20	265.30	252.10	235.40	222.90	222.20	221.20	221.20
SD OF TEMPERATURE(K)	2.50	3.00	3.50	3.50	3.50	3.50	3.50	5.00	5.00	2.00	2.00
DEW PT DEPRESSION(K)	3.50	4.00	5.20	7.40	9.00	9.90	9.40	16.70	39.00	38.00	40.00
GRADIENT OF T(K/KM)	0.00467	0.00467	0.00467	0.00467	0.00400	0.00333	0.00200	0.00200	0.00267	0.00467	0.00667
GRADIENT OF D(K/KM)	0.00000	0.00000	0.00000	0.00133	0.00333	0.00333	0.00200	0.00200	0.00267	0.00467	0.00667
MEAN VN(M/S)	0.50	0.60	0.90	1.00	0.80	0.10	0.00	0.00	0.00	0.00	0.00
MEAN VP(M/S)	-1.40	-2.40	-4.50	-6.50	-8.80	-11.20	-13.30	-13.60	-11.70	-7.00	5.00
SD OF VELOCITY(M/S)	3.00	3.70	5.50	7.60	10.10	12.60	15.00	14.00	10.00	4.50	2.00
MEAN W(MB/S)	0.00000	0.00000	0.00000	0.00000	0.00005	0.00010	0.00009	0.00003			
SD OF W(MB/S)	0.00001	0.00002	0.00004	0.00008	0.00010	0.00020	0.00018	0.00006			

TABLE 2.3 SAHEL ZONE JANUARY

LATITUDE 15.0N LONGITUDE 0.0E

MEAN PRESSURE 1013.0 MEAN TEMPERATURE 298.6 MU 1.3

ATMOSPHERIC LEVEL	11	10	9	8	7	6	5	4	3	2	1
MEAN TEMPERATURE(K)	296.00	294.50	291.00	284.80	273.30	258.50	243.00	227.50	211.00	201.00	213.00
SD OF TEMPERATURE(K)	2.20	2.20	2.25	2.10	1.80	2.10	2.40	2.20	2.35	2.40	3.20
DEW PT DEPRESSION(K)	20.00	22.50	28.00	23.80	20.30	16.50	15.00	12.50	11.00	18.00	30.00
GRADIENT OF T(K/KM)	0.00270	0.00270	0.00270	0.00270	0.00270	0.00260	0.00255	0.00290	0.00370	0.00510	0.00350
GRADIENT OF D(K/KM)	-0.01400	-0.00930	-0.00630	-0.00160	0.00000	0.00070	0.00075	0.00290	0.00370	0.00510	0.00350
MEAN VN(M/S)	1.50	1.50	1.50	1.50	1.20	0.30	-0.60	-1.10	-1.40	0.00	1.40
MEAN VP(M/S)	-2.00	-2.00	-1.60	-0.40	2.80	7.40	7.60	2.40	-3.20	-8.00	3.00
SD OF VELOCITY(M/S)	2.80	3.10	3.50	4.20	5.40	7.10	8.70	9.40	9.40	6.50	3.50
MEAN W(MB/S)	-0.00008	-0.00003	0.00008	0.00018	0.00026	0.00033	0.00036	0.00035			
SD OF W(MB/S)	0.00015	0.00006	0.00016	0.00036	0.00053	0.00067	0.00067	0.00069			

TABLE 2.4 SAHEL ZONE JULY

LATITUDE 15.0N LONGITUDE 0.0E

MEAN PRESSURE 1011.0 MEAN TEMPERATURE 300.0 MU 4.8

ATMOSPHERIC LEVEL	11	10	9	8	7	6	5	4	3	2	1
MEAN TEMPERATURE(K)	299.00	298.00	296.00	287.00	274.50	260.50	246.00	229.50	211.00	202.50	219.00
SD OF TEMPERATURE(K)	2.10	2.00	1.85	1.60	1.60	1.65	1.80	1.95	2.10	2.40	2.80
DEW PT DEPRESSION(K)	4.00	9.00	18.00	14.00	9.00	5.00	5.00	3.50	3.00	19.50	36.00
GRADIENT OF T(K/KM)	0.00065	0.00130	0.00200	0.00280	0.00350	0.00360	0.00285	0.00180	0.00200	0.00320	0.00350
GRADIENT OF D(K/KM)	-0.00205	-0.00110	-0.00160	-0.00080	0.00052	0.00360	0.00285	0.00180	0.00200	0.00320	0.00350
MEAN VN(M/S)	0.40	0.25	0.00	-0.20	-0.30	-0.30	-0.10	0.50	1.85	2.60	1.40
MEAN VP(M/S)	1.00	0.60	0.80	2.40	4.40	2.40	-1.00	2.00	10.00	18.30	22.00
SD OF VELOCITY(M/S)	2.50	3.20	4.10	4.70	5.00	4.80	5.60	6.30	6.60	5.50	2.80
MEAN W(MB/S)	-0.00001	-0.00001	-0.00004	-0.00008	-0.00012	-0.00017	-0.00020	-0.00020			
SD OF w(MB/S)	0.00002	0.00003	0.00008	0.00015	0.00024	0.00034	0.00040	0.00040			

3. Hydrology and soil moisture

3.1 Introduction

3.2 Modelling hydrology

3.2.1 Introduction to the hydrological balance of the surface
3.2.2 Review of hydrology and soil moisture processes
3.2.3 Review of hydrological parametrizations for AGCMs

3.3 Development of a hydrological parametrization.

3.3.1 Gravitational drainage
3.3.2 Soil moisture models
3.3.3 Infiltration and surface runoff
3.3.4 Modification of infiltration by vegetation.
3.3.5 Summary of new hydrological parametrization.

3.4 One dimensional model studies of the dependence of runoff on soil type.

3.5 AGCM studies of the new hydrological parametrization.

3.5.1 Introduction
3.5.2 Comparison of new hydrology with 'bucket' model.
3.5.3 Sensitivity of atmospheric variables to soil type.
3.5.4 Conclusions

3.6 Summary and Conclusions

3.7 References

3. Hydrology and soil moisture

3.1 Introduction

Hydrological processes are treated in a rather rudimentary fashion in general circulation models, if they are treated at all. Recently, as interest in the effect of land surface processes on climate has increased, so also has the need to improve the parametrization of hydrological and soil moisture processes, thereby improving estimates of evaporation (Rowntree (1982), (1983)). Hydrological processes, which include movement of water in soils, river flow, ground water storage, reservoir or lake storage, and evapotranspiration, are complex and still not totally understood (Erichsen and Nordseth (1984)). Micro-scale variations in basic hydrological variables and parameters present formidable problems for mathematical description of hydrological processes on the macroscale. For example, hydraulic conductivity, which is dependent on soil moisture concentration, is reported to vary by several orders of magnitude over a relatively short distance (Price and Bower (1984)) and Dooge (1982) has pointed out that mathematical descriptions of soil moisture behaviour which are appropriate on the micro-scale may not be applicable on the macro-scale due to the highly heterogeneous nature of the land surface and subsurface. Empirical/statistical models have been used widely in hydrology but more recently physically based models usually referred to as deterministic or distributed models have been developed. Anderson and Burt (1985) give a useful review of hydrological modelling and show that the subject is still developing and that there are difficult problems to overcome. An example of deterministic catchment modelling by Beven et al (1984) shows the amount of data required for simulation on that scale and the difficulties in predicting peak runoff rates. However the catchment water balance was simulated to a satisfactory level of accuracy (within 4%). Fortunately the climate modeller is primarily interested in the water balance rather than the shape of river hydrographs. However he is working on a much larger space scale, will have little data available and will be unable to develop a distributed model on a global scale. In fact, availability of data presents a major limitation on the type of parametrization that can be realistically used in global climate modelling. Another limitation is the large amount of computing time generally required by more complex hydrological models.

Given the problems and the uncertainty surrounding hydrological modelling, especially in data sparse areas, a relatively simple but physically based parametrization has been derived. Its behaviour is tested in both ODM and AGCM integrations and appears to be satisfactory although there are few data with which to verify such models.

In this section the term hydrological processes will be taken to refer to all aspects of the hydrological cycle but the term hydrology will refer more specifically to river flow and will be differentiated from soil water modelling. There are various measures of soil moisture but we will use the volumetric soil moisture concentration, θ, defined as the ratio of the total volume of moisture to the total soil volume. We also refer to the volumetric soil moisture content at saturation, θ_s, at field capacity, θ_f, and at wilting point θ_w. These terms are explained in detail in section 3.3.2.

3.2 Modelling hydrology

3.2.1 Introduction to the hydrological balance of the surface.

The moisture balance of a surface layer of soil can be written simply as in equation 3.1.

$$\frac{d\hat{\theta}}{dt} = \frac{1}{D} (R + SM - \nu E_d - (1-\nu)E_s - Y_g - Y_s) \quad (3.1)$$

where $\hat{\theta}$ is the mean soil moisture concentration and D is the depth of the layer. R is incident rainfall which is replaced by throughfall (T_f) in the presence of vegetation. Throughfall is the portion of incident rainfall reaching the ground beneath a canopy (see section 4.3.3). SM is snowmelt, E_d and E_s are transpiration from a dry vegetation canopy and direct soil evaporation respectively, ν is the proportion of vegetated surface, Y_g is drainage from the base of the layer and Y_s is runoff from the surface, ie water which has not entered the surface. Y_s is only operative providing there is rainfall or snowmelt. If further layers of soil were included then there would be an exchange term between this layer and a deeper one. In this section we are concerned primarily with the Y terms and the movement of moisture within the soil rather than evaporation.

Hydrology and soil water modelling are important in climate modelling primarily because the evaporation rate which is dependent on the soil moisture concentration plays an important part in the energy balance of the surface.

As the other terms in Eq. 3.1 affect the soil moisture concentration they may also affect evaporation rates. It is useful to know that where θ remains high (usually in high rainfall regions), evaporation is at the potential rate and is largely independent of θ, so that in such regions errors in Y are not generally significant in climatic terms. Similarly where θ is persistently low, rainfall, evaporation and runoff are low and runoff errors are not very significant. However there are large regions where θ does influence the evaporation rate, eg in Western Europe in summer and where it is important to estimate runoff to a higher degree of accuracy. Evaporation is dealt with in detail in section 4.

3.2.2 Review of hydrology and soil moisture processes.

Movement of soil moisture is governed by Darcy's law (extended by Richards (1931)) (Eq. 3.2)

$$Q = - K(\psi)\nabla H_\theta \quad (3.2)$$

where Q is the moisture flux, K hydraulic conductivity, ψ is matric potential and H_θ is the total energy potential defined as

$$H_\theta = \psi - z \quad (3.3)$$

where z is taken as positive in the vertically downwards direction and is the gravitational component of the energy potential (in units of length).

In soil water modelling it is useful to deal in terms of energy potential of soil water with respect to some fixed energy level, in order to describe the movement of water in the soil. The force acting on soil water is given as the negative of the potential gradient since flow occurs from high to low potential. Matric potential is that part of the total energy potential which is a result of the forces binding soil water to the soil by adsorption and capillarity. Matric potential is generally negative. For a very readable treatise on the physics of soil water see for example Ch3 of Hillel (1971).

Eq. 3.2 is valid for steady flow but for transient flow it is also necessary to include the mass balance Eq. 3.4

$$\partial\theta/\partial t = - \nabla.Q \qquad (3.4)$$

Eqs. 3.2 and 3.4 may be solved analytically for only a few special cases; otherwise numerical solution is required. Between rainfall events soil moisture slowly redistributes itself under gravitational and matric forces. During rainfall events the near surface becomes saturated and a fairly sharp wetting front develops and subsequently moves downwards under the influence of these forces (see for example Kirkby (1985)). The existence of sharp gradients in soil moisture means that a relatively fine mesh is required to model wetting and drying of soils accurately. Solution of Eqs. 3.2 and 3.4 is further complicated by hysteresis of the conductivity curves between wetting and drying, although this is often ignored in modelling soil moisture movement.

Inhomogeneities within soils are more important for soil moisture movement than for heat flow and can lead to marked spatial variations in soil moisture and conductivity (Price and Bauer (1984)). The above equations ignore the important contributions that natural 'pipes', burrows, decayed root channels and cracks make to the redistribution of water in the soil and especially to runoff processes. Roots of plants can remove water from any depth within the soil so that in vegetated areas the predominant pathway taken by soil moisture to the atmosphere is not vertical but to the nearest roots.

Runoff processes are extremely complex, depending on the soil profile, soil type, vegetation cover and type, land morphology, underlying geology and antecedent moisture characteristics. Two runoff components are generally identified (1) Quick runoff; that part of the hydrograph which responds quickly to rainfall events and (2) slow runoff which as its name suggests takes place for some considerable time after rainfall events. This is a fairly inexact distinction as it relates to hydrograph shape rather than physical mechanisms. Kirkby (1985) gives a useful introduction to runoff generating mechanisms. These are summarised as follows: (1) Hortonian or infiltration excess overland flow caused when local rainfall intensity exceeds infiltration capacity (surface infiltration rate); (2) Saturation excess overland flow, caused where rain falls on areas where the soil is saturated and cannot accept any more water. These areas are relatively small and tend to be found close to streams, but may grow and contract during the passage of a rainfall event; (3) saturation through flow, occurring at less permeable levels in the soil which having become

saturated enable moisture to move parallel to the soil horizons in a downslope direction rather than vertically and (4) deep percolation to the water table and thence to surface drainage.

There are variations in these basic types and the contribution from each varies from location to location. Broadly Hortonian flow is most significant in arid areas and fairly insignificant in humid forested regions. Saturation overland flow and throughflow are more common in humid regions and percolation is fairly ubiquitous. Beven et al (1984) report that the contributing area (where saturation overland flow occurs) is difficult to define and show that the relationship between peak runoff and contributing area varies greatly between catchments. Other aspects of the complexity of runoff are discussed by Erichsen and Nordseth (1984) and Ward (1984).

3.2.3 Review of hydrological parametrizations for AGCMs

Carson (1982) has reviewed various parametrizations of hydrology. Most schemes are highly empirical and the most common type consists of a soil moisture store which empties and fills in response to evaporation and rainfall respectively. Referred to as a 'bucket' model, runoff is only generated when the store is full and the 'bucket' overflows. Runoff is therefore instantaneous and only occurs during rainfall or snowmelt and at high soil moisture concentrations. Slow drainage of soil moisture following rainfall is ignored as is quick runoff during precipitation on dry soils. Carson (1982) reports that some climate modellers (eg Gates and Schlesinger (1977) and Shukla (1978)) have introduced a soil moisture dependence to their formulation of runoff. Their model's behaviour is shown in figure 3.1. The net effect of such models will be reduced soil moisture since a proportion of incident rainfall will no longer be added to the soil. Such an approach is realistic but empirical in that it is not related directly to any physical processes although both Hortonian and saturation excess overland flow could be considered to be relevant mechanisms.

Another approach is to model the flow of moisture using a finite difference approximation of Eqs. 3.2 and 3.4. Mahrt et al (1984) and Dickinson (1984) both suggest 2-layer models, the top layer being much thinner than the bottom layer. Both suggest that it is necessary to have at least two layers to model bare soil evaporation correctly. They allow gravitational drainage through the lowest boundary, and Mahrt et al limit infiltration thereby allowing surface runoff. Dickinson refers to the need to tune surface runoff depending on soil moisture or to assume a sub-grid scale variation of rainfall intensity but gives no example.

The same approach is taken by Milly and Eagleson (1982a) with detailed modelling of infiltration and exfiltration. They found that a single level model could perform better than a two layer model providing the depth of the layer was chosen carefully for the climatic conditions of the experiment. It was found in fact that the optimum depth varied from storm to storm, so that an alternative approach was taken in which the soil cell size and soil moisture were allowed to vary to simulate moisture redistribution following a rainfall event.

Milly and Eagleson (1982b) have also considered the inhomogeneity of the land surface and its effect on evaporation and infiltration. Among their conclusions they note that either spatially variable rainfall or soil moisture leads to increased runoff compared to the use of mean values.

In conclusion two main approaches have been taken so far: (1) an empirical approach and (2) a physically based soil moisture modelling. The first has the obvious limitations of any empirical system but is easy to use. The second removes or reduces the need for tuning but introduces problems regarding available data and the representativeness of essentially local models in an AGCM grid square context. So far as is known the second approach has not actually been used in any AGCM experiments.

3.3 Development of a hydrological parametrization

3.3.1 Gravitational drainage

A relatively simple parametrization has been developed based on Milly and Eagleson (1982a) but with considerable simplification. Two components of runoff were considered to be important for modelling in the AGCM context: surface or Hortonian runoff and gravitational drainage. Saturation excess overland flow might also require to be modelled but has not been considered due to the difficulty in specifying a typical average relationship. To some extent it will be implicit in the other two runoff formulations.

Combining Eqs. 3.2 and 3.4 gives

$$\partial\theta/\partial t = \nabla.(K(\psi)\nabla(H_\theta)) \qquad (3.5)$$

Assuming that important soil moisture redistribution only occurs vertically we can write Eq. 3.5 for the z direction alone. Locally this will not be true, especially on hill slopes but this point is discussed later. For the z direction (taking z downwards as positive) Eq. 3.5 becomes (using Eq. 3.3)

$$\partial\theta/\partial t = \partial/\partial z(K(\psi)(\partial\psi/\partial z - 1)) \qquad (3.6)$$

If it is assumed that there is a single active soil layer, ie a layer which interacts with the atmosphere, its depth is taken to be equal to the average root depth in vegetated areas and a shallow layer, of depth to be determined, in areas of bare soil. Then integrating Eq. 3.6 over a layer of depth D gives

$$\int_0^D \partial\theta/\partial t \, dz = [\, K(\theta)\,(\partial\psi/\partial z - 1)\,]_0^D \qquad (3.7)$$

noting that $K(\theta) \equiv K(\psi)$ as $\psi = \psi(\theta)$.

At the surface (z=0) the term on the right hand side of Eq. 3.7 is the balance between infiltration and evaporation both of which are treated separately. Noting that the mean moisture concentration throughout the layer is $\hat{\theta} = \int_0^D \theta dz/D$, we can write Eq. 3.7 as

$$D\partial\hat{\theta}/\partial t = I_f - \nu E_d - (1 - \nu)E_s + K(\theta_D)\,((\partial\psi/\partial z)_D - 1) \qquad (3.8)$$

where I_f is surface infiltration and E_s is soil evaporation. Local infiltration is defined as

$$I_f = \min [T_f + SM, F] \tag{3.9}$$

where F is the maximum infiltration rate or infiltration capacity.

A further assumption is made that the soil moisture gradient is fairly low within the active zone, such that $\theta_D \sim \hat{\theta}$. This may appear to be a rather gross assumption and is likely to be wrong during rainfall events and strong evaporation over bare soil. However there are two aspects of soil moisture movement which make this assumption more reasonable. The first is that in vegetated areas, moisture is removed by roots from all levels in the active zone and the profile will tend to be evened out. Secondly during rainfall, fairly rapid horizontal removal of soil moisture occurs along natural pipes and cavities so that there will be a tendency to remove extreme vertical variability within a soil profile over a period of time. These assumptions may be more reasonable when we consider spatial averages. Because of horizontal redistribution and removal of moisture it is quite possible that the horizontal average of the vertical gradient of ψ again tends to a small value, such that $(\partial\psi/\partial z)_D \to 0$. This assumption is further made here.

Making these simplifications and denoting grid box averages with a bar, Eq. 3.8 becomes

$$D\,\partial\bar{\hat{\theta}}/\partial t = -\overline{K(\hat{\theta})} + \bar{I}_f - \nu\bar{E}_d - (1-\nu)\bar{E}_s \tag{3.10}$$

A final assumption is made that $\overline{K(\hat{\theta})} \equiv K(\bar{\hat{\theta}})$. Due to the non linear nature of $K(\theta)$ this will lead to a bias in the $K(\theta)$ term but is a necessary simplification until a horizontally spatial variation in θ is assumed.

The first term on the right hand side is gravitational drainage of moisture from the active layer to ground water which eventually will reach streams. No attempt is made to model changes in the level of ground water and it is assumed that there is no movement of water from the water table to the surface. Evaporation is treated in section 4. From Eq. 3.9 local surface runoff is defined in Eq. 3.11 as

$$Y_s = T_f + SM - I_f \tag{3.11}$$

Due to the highly variable nature of rainfall, Y_s for the grid square is computed making some assumptions about the likely rainfall distributions. Infiltration and surface runoff are dealt with more fully in sub sections 3.3.3 and 3.3.4.

3.3.2 Soil moisture models

It is necessary to have representative values of soil moisture characteristics for use in the hydrology parametrization. A review of the literature reveals a wide range of values and not a few soil moisture models. In this section a comparison of several results is made and some

suitable values chosen. The possible errors are large, yet they are not excessive compared to other possible errors such as those due to the formulation of runoff and the specification of rainfall.

Various sources of data have been used with the emphasis being on results from Eagleson (1978), Koch (1985) and Clapp and Hornberger (1978). A useful summary of some soil moisture characteristics is given by Mahrt et al (1984). In considering the problem we need a model for $K(\theta)$ where K is the soil moisture conductivity and θ the soil moisture volume concentration. Eagleson (1978) gives

$$K(\theta) = K_s \ ((\theta-\theta_w)/(\theta_s-\theta_w))^{c} \qquad (3.12)$$

where θ_s is the porosity or saturation value of θ and θ_w is the residual value of θ at the wilting point. At θ_s it is assumed that all voids between soil particles are filled with water, although this is not usually achieved in practice since a small fraction of air becomes trapped. The residual value of θ or wilting point (θ_w) is taken to be a constant defined as the soil water concentration at which it becomes virtually impossible for plants to remove water from the soil. As Hillel (1971) discusses however, wilting point can depend on the rate of uptake within a plant and so depends to some extent on atmospheric demand as well as soil moisture concentration. It appears (see fig. 3.2) that Koch (1985) in using the same relationship between soil moisture and conductivity as Eagleson, has defined θ_w to be the field capacity (θ_f).

Other forms of Eq. 3.12 are given by Clapp and Hornberger (1978) viz

$$K(\theta) = K_s \ (\theta/\theta_s)^{2b+3} \qquad (3.13)$$

where also $\psi(\theta) = \psi_s(\theta/\theta_s)^{b}$

thus ignoring the effect of residual concentration explicitly and implicitly including it in the chosen value of b.

Since we are interested in the behaviour of soil water in the natural setting it was decided to retain θ_w and so use Eq. 3.12. It will be noticed that field capacity is not considered explicitly. This is because it is not a true physical property of soils and its definition is somewhat arbitrary (the concentration at which gravitational drainage effectively ceases (Hillel (1971)). However it is useful to compare quoted values of field capacity as this concept is currently used in the AGCM.

Figure 3.2 shows the relationship between θ_s, θ_f, and θ_w for various soil types given by different authors. Values of c from Eagleson (1978) are also given showing that c is approximately related to soil type. Using this relationship between c and soil type it was possible to plot K_s (saturated conductivity) as a function of c using data from Eagleson (1978), Koch (1985), Clapp and Hornberger (1978) and Brakensiek (1979). Figure 3.3 shows that for a given c there is an order of magnitude variation in K_s, possibly due to differences in soil samples but perhaps, as pointed out by Brakensiek (1979) because conductivity is difficult to ascertain near saturation. For our purposes a geometric mean of K_s is taken to yield an average relationship between K_s and c as shown in figure

3.3. This curve gives values which mostly compare well with final infiltration rates quoted by Hillel (1971) (infiltration rates tend to K_s after prolonged rainfall).

Average values of θ_s, θ_f and θ_w are shown in figure 3.4. The values for sand are assumed to occur at c=2. By inspection of data from Eagleson and Koch it was decided to define field capacity as the point at which the hydraulic conductivity falls to 0.03 mmh^{-1}. Using the values of θ_w, θ_s, K_s and c in figures 3.3 and 3.4 and Eq. 3.12, θ_f was re-calculated and is shown in figure 3.4. The values given are slightly larger for high c values and lower for low c but at least we have a climatologically consistent definition of field capacity.

Figure 3.5 shows the available soil water at field capacity and at saturation for 1m of soil. Currently a field capacity of 15 cm is used in the bucket model, which corresponds here to a soil with c = 6.6 and D=1m. Such a soil was used as a test soil to compare performance of the new hydrology scheme with the bucket model (section 3.5.2).

To allow some variation in soil characteristics globally, soil type was related to the Wilson and Henderson-Sellers (1985) categories. Figure 3.6 shows the relationships between c and the percentage of clay in the soil (from Clapp and Hornberger (1978)). Wilson and Henderson-Sellers (1985) define 3 soil types dependent on texture: coarse, medium and fine. These are also shown in Figure 3.6.

Medium texture soils also include loams and silts with lower clay fractions than implied here. For that reason medium soils were assigned a value of c = 8 which is the median value of the whole range of c. Rather than use extreme values, coarse soils were assigned c = 5 and fine c = 11. The soil parameters for different soil types are summarised in Table 3.1 below.

TABLE 3.1

Soil Type by Texture	c	K_s (ms^{-1} (mmh^{-1})) x10^{-6}		θ_s	θ_w	θ_f
COARSE	5.0	8.06	(29.0)	0.420	0.055	0.150*
MEDIUM	8.0	1.81	(6.5)	0.460	0.105	0.290
FINE	11.0	0.36	(1.3)	0.490	0.180	0.400
TEST	6.6	3.61	(13.0)	0.445	0.080	0.230

*An error in deriving these values meant that 0.13 was used in all integrations; the effect would be relatively small.

These categories of soil types give a reasonable spread and yet do not contain extreme values. Although the values have been derived in a rather empirical manner yet they are useful order of magnitude values which may be justified on the grounds that there are large subgrid scale variations in soil types and characteristics, and that possible errors in the runoff scheme may be equally large. Gravitational drainage for three soil types in table 3.1 is shown in figure 3.7. The values are those actually used in the experiments.

3.3.3 Infiltration and Surface Runoff

It has already been noted that local infiltration depends on both the rainfall rate and the infiltration capacity (Eq. 3.9) which in turn depends on initial soil moisture conditions and the evolution of the rainfall event (Smith (1982)). Broadly, the initial infiltration capacity can be high but declines to a final value after about an hour (depending on soil type and rainfall rate etc.) as the soil becomes saturated. Infiltration capacity varies spatially by quite large amounts (Tricker (1977)) and depends on soil type, underlying geology, vegetation cover and crusting of bare soil. Because of these other uncertainties it was decided to assume constant infiltration capacities equal to the saturated conductivity as given in table 3.1. The effect of vegetation is considered in section 3.3.4.

It was considered necessary to allow for spatial variations in rainfall as otherwise surface runoff would be greatly underestimated. From Eqs. 3.9 and 3.11 local surface runoff of rainfall on bare soil can be written as

$$Y_s = \max [0, R - F] \qquad (3.14)$$

where $T_f + SM$ has been replaced by R.

Let the proportion of a grid square likely to be instantaneously affected by rain during a rainfall event be ε. Let the probability distribution of rainfall within the rainfall area be given by the probability density function f(R) such that $\int_0^\infty f(R)dR = 1$. Then the average grid box rainfall is defined by

$$\bar{R} = \varepsilon \int_0^\infty Rf(R)dR \qquad (3.15)$$

where $\bar{R}$ is generated by the rainfall parametrizations in an AGCM. Assuming F is constant over the area, average runoff $\bar{Y}_s$ is given by

$$\bar{Y}_s = \varepsilon \int_F^\infty (R - F)\, f(R)dR \qquad (3.16)$$

since $Y_s = 0$ for $R \leq F$.

By assuming that the probability distribution is exponential we define:

$$f(R) = \varepsilon/\bar{R} \exp (-\varepsilon R/\bar{R}) \qquad (3.17)$$

and by substituting Eq. 3.17 into Eq. 3.16 we have:

$$\bar{Y}_s = \bar{R} \exp (-\varepsilon F/\bar{R}) \qquad (3.18)$$

ε was set to 1 for large scale rain and 0.3 for convective rain and used in all experiments in this report. These are likely to be conservatively high values. Eagleson and Qinliang (1985) explore the likely coverage of a rainfall area for different catchment sizes and suggest that for an AGCM grid square more appropriate values for ε would be 0.6 and 0.05 respectively.

In section 4 interception of rainfall is introduced, in which case a diminished amount reaches the ground as throughfall T_f. Where interception is included, R is replaced by T_f in Eq. 3.18. For snowmelt R is replaced by SM in Eq. 3.18 and ε is set to 1.0.

The relationship between surface runoff and grid square average rainfall is shown in figure 3.8 for the values of ε used in the experiments.

3.3.4 Modification of infiltration by vegetation

Infiltration capacity depends on the soil covering. Infiltration rates quoted for each soil type in table 3.1 assume uncrusted bare soil. There is little information on infiltration rates in the presence of vegetation but the consensus is that they are generally much higher. By contrast bare soil usually develops a crust which tends to reduce infiltration rates. Clay soils respond in a more complex fashion due to the tendency for cracks to appear in dry soil thereby enhancing infiltration rates. Vegetation, especially forest, provides a protecting layer of humus and improves soil structure, thereby allowing higher infiltration rates. Trimble and Weitzman (1954) quote infiltration rates for different vegetation types for medium textured soils and Tricker (1977) notes the pre-eminence of vegetation in determining infiltration rates.

Initially it was decided that bare soil and vegetation rates could be treated separately so that

$$F = \nu F_v + (1- \nu)F_s \qquad (3.19)$$

where ν is the vegetated fraction, F_v the vegetation infiltration rate and F_s the bare soil infiltration rate (equivalent to K_s). This form was used in the AGCM integration of section 3.6. Later it was decided to let F_v be a function of soil type, so F was redefined as

$$F = (\nu \beta_v + 0.5(1- \nu))F_s \qquad (3.20)$$

where β_v is a factor used to modify bare soil infiltration in the presence of vegetation and the factor of 0.5 allows for crusting of bare soils. Eq. 3.20 was used in ODM integrations.

The justification for either of these forms of the infiltration capacity is somewhat tenuous, but some means of accounting for the effect of vegetation on infiltration is required. Infiltration rates quoted in small catchment studies, eg by Beven et al (1984) show considerable spatial variability and reveal the difficulty in arriving at realistic values which might be appropriate to an area the size of a grid square. A future approach may be to allow some statistical distribution of infiltration rates, but this has the disadvantage that yet more unknown parameters need to be estimated.

3.3.5 Summary of new hydrological parametrization.

In the previous sections a relatively simple parametrization of hydrology has been derived. There are two components. The first deals with surface runoff and is rainfall dependent, the second concerns gravitational drainage and is soil moisture dependent. Together they simulate some

important aspects of runoff, namely, quick response during rainfall and slow drainage once rainfall has ceased. The total runoff is given in Eq. 3.21, omitting bar signs denoting areal averages.

$$Y = Y_s + Y_g = R \exp(-\varepsilon F/R) + K_s((\theta-\theta_w)/(\theta_s-\theta_w))^c \qquad (3.21)$$

where F is given by Eq. 3.20 and R is changed to throughfall, T_f, if canopy storage is included or SM for snowmelt.

3.4 One dimensional model studies of the dependence of runoff on soil type

Three ODM integrations were carried out for southern England over one annual cycle, in order to compare the effect of soil on runoff. The soils quoted in table 3.1 were used. The ODM used the evaporation and interception routines developed in section 4. The land surface data were those presented in section 5. For each integration a land type of long grass was used. A program error in the calculation of F meant that F was underestimated by a factor of 0.68 which meant that surface runoff was greater than it should have been. However as Y_s is typically about 10% of Y_g, this error was not considered to be too serious. The actual values of F which were used in the integrations are quoted in table 3.2 along with mean or total values for some hydrological variables computed from the integrations.

From the three columns on the left hand side of table 3.2 it can be seen that there are 2 opposing tendencies. As the texture becomes finer, the field capacity (SMC_f) increases allowing more rainfall to remain in the soil, however infiltration capacity decreases, leading to increased surface runoff. The result is that total runoff does not vary monotonically with soil texture. Evaporation is inversely related to runoff but there is a smaller difference in evaporation because it is only controlled by the soil moisture content (SMC) when $SMC<SMC_c$. SMC_c, the 'critical' value of SMC, is given in table 3.2 and is the point at which evaporation becomes limited by reduced availability of soil moisture.

The control of evaporation by soil moisture is discussed in section 4.2. From the point of view of this section we note that the ratio of actual evaporation to potential evaporation is β and $\beta < 1$ for $SMC<SMC_c$ and proportional to SMC. β is defined in equation 4.4.

For Southern England $SMC<SMC_c$ only occurs for a proportion of the year. Figures 3.9 to 3.11 show the variation of soil moisture for each soil type. Table 3.3 summarises the durations over which $SMC < SMC_c$ for each soil type along with the times when SMC falls below and rises above the critical point. The amount of drying is also important as is the time of year. In the coarse soil case evaporation falls below the potential rate near the time of maximum insolation so that the effect on evaporation rates is potentially greatest.

From these integrations it can be concluded that coarse soil will generally be drier than the others and that evaporation will be reduced. The medium soil would appear to be the wettest and give the greatest evaporation but the results may well depend on the climatic regime, particularly on the frequency of rainfall.

Table 3.2

Summary of ODM Integrations for 3 soil types in Southern England (Annual means or totals)

Soil Texture	SMC_f (cm)	SMC_c (cm)	F (ms^{-1} (mmh^{-1}))	T* (°C)	SMC (cm)	Total R (mm)	Total Y (mm)	Total E (mm)
Coarse	9.5	2.5	9.67×10^{-6} (34.8)	8.90	5.39	657.9	192.7	473.9
Medium	18.5	6.5	2.17×10^{-6} (7.8)	8.56	10.20	667.5	101.6	531.7
Fine	22.0	7.0	0.44×10^{-6} (1.6)	8.70	9.52	664.9	137.5	511.6

Table 3.3

Duration for which actual evaporation becomes less than potential evaporation.

Soil Texture	1st Day when SMC < SMC_c	1st Day when SMC > SMC_c	Duration (days)
Coarse	~ 163	~ 280	~ 100
Medium	~ 210	~ 280	~ 70
Fine	~ 193	~ 333	~ 140

3.5 AGCM studies of new hydrological parametrization

3.5.1 Introduction

The work described in this section has been discussed by Warrilow (1986) and concerns 2 distinct experiments. The first experiment used the new hydrology scheme with a test soil defined in table 3.1. An 18 month integration was carried out and results compared to a control integration which used a simple 'bucket' model with a capacity of 15 cm (see section 3.2.3). The AGCM was run with fixed cloud, uniform surface resistance of 60 sm^{-1}, no canopy interception and a single layer to predict soil temperatures. The second experiment consisted of two 6 month integrations one with coarse soil and the other with fine. The aim of this second experiment was to test the sensitivity of the global model to soil type. The results are presented in the following subsections.

3.5.2 Comparison of new hydrology with 'bucket' model

Each integration began at the end of a model February. The experiment test soil had been chosen so as to have a similar field capacity to that of the control. Therefore a root depth of 1m was used giving a nominal field capacity of 15cm. The new hydrology scheme might be expected to lead to drier soil conditions where SMC<15 cm, since from Eq. 3.21 we see that only a fraction of the rainfall can enter the soil, especially in convective situations, because of the surface runoff term, and gravitational drainage occurs all the time, albeit at a low rate when the soil moisture content is less than field capacity. Figures 3.12 and 3.13 show the soil moisture content during the first northern hemisphere summer and the change with respect to the control. The expected drying is observed over large areas but it should be noticed that those areas were already fairly dry and that in moist regions (SMC > 15cm) soil moisture has increased as there is no

longer an upper limit to soil moisture in the new hydrology scheme. There is therefore some enhancement of the soil moisture difference between wet and dry regions, although the effects of random variability in the rainfall are superimposed on this broad trend. An area of consistent drying can be observed along the edge of dry areas of both North America and Asia between 50N and 60N. A correspondng reduction in both precipitation and evaporation occurs in these areas. A similar effect was observed during the following summer about 5° of latitude farther south, accompanied by a more general reduction in soil moisture in northern mid-latitudes.

Total runoff changes relatively little. Figures 3.14 and 3.15 show total annual runoff for the experiment and control respectively. Largest area of consistent change appear to be northern Australia and the southern United States where runoff has increased. Figure 3.16 shows the annual gravitational component of runoff. This is similar to the total control runoff. Figure 3.17 shows the annual component of surface runoff. It would appear from this that the increased runoff noted in the United States is due to this component. Elsewhere, significant surface runoff has merely subtracted from gravitational drainage, so that the total is little different from the control.

Comparison of total runoff from the new scheme with a map of annual runoff published by Manabe and Holloway (1975) from original work by Lvovitch and Ovtchinnikov revealed that the new scheme performs quite well. It needs to be remembered however that runoff as defined in the AGCM context is not necessarily the same as that taken from observational studies, which may either be based on river flow observations or estimates based on water balance studies. Moreover estimates of runoff are necessarily difficult to make as each component of the hydrological cycle, including precipitation has observational uncertainty of at least 10% (IAHS 1983).

For the parameters used in this experiment, the gravitational component of runoff is generally larger than surface runoff except in a few locations as noted above. This is largely as expected especially as the infiltration capacity has been increased by the presence of vegetation in these experiments by a factor of 2.3 (using Eq. 3.19) giving an actual infiltration capacity of $7.36 \times 10^{-6} ms^{-1}$ ($26.5\ mmh^{-1}$). Work done after these experiments were carried out led to a revision of the effect of vegetation type on infiltration capacity as defined by Eq. 3.20 (see section 3.3.4).

3.5.3 Sensitivity of atmospheric variables to soil type

Two six month AGCM integrations were carried out using parameters for either a fine or coarse textured soil as given in table 3.1. It might have been useful to have looked at the medium soil case but when these integrations were carried out it was assumed that the medium soil would be intermediate. The same vegetation characteristics were used as in the first AGCM hydrology experiment. The infiltration capacities for each soil in the presence of vegetation were $F = 8.25 \times 10^{-6} ms^{-1}$ ($29.7\ mmh^{-1}$) for coarse soil and $F = 6.72 \times 10^{-6} ms^{-1}$ ($24.2\ mmh^{-1}$) for fine soil (from Eq. 3.19). As discussed in section 3.3.4 it was decided to let infiltration capacity in vegetated areas depend on soil type as well as vegetation type as in Eq. 3.20. Use of Eq. 3.19 led to a surface infiltration capacity that was probably too high, however there is considerable uncertainty in

Table 3.4

Zonal means of some surface variables, showing sensitivity to soil type

Latitude Band	SMC (cm)		Precipitation ($mmday^{-1}$)		Evaporation ($mmday^{-1}$)		Sensible Heat Flux (Wm^{-2})	
	Coarse	Fine	Coarse	Fine	Coarse	Fine	Coarse	Fine
90N-30N	4.52	12.35	2.305	2.472	1.973	2.198	25.4	21.7
	+173%		+7.0%		+11.4%		-14.6%	
30N-Equator	4.22	8.79	5.479	5.492	4.474	4.462	22.3	21.7
	+108%		+0.3%		-0.3%		-2.7%	
Equator-30S	1.76	4.99	2.598	2.674	4.471	4.720	22.3	20.8
	+184%		+3.0%		+5.6%		-6.7%	
30S-90S	5.18	11.40	3.085	3.091	2.590	2.377	16.9	15.5
	+120%		+0.2%		-8.2%		-8.3%	

this aspect of the work. Figures 3.18 and 3.19 show the soil moisture distributions for the Northern Hemisphere summer (second 3 months of integration) and reveal large differences which stem from the different abilities of each soil to hold moisture. However as discovered in the ODM studies the effect on other fields is somewhat less marked. Results for broad latitude bands are summarised in table 3.4, together with the percentage differences between coarse and fine soils. Although the values given include sea points, except for soil moisture, it does give an overall impression of the impact of soil type on the atmospheric processes. The relatively small effect of changing soil type, is likely to be, as we have seen in section 3.4, due to a lack of variation in β, Figures 3.20 and 3.21 give maps of β for the summer period for each soil type. It is apparent that there are substantial areas where $\beta \sim 1$ and $\beta \sim 0$ is common to both soil types, for which there can be little change in evaporation. In fact the two charts are very similar although dry areas are more extensive in the coarse soil case.

There are however some important local variations. Figures 3.22 to 3.25 show precipitation and evaporation for each soil type separately. Over Europe precipitation is larger over a wide area in the fine soil case and over the Caucasus it is almost doubled. Evaporation is likewise greater over Europe but over the Caucasus it is the same. However the areas surrounding the Caucasus exhibit higher evaporation and presumably account for the higher precipitation. Consideration of β in figures 3.20 and 3.21 show that β varies greatly over Europe thereby accounting for the differences in evaporation and precipitation. Other local areas where substantial differences exist can be found, so clearly on a local scale soil type is important.

3.5.4 Conclusions

AGCM studies confirm that the new hydrology scheme produces fairly small changes in runoff and soil moisture when the field capacity is chosen to be the same although as expected it is slightly drier. For the parameters chosen, surface runoff is a much smaller component than gravitational drainage but nevertheless makes an important contribution to runoff in some relatively dry tropical areas.

Soil moisture depends strongly on soil type but the dependence of other fields on soil type is weaker, although some local exceptions have been observed. This can be understood by considering the parameter β which shows much less variability between soil types.

3.6 Summary and Conclusions

Major problems face anyone trying to model hydrological processes on any time or space scale. Hydrological modelling has often drawn heavily on statistical and empirical techniques. These have been successful in various engineering applications but suffer from being limited to the catchments for which the models were designed. An alternative path which is being followed increasingly is to use physically based models, in which the basic equations governing moisture flow in the soil are solved. These however suffer from the disadvantage of requiring large amounts of data which can often only be found by detailed field measurements. These problems are considerable on a catchment scale but become impossible on a

global scale. A review of hydrological parametrizations shows that highly simplified but physical based approaches have been taken recently, replacing early empirical schemes.

In this section a parametrization has been developed in which highly simplifying assumptions have been made to the basic flow equations. An attempt has been made to relate runoff to soil type, soil moisture, rainfall and vegetation. Despite its simplicity, fairly realistic mean annual runoff values have been derived from some AGCM integrations. The basic parametrization gives results similar to the bucket model if the field capacities are similar. Soil moisture is highly dependent on soil type, but evaporation, runoff and precipitation are less dependent overall.

Further work is needed to investigate the sensitivity of the model to the spatial distribution of rainfall, soil type and vegetation type. The need for further moisture layers should be considered along with the need for modelling the effect of high water tables on runoff and evaporation.

3.7 References

Anderson, M.G. and Burt, T.P. 1985 Modelling strategies. Hydrological forecasting, Ch1, Edt. by Anderson M.G. and Burt T.P., John Wiley and Sons, Chichester.

Beven, K.J., Kirkby, M.J., Schofield, N. and Tagg, A.F. 1982 Testing a physically-based flood forecasting model (TOPMODEL) for three UK catchments. Journal of Hydrology, 69, 119-143.

Brakensiek, D.L. 1979 Comments on 'Empirical Equations for some Soil Hydraulic Properties' by Roger B. Clapp and George M. Hornberger. Water Res. Res., 15, 989-990.

Carson, D.J. 1982 Current parametrizations of land-surface processes in atmospheric general circulation models. Land surface processes in atmospheric general circulation models, Edt by Eagleson P.S., Cambridge University Press, Cambridge.

Clapp, R.B. and Hornberger, G.M. 1978 Empirical equations for some soil hydraulic properties. Water Res. Res. 14, 601-604.

Cosby, B.J., Hornberger, G.M. Clapp, R.B. and Ginn, T.R. 1984 A statistical exploration of the relationships of soil moisture characteristics to the physical properties of soils. Water Res. Res., 20, 682-690.

Dickinson, R.E.	1984	Modelling evapotranspiration for three dimensional global climate models. Climate Processes and Climate Sensitivity, Geophysical Monograph 29, Maurice Ewing Vol 5.
Dooge, J.C.I.	1982	Parametrization of hydrologic processes. Land surface processes in atmospheric general circulation models, Edt by Eagleson P.S., Cambridge University Press, Cambridge.
Eagleson, P.S.	1970	Dyanmic Hydrology, McGraw-Hill, New York.
Eagleson, P.S.	1978	Climate, Soil, and Vegetation. Water Res. Res., 14, 705-776.
Eagleson, P.S. and Qinliang, W.	1985	Moments of catchment storm area. Water Res. Res., 21, 1185-1194.
Erichsen, B. and Nordseth, K.	1984	Runoff models - do they tell what actually happens! Nordic Hydrology, 15, 273-282.
Gates, W.L. and Schlesinger, M.E.	1977	Numerical simulation of the January and July global climate with a two-level atmospheric model. J. Atmos. Sci., 34, 36-76.
Hillel, D.	1971	Soil and Water. Academic Press, New York.
Kirkby, M.J.	1985	Hillslope hydrology. Hydrological forecasting CH3. Edt. by Anderson M.G. and Burt T.P., John Wiley and Sons, Chichester.
Koch, R.W.	1985	A stochastic streamflow model based on physical principles. Water. Res. Res., 21, 545-553.
Lee, R.	1980	Forest Hydrology, Columbia Univ. Pr., New York.
Mahrt, L., Pan, H., Paumier, J. and Troen, Ib.	1984	A boundary layer parametrization for a general circulation model. Oregon State University. Department of Atmospheric Sciences. Corvallis Oregon.

Manabe, S. and Holloway, J.L. 1975 A seasonal variation of the hydrologic cycle as simulated by a global model of the atmosphere. Journal of geophysical Research, 80, 1617-1649.

Marshall, T. and Holmes, J. 1979 Soil Physics. Cambridge Univ. Press., Cambridge.

Milly, P.C.D. and Eagleson, P.S. 1982a Parameterization of moisture and heat fluxes aross the land surface for use in atmospheric general circulation models. Report No. 279., Dept. of Civil Eng., Massachusetts. Institute of Technology, Cambridge, Mass.

Milly, P.C.D. and Eagleson, P.S. 1982b Infiltration and evaporation at inhomogeneous land surfaces. Report No 270, Dept. of Civil Eng., Massachusetts Institute of Technology, Cambridge, Mass.

Price, A.G. and Bauer, B.O. 1984 Small scale heterogeneity and soil-moisture variability in the unsaturated zone. Journal of Hydrology, 70, 277-293.

Richards, L.A. 1931 Capillary conduction of liquids in porous mediums. Physics 1, 318-333.

Rowntree, P.R. 1982 Sensitivity of general circulation models to land surface processes Met O 20 Technical Note No II/192 Meteorological Office, Bracknell. (Unpublished).

Rowntree, P.R. 1983 Land surface processes in climate models - parametrization and model sensitivity. Met O 20 Technical Note No II/201.

Rutter, A.J. 1975 The hydrological cycle in vegetation. In: Vegetation and the atmosphere, Vol 1, Edt. Monteith J.L., Academic Press, London, 111-154.

Shukla, J. 1978 Private Communication to Carson, D.J.

Smith, R.E. 1982 Rational Models of infiltration Hydrodynamics. In: Modelling Components of hydrologic cycle, Edt. Singh V.P. Littleton, Col., 107-126.

Tricker, A.S.	1977	Infiltration characteristics of a small Pennine catchment in Derbyshire. The East Midland Geographer, 6., 328-336.
Trimble, G.R. Jr. and Weitzman, S.	1954	Effect of a hardwood forecast canopy on rainfall intensities. Trans. American Geophysical Union, 35, 226-234.
Ward, R.C.	1984	On the response to precipitation of headwater streams in humid areas. Journal of Hydrology, 74, 171-189.
Warrilow, D.A.	1986	The sensitivity of the UK Meteorological Office Atmospheric General Circulation Model to recent changes to the parametrization of Hydrology. To appear in Proc. Conf. on Parametrization of Land-surface Characteristics, Use of Satellite Data in Climate Models, and First Results of ISLSCP, Rome 2-6 December 1985.
Wilson, M.F. and and Henderson-Sellers, A.	1985	A global archive of land cover and soils data for use in General Circulation Climate Models. Journal of Climatology, 5, 119-143.

Figure 3.1 Runoff parametrizations.

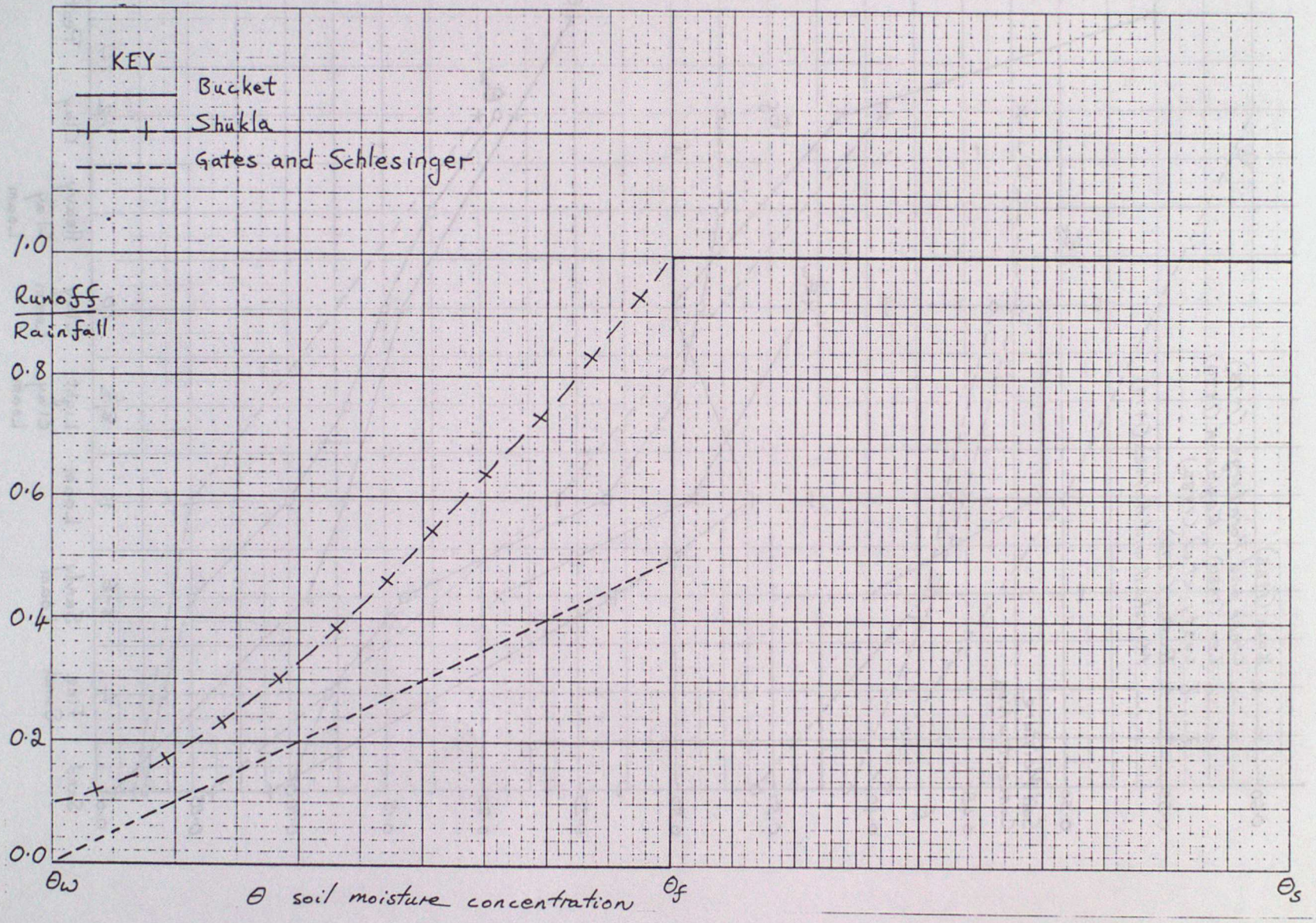

Figure 3.2 Soil moisture concentration at saturation, field capacity and wilting point for different soil types.

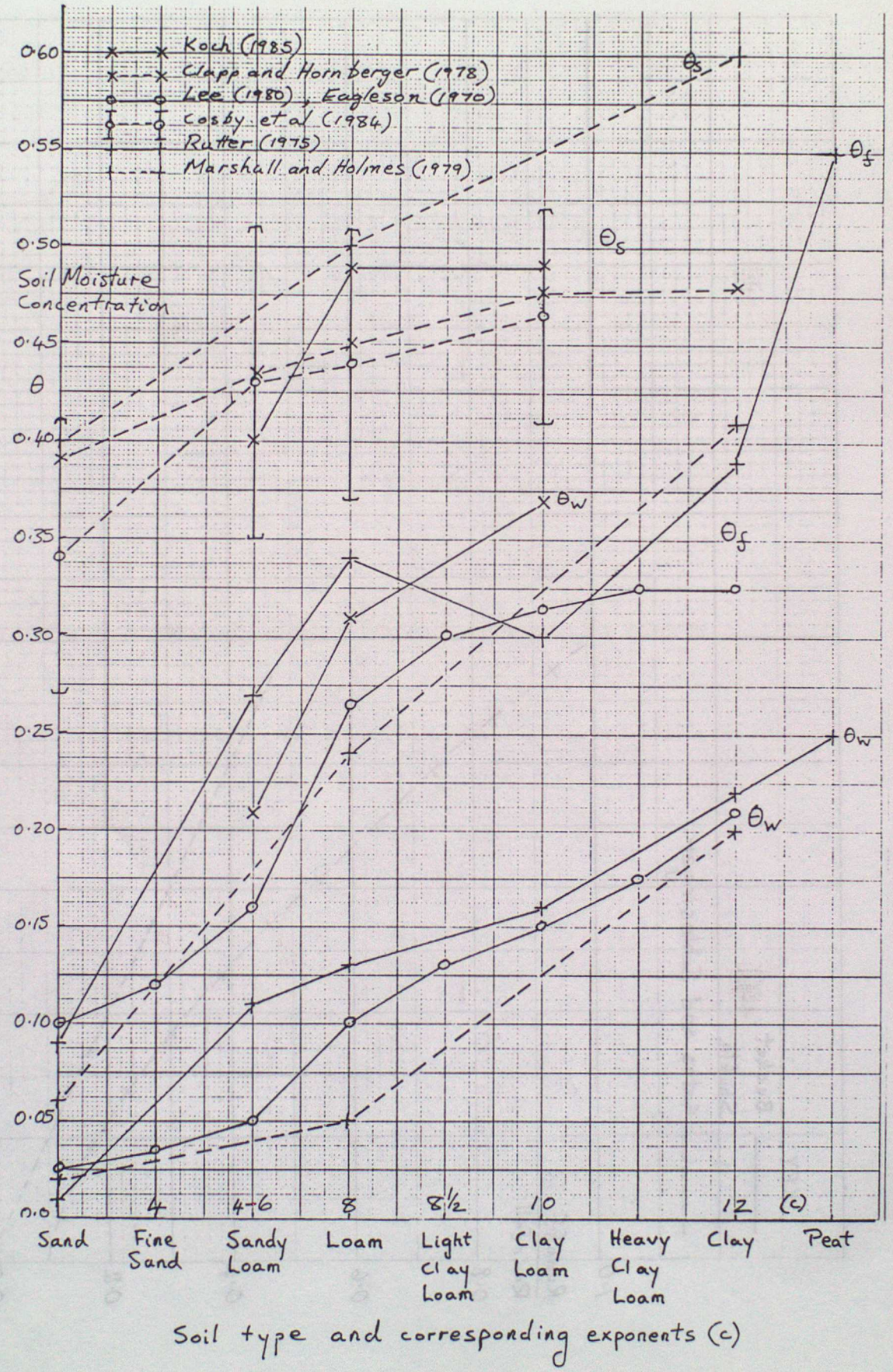

Figure 3.3 Saturated conductivity for different soil types.

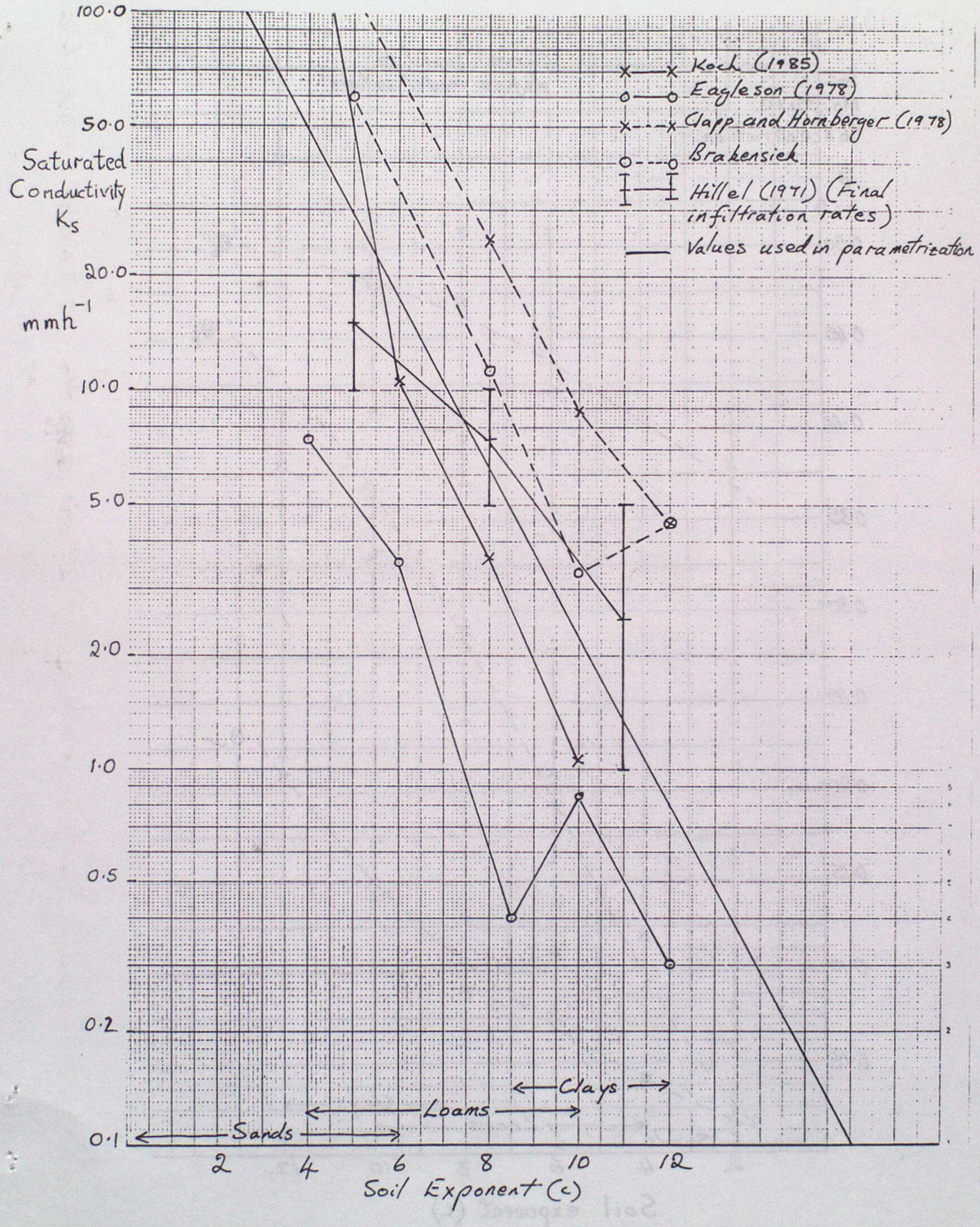

Figure 3.4 Mean and model values of soil moisture concentration at saturation, field capacity and wilting point.

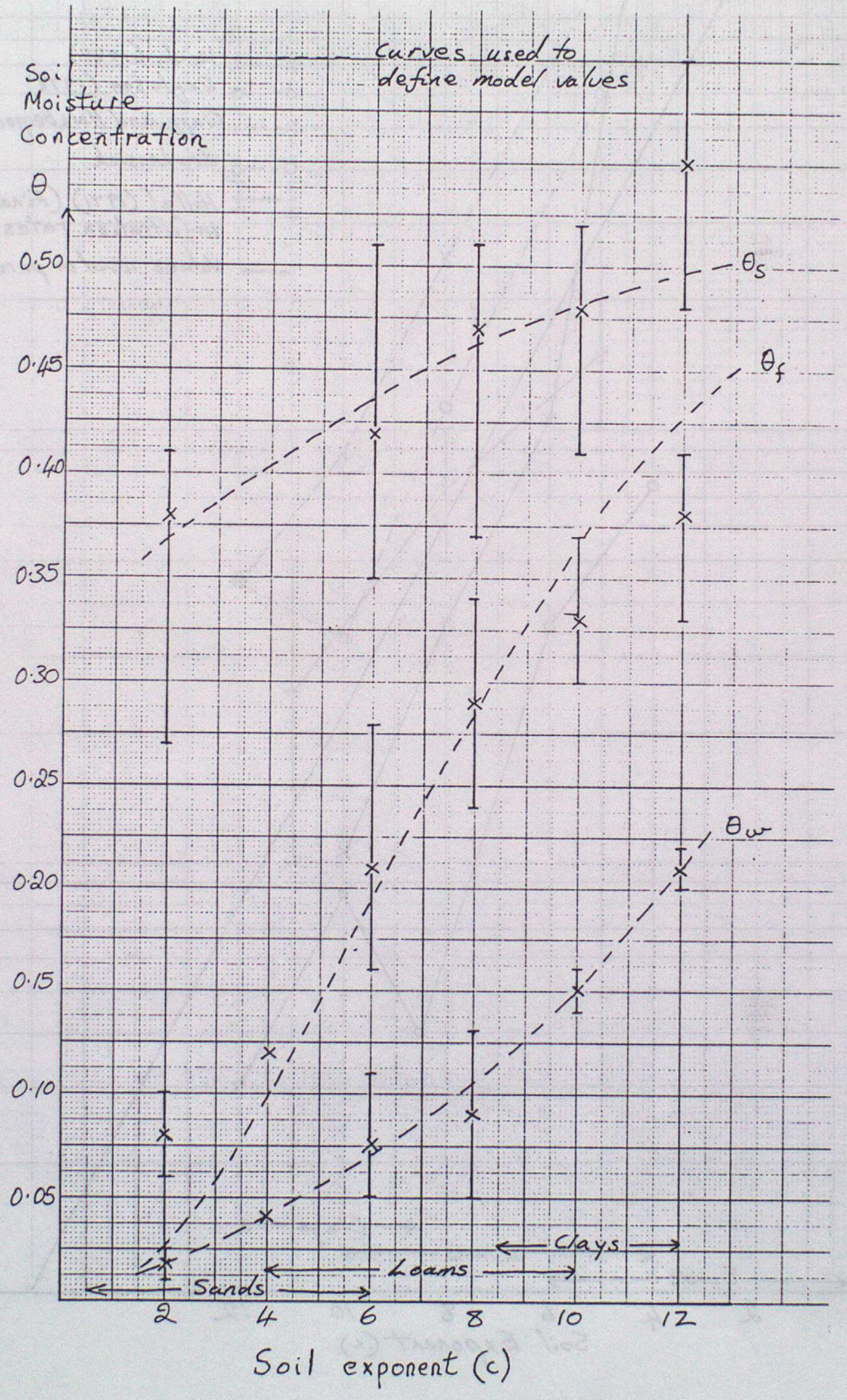

Figure 3.5 Available soil moisture content for 1m of soil in model.

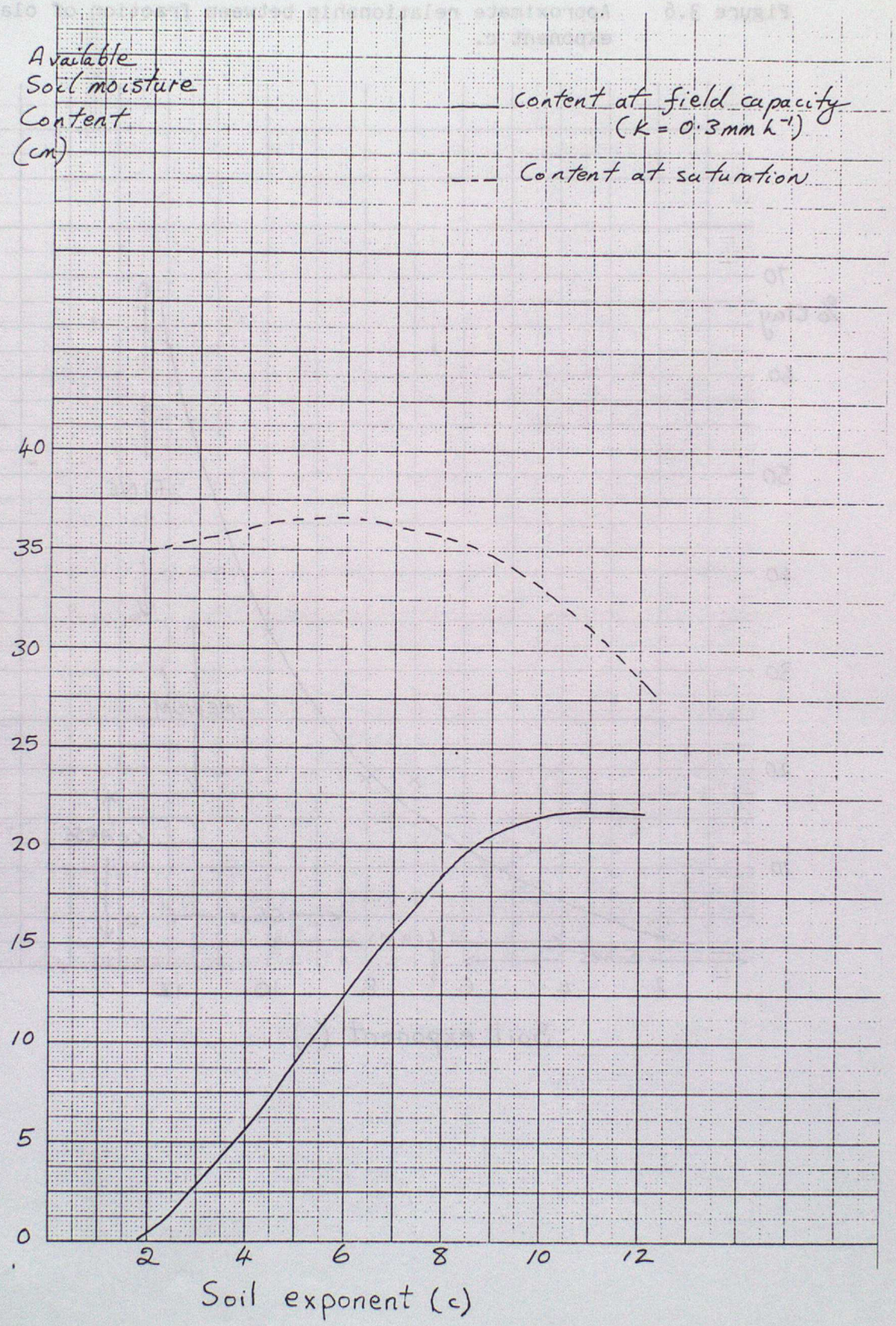

Figure 3.6 Approximate relationship between fraction of clay and exponent c.

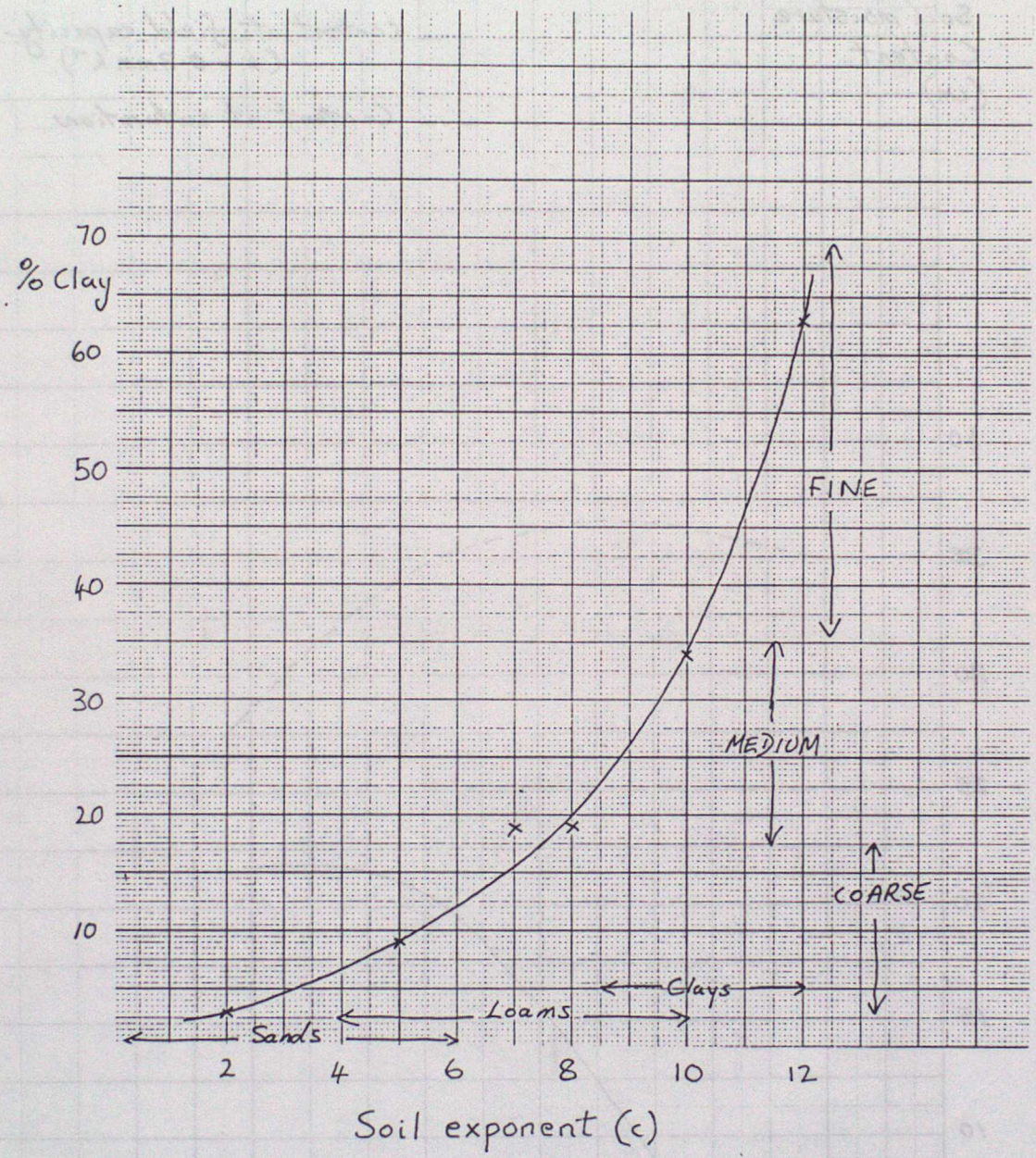

Figure 3.7 Gravitational drainage as a function of available soil moisture for three soil types.

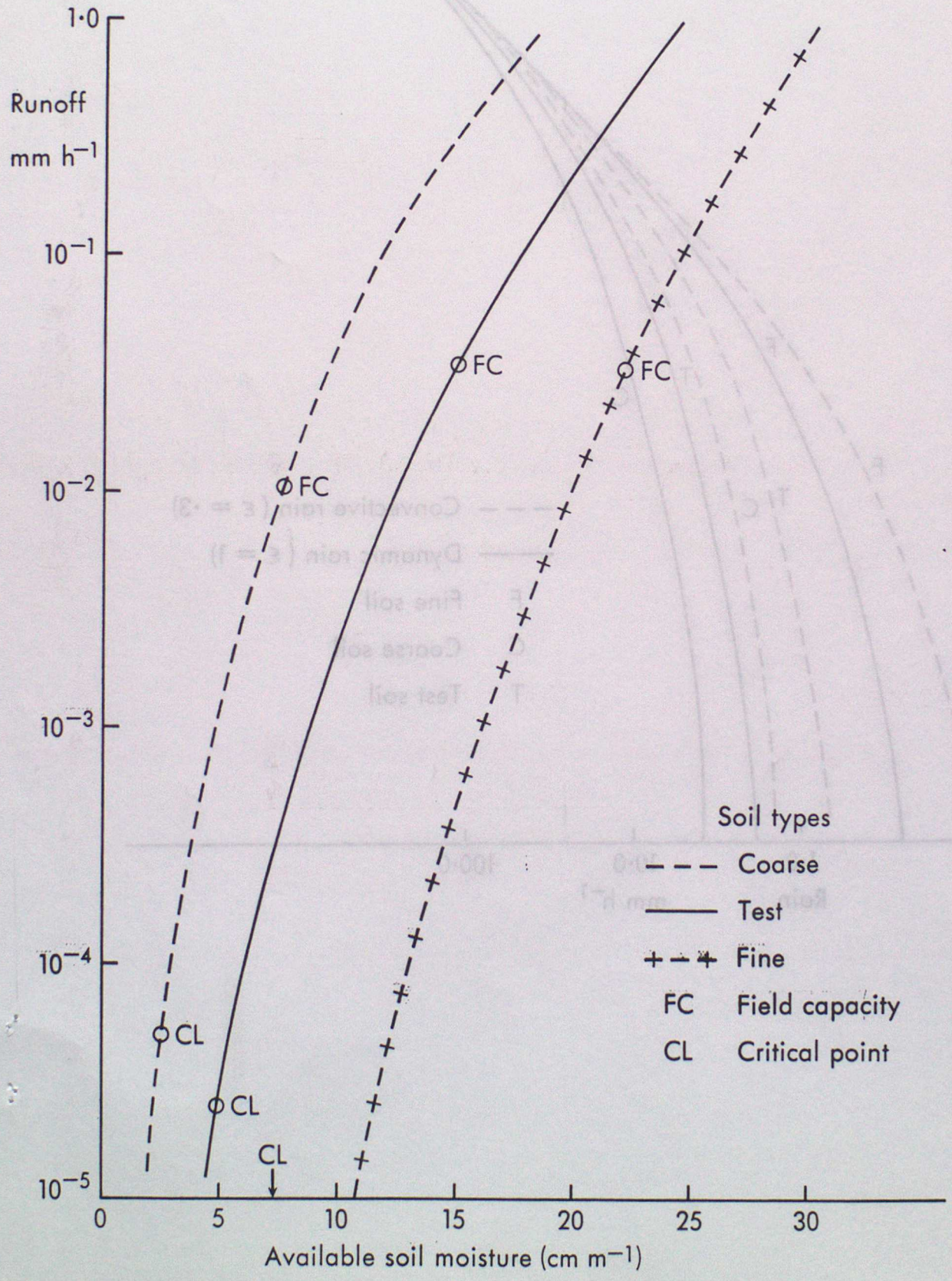

Figure 3.8 Surface runoff as a function of rainfall for three soil types.

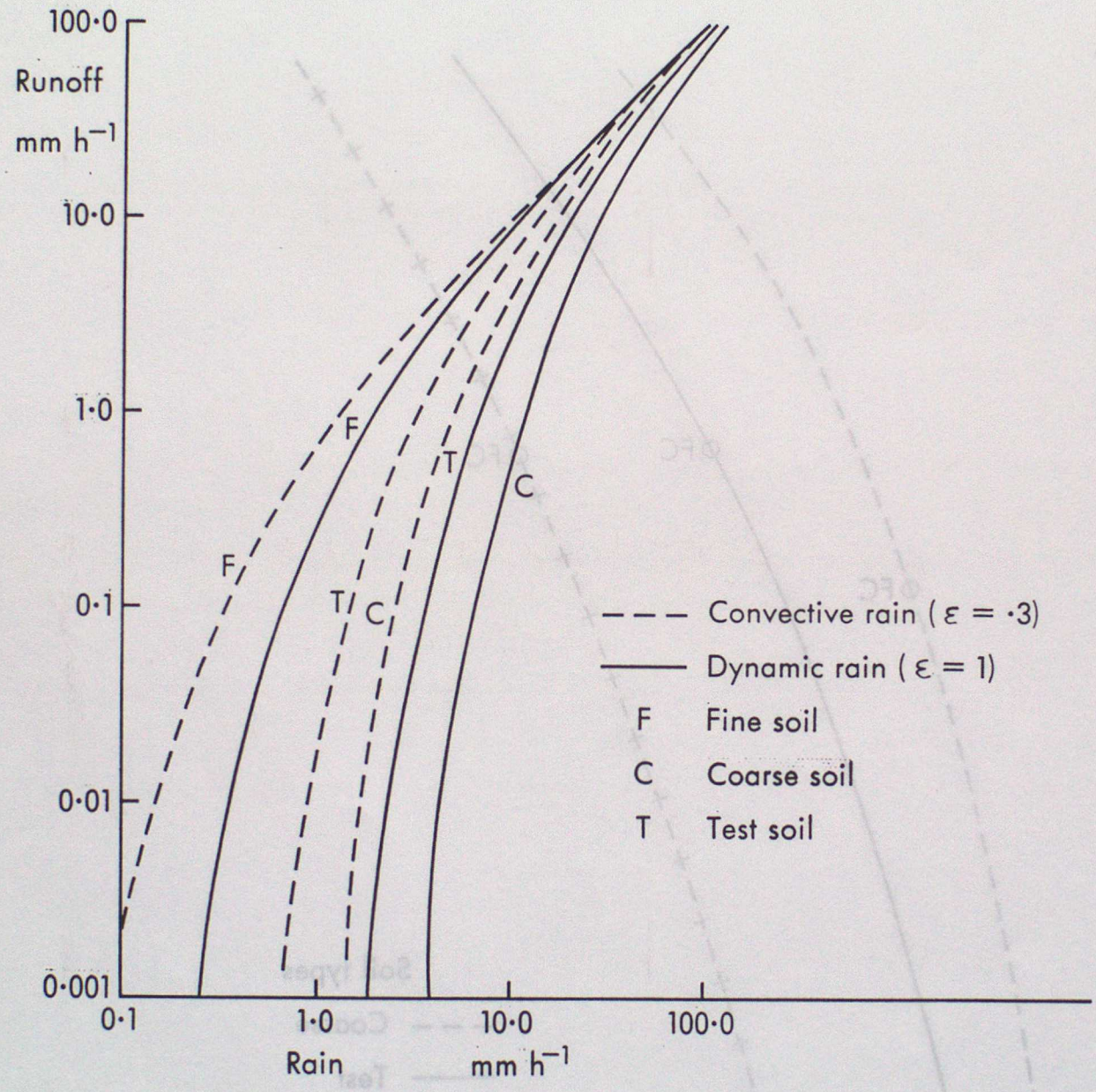

FIGURE 3.9 ANNUAL CYCLE SOUTHERN ENGLAND
COARSE SOIL. TALL GRASS

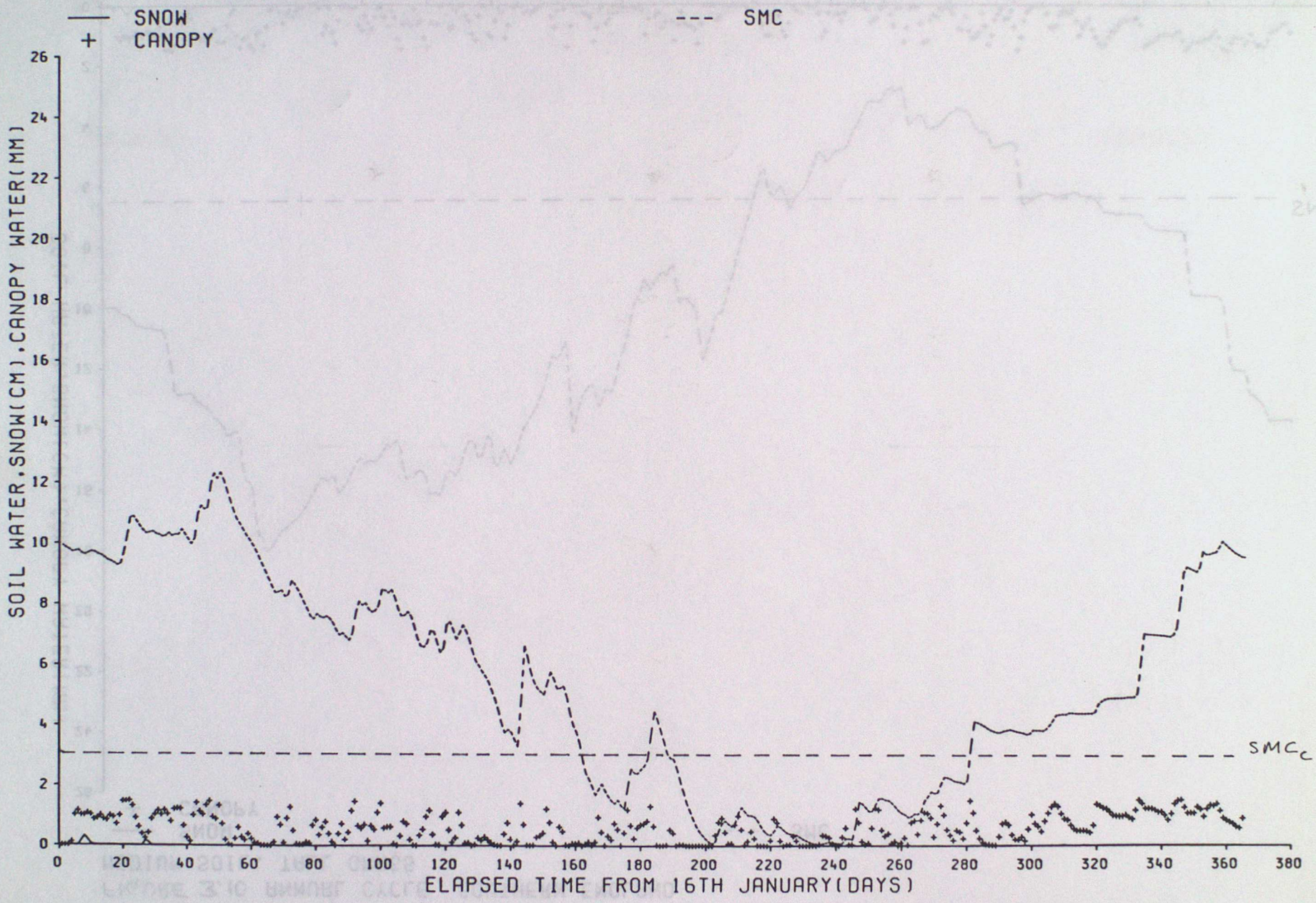

FIGURE 3.10 ANNUAL CYCLE SOUTHERN ENGLAND
MEDIUM SOIL. TALL GRASS

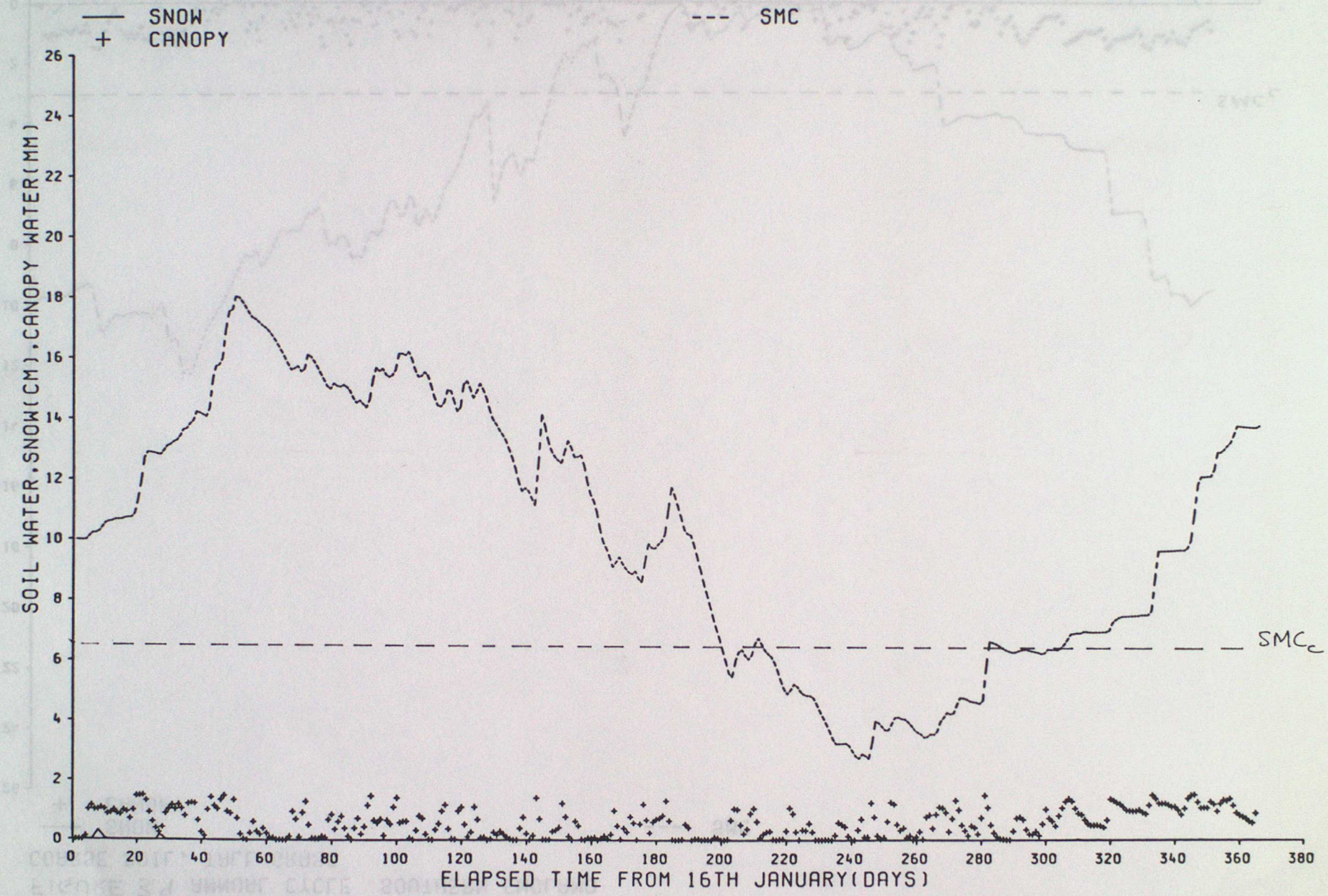

FIGURE 3.11 ANNUAL CYCLE SOUTHERN ENGLAND
FINE SOIL. TALL GRASS

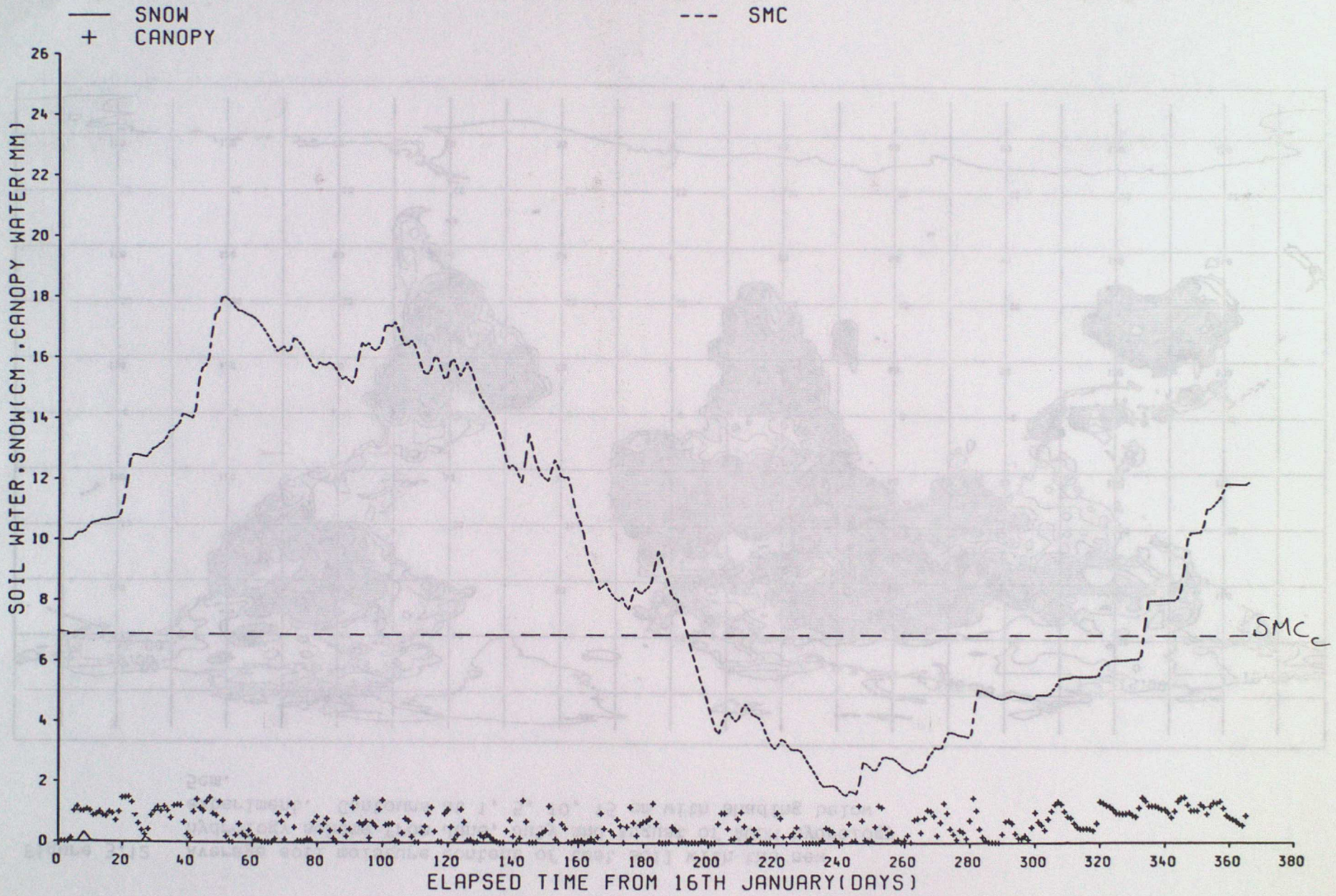

Figure 3.12 Average soil moisture content of test soil with the new hydrology scheme from June, July and August of AGCM hydrology experiment. Contours at 1, 5, 10, 15 cm with shading below 5cm.

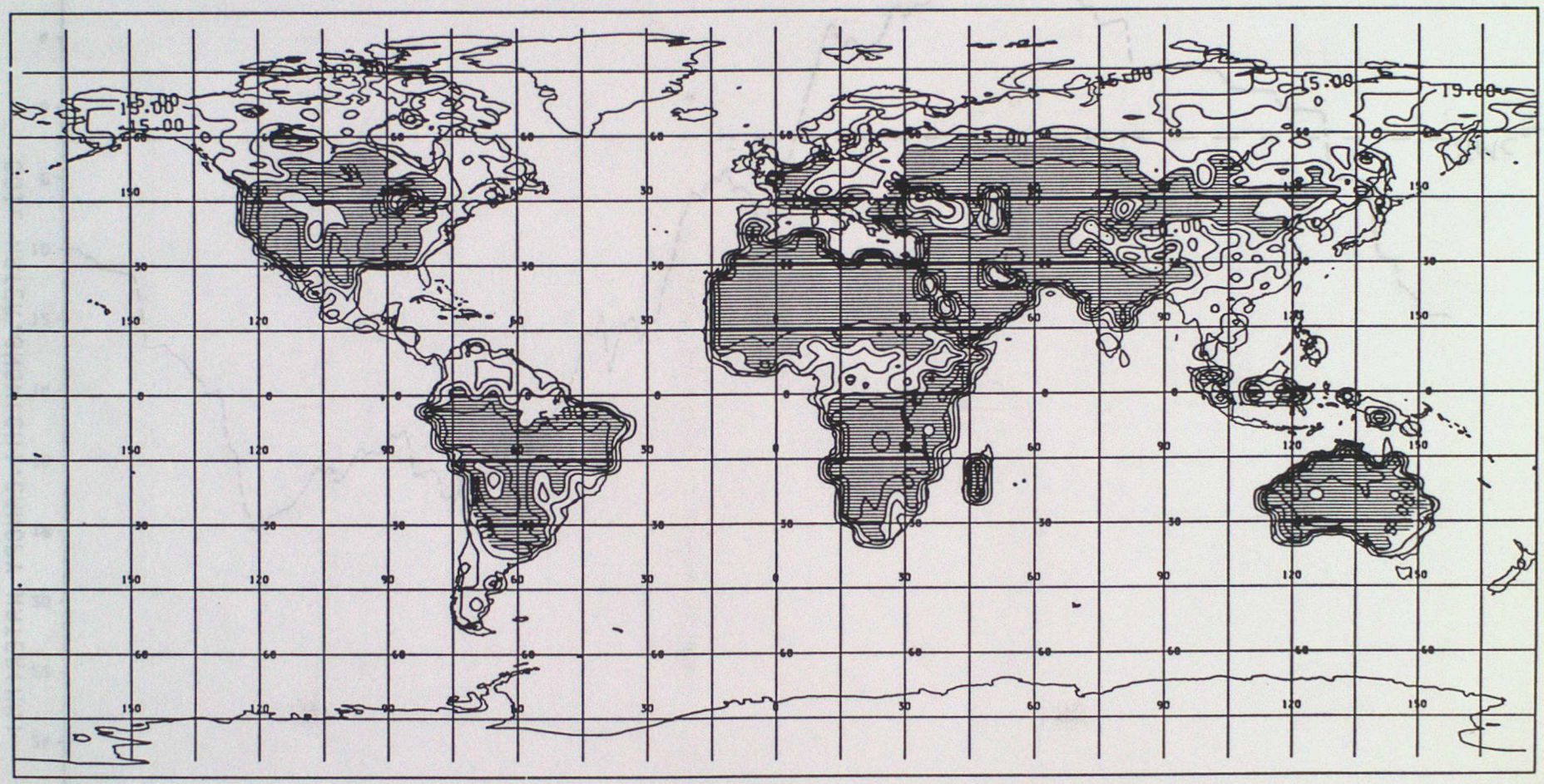

Figure 3.13 Average difference in soil moisture content between the new hydrology scheme AGCM experiment and a 15cm 'bucket' model control experiment for June, July and August. Dark shading denotes differences greater than 2cm and light shading differences less than -2cm.

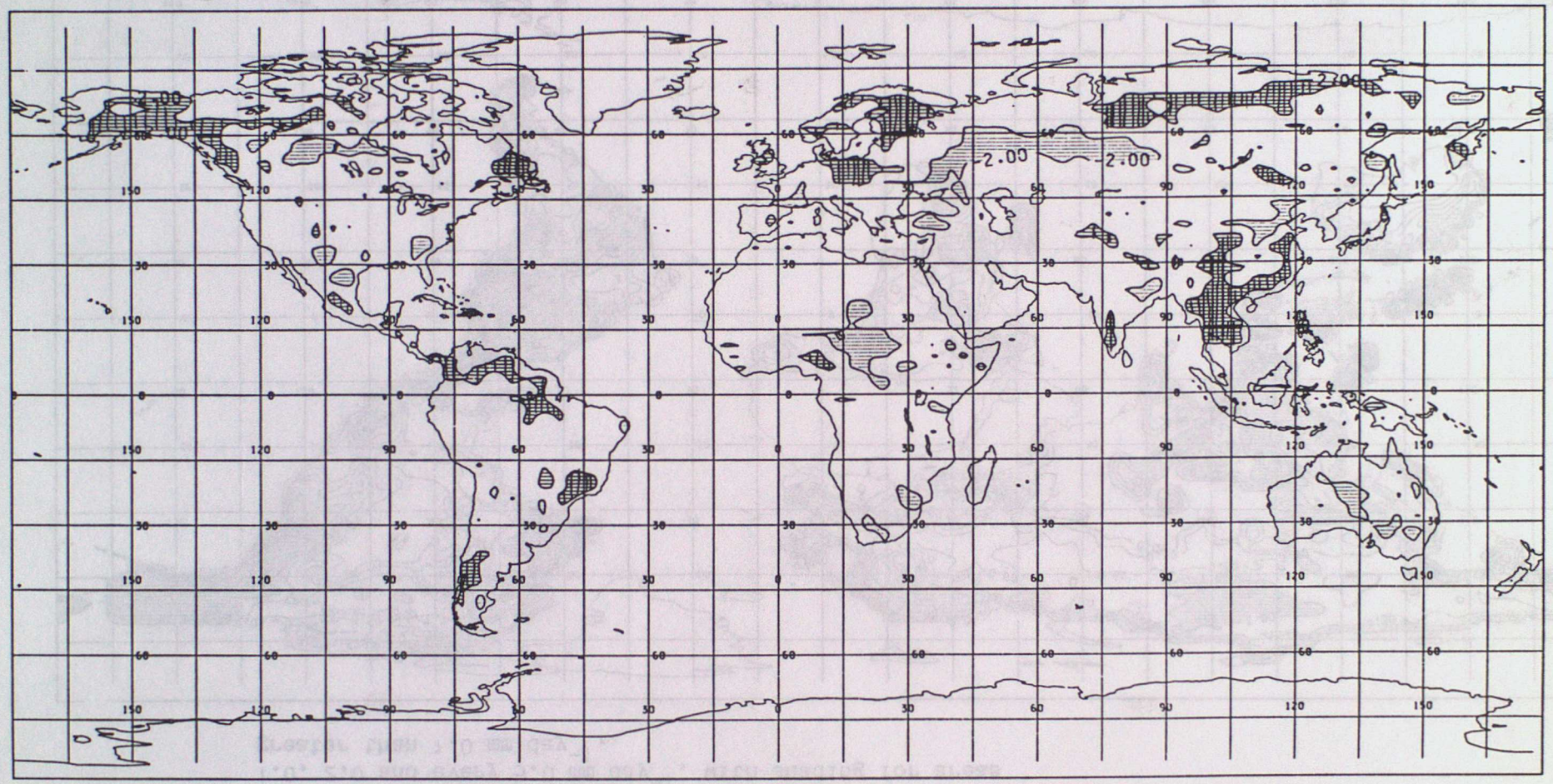

Figure 3.14 Total annual runoff for test soil with new hydrology scheme from AGCM hydrology experiment. Contours at 0.05, 0.1, 0.5, 1.0, 2.0 and every 5.0 mm day^{-1}, with shading for areas greater than 1.0 mm day^{-1}.

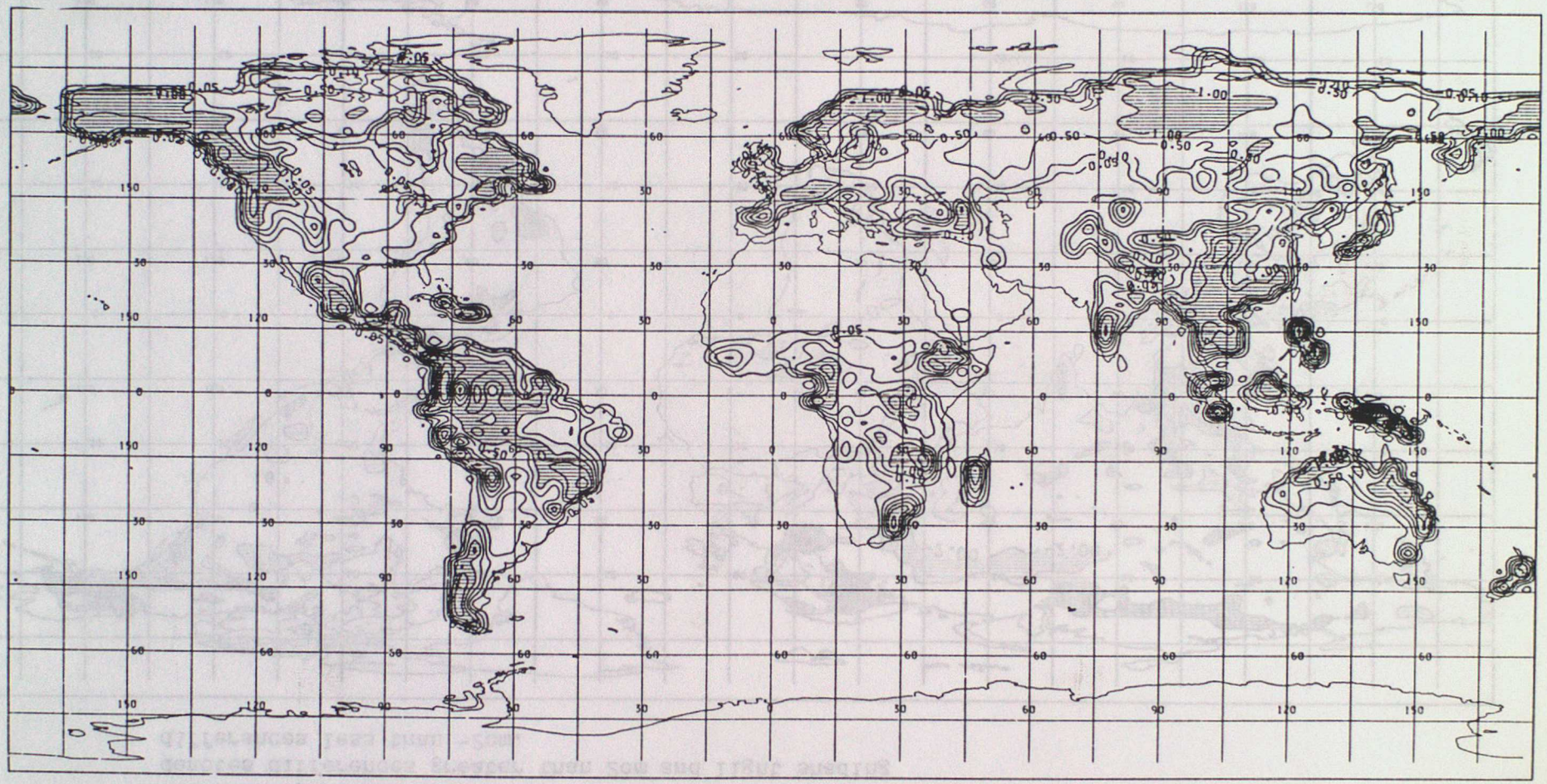

Figure 3.15 Total annual runoff from 15 cm 'bucket' model AGCM control experiment for the corresponding period to that in figure 3.14. Contours as in figure 3.14.

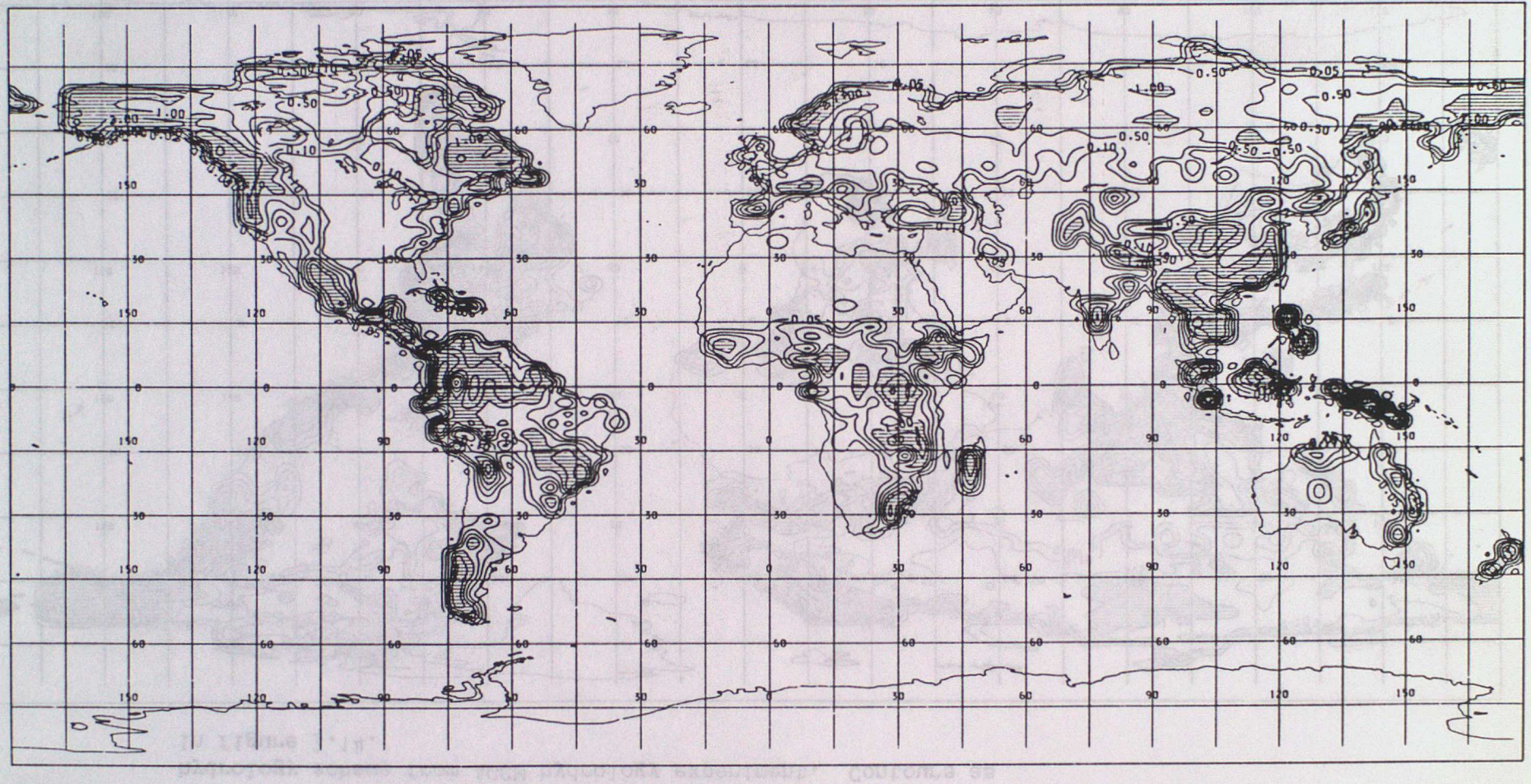

Figure 3.16 Total annual gravitational drainage for test soil with new hydrology scheme from AGCM hydrology experiment. Contours as in figure 3.14.

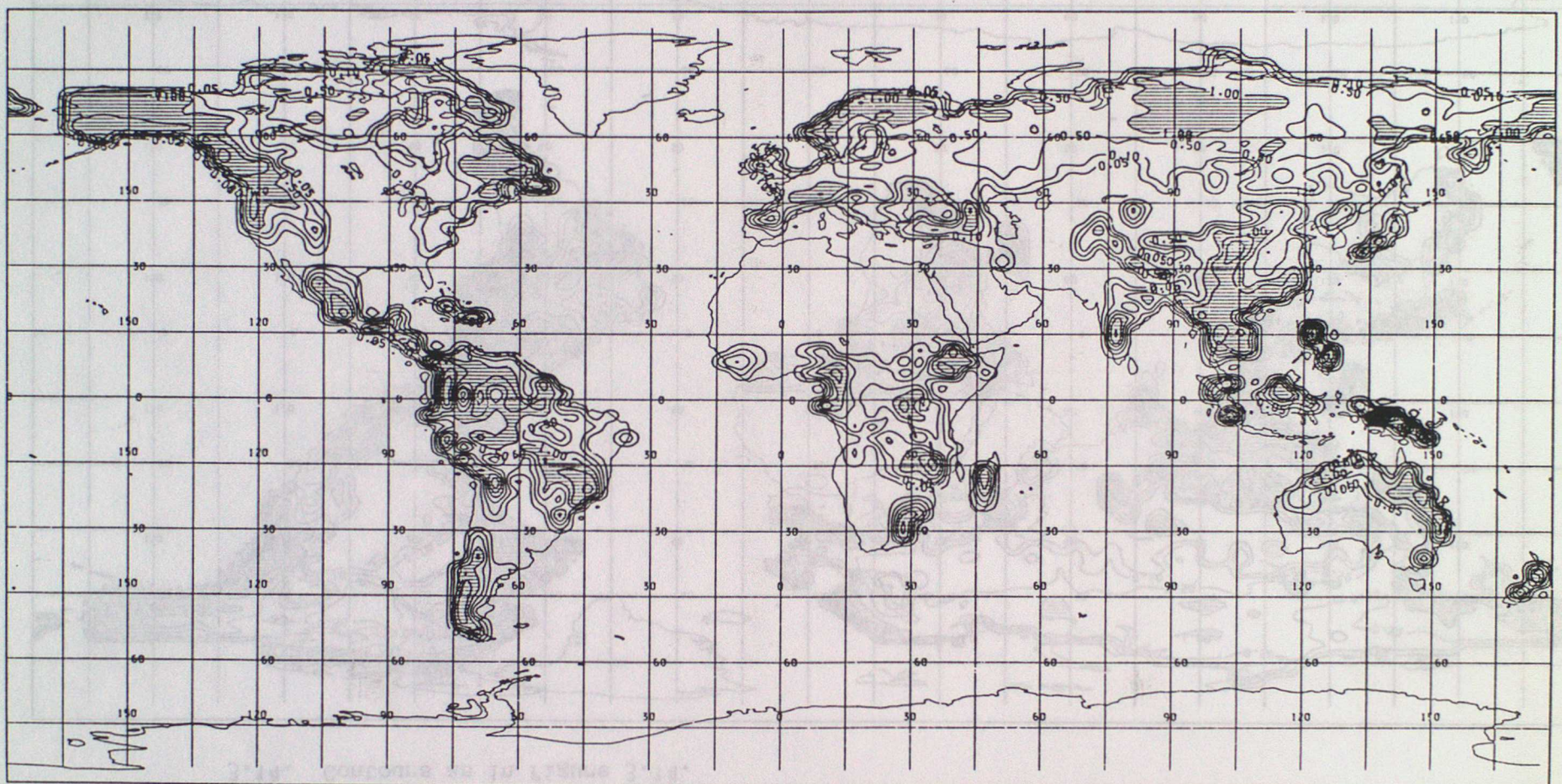

Figure 3.17 Total annual surface runoff for test soil with new hydrology scheme from AGCM hydrology experiment. Contours as in figure 3.14.

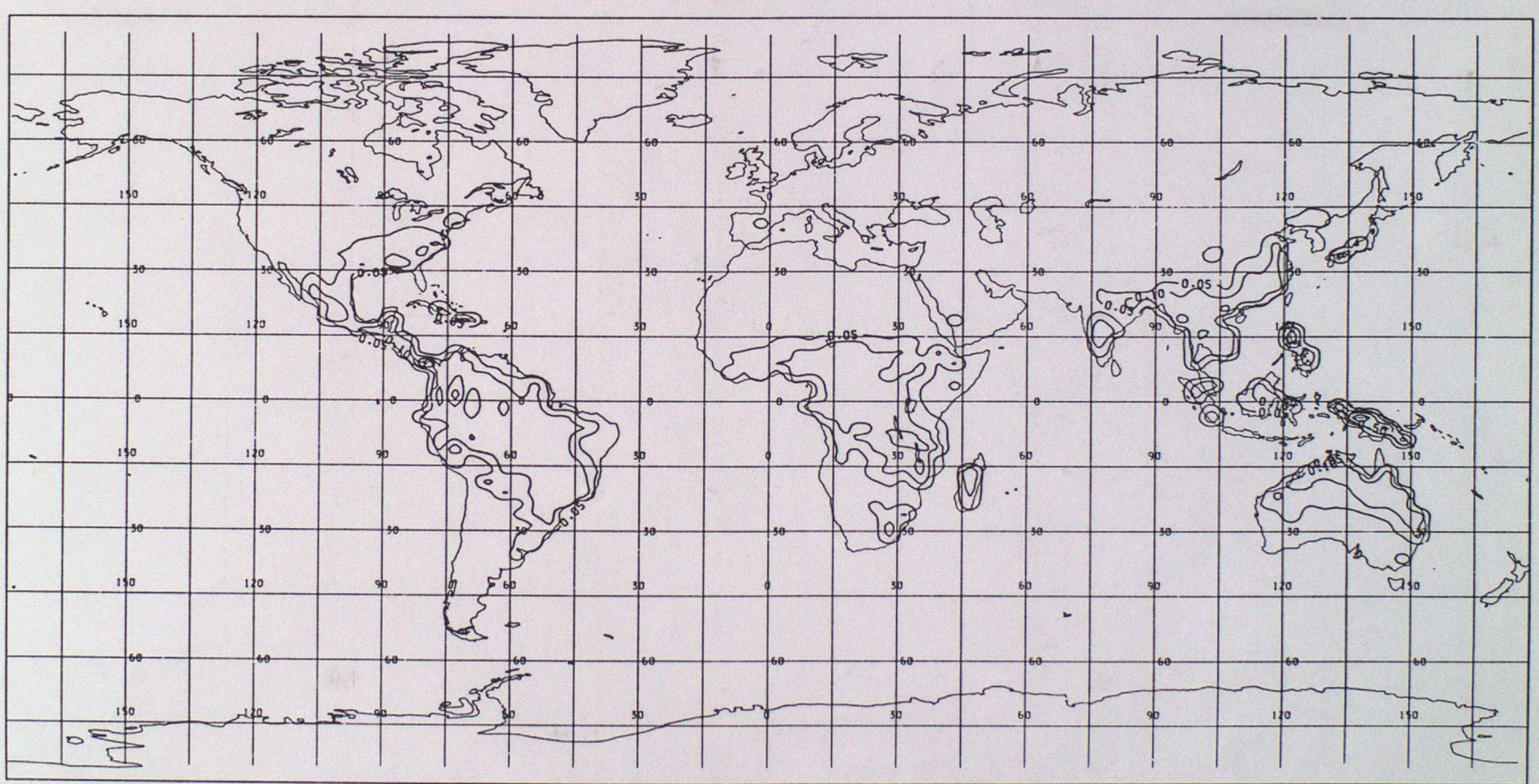

Figure 3.18 Average soil moisture content for coarse soil with new hydrology scheme from June, July and August of AGCM soil type experiment. Contours at 1, 5, 10, 15cm and shaded below 5cm.

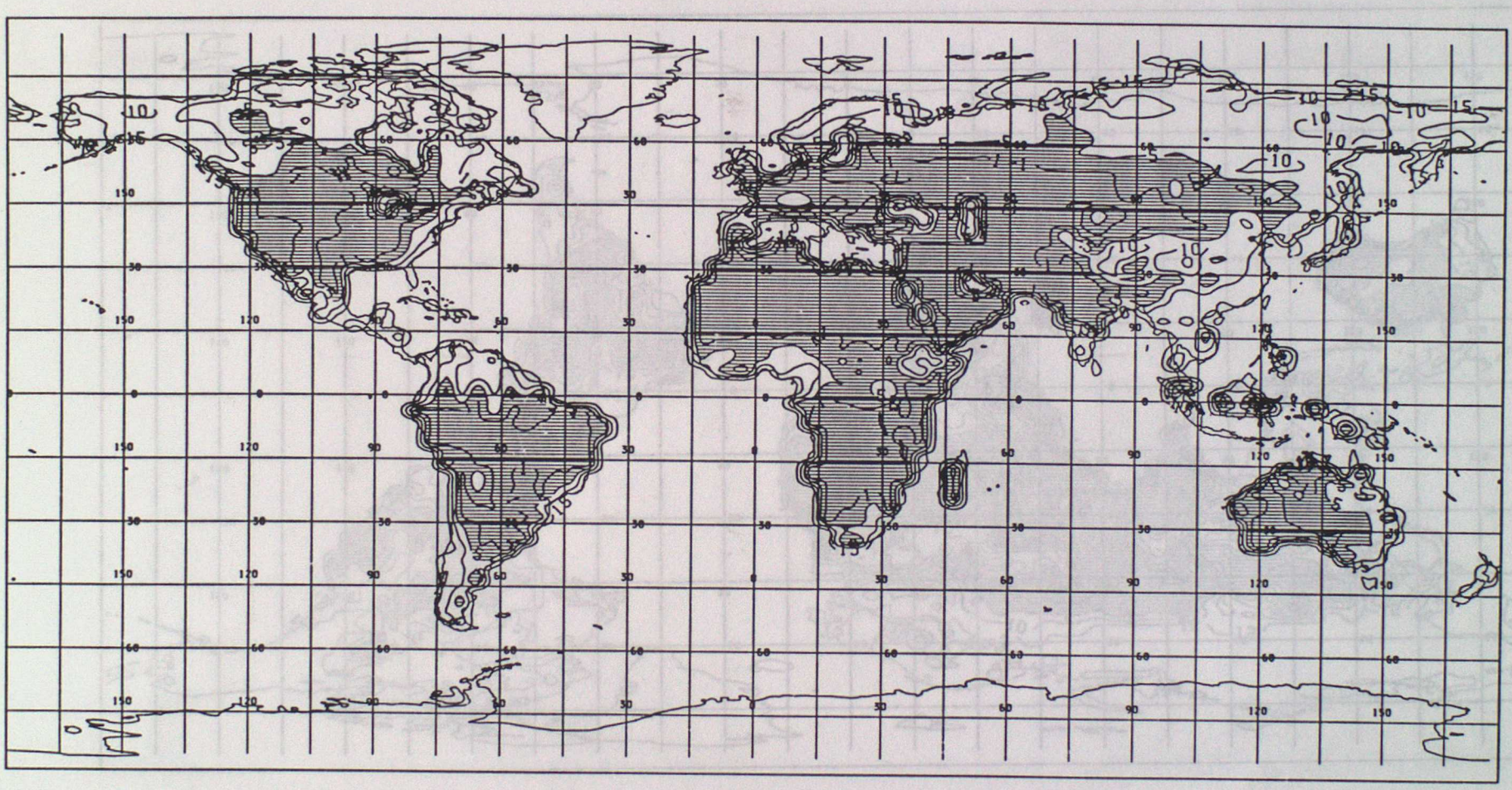

Figure 3.19 Average soil moisture content for fine soil with new hydrology scheme from June, July and August of AGCM soil type experiment. Contours as in figure 3.18.

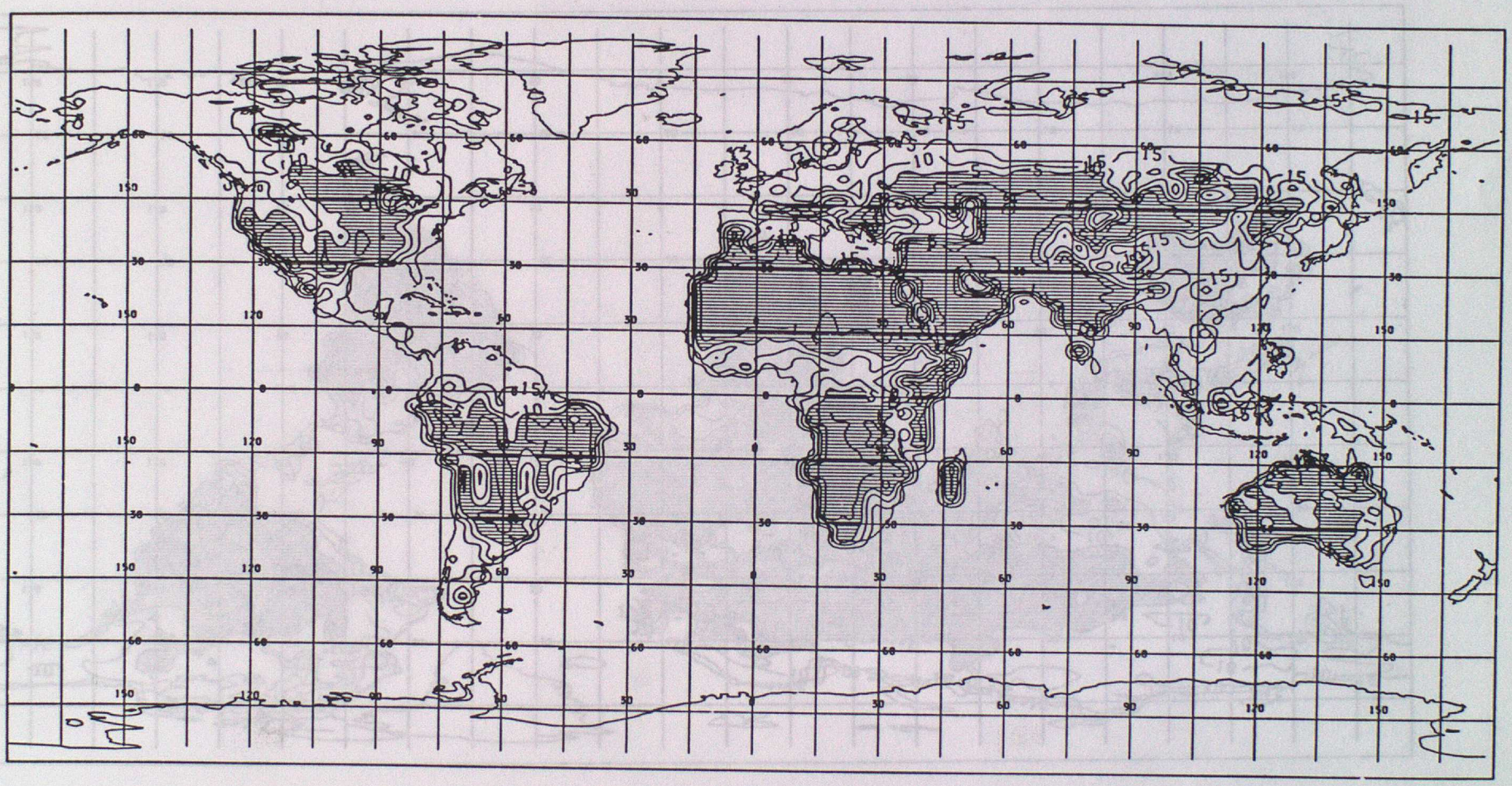

Figure 3.20 The ratio of average soil moisture content from figure 3.18 to the critical soil moisture content for coarse soil. Contours at 0.05, 0.5 and 0.95 with shading between 0.05 and 0.95.

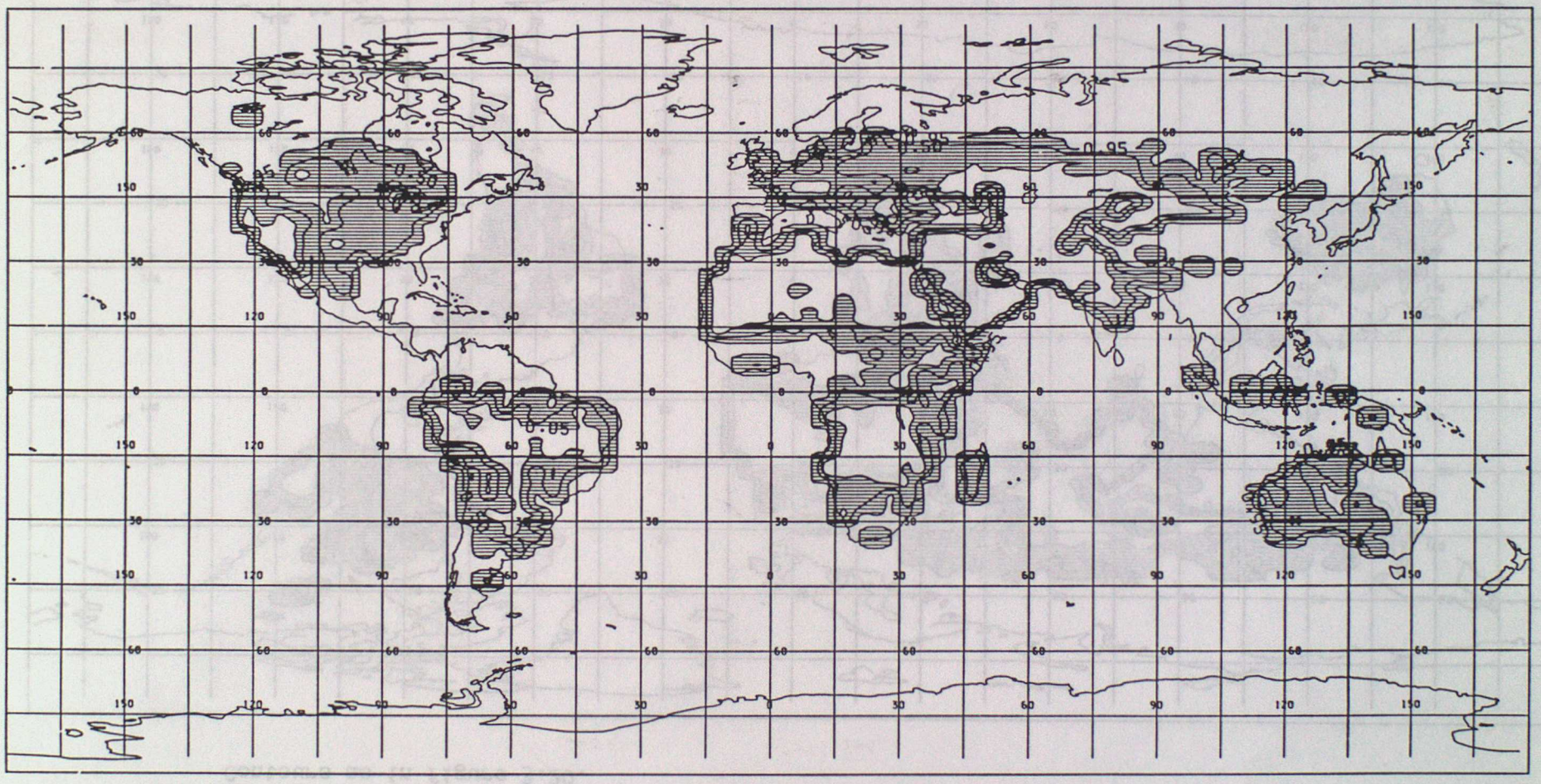

Figure 3.21 The ratio of average soil moisture content from figure 3.19 to the critical soil moisture content for fine soil. Contours as in figure 3.20.

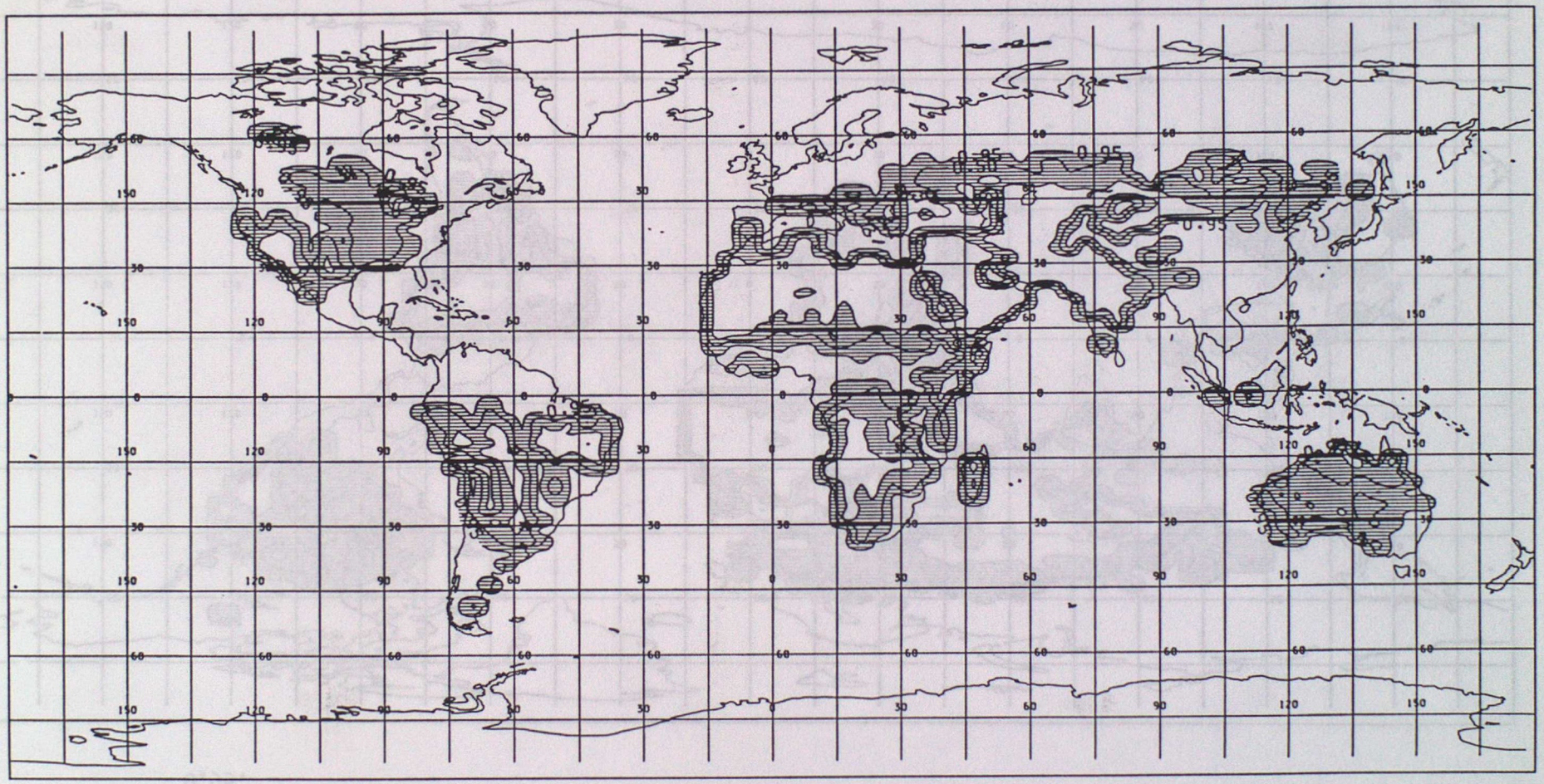

Figure 3.22 Average precipitation for coarse soil with new hydrology scheme from June, July and August of AGCM soil type experiment. Contours at 0.1, 1.0, 2.0, 5.0, 10.0 and every 20.0 mm day^{-1} with shading above 5.0 mm day^{-1}.

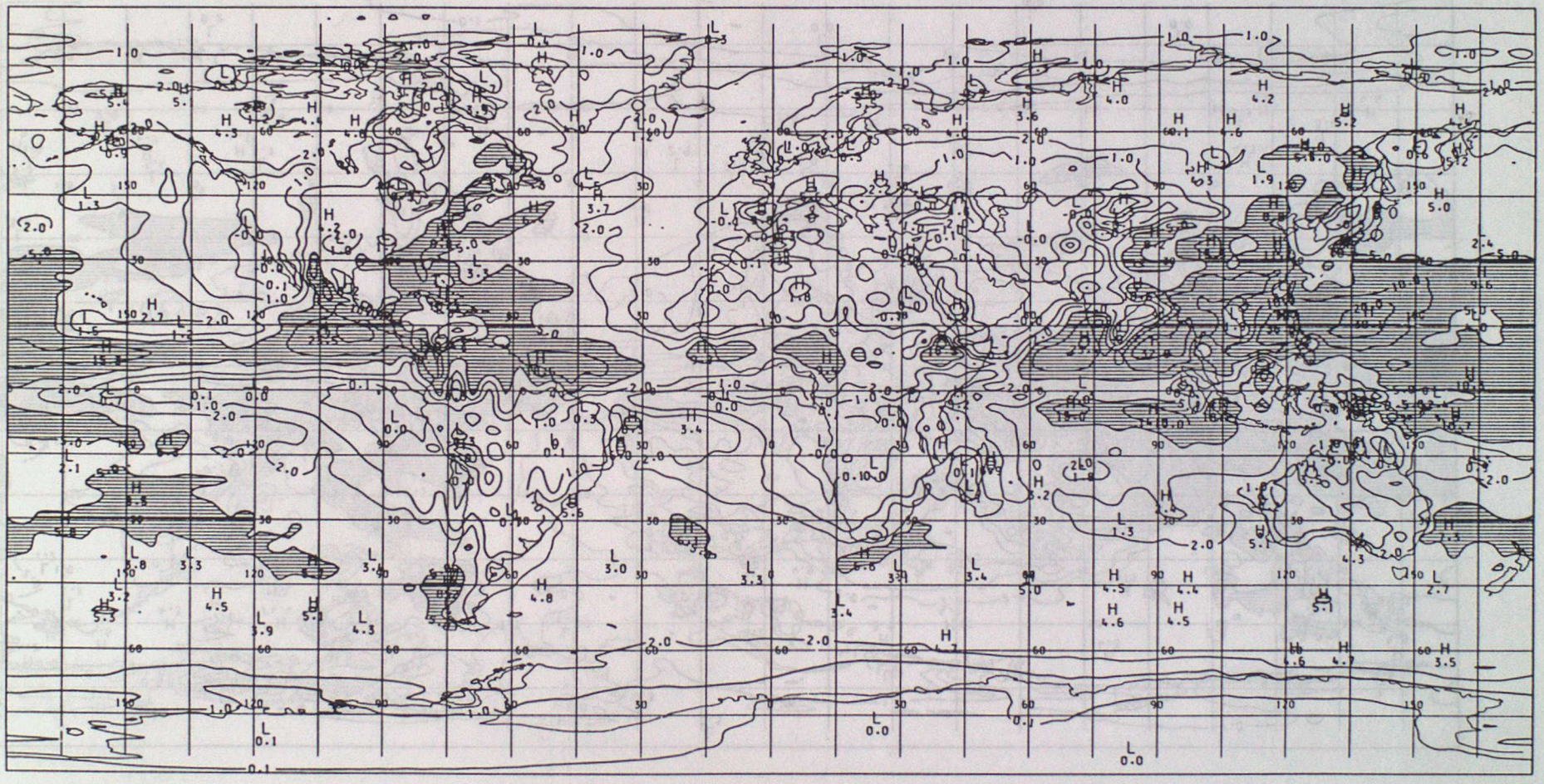

Figure 3.23 Average precipitation for fine soil with new hydrology scheme from June, July and August of AGCM soil type experiment. Contours as in figure 3.22.

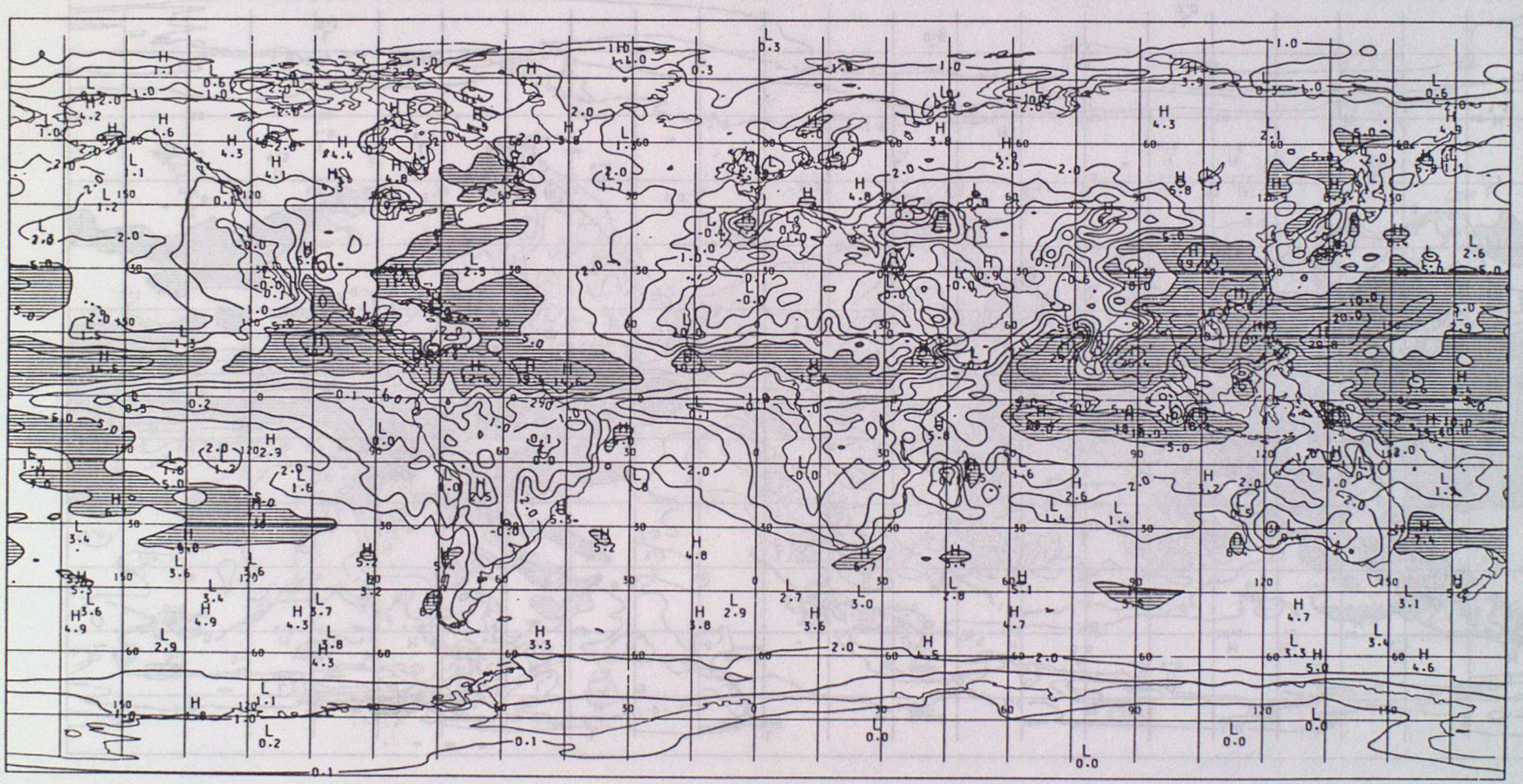

Figure 3.24 Average evaporation for coarse soil with new hydrology scheme from June, July and August of AGCM soil type experiment. Contours at 1.0 mmday^{-1} intervals and at 0.1 mmday^{-1} and shading above 5.0 mmday^{-1}.

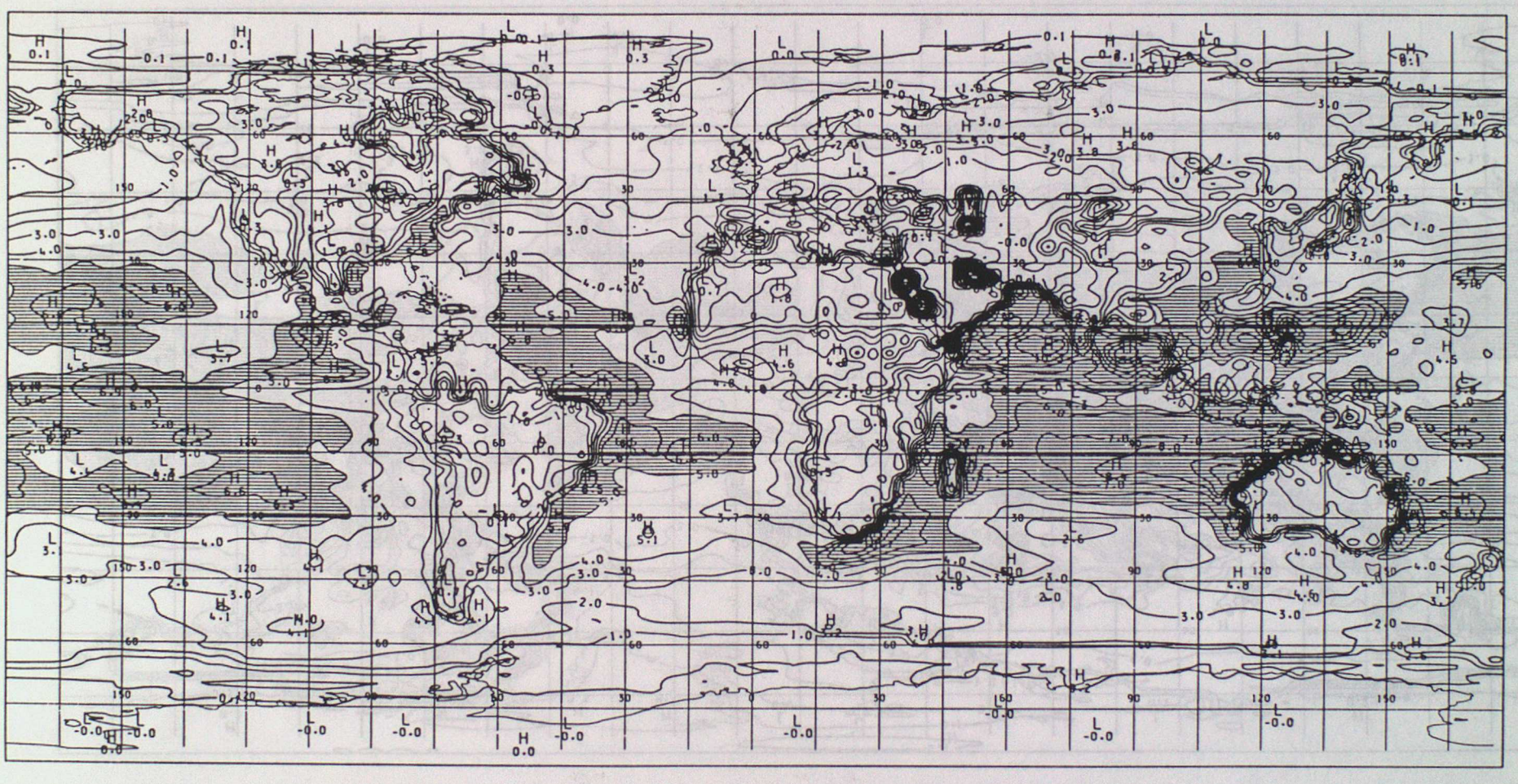

Figure 3.25 Average evaporation for fine soil with new hydrology scheme from June, July and August of AGCM soil type experiment. Contours as in figure 3.24.

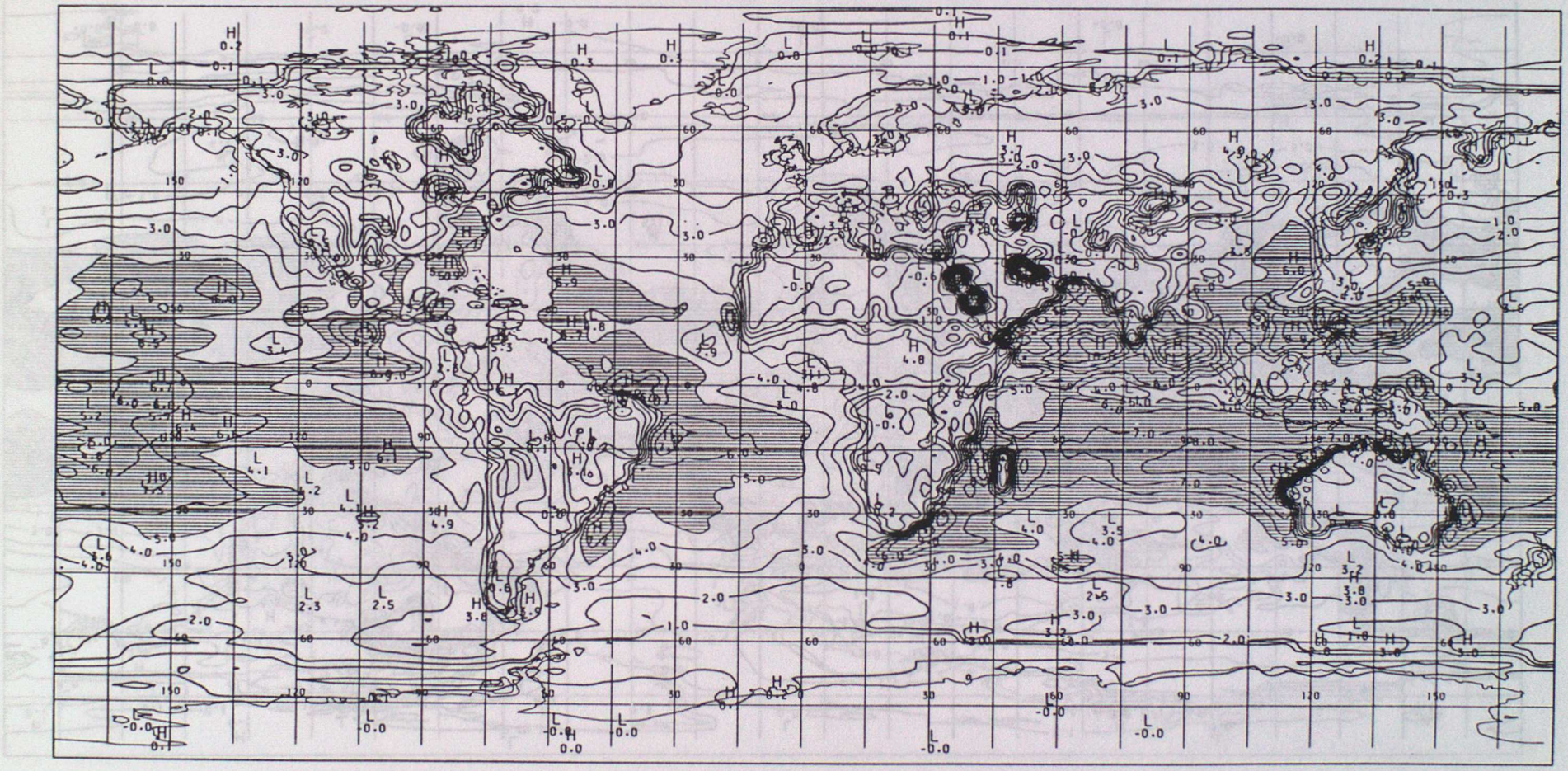

4. Evaporation and Interception

4.1 Introduction

4.2 Surface resistance and evaporation.

4.2.1 Introduction to evaporation.
4.2.2 AGCM study of the use of surface resistance.
4.2.3 Sensitivity of evaporation to surface resistance and root depth in a one dimensional model.

4.3 Canopy interception and evaporation.

4.3.1 The relevance of interception to land surface processes.
4.3.2 Physical aspects of interception.
4.3.3 Modelling interception.
4.3.4 Interception capacities.
4.3.5 A one dimensional model sensitivity study.

4.4 Conclusions

4.5 References

4. Evaporation and Interception

4.1 Introduction

Three aspects of the impact of vegetation on evaporation are considered in this section. Since large areas of the land surface are vegetated it is necessary to take into account the modification of land surface processes by plant canopies. More specifically, evaporation is considered as it is an important component of the surface thermal and moisture balance and of the hydrological cycle. The influence of evaporation on continental rainfall means that it is necessary to model it with some degree of accuracy.

Firstly the controlling influence of vegetation on moisture transport from the soil to the atmosphere by means of stomatal resistance is investigated in ODM and AGCM studies. Integrations are compared for surface resistances of 0 and 60 sm^{-1}. It is shown that inclusion of surface resistance leads to more realistic partitioning of available energy between latent and sensible heat fluxes.

Secondly the importance of root depth, which controls the maximum available soil moisture, is looked at briefly in the context of some ODM studies. This parameter would appear to be as important as surface resistance in controlling evaporation but it does so by varying the duration for which evaporation drops below the potential rate at low soil moisture concentrations.

Lastly interception of rainfall is modelled using a single canopy store. Although interception capacity is small compared to soil moisture capacity, its effect can be quite large as intercepted rainfall can evaporate at a surface resistance of 0 sm^{-1}. The effect is greatest when there are mainly frequent low intensity rainfall events. Soils remain drier than they would without a canopy store and evaporation increases. There is evidence from an ODM study that convective rainfall is enhanced.

4.2 Surface resistance and evaporation

4.2.1 Introduction to evaporation

As discussed in the introduction to section 4, evaporation from the earth's surface is controlled by the nature of the surface. Evaporation from bare ground depends on the ability of moisture to move within the soil matrix towards the surface under a controlling potential gradient. Where vegetation is present, moisture moves under the potential gradient to plant roots, whence it is drawn by suction forces to the leaves. Small variable openings in the leaves of plants, known as stomata, control the flow of water vapour between the leaf and the outside air. Such a control is commonly referred to as stomatal resistance by analogy with Ohm's law. The stomatal resistance can vary according to the type and state of vegetation, and external environmental factors, such as solar radiation. These are discussed by Feldlake and Boyer (1985) and Avissar et al (1985) for example. Stomatal resistances can be treated as resistances in parallel within a vegetation canopy. This is important as a canopy has a surface area greater than its projected area on the ground. The ratio of the leaf area to the projection is known as the leaf area index (LAI) and can be

used to adjust the stomatal resistance to the resistance of the canopy. More complex treatments may also include the differential demand on leaves at different levels within a canopy. (For example Sellers and Lockwood (1981)). In the following study the total canopy (or soil) resistance is referred to as surface resistance (r_s).

Between the surface and a reference atmospheric level there is an 'aerodynamic resistance' (r_a) which depends on atmospheric stability and wind velocity at the reference level.

From Slingo (1985) evaporation in the Meteorological Office AGCM is calculated as in Eq. 4.1

$$E_p = -\rho^* (q_{11} - q^*)/(r_a + r_s) \qquad (4.1)$$

where ρ^* and q^* are near surface values of air density and specific humidity respectively, q_{11} is the reference level humidity, and E_p is potential evaporation for vegetation freely supplied by water. r_a is defined in Eq. 4.2

$$r_a = 1/C_E \, |v_{11}| \qquad (4.2)$$

where C_E is the roughness dependent bulk transfer coefficient for moisture and v_{11} is the horizontal wind velocity at the lowest atmospheric level.

Originally, r_s was not included in the evaporation calculation and it had become apparent that evaporation rates were too high compared to the sensible heat flux.

A global value for r_s of 60 sm^{-1} was chosen based on data in Thompson et al (1982) and after some short AGCM studies (presented in section 4.2.2), was adopted in the Meteorological Office climate and forecast models. Different values of r_s were assigned to different vegetation types in ODM studies to test the sensitivity of evaporation to r_s (section 4.2.3).

Actual evaporation (E_a) is calculated from potential evaporation by assuming that at some critical value of soil moisture concentration, θ_c, matric forces exert a restraining influence on the flux of soil moisture to the surface or to plant roots. E_a is defined as

$$E_a = \beta E_p \qquad (4.3)$$

$$\text{where } \beta = \min [1, (\theta-\theta_w)/(\theta_c-\theta_w)] \qquad (4.4)$$

and $\theta \geq \theta_w$

The critical point at which soil moisture controls evaporation (θ_c) is not well defined and to some extent depends on the depth of soil layer being considered. For simplicity and in line with previous practice θ_c was defined as follows:

$$\theta_c = \theta_w + {}^1/_3 (\theta_f - \theta_w) \qquad (4.5)$$

It would be better in future work to allow r_s to vary with θ and calculate actual evaporation using Eq 4.1.

4.2.2 AGCM study of the use of surface resistance

A short AGCM experiment comparing r_s = 0 sm^{-1} with r_s = 60 sm^{-1} was carried out for an August simulation, in which recent developments in the treatment of radiation in the AGCM were included (Slingo and Wilderspin 1986). These included improved treatment of longwave infra-red radiation and radiative absorption characteristics of CO_2, variable cloud and new surface albedos which were used in subsequent AGCM experiments discussed in this report, based on work by Wilson and Henderson-Sellers (1985).

As might be expected evaporation decreased over most land areas, although not surprisingly most of the reduction occurred in areas which were already moist. Reductions of 1 mm day^{-1} were common (Figures 4.1 and 4.2). As a result, in these areas where evaporation decreased significantly the sensible heat flux increased locally by up to 30 Wm^{-2} (figures 4.3 and 4.4). There appears to be a feed back effect on precipitation which generally shows a decrease of up to 1 mm day^{-1} over the moist areas (figure 4.5) a change which can largely be traced to a reduction in convective precipitation. Soil moisture shows a variable response as does surface temperature (T*) although there are significant areas where T* increased by at least 1K (Figure 4.6).

For central Europe, which is moist during this integration, the Bowen ratio ($H/_{LE}$) changes from 0.09 to 0.23 when r_s is increased to 60 sm^{-1}. A typical value for the Bowen ratio quoted by Rowntree (1983) is 0.25. As r_s = 60 sm^{-1} is a fairly typical average day time value for surface resistance (Thompson et al (1982)) and its inclusion gave a more realistic Bowen ratio, it was decided to include it in the 11 level AGCM over all land areas. Surface resistance was also included in the operational forecast model. Further studies of the sensitivity of evaporation to r_s were carried out in the ODM as described in the next section.

4.2.3 Sensitivity of evaporation to surface resistance and root depth in a one-dimensional model

The ODM discussed in section 2 was used to simulate the climate over 1 annual cycle in Southern England for 3 different surface resistances (0sm^{-1}, 60 sm^{-1}, 120 sm^{-1}). In these experiments canopy interception and evaporation as described in section 4.3 were also included. Using a medium soil and long grass (parameters in tables 5.2 and 5.3) we find that for the year evaporation and the sensible heat flux vary largely as expected. Results are quoted in table 4.1.

Table 4.1

Variation of various ODM parameters with surface resistance over one annual cycle of a Southern England simulation.

Surface resistance (sm^{-1})	0.0	60.0	120.0
Ave. latent heat flux (Wm^{-2})	45.93	42.00	38.32
Ave. sensible heat flux (Wm^{-2})	8.61	12.75	17.73
Bowen Ratio	0.19	0.30	0.46
Ave. net radiation at the top of the atmosphere (Wm^{-2})	-72.84	-71.74	-69.52

Ave. net radiation at the surface (Wm^{-2})	54.65	54.86	56.17
Ave. soil moisture content (cm)	8.30	10.20	11.87
Ave. canopy content (mm)	0.62	0.57	0.55
Total precipitation (mm)	693.8	673.6	662.2
Ave. surface temperature (°C)	8.30	8.56	8.88

Given that these are annual mean values results are consistent with those noted for Europe in the AGCM integration. $r_s = 60 sm^{-1}$ gives a Bowen ratio slightly larger than that quoted by Rowntree (1983). A 5% change in latent heat flux results from changing r_s by 30 sm^{-1}, for this location and land type. It can be noted that there is a direct relationship between the Bowen ratio and surface temperature and an inverse relationship with rainfall. Differences in the latter do not appear to be as great as were noted in the AGCM integration, but as those were for a Northern Hemisphere summer integration, when convection is important, we might expect a lower difference in this model. Also here we are considering a local area and relatively strong advection from an external climate which is deemed to be unchanged.

It is interesting to note that soil moisture increases with r_s, despite the reduction in rainfall with r_s. Clearly reduced evaporation allows soils to remain moist over a longer period. However there is a contrary effect which occurs once the critical soil moisture concentration is reached. The low resistance, high evaporation case can reach the critical point more quickly, and from that point evaporation rates decrease below the potential rate whereas the high resistance, lower evaporation case may not even reach the critical point. There are therefore two processes which affect evaporation over a long period of time and may eventually cancel each other. Evaporation therefore depends not only on r_s but also on the root depth and temporal rainfall sequence.

This effect is seen graphically in figures 4.7 and 4.8 comparing soil moisture content for $r_s = 0.0$ and $r_s = 120$ sm^{-1} cases respectively. For the second case the soil moisture content barely falls below the critical point and potential evaporation is maintained throughout. The effect on surface temperatures reveals some other important processes (Figures 4.9 and 4.10). When $r_s = 120$ sm^{-1} the annual temperature wave follows solar radiation quite closely, but when $r_s = 0$, the highest daily means occur towards the end of the summer, when the soil has dried out, whereas temperatures are suppressed in the spring due to the higher evaporation rates. It is interesting also to note that daily minima vary little between integrations, but that maxima are reduced typically by 5°C in spring and early summer for the zero resistance case. Thus varying r_s not only changes average values but affects the diurnal and annual cycle.

Further integrations were carried out to compare the effect of root depth on evaporation for $r_s = 60$ sm^{-1}. Results are given in table 4.2.

Table 4.2

Variation of various ODM parameters with root depth over one annual cycle of a Southern England simulation.

Root depth (m)	0.1	0.5	1.0
Ave. latent heat flux (Wm^{-2})	29.41	36.92	42.00
Ave. sensible heat flux (Wm^{-2})	27.34	17.74	12.75
Bowen Ratio	0.93	0.48	0.30
Ave. net radiation at the top of the atmosphere (Wm^{-2})	-67.06	-70.58	-71.74
Ave. net radiation at surface (Wm^{-2})	56.87	54.77	54.86
Ave. soil moisture content	1.06	5.32	10.20
Ave. canopy content (mm)	0.55	0.56	0.57
Total precipitation (mm)	652.6	662.2	673.6
Ave. surface temperature (°C)	9.50	8.94	8.56

Root depth affects soil moisture capacity directly and thereby affects evaporation. Taking r_s = 60 sm^{-1} and root depth as 1 m, we see that doubling r_s has virtually the same effect on the Bowen ratio as halving the root depth with r_s = $60sm^{-1}$. As with surface resistance, root depth affects the distribution of evaporation throughout the year, the important parameter being the time at which soil moisture dries below the critical soil moisture concentration. The shallower the root depth, the earlier this occurs each year. Comparing soil moisture contents in figures 4.11 and 4.12 for 50 cm and 100 cm root depths respectively and critical points (SMC_c) of 3.75 and 6.5 cm respectively, we see that soil moisture is substantially less than the critical point for 120 and 65 days respectively. However figure 4.13 shows that when the root depth is only 10 cm (SMC_c = 0.65 cm), $\theta < \theta_c$ for only 90 days and then the dry periods are not contiguous. However they occur more centrally about the time of maximum radiation and so affect evaporation more strongly. Thus the effect of varying root depth is not simple and annual averages hide a good deal of complex behaviour.

4.3 Canopy interception and evaporation

4.3.1 The relevance of interception to land surface processes

In highly vegetated areas, notably forested regions of mid latitudes, interception of rainfall by a vegetation canopy plays an important part in the soil moisture budget, affecting both runoff and evaporation. The effect is greatest where rainfall is frequent but of low intensity. The net result is that soils are drier than they would be in the absence of vegetation, and rainfall is considered to be 'lost' to the soil. Runoff volumes are generally considered to be reduced which can have important consequences for water resources (Reifsnyder (1982)). However, observations in this regard have shown that the effect on runoff of removing vegetation is of variable magnitude. Baker (1986) quotes increases in water yield of 15-45% in the first year following deforestation. Hewlett and Bosch (1984) report a detectable but unimportant increase in runoff from individual high intensity storms. From an atmospheric point of view, canopy interception allows rainfall to re-evaporate more easily as it can do so at the potential rate with a

surface resistance of zero. In this section some physical aspects of interception are discussed, a simple parametrization is proposed and results from a ODM study are presented.

4.3.2 Physical aspects of interception

A vegetation canopy is a complex structure of small elements (leaves) and branches and stems. Canopy density may have more than one maximum in the vertical. The canopy is not static and may change its characteristics with wind flow and rainfall and from season to season. It will not be uniform spatially especially over an area the size of an AGCM grid square.

Rowe and Hendrix (1951) give a useful discussion on the processes involved in interception and these are summarised as follows. Rainfall is intercepted by vegetation surfaces; a certain proportion however reaches the ground directly. The uppermost parts of the canopy intercept more rainfall than the lower parts initially; however as the upper surfaces become saturated, water begins to drip from leaves, some onto lower leaves and some reaching the ground. Eventually if rainfall is heavy enough and persists long enough the whole canopy becomes saturated. Branches and stems can play an important part in storing moisture especially in tropical forests (Herwitz (1985)). Water may also reach the ground as stem flow, although this is generally less important than leaf drip (4% of precipitation compared to 84% for throughfall (Rowe and Hendrix (1951)). The amount of water stored on vegetation depends not only on the so called interception capacity (which we might relate to the surface area) but on external factors such as rainfall rate, wind velocity and evaporation rate.

After rainfall has ceased, leaf drip and stem flow may continue for some time although the exact point of cessation is not well defined (Rutter et al (1971)). In this section we take throughfall to be the sum of leaf drip, stem flow and precipitation reaching the ground directly.

Once rainfall has ceased, evaporation removes intercepted rainfall within 6 to 12 hours (Rutter et al (1971)). The upper parts of the canopy dry first and as the leaves dry, transpiration begins again. The partitioning of energy for evaporation between wet and dry parts of the canopy has been studied by Hancock et al (1983) who showed that there is a consistent lowering of the water source within a forest canopy and an increase in transport resistance as the canopy dries.

As a post script, Morton (1984) has questioned the conclusions generally made concerning canopy interception and evaporation and in particular the applicability of the Ohms Law analogue. He also suggests that it is possible for vegetation to absorb intercepted water and convey it to the soil, although he admits that evidence for this is not conclusive.

4.3.3 Modelling interception

Sellers and Lockwood (1981) have used a multilayer vegetation model to study the effect of interception on a small catchment water balance and Massman (1980) has investigated a general equation for interception and evaporation for a single layer canopy. The former approach is probably unnecessarily complex for an AGCM application and the latter requires specification of some empirical constants. The simpler Rutter model

(Rutter et al (1971)) compares favourably with the multilayer model although it has shortcomings. The approach adopted here is to use a relatively simple model and to test the sensitivity of the atmosphere to that model.

Let S_m be the maximum canopy storage or canopy capacity and S be the amount stored at any one time. For a homogeneous canopy we have

$$\frac{dS}{dt} = I_s - D_r - E_c \tag{4.5}$$

where I_s is the rate of interception, D_r the drainage rate and E_c the rate of wet canopy evaporation.

$$I_s = \Lambda R \tag{4.6}$$

where R is the rainfall rate at the top of the canopy and Λ is the probability of rainfall being intercepted. Throughfall can then be defined as

$$T_f = (1 - \Lambda)R + D_r \tag{4.7}$$

Rutter et al (1971) suggest that evaporation from wet and dry portions of the canopy can be treated separately. For a local canopy, Hancock et al (1983) have shown that some interaction should be included; however, over a large area it is probably reasonable to treat the wet and dry portions separately.

Then we define canopy evaporation as follows

$$E_c = (S/S_m)E_p \quad (r_s=0) \tag{4.8}$$

where E_p is potential evaporation.

Dry canopy evaporation is then given by E_d where

$$E_d = (1 - S/S_m)\, \beta E_p \quad (r_s \neq 0) \tag{4.9}$$

To describe the process of filling the interception store, further simplifying assumptions are made, ie $\Lambda \to 1$ and locally $D_r = R$ where the canopy is full and $D_r = 0$ when the canopy is empty, thus we assume that

$$D_r = (S/S_m)R \tag{4.10}$$

Eq. 4.10 is reported by Massman (1980) to be extensively used although he notes that in the model the early buildup of water is too low and the drip rate is zero once rainfall has ceased. From our viewpoint this is no bad thing as spatial rainfall variations will probably keep parts of the canopy drier for longer. We have not explicitly studied the effect of rainfall spatial variability in the context of canopy interception, since it is complicated by unknown factors such as storm movement. Dickinson (1984) has used

$$D_r = \begin{cases} 0 & S < S_m \\ I_s & S \geq S_m \end{cases} \tag{4.11}$$

Combining Eq. 4.5 with Eqs. 4.6, 4.7 and 4.10 and setting $\Lambda = 1$ gives

$$\frac{dS}{dt} = R(1 - S/S_m) - (S/S_m)E_p \quad (r_s = 0) \qquad (4.12)$$

Eq. 4.12 gives the time variation of S over the area where vegetation is homogeneous. In modelling the land surface it can be assumed that a proportion ν of the grid square will be vegetated and the remainder will have bare soil. Then, for a grid box the total throughfall is defined in Eqs. 4.13 and 4.14

$$T_f = (1- \nu)R + \nu(S/S_m)R \qquad (4.13)$$

$$= R(1 - \nu (1 - S/S_m)) \qquad (4.14)$$

Total evaporation E is given by

$$E = \nu (E_c + E_d) + (1- \nu)E_s \qquad (4.15)$$

$$= \nu (S/S_m)E_p(r_s=0) + \nu(1-S/S_m)\, \beta E_p(r_s = r_{sc}) + (1- \nu)\beta E_p(r_s=r_{ss}) \qquad (4.16)$$

Where soil resistance (r_{ss}) and vegetation resistance (r_{sc}) are not distinguished for evapotranspiration, we set $r_{ss} = r_{sc}$ and then have

$$E = \nu(S/S_m)E_p(r_s=0) + (1 - \nu S/S_m)\, \beta E_p(r_s=r_{sc}) \qquad (4.17)$$

Evaporation is subject to there being moisture available. Strictly speaking evaporation from bare soil (E_s) should be treated separately, but in our experiments it was included with dry canopy evaporation. (Over the European area the fraction of bare soil is small). From Eq. 3.3 the soil moisture balance is given by

$$\frac{d\theta}{dt} = \frac{1}{D}(T_f + SM - \nu E_d - (1-\nu)E_s - Y_g - Y_s) \qquad (4.18)$$

$$= \frac{1}{D}(T_f + SM - (1 - \nu S/S_m)\, \beta E_p(r_s=r_{sc}) - Y_g - Y_s) \qquad (4.19)$$

Eq. 4.19 for soil moisture balance and Eq. 4.12 for the canopy balance have been used in the ODM to test sensitivity to canopy capacity. These equations have not yet been programmed into the AGCM. Due to the different capacities of vegetated and bare soil and their different behaviour under infiltration and evaporation it may be better to have separate soil moisture stores for vegetated areas and bare areas.

4.3.4 Interception capacities

Interception capacity estimates for vegetation vary widely as might be expected. The values given will depend on local site conditions such as vegetation age, height, density and type. Both Thompson et al (1982) and Dickinson (1984) suggest that canopy capacity (S_m) is linearly related to leaf area index (LAI). Dickinson uses a projected area LAI which is the total leaf area divided by 2 for flat leaves and divided by π for needles; he also includes stem area index (SAI), the total area of stems and

branches. It is not clear what this means in terms of cereals and grass. Thompson et al (1982) appear to use the projected area LAI also. We will refer to this as LAI_1. Other authors, eg Herwitz (1985) use the total area index, LAI_2, and others do not say explicitly what they use. We will refer to the total vegetation area index (VAI) as the sum of LAI_2 and SAI.

There is considerable variability in estimates of LAI as might be expected and naturally LAI for a single tree may not be appropriate for use as a grid box average, not withstanding differences in definition. Thompson et al (1982) give a list of typical values of LAI_1, and the question that arises is whether these should be increased to account for water splashing onto the underside of leaves and completely covering pine needles.

Various individual studies referred to in table 4.3 have been plotted in figure 4.14 and show that the suggested relationship of

$$S_m = 2. \times 10^{-4} \text{ VAI} \qquad (4.20)$$

is a reasonable fit (S_m, in metres). Defining appropriate values of VAI may be more difficult. Values of S_m for different vegetation types without quoted values of LAI are plotted as circles on the line of S_m against VAI. The range of possible canopy capacity values is fairly limited. Mintz et al (1983) quote values in the range 1 to 3 mm. Using figure 4.14 and various quoted values for LAI, S_m was estimated for various land types as given in table 4.4.

Table 4.3

List of studies for which data are given in figure 4.14 and table 4.4.

Reference	Author(s)	Vegetation type
H_1	Halldin et al (1984)	Broadleaf (Oak)
H_2	Hancock et al (1983)	Needleaf (Sitka Spruce)
H_3	Herwitz (1985)	Tropical
C	Calder et al (1984)	Shrub (Heather)
E	Eagleson (1970)	Needleaf (Ponderosa Pine)
M	Monteith (1976)	Various
T	Thompson et al (1982)	Various

Table 4.4

Canopy capacity for different land types.

Land Type	Local Capacity (m) S_m	Vegetated Fraction ν	Grid Box Capacity νS_m(m)
Forest	2.5×10^{-3}	0.9	2.25×10^{-3}
Woodland	2.0×10^{-3}	0.9	1.80×10^{-3}
Shrubs	1.7×10^{-3}	0.85	1.45×10^{-3}
Tall grass/crops	1.5×10^{-3}	0.85	1.28×10^{-3}
Short grass/crops	1.0×10^{-3}	0.85	0.85×10^{-3}
Semi Desert	0.5×10^{-3}	0.5	0.25×10^{-3}
Desert	0.2×10^{-3}	0.01	0.002×10^{-3}
Swamp	1.0×10^{-3}	0.5	0.5×10^{-3}
Tundra	0.2×10^{-3}	0.8	0.160×10^{-3}

There is a case for treating tropical vegetation separately; however for the time being, given the uncertainty in the data, it was considered necessary to first find the sensitivity to S_m. An ODM study with and without a canopy present are given in the next section.

4.3.5 A one dimensional model sensitivity study

Two ODM integrations were carried out for southern England to ascertain the sensitivity to canopy storage. The land type of forest was used and in one experiment the canopy capacity was set to zero. A programming error meant that the local storage was 2.8mm rather than 2.5mm. Both experiments were run over an annual cycle but results have only been presented for a 60 day period from mid-May to mid-July (days 120 to 179). These are summarised in table 4.5. As might be expected, by including canopy storage, evaporation has increased at the expense of the sensible heat flux, leading to a marked decrease in the Bowen ratio. Not surprisingly, average soil moisture is lower since a fraction of rainfall no longer reaches the soil but is intercepted and re-evaporated. An interesting result is the enhancement of convective rainfall, presumably as a result of the increase in evaporation. As the increase in evaporation must take place whilst the canopy is wet, it suggests that existing rainfall events are enhanced rather than new ones generated.

Table 4.5

ODM Study of the effect of canopy interception (60 day integration)

	With Canopy	Without Canopy	Difference
Canopy capacity(mm)	2.8	0.0	2.8
Average surface temperature (K)	287.4	287.9	-0.5
Average SMC (cm)	17.8	20.1	-2.3
Average Canopy Storage (mm)	.49	0	.49
Average Latent Heat (Wm^{-2})	67.6	55.5	12.1
Average Sensible Heat (Wm^{-2})	54.2	66.7	-12.5
Bowen ratio	0.80	1.20	-0.4
Total Dynamic Rain (mm)	44.1	43.1	1.0
Total Convective Rain (mm)	91.6	79.6	12.0

Figures 4.15 and 4.16 confirm that this is indeed the case although a few new events have appeared close to existing rainfall events. New events will not be generated during dry periods as figure 4.17 shows that canopy stored water is removed quickly once rainfall has ceased. It is not obvious what would happen in an AGCM context. Clearly local rainfall would be enhanced but whether events would last longer or become more extensive would need to be tested in an AGCM experiment. Certainly a 22% increase in evaporation and 15% increase in rainfall during a summer period, suggests that canopy storage has a significance beyond its size and should be included in any climate model.

4.4 Conclusions

Evaporation plays an important part in the surface energy and moisture budget and can affect the rainfall distribution over continental areas in quite a major way by providing moisture particularly for convective systems. It is therefore important to calculate evaporation rates with a reasonable degree of accuracy. It was observed that without taking surface resistance into account, evaporation rates were too high. Inclusion of a surface resistance of 60 sm^{-1} had a beneficial effect on evaporation rates and has been included in the AGCM.

Canopy storage has been shown to have a potentially large effect on soil moisture, evaporation and rainfall and needs to be investigated further. ODM studies suggest that convective rainfall events are enhanced rather than new ones generated although this needs to be tested in an AGCM context.

The dependence of evaporation on soil moisture parameters such as soil type and root depth is also important and sensitivity to root depth is comparable to sensitivity to surface resistance.

Future work needs to look at the appropriateness of the present formulation used to control evaporation at low soil moisture concentrations, and the dependence of surface resistance on other physical processes. More complex canopy models which have recently been developed by some workers need to be evaluated in a climate modelling context to see if such complexity is in fact needed to model the energy and moisture balance at the earth's surface.

4.5 References

Avissar, R., Avissar, P., Mahrer, Y. and Bravdo, B.A. 1985 A model to simulate response of plant stomata to environmental conditions. Agric. and Forest Meteorology, 34, 21-29.

Baker, M.B. Jr., 1986 Effects of Ponderosa Pine Treatments on Water Yield in Arizona. Water. Res. Res., 22, 67-73.

Calder, I.R., Hall, R.L., Harding, R.J. and Wright, I.R. 1984 The use of wet-surface weighing lysimeter in rainfall interception studies of heather. Journal of Climate and Applied Meteorology, 23, 461-473.

Dickinson, R.E. 1984 Modelling evapotranspiration for three-dimensional global climate models. Geophysical Monograph 29, Maurice Ewing, vol 5.

Eagleson, P.S. 1970 Dynamic Hydrology, McGraw Hill, New York.

Feldlake, C.M., and Boyer, D.G. 1985 Resistance to water loss from warm and cool-season forage canopies in a growth chamber. Agric. and Forest Meteorology, 34, 269-275.

Halldin, S., Saugier, B., and Pontailler, J.Y. 1984 Evapotranspiration of a deciduous forest: simulation using routine meteorological data. Journal of Hydrology, 75, 323-341.

Hancock, N.H., Sellers, P.J. and Crowther, J.M. 1983 Evaporation from a partially wet forest canopy. Annales Geophysicae, 1, 139-146.

Herwitz, S.R. 1985 Interception storage capacities of tropical rainforest canopy trees. Journal of Hydrology, 77, 237-252.

Hewlett, J.D., and Bosch, J.M.	1984	The dependence of storm flows on rainfall intensity and vegetal cover in South Africa. Journal of Hydrology, 75, 365-381.
Massman, W.J.	1980	Water storage on forest foliage: a general model. Water Res. Res., 16, 210-216.
Mintz, Y., Sellers, P.J. and Willmott, C.J.	1983	On the design of an interactive biosphere for the GLAS general circulation model. NASA Technical Memorandum 84973, Goddard Space Flight Center, Greenbelt, (Unpublished).
Monteith, J.L. (Edt)	1976	Vegetation and the atmosphere, Vol. 2. Academic Press, London.
Morton, F.I.	1984	What are the limits on forest evaporation? Journal of Hydrology, 74, 373-398.
Reifsnyder, W.E.	1982	The role of forests in the global and regional water and energy balances. WMO. CAgM Report No. 8.
Rowe, P.B., and Hendrix, T.M.	1951	Interception of rain and snow by second-growth Ponderosa Pine. Trans. Amer. Geophysical Union, 32, 903-908.
Rowntree, P.R.	1983	Land surface processes in climate models - parametrization and model sensitivity. Int. Counc. Sci. Union, W.M.O., World Clim. Res. Prog., Rep. Fourth Session. Joint Sci. Comm., Venice, 1-8 March 1983, 57-75.
Rutter, A.J., Kershaw, K.A., Robins, P.C. and Morton, A.J.	1971	A predictive model of rainfall interception in forests, 1. Derivation of the model from observation in a plantation of Corsican Pine. Agric. Meteorol., 9, 367-384.
Sellers, P.J., and Lockwood, F.G.	1981	A computer simulation of the effects of differing crop types on the water balance of small catchments over long time periods. Quart. Journal of Royal Met. Soc., 107, 395-414.

Sellers, P.J., Mintz, Y. and Sud, Y.C.	1985	A simple biosphere model (SIB) for use within general circulation models. University of Maryland. (Unpublished).
Slingo, A. (Edt.)	1985	Handbook of the Meteorological Office 11-layer atmospheric general circulation model. Volume 1, Model description. Met O 20 DCTN 29, Meteorological Office, Bracknell. (Unpublished).
Slingo, A. and Wilderspin R.C.	1984	Development of an improved GCM radiation scheme. Met O 20 DCTN 6, Meteorological Office, Bracknell (Unpublished).
Thompson, N., Barrie, I.A. and Ayles, M.	1982	The Meteorological Office rainfall and evaporation calculation system: MORECS (July 1981). Meteorological Office, Bracknell.
Wilson, M.F. and Henderson-Sellers, A.	1985	A global archive of land cover and soil data for use in general circulation climate models. Journal of Climatology, 5, 119-143.

Figure 4.1 Average August evaporation from AGCM experiment with r_s = 60sm^{-1}. Contours every 1.0mm day^{-1} and at 0.1 mm day^{-1} with shading above 5.0mm day^{-1}.

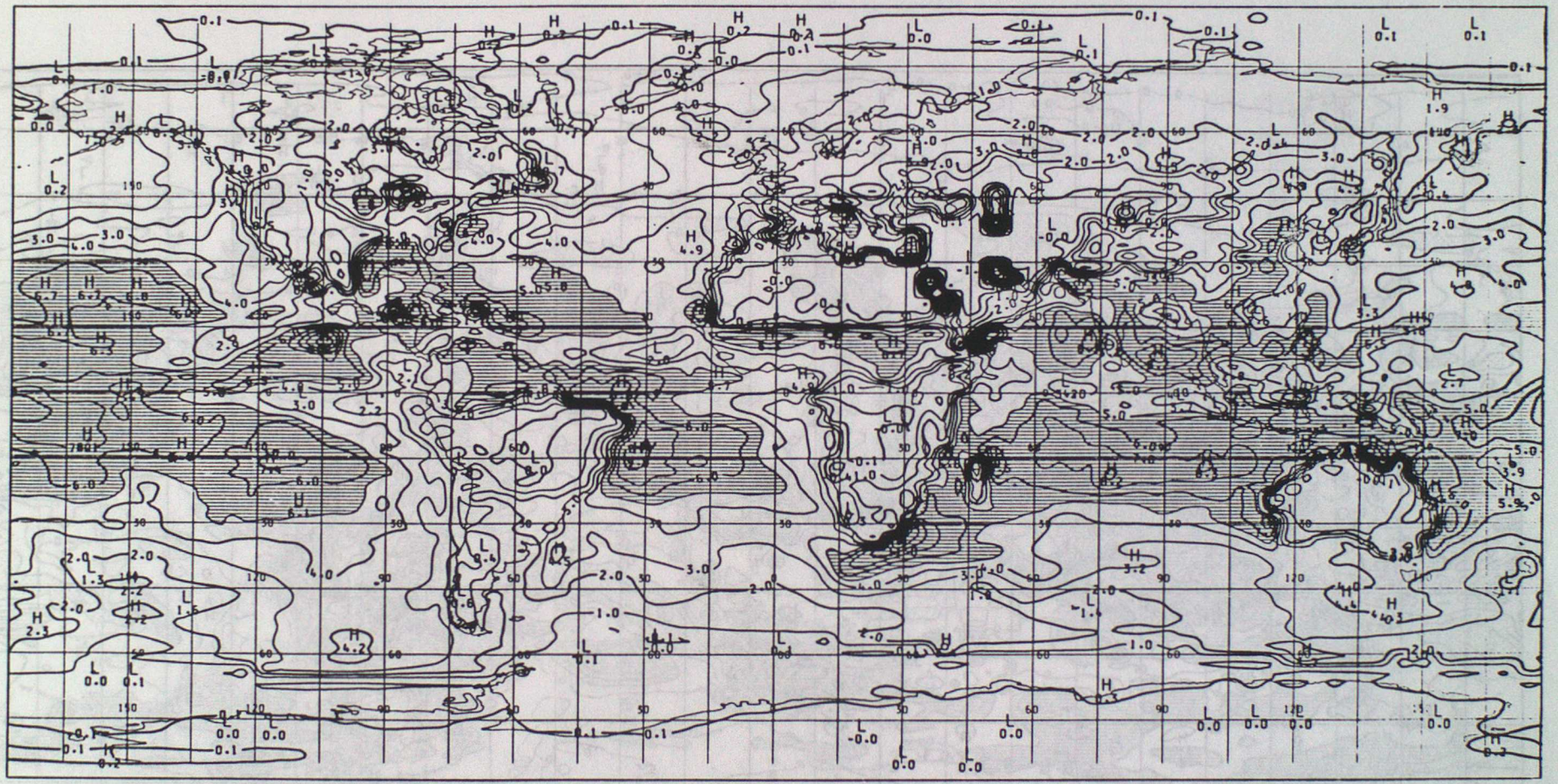

Figure 4.2 Difference in August evaporation between experiment (r_s = 60sm^{-1}), and control (r_s = 0sm^{-1}). Contours every 0.5 mm day^{-1} with areas greater than 0.5 mm day^{-1} stippled and less than -0.5 mm day^{-1} shaded.

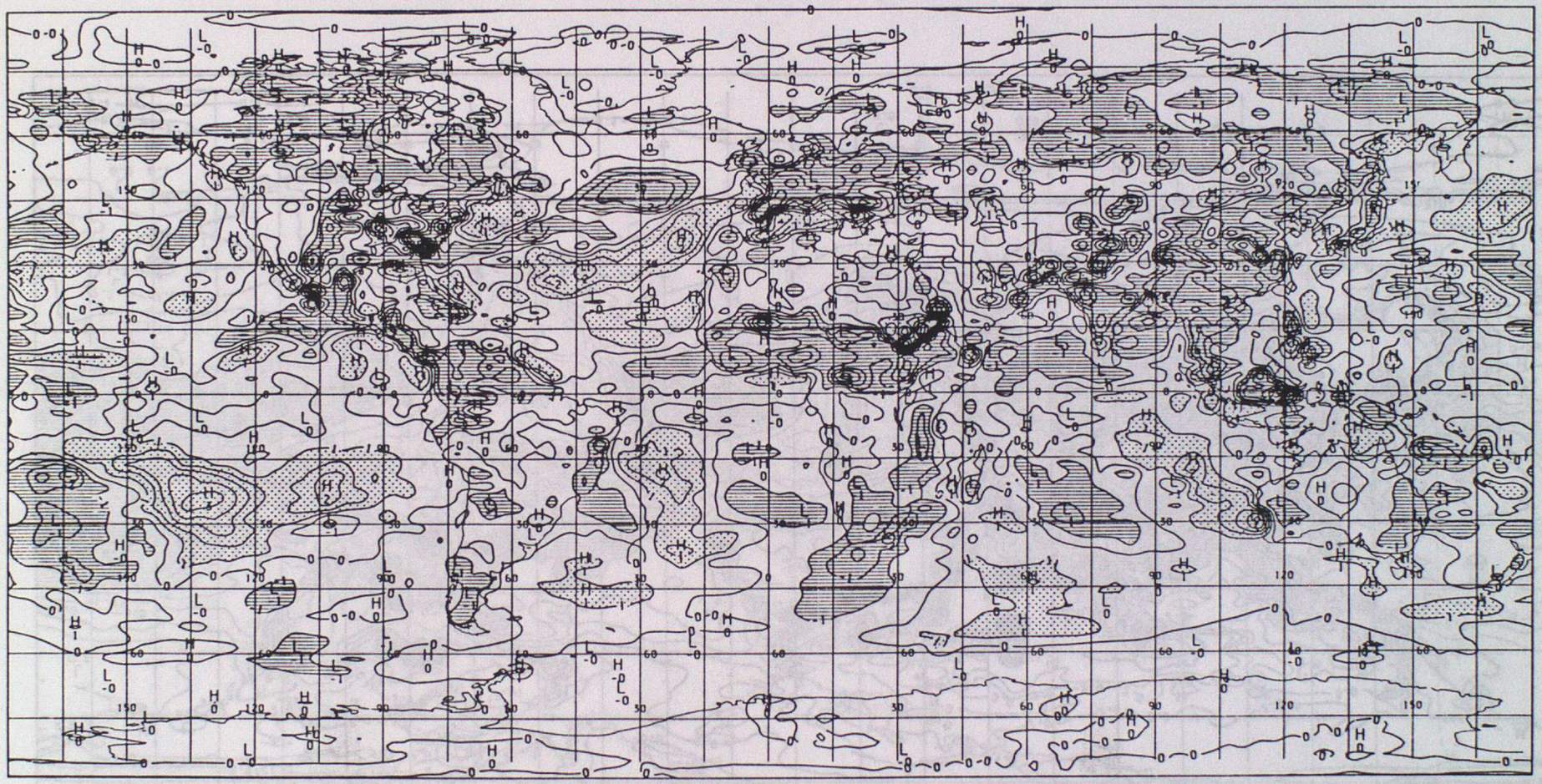

Figure 4.3 Average August sensible heat flux from AGCM experiment with $r_s = 60\ sm^{-1}$. Contours every 50.0 Wm^{-2} and at ±12.5 and ±25.0 Wm^{-2} with negative areas shaded.

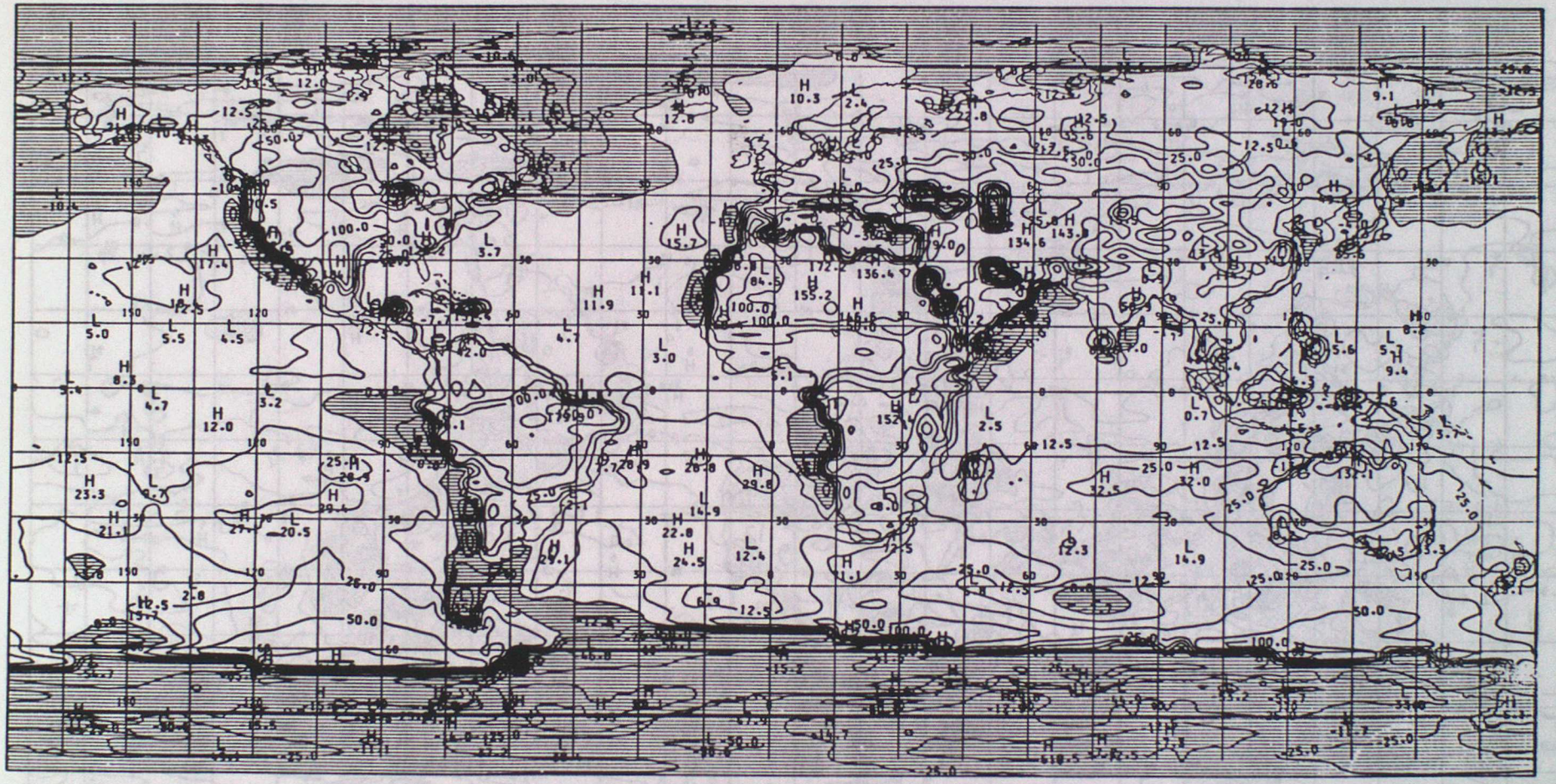

Figure 4.4 Difference in August sensible heat flux between experiment (r_s = 60 sm^{-1}) and control (r_s = 0 sm^{-1}). Contours every 15.0 Wm^{-2} with areas greater than 15.0 Wm^{-2} stippled and less than -15.0 Wm^{-2} shaded.

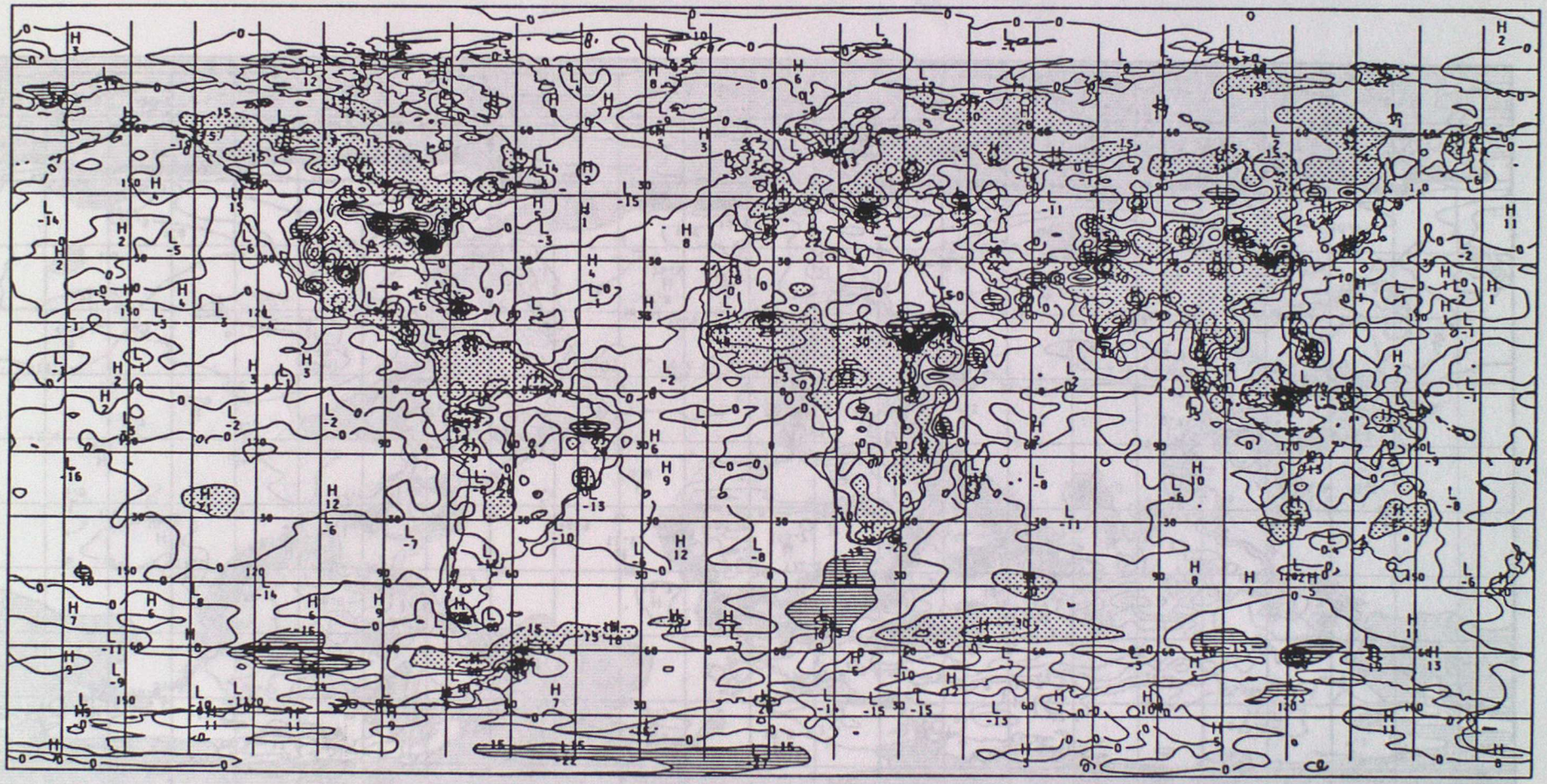

Figure 4.5 Difference in August precipitation between experiment (r_s = 60 sm^{-1}) and control (r_s = 0 sm^{-1}). Contours every 1 mm day^{-1} with areas greater than 1 mm day^{-1} stippled and less than -1 mm day^{-1} shaded.

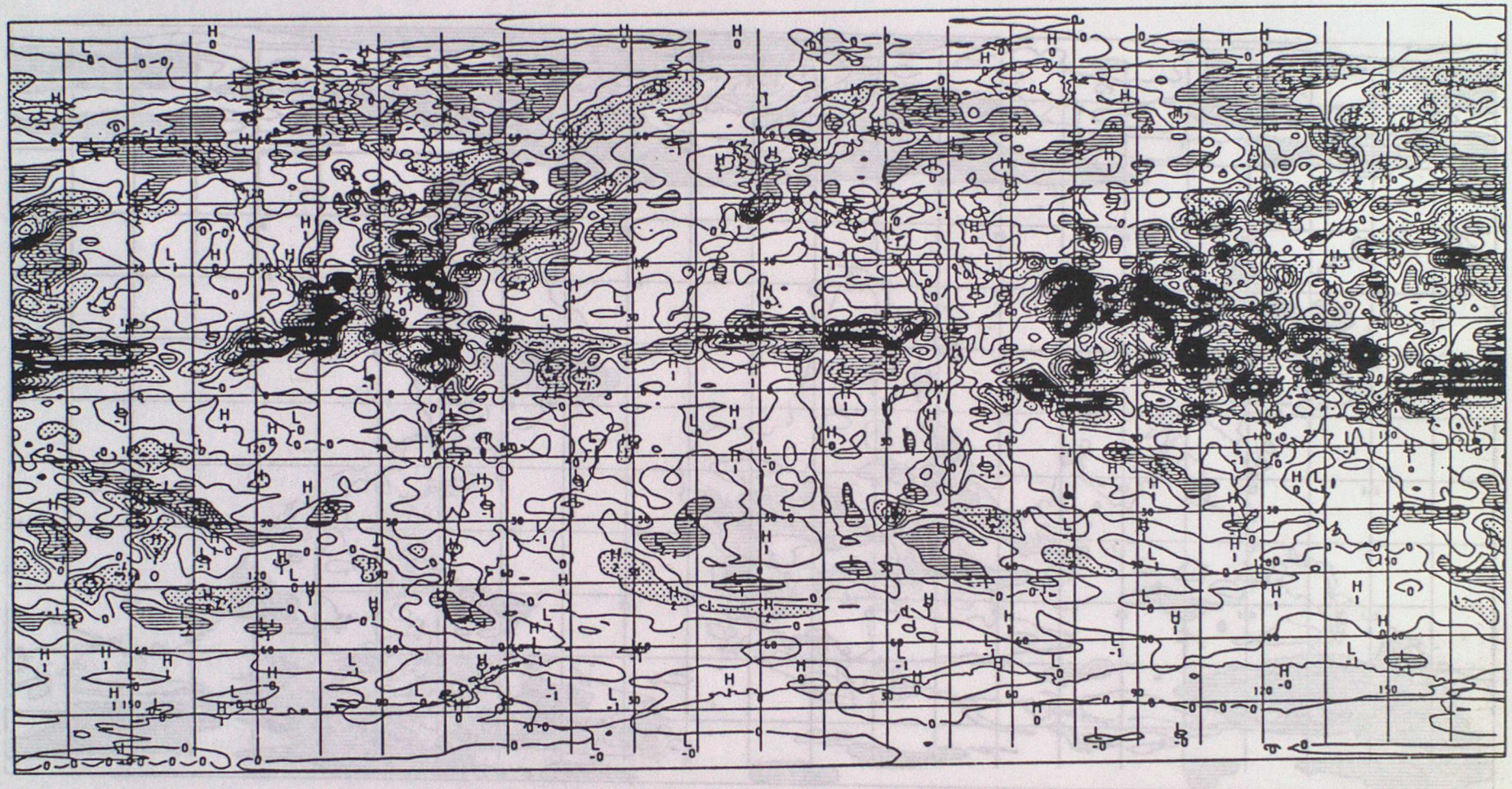

Figure 4.6 Difference in August mean surface temperature between experiment (r_s = 60 sm^{-1}) and control (r_s = 0 sm^{-1}). Contours every 2K and negative areas shaded.

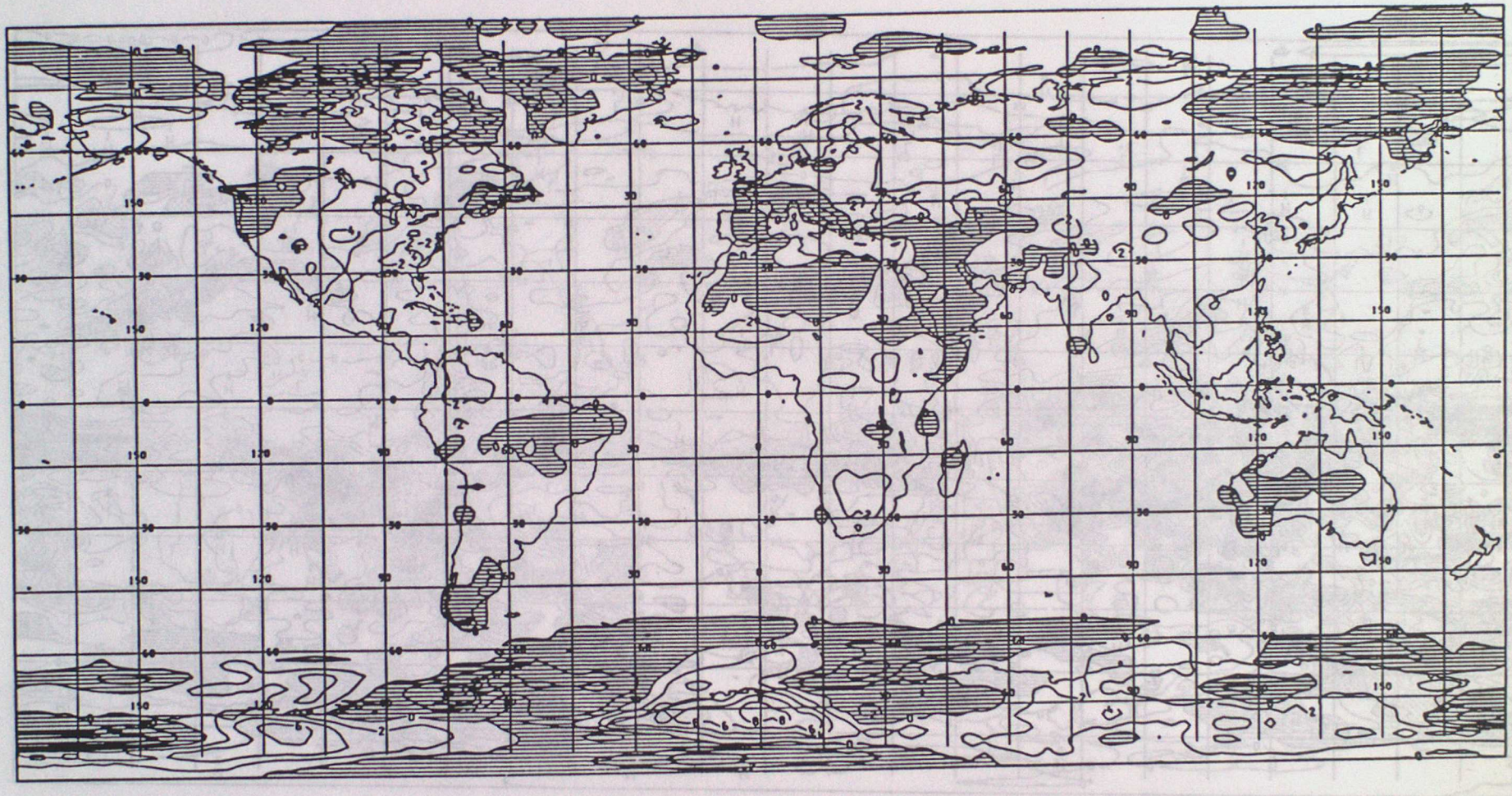

FIGURE 4.7 ANNUAL CYCLE SOUTHERN ENGLAND
MEDIUM SOIL. TALL GRASS(RS=OS/M)

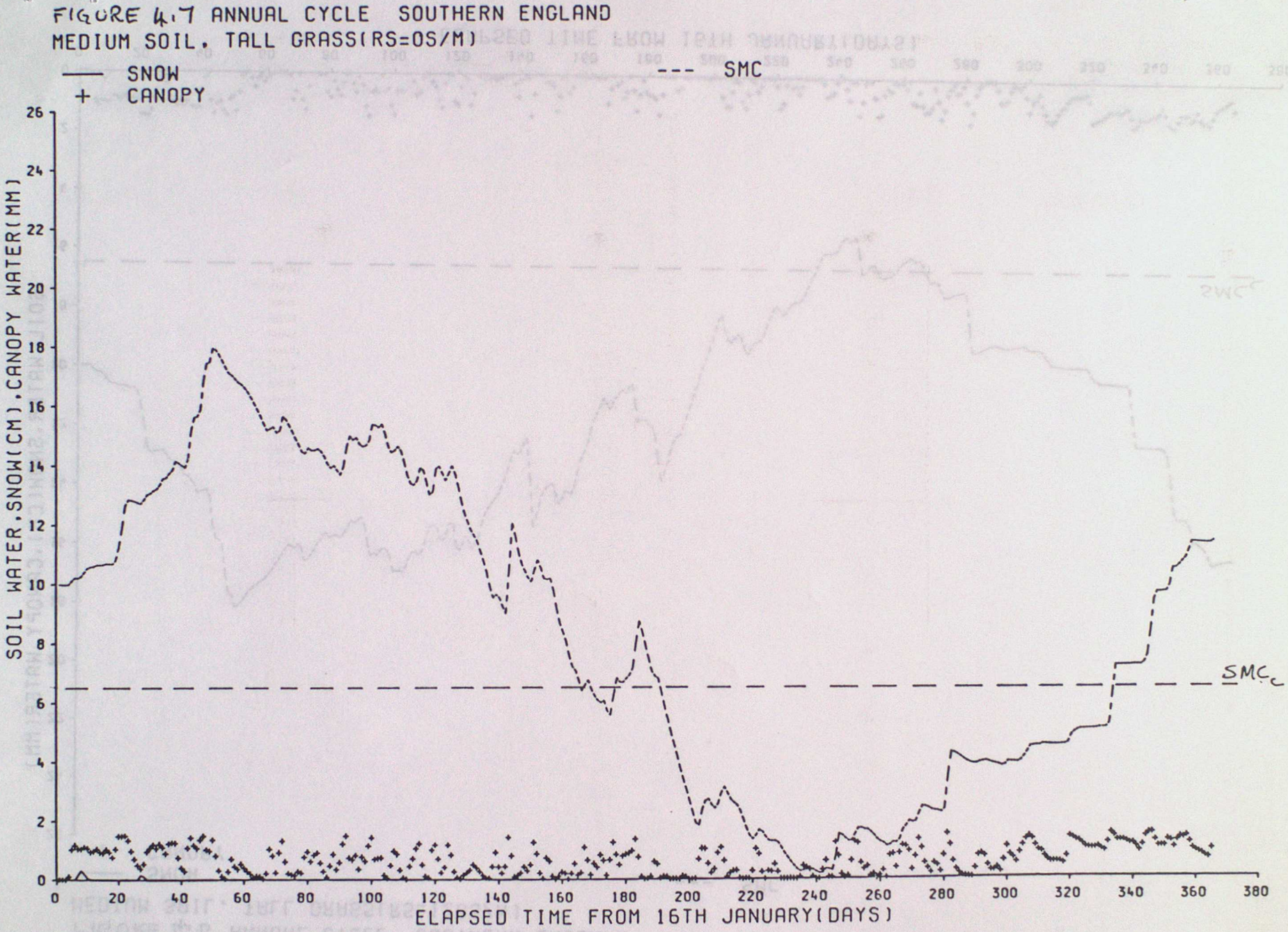

FIGURE 4.8 ANNUAL CYCLE SOUTHERN ENGLAND
MEDIUM SOIL. TALL GRASS(RS=120S/M)

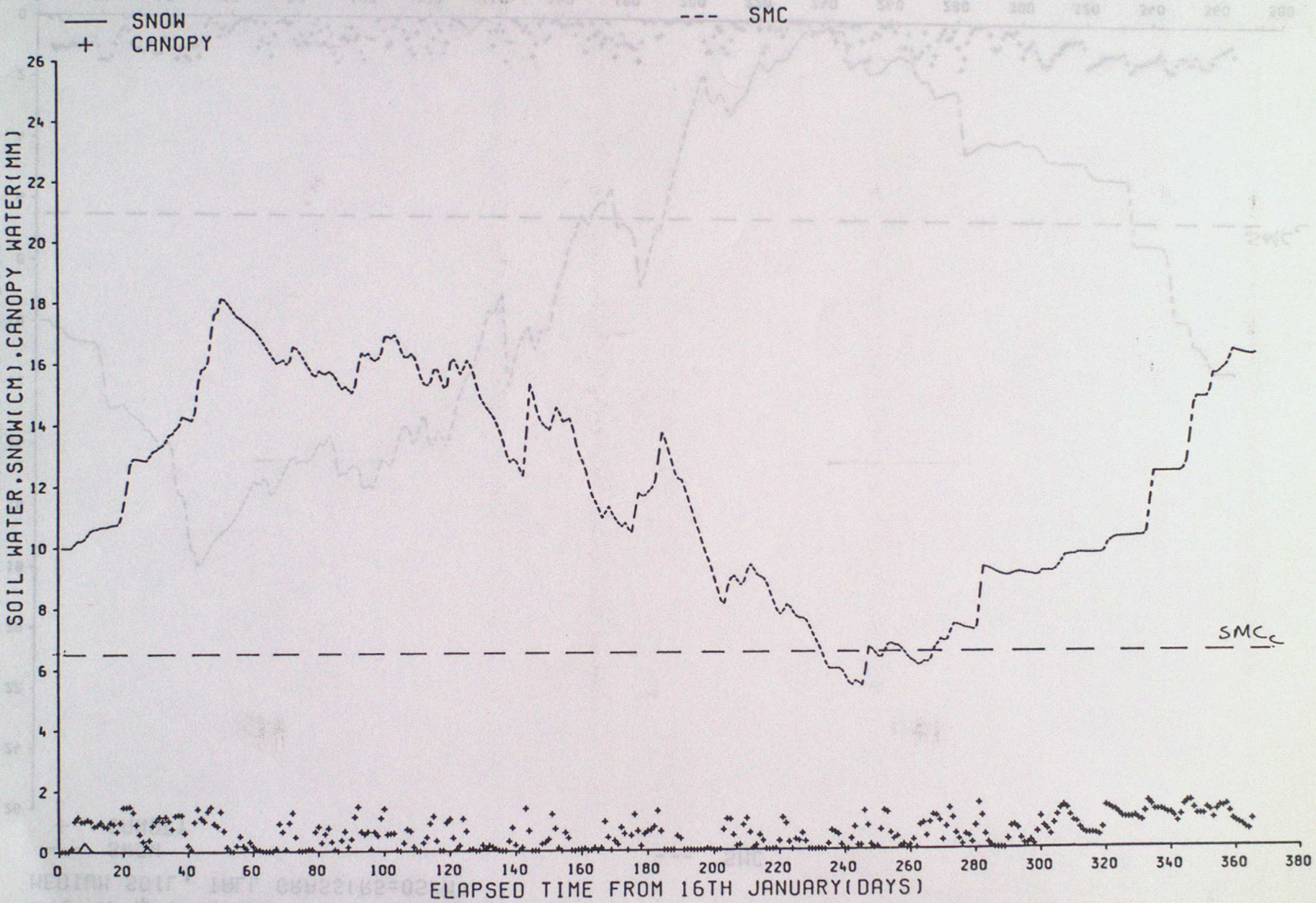

FIGURE 4.9 ANNUAL CYCLE SOUTHERN ENGLAND
MEDIUM SOIL. TALL GRASS(RS=OS/M)

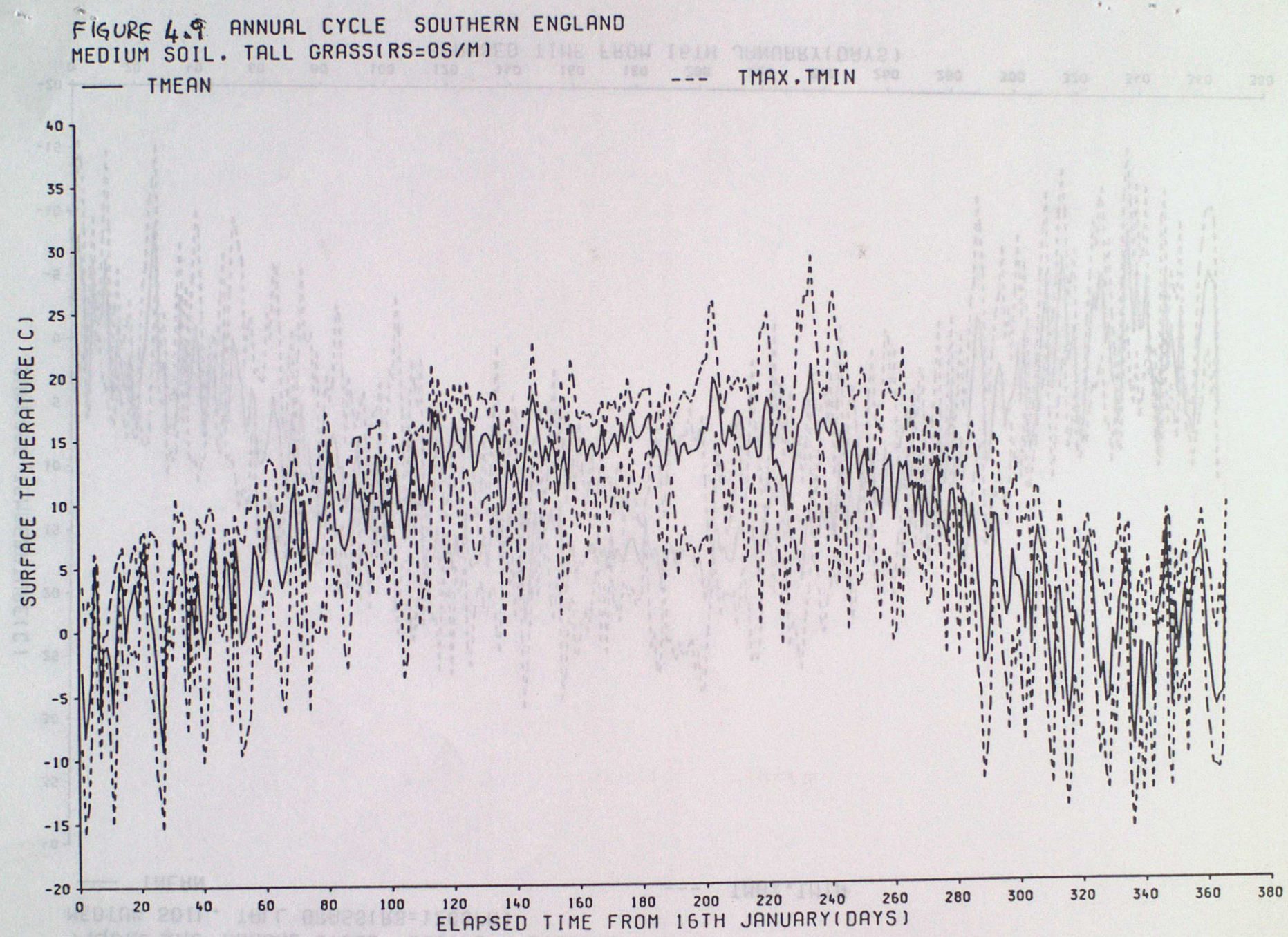

FIGURE 4.10 ANNUAL CYCLE SOUTHERN ENGLAND
MEDIUM SOIL. TALL GRASS(RS=120S/M)

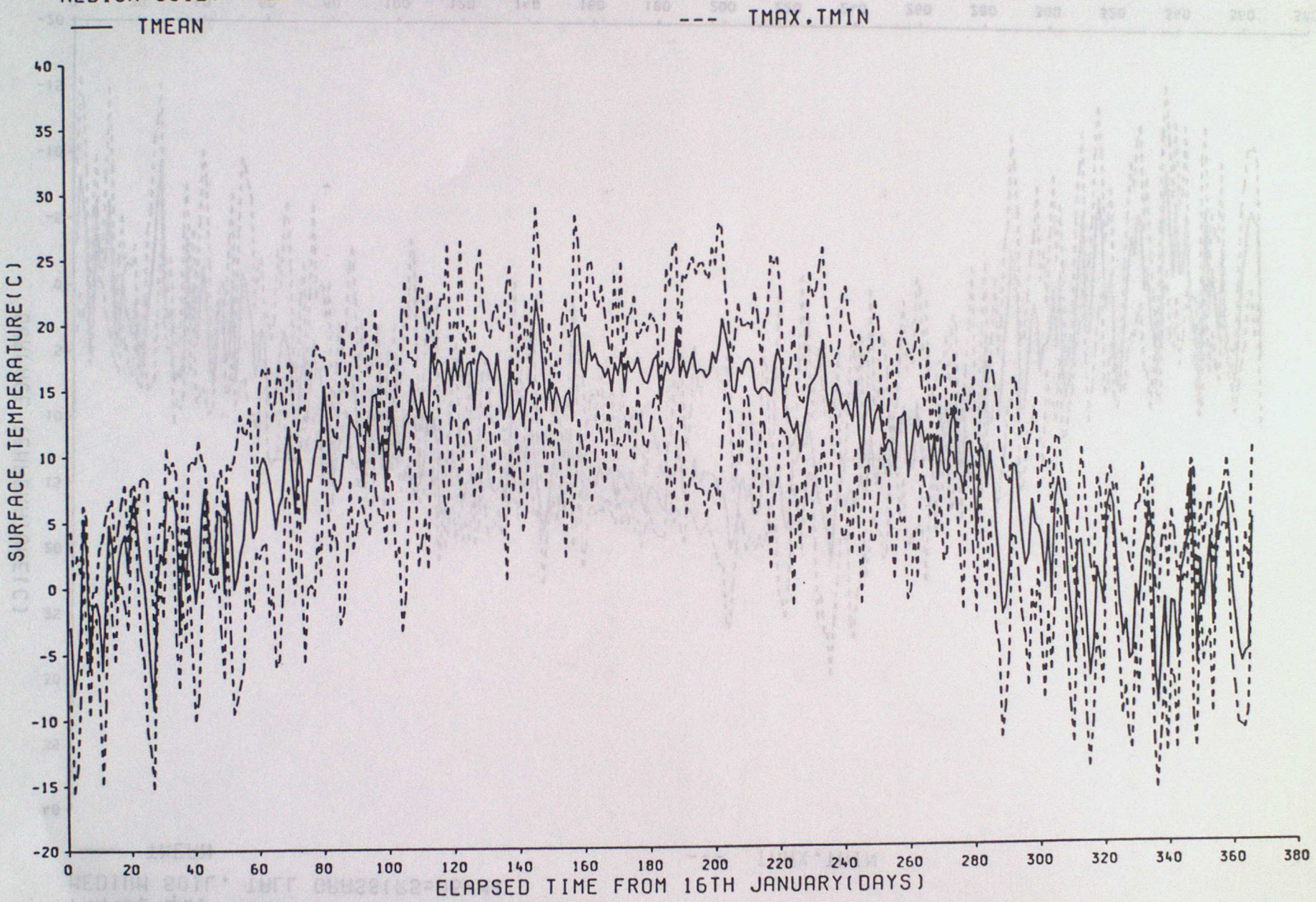

FIGURE 4.11 ANNUAL CYCLE SOUTHERN ENGLAND
MEDIUM SOIL. TALL GRASS(D=50CM)

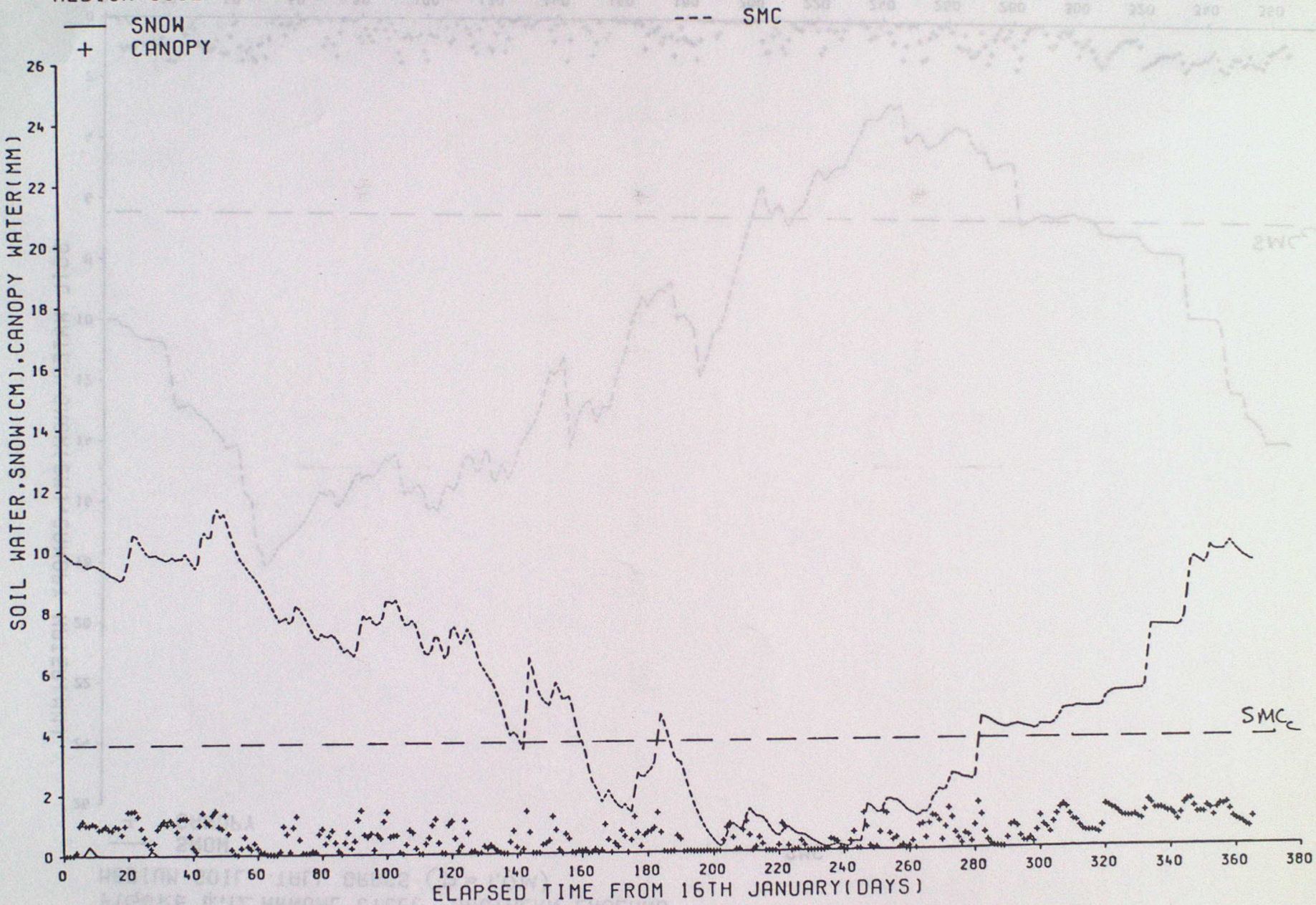

FIGURE 4.12 ANNUAL CYCLE SOUTHERN ENGLAND
MEDIUM SOIL. TALL GRASS (D = 1.0M)

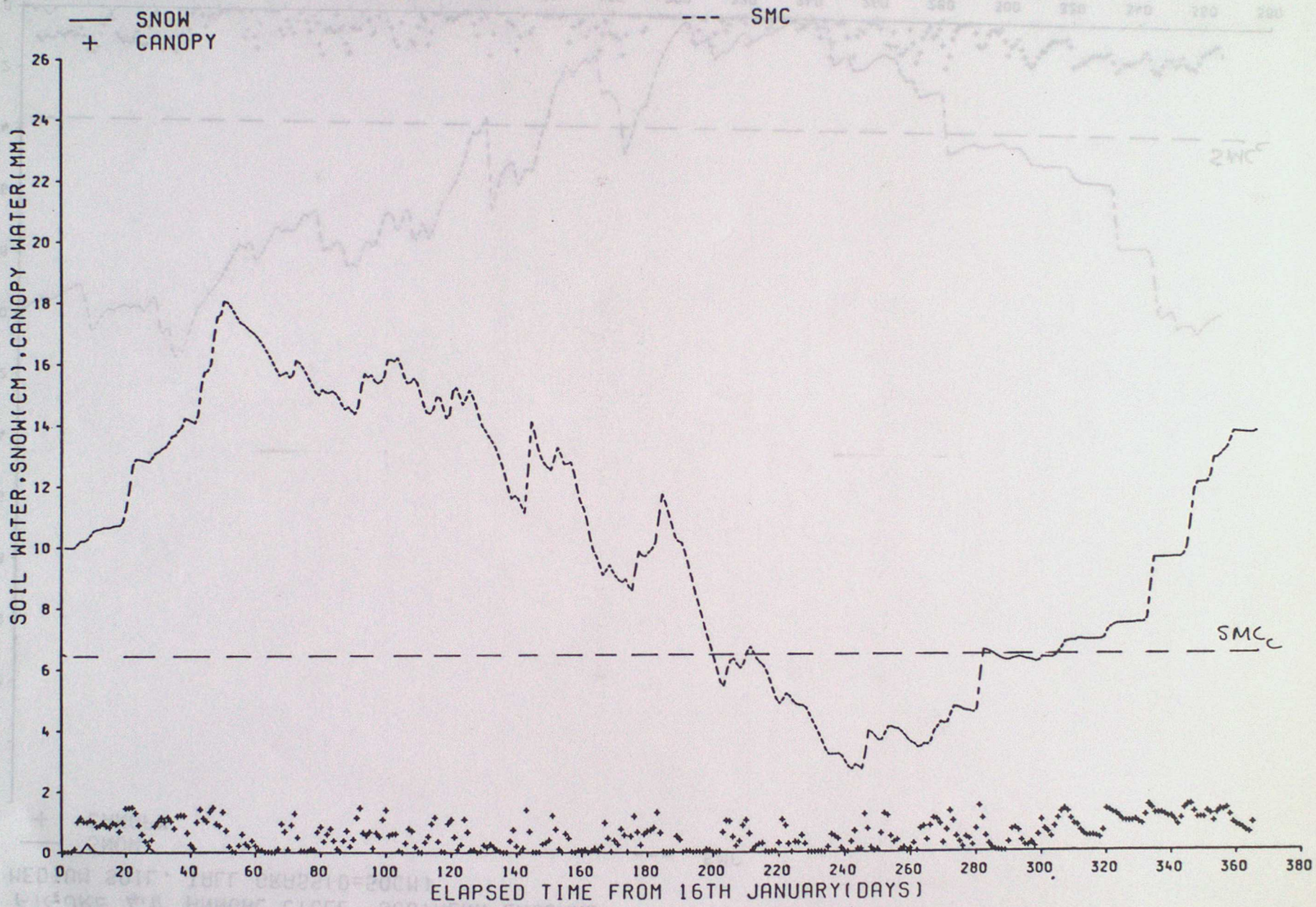

FIGURE 4.13 ANNUAL CYCLE SOUTHERN ENGLAND
MEDIUM SOIL. TALL GRASS(D=10CM)

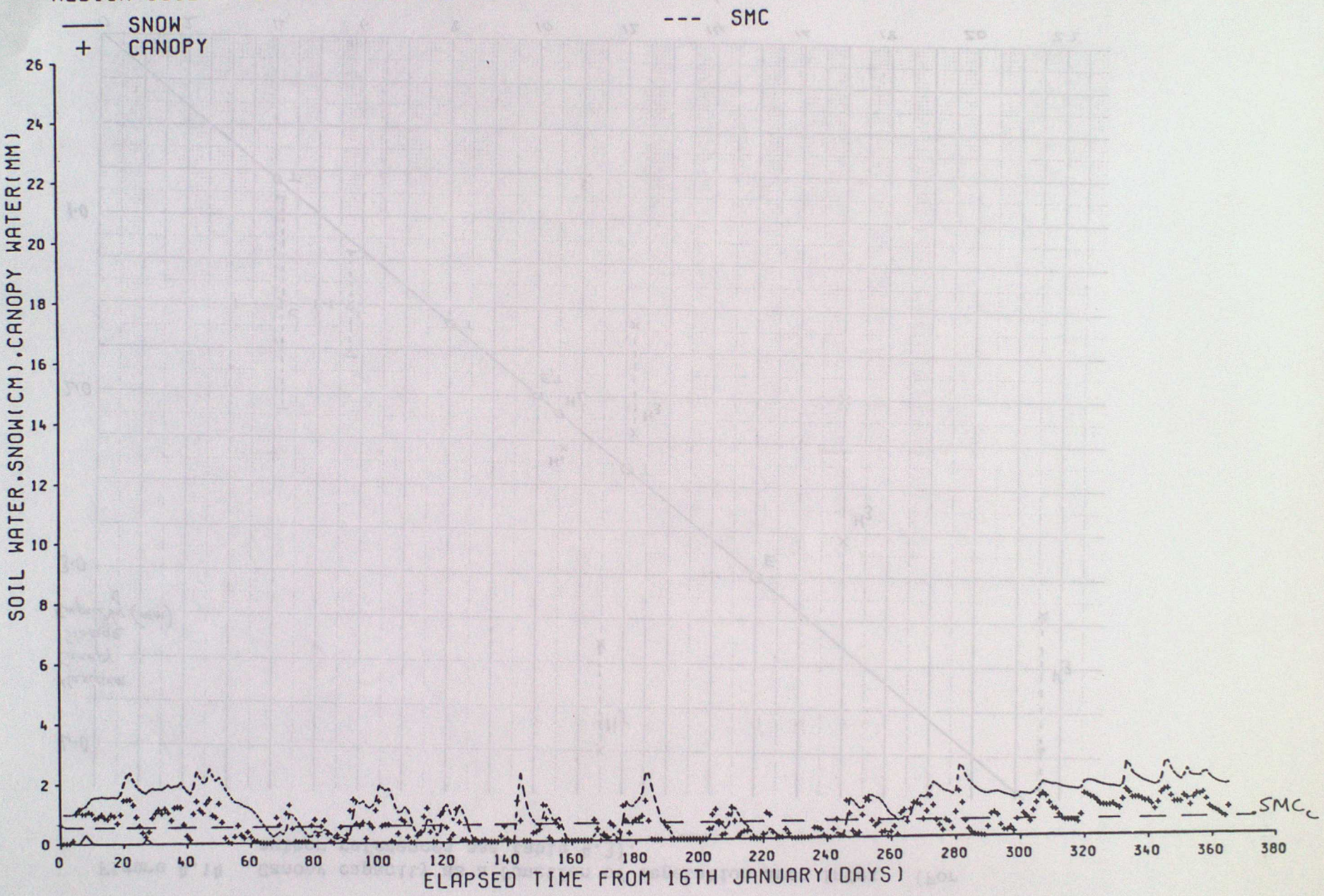

Figure 4.14 Canopy capacity as a function of vegetation area index. (For author references see table 4.3).

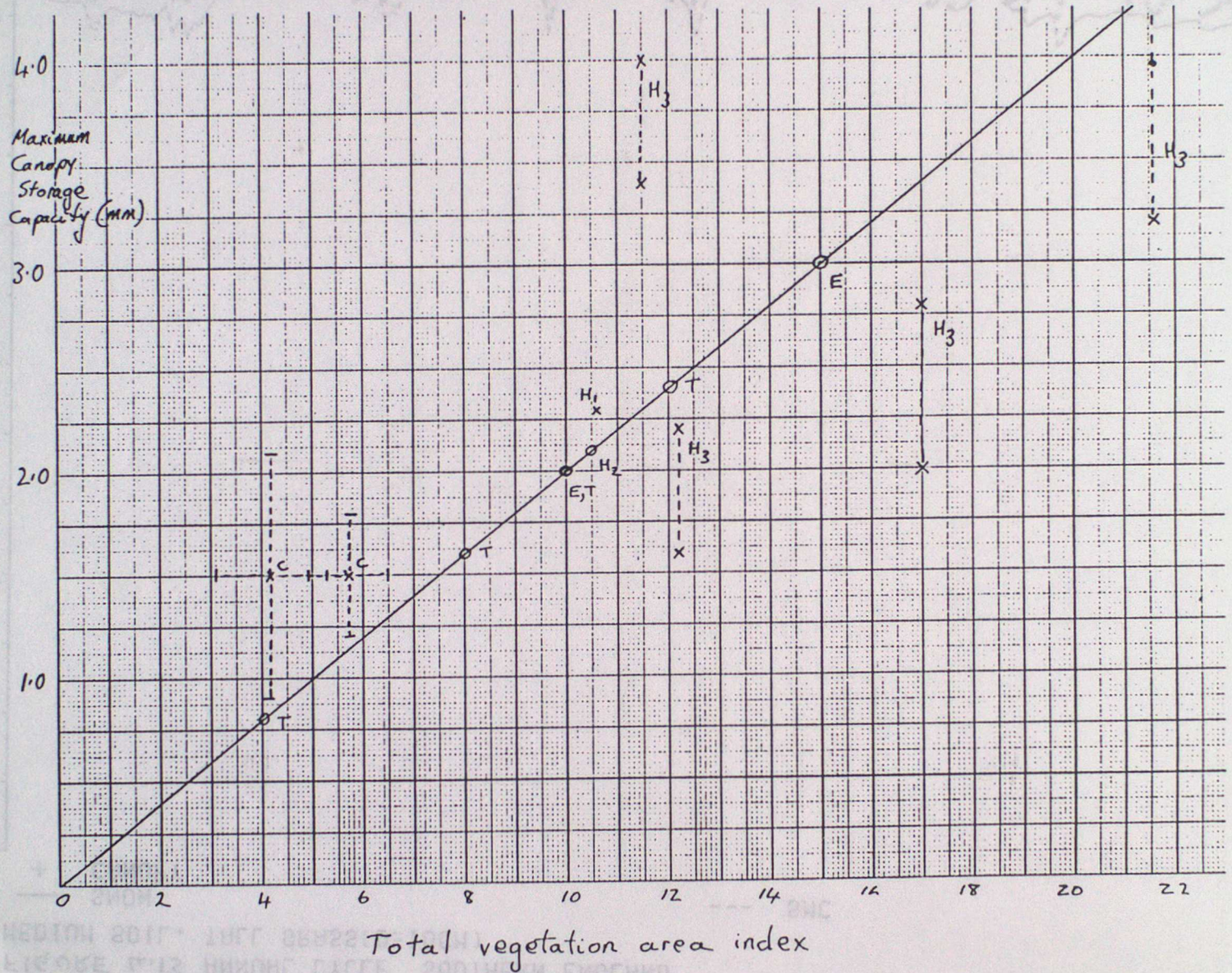

FIGURE 4.15 DAYS 120-180 SOUTHERN ENGLAND
MEDIUM SOIL FOREST(S=0.0MM)

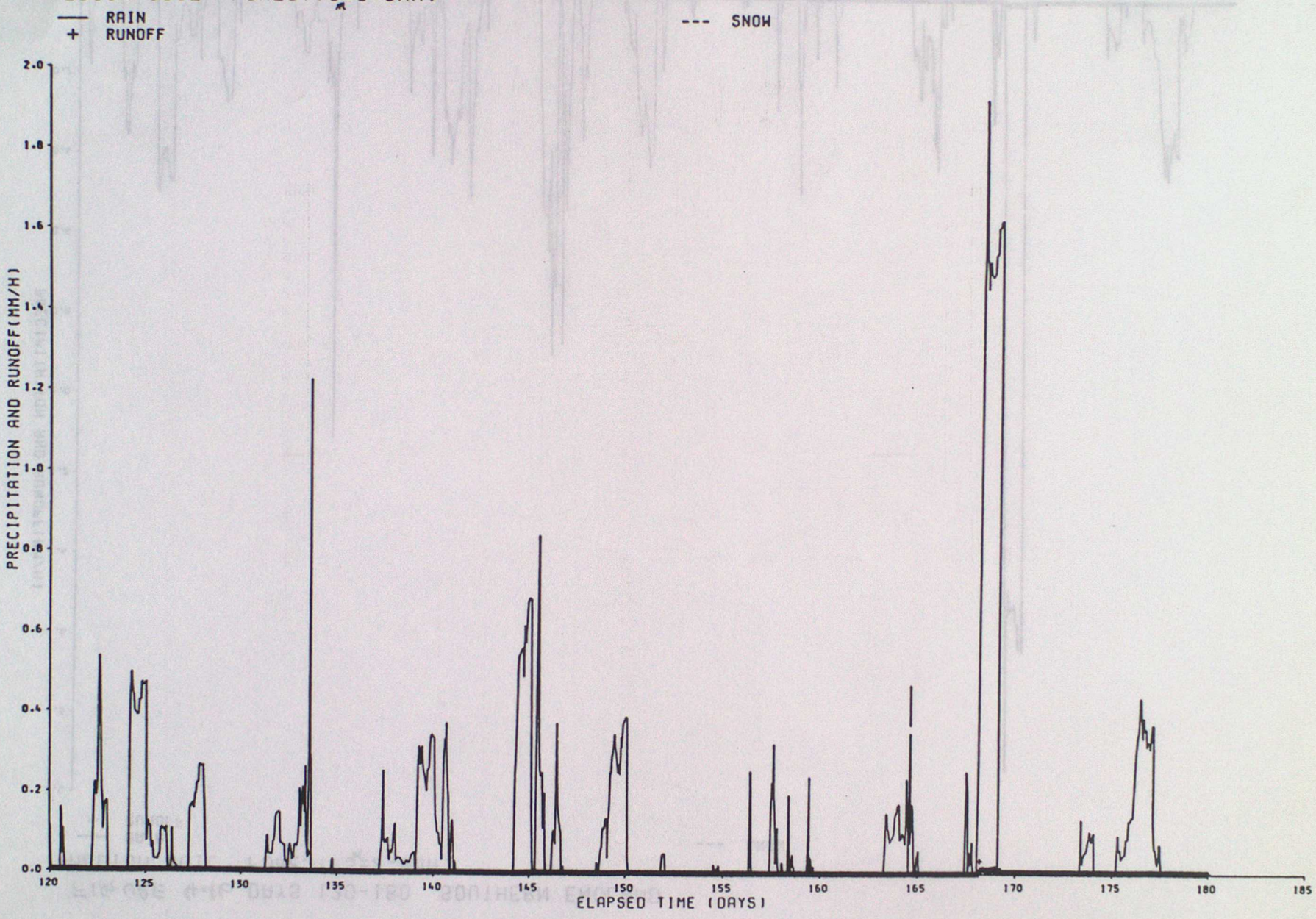

FIGURE 4.16 DAYS 120-180 SOUTHERN ENGLAND
MEDIUM SOIL FOREST(S_r=2.8MM)

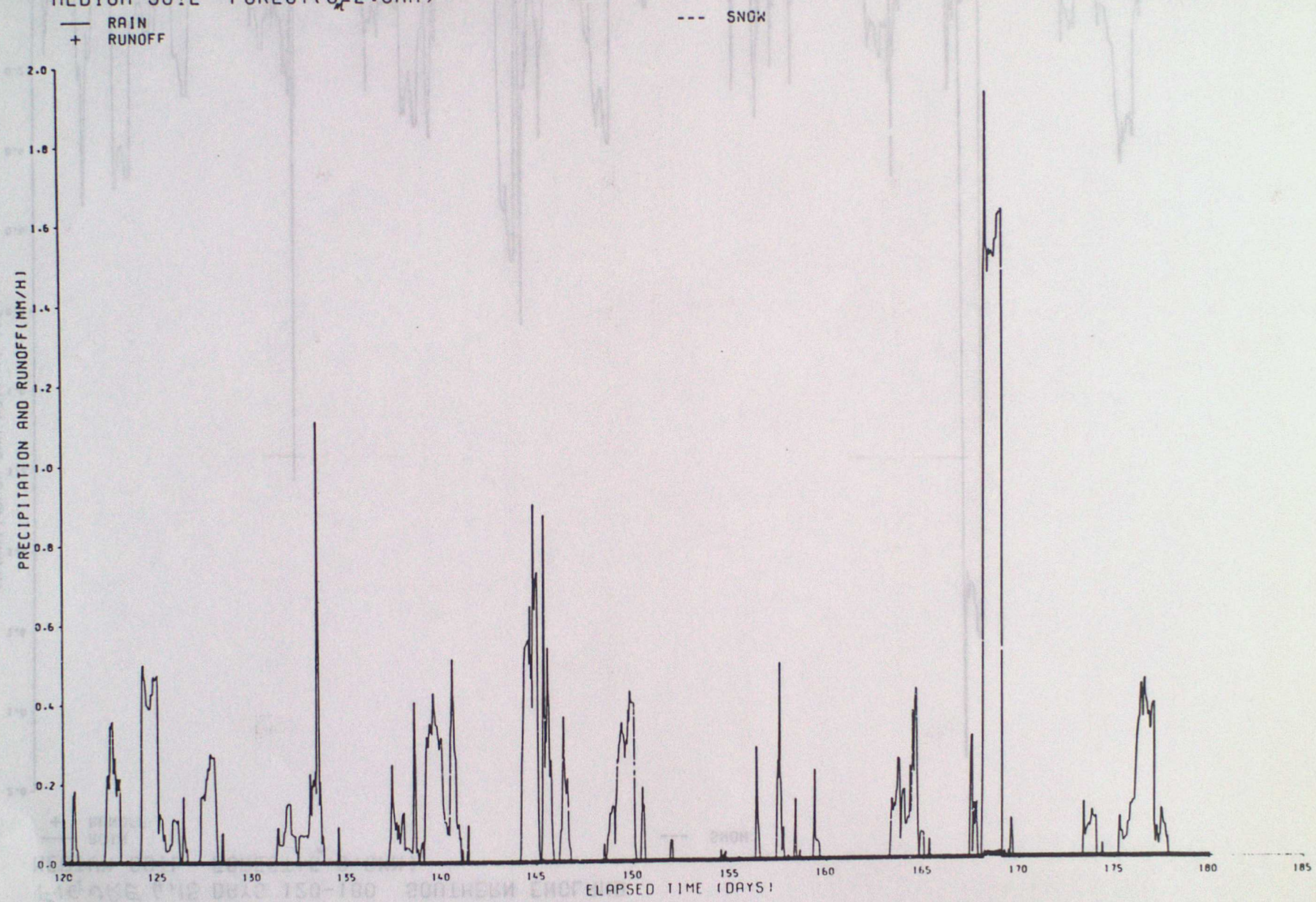

FIGURE 4.17 DAYS 120-180 SOUTHERN ENGLAND
MEDIUM SOIL FOREST(S_m=2.8MM)

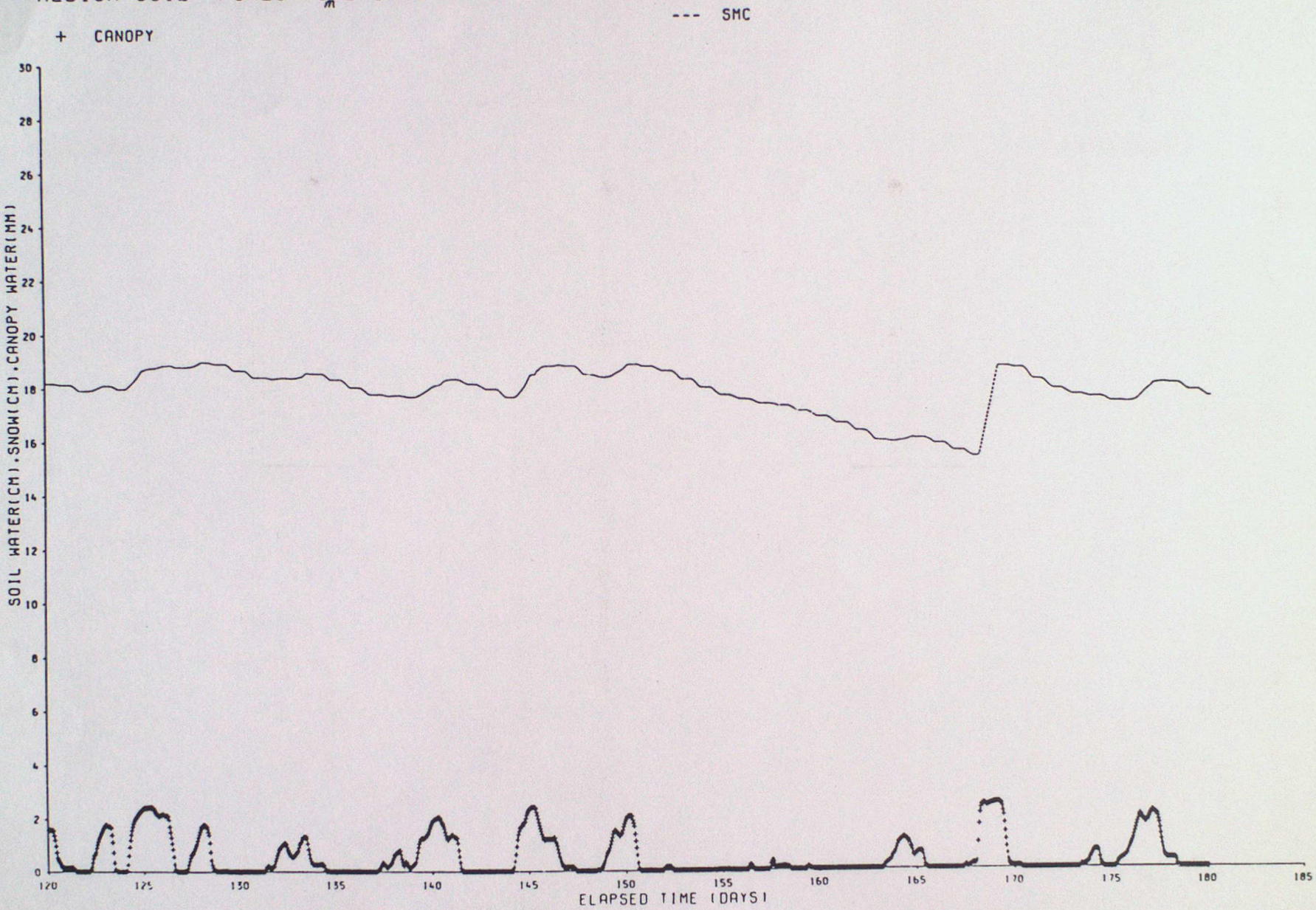

5. Land Surface Data

5.1 Introduction

5.2 Data sources

5.3 Interim division of land and soil types

5.4 Conclusions

5.5 References

5. Land Surface Data

5.1 Introduction

As more detailed modelling of land surface processes takes place so the requirement for information on various land surface parameters grows. Since different models require different amounts of information and since some parameters are difficult to measure directly, the general approach has been to map vegetation and soil types and relate surface modelling parameters to these types. The assumption is that there are fairly unique relationships between soil and vegetation types and model parameters. Clearly this is an over-simplification but it is a useful first step in a subject where global data are sparse and where the relationship between model parameters and vegetation and soil types have often been derived from a few very local studies. Other factors may play an important role, such as vegetation density, vegetation and soil spatial variability, geomorphology and underlying geology.

Whilst on the one hand there is the need to gather data on land surface types and parameters and to test various land surface models for AGCM modelling, there is a need to consider the sensitivity of any model atmosphere to land surface variability so that we have some idea which parameters need to be ascertained first and to what degree of precision. In this section an interim classification of land types and parameters is presented.

5.2 Data Sources

The majority of published surface data are derived from surface based observational studies. For AGCM purposes the spatial distribution of land surface parameters is required. However generally speaking only the spatial distribution of vegetation or soil types is available and information on parameters can only be found in detailed local studies. The need therefore is to relate the local studies to the large scale studies of land type. In recent years the possibility of quantitative observation of the land surface by satellite has become a reality, although the subject is still in its infancy. Available land surface data and requirements are reviewed by Bolle and Rasool (1985).

Although more data will be available in the future, for the present there are two machineable archives of global land use data, including vegetation types and soil characteristics which are generally available. These have been prepared by Wilson and Henderson-Sellers (1985) and Matthews (1984). The former archive was already available in the Meteorological Office and so has been used as a basis for our work. Surface albedos based on Wilson and Henderson-Sellers are currently used in AGCM integrations.

5.3 Interim division of land and soil types

The Wilson and Henderson-Sellers datasets have a resolution of 1°. They are divided into 53 vegetation and 21 soil types and both primary and secondary vegetation categories are provided. For testing purposes this was considered to be a rather large number of categories to work with so that as an interim measure 3 soil textural classes were defined (as in section 3) and 9 land/vegetation categories. This was deemed to be

realistic as a substantial number of Wilson and Henderson-Sellers categories accounted for much less than 1% of all grid squares. Future work will use the Wilson and Henderson-sellers data sets directly.

The relationship between the code numbers of the Wilson and Henderson-Sellers land type categories and those used in our work is given in table 5.1. The relationship between code numbers and land type is given in table 5.2 along with parameter values used in the experiments (unless stated otherwise).

Parameter values have been taken from the following sources: Surface resistance from Thompson et al (1982), Haldin et al (1984) and Lockwood (1985); root depth and surface roughness from Eagleson (1970) and snow albedo from Matthews (1984) and Robinson and Kukla (1984).

Table 5.1 Relationship between land type categories of Wilson and Henderson-Sellers and those of Warrilow.

W and H-S	W	W and H-S	W
00	Water	31	5
01	Water	32	4
02	8	33	4
03	Ice	34	5
04	8	35	5
05	8	36	6
		37	4
10	1	38	-
11	2	39	5
12	1	40	5
13	2	41	5
14	2	42	-
15	2	43	4
16	3	44	4
17	2	45	3
18	1	46	2
19	1	47	3
20	1	48	4
21	2	49	4
22	-	50	1
23	2	51	2
24	2	52	1
25	1	61	9
26	2	62	9
27	3	70	7
28	3	71	6
29	-	72	-
30	5	73	6
		80	6

Table 5.2 Land Type Parameters

Type	Index	Vegetated Fraction,	Root Depth, D. (m)	Albedo Snow Free	Albedo Deep Snow	Stomatal Resistance r_s. (sm^{-1})	Surface Roughness, z_o. (m)	Canopy Capacity S_m. (m)	Vegetation infiltration enhancement factor, β_v
Forest	1	0.90	1.50	0.14	0.25	150.0	2.0000	0.0025	6.0
Woodland	2	0.90	1.30	0.16	0.40	100.0	1.5000	0.0020	4.0
Scrubland	3	0.85	1.20	0.17	0.60	100.0	0.1400	0.0017	3.0
Tall grass or crops	4	0.85	1.00	0.20	0.60	60.0	0.0600	0.0015	2.0
Short grass or crops	5	0.85	0.60	0.20	0.80	50.0	0.0200	0.0010	1.5
Semi desert	6	0.50	0.40	0.25	0.80	100.0	0.0050	0.0005	1.0
Desert	7	0.01	0.10	0.30	0.80	100.0	0.0003	0.0002	1.0
Swamp	8	0.50	2.00	0.15	0.80	0.0	0.0010	0.0010	1.0
Tundra	9	0.80	0.40	0.17	0.80	100.0	0.0200	0.0002	1.0

Table 5.3 Soil Type Parameters

Type (Texture)	Index	Wilting Point, θ_w	Critical Point, θ_c	Field Capacity θ_f	Saturation θ_s	Exponent c	Saturated Conductivity K_s (ms^{-1} (mmh^{-1}))	Heat Capacity ($Jm^{-3}K^{-1}$)	Heat Conductivity ($Jm^{-1}K^{-1}s^{-1}$)
Test	1	0.080	0.130	0.230	0.445	6.6	3.611×10^{-6} (13.0)	2.34×10^{6}	0.56
Coarse	2	0.055	0.087	0.150	0.420	5.0	8.056×10^{-6} (29.0)	1.92×10^{6}	0.49
Medium	3	0.105	0.170	0.290	0.460	8.0	1.806×10^{-6} (6.5)	2.22×10^{6}	0.47
Fine	4	0.180	0.250	0.400	0.490	11.0	3.611×10^{-7} (1.3)	2.87×10^{6}	0.73

Soil parameters are summarised in table 5.3, as derived in section 3. Thermal characteristics have also been included based on data given by Van de Griend et al (1985). These were derived after most of the experiments discussed in section 6 and so are not used in any of these.

5.4 Conclusions

Land surface and soil parameters have been assigned to 9 broad categories of land type and 3 soil textural classes. A global distribution on a 1° x 1° resolution was derived using the archive of Wilson and Henderson-Sellers (1985) as a basis for testing the sensitivity of the AGCM to variable surface characteristics. Although highly simplified the simple land types have enough variability to test the sensitivity of the atmospheric models to variations in vegetation and soil. In this report a sensitivity study has been carried out for Europe using the ODM and the results are summarised in section 7. Time did not allow AGCM experiments to be carried out with spatially varying land surface or soil types, although the AGCM is currently used with a variable albedo data set based on Wilson and Henderson-Seller's archive. Future research needs to ascertain which parameters are required and to what degree of precision and to investigate the viability of satellite derived data.

5.5 References

Bolle, H.J. and Rasool, S.I. 1985 Development of the implementation plan for the International Satellite Land-Surface Climatology Project. WMO/TD- No 46., WCP94, World Meteorological Organization.

Eagleson, P.S. 1970 Dynamic Hydrology, McGraw Hill, New York.

Haldin, S., Saugier, B., and Pontailler J.Y. 1984 Evapotranspiration of a deciduous forest: simulation using routine meteorological data. Journal of Hydrology, 75, 323-341.

Lockwood, J.G. 1985 World Climate Systems Edward Arnold, London.

Matthews, E. 1984 Prescription of land-surface boundary conditions in GISS GCMII: A simple method based on high-resolution vegetation data bases. NASA Technical Memorandum 86096. Goddard Space Flight Center Institute for Space Studies New York.

Robinson, D.A. and Kukla, G. 1984 Albedo of a dissipating snow cover. Journal of Clim. and Applied Met., 23, 1626-1634.

Thompson, N., Barrie, I.A. and Ayles, M. 1982 The Meteorological Office rainfall and evaporation calculation system: MORECS (July 1981). Hydrological Memorandum No. 45. Meteorological Office, Bracknell.

Van de Griend, A.A., Camillo, P.J. and Gurney, R.J. 1985 Discrimination of soil physical parameters, thermal inertia and soil moisture from diurnal surface temperature fluctuations. Water Res. Res., 21, 997-1009.

Wilson, M.F. and Henderson-Sellers, A. 1985 A global archive of land cover and soils data for use in General Circulation Climate Models. Journal of Climatology, 5, 119-143.

6. Parametrization of Land Surface Temperatures

6.1 Introduction

6.2 General relationships controlling soil temperatures and heat exchange at the Earth's surface

6.3 Analysis of the behaviour of land surface temperature parametrizations

- 6.3.1 Solution of the basic equations and a framework for analysis
- 6.3.2 Amplitude phase response of a single layer
- 6.3.3 The force restore models

6.4 Parametrization of surface temperatures using multi-layer models

- 6.4.1 General equations
- 6.4.2 Amplitude phase response of a multi-layer model
- 6.4.3 Particular models
- 6.4.4 Initialisation

6.5 One dimensional model studies

- 6.5.1 Introduction
- 6.5.2 Results of experiments
- 6.5.3 Conclusions

6.6 AGCM studies of soil temperatures

- 6.6.1 Introduction
- 6.6.2 Results of experiments
- 6.6.3 Conclusions

6.7 Discussion and conclusions

6.8 References

Appendix 6 Derivation of λ and C

6. Parametrization of Land Surface Temperatures

6.1 Introduction

The modelling and parametrization of any surface process can be difficult due to the large variability of surface characteristics (eg morphology, vegetation, soil type, soil moisture etc) and the variability of weather on a local scale which in turn affects and is affected by the surface characteristics. On a numerical model grid scale detailed modelling of surface processes is unlikely to be a viable option. The aim should be to describe adequately the processes which affect the general circulation and major mass and heat exchanges at the surface. Most studies of surface heating have been on a micrometeorological scale and it is not obvious that relationships which have been derived for largely homogeneous situations are necessarily applicable to a large heterogeneous area (Dooge (1982)). In modelling surface temperatures it is considered necessary to take into account long term temperature fluctuations due to slow temperature changes of deeper layers as well as the more rapid temperature changes experienced at the surface. The present UK Meteorological Office scheme (MO scheme) treats the land surface as a single slab of constant heat capacity and homogeneous temperature, 'forced' by heat input at the surface. It implicitly takes into account the heat flux to and from deeper layers, related to diurnal forcing. However, because of the limited heat capacity of the slab, the scheme tends to amplify long period temperature oscillations (such as the annual cycle) and attenuate sub-daily oscillations relative to the true situation. The phase difference between the forcing flux and the temperature wave is also modelled incorrectly. Carson (1982) gives a useful review of land temperature parametrization schemes and has proposed (unpublished) an extension of the Deardorff 'force restore' scheme to take account of the annual cycle (Deardorff (1978)). This paper looks at the amplitude and phase response of Carson's proposed scheme along with related schemes and compares them to the behaviour of an multi-layer model.

It is found that the 'force restore' type of scheme has some limitations and that a better response can be achieved using a 4-level soil model.

6.2 General relationships controlling soil temperatures and heat exchange at the Earth's surface

For any solid body the flow of heat is determined by the relations

$$\underline{G} = -\lambda \nabla T \qquad (6.1)$$

$$\frac{\partial T}{\partial t} = -{}^{1}/_{C}\, \nabla . \underline{G} \qquad (6.2)$$

where G is the heat flux and T the temperature. λ is the conductivity for heat and C is volumetric specific heat, also referred to in the text as

heat capacity. ∇ is the usual differential operator. Eqs. 6.1 and 6.2 may be combined to give the following

$$\frac{\partial T}{\partial t} = \frac{\lambda}{C} \nabla^2 T + \frac{1}{C} \nabla\lambda.\nabla T \qquad (6.3)$$

In these equations it is not assumed that λ or C are invariant with respect to time or space. At the earth's surface variations in soil types and soil moisture will affect the values of C and λ so that they are unlikely to be homogeneous. Furthermore, movement of water in the soil can bring about changes in heat content, capacity and conductivity; phase changes of water can produce heat sources and sinks within the soil, and so there is considerable complexity in the thermal behaviour of the soil. However, in AGCM modelling a number of simplifying assumptions have to be made which enable a tractable solution of Eqs. 6.1 to 6.3 to be found. These assumptions will be discussed in turn.

(a) Homogeneity

An important simplification is to assume that soil grid scale characteristics may be treated as being homogeneous, ie λ and C are invariant with respect to time and space. In fact this condition could be relaxed slightly in finite difference schemes by allowing λ and C to vary with time. Lettau (1954) in a treatment of soil temperatures has shown that local time and space dependence of λ and C accounts for surface temperature fluctuations which are harmonics of the daily cycle. Nevertheless the amplitudes of the harmonics are likely to be considerably less than those of the daily cycle and are unlikely to be coherent over an area the size of a model grid square. By assuming that λ and C are spatially constant, Eq. 6.3 becomes the better known diffusion equation

$$\frac{\partial T}{\partial t} = \frac{\lambda}{C} \nabla^2 T \qquad (6.4)$$

(b) One dimensional heat flow

In general, it is observed that the strongest temperature gradients in the soil are perpendicular to the surface. Although local temperature gradients will exist in the horizontal they are insignificant compared with those in the vertical. Therefore it is generally assumed in AGCM modelling that only vertical heat flow and temperature gradients are significant and that soil heat flow between grid squares will be negligible.

(c) Boundary conditions

It is usually assumed that there is some deep soil temperature which is constant and that the surface temperature varies in a periodic (if not exactly sinusoidal) manner with periodicities of 1 day and 1 year being important. These boundary conditions have led to the

development of an important class of schemes, originally proposed by Bhumralkar (1975), and Deardorff (1978) which will be looked at in detail in section 6.3. An alternative condition, more appropriate for climate modelling, is to set the heat flux across the lowest boundary to be zero.

(d) The solid body assumption

In most models the land is treated as a solid body in which heat diffuses in a simple way determined by Eqs. 6.1, 6.2 and 6.4, and the surface is treated as a simple boundary at which heat and moisture are exchanged with the atmosphere. Vegetation is treated implicitly (ie in so far as it affects the values of roughness, albedo, surface storage and the hydrological variables etc) rather than explicitly as a layer in which complex interactions are taking place. More recently, attempts to treat vegetation explicitly (having its own characteristics and physical processes) have been made (see for example Deardorff (1978), Mintz et al (1983)).

The temperature at the top surface of a vegetation canopy is not necessarily the same as that at the surface of the soil. So for this and other reasons related to surface fluxes and hydrology, it will be necessary in the future to consider vegetation explicitly in a parametrization, especially if vegetation change experiments are envisaged. On the other hand the effect of a solid body assumption on heat fluxes is likely to be small as a canopy has a very low heat capacity.

(e) Unique surface temperature assumption.

Most, if not all, AGCMs use a single surface temperature to calculate both the upward longwave radiative flux and the turbulent fluxes of heat and moisture. However, the true surface temperature can be rather high (locally up to 80°C in the tropics), and a good temperature parametrization should reflect this. Such a temperature will be appropriate for calculation of the long wave radiative flux, but may not necessarily be appropriate for calculation of boundary layer fluxes which are based on the assumption of turbulent transport. Chang (1958) quotes some observed lapse rates of about 10^3 times the dry adiabatic lapse rate (Γ) in the first few feet and $2 \times 10^5 \times \Gamma$ in the first centimetre of the atmosphere. Such high gradients can exist because the predominant processes for heat transport very near the surface are conduction and diffusion rather than turbulent transport. Further improved surface temperature parametrizations may thus require parallel development of boundary layer schemes.

These foregoing assumptions allow the treatment of surface temperatures to be made in a straightforward manner. In the next section various surface temperature parametrizations which have been considered for use in the MO AGCM will be analysed with regard to their amplitude and phase response characteristics and their applicability in AGCMs.

6.3 Analysis of the behaviour of land surface temperature parametrizations

6.3.1 Solution of the basic equations and a framework for analysis.

Rewriting Eqs. 6.1, 6.2 and 6.4 in one dimension gives:

$$G = -\lambda \partial T/\partial z \quad (6.5)$$

$$\partial T/\partial t = -1/C \partial G/\partial z \quad (6.6)$$

$$\partial T/\partial t = \lambda/C \partial^2 T/\partial z^2 \quad (6.7)$$

From Jacobsen and Heise (1982) a general solution of Eqs. 6.5 to 6.7 is given by (here taking z downwards as positive):

$$T = \bar{T} + \sum_j \Delta T_j \, e^{-z/\delta_j} \, e^{i(\omega_j t - z/\delta_j)} \quad (6.8)$$

and $$G = \lambda(1+i)\sum_j \frac{\Delta T_j}{\delta_j} e^{-z/\delta_j} e^{i(\omega_j t - z/\delta_j)} \quad (6.9)$$

where $\delta_j = \sqrt{(\frac{2\lambda}{C\omega_j})}$ is the e-folding depth at frequency ω_j,

ΔT_j the amplitude of the jth temperature wave and $i = \sqrt{-1}$. Now for a single forcing frequency ω, and considering the surface (z=0) temperatures and fluxes, Eqs. 6.8 and 6.9 become, omitting subscript j,

$$T = \bar{T} + \Delta T e^{i\omega t} \quad (6.10)$$

and $$G = \frac{\lambda(1+i)\Delta T e^{i\omega t}}{\delta} \quad (6.11)$$

We may also define $$G = \Delta G e^{i\omega t} \quad (6.12)$$

Thus $$\Delta T = \frac{(1-i)\delta \Delta G}{2\lambda} \quad (6.13)$$

$$= |\Delta T| e^{i\chi} \text{ where } \chi \text{ is a phase constant} \quad (6.14)$$

For any surface temperature parametrization let the surface flux be G given by Eq. 6.12 and the surface temperature be T' in Eq. 6.15.

$$T' = \bar{T}' + \Delta T' e^{i\omega t} \quad (6.15)$$

where $$\Delta T' = |\Delta T'| e^{i\chi'} \quad (6.16)$$

Then the ratio (A) at frequency ω, of the parametrized solution to the analytical solution is given from Eqs. 6.14 and 6.16 as

$$A = \frac{\Delta T'}{\Delta T} = \frac{|\Delta T'|}{|\Delta T|} e^{i(\chi' - \chi)} \quad (6.17)$$

The temperature amplitude response of the parametrization is defined in Eq. 6.18

$$|A| = \left|\frac{\Delta T'}{\Delta T}\right| \tag{6.18}$$

and the phase response ARG(A) in Eq. 6.19

$$ARG(A) = \chi' - \chi \tag{6.19}$$

From the above it is apparent that surface temperatures may respond to forcing at all frequencies. However since all models are necessarily limited, there must be some degradation of the response over some ranges of frequencies. The framework given in Eqs. 6.10 to 6.19 allow the amplitude and phase response of any parametrization to be studied and designed for optimum response defined by an a priori requirement. There are broadly speaking three categories of surface temperature parametrization.

(i) a single slab, eg as in the MO AGCM.

(ii) variations on the force restore method (eg Deardorff (1978)).

(iii) finite difference, n-layer schemes (eg Benoit (1976)).

Each of these schemes will be studied in turn.

6.3.2 Amplitude phase response of a single layer

The Meteorological Office AGCM and Numerical Weather Prediction (NWP) models have used a single layer to specify soil temperatures. In these models the layer has a heat capacity equivalent of 5 cm of water. The equation is of the form given in Eq. 6.20.

$$\frac{\partial T_1}{\partial t} = \frac{G}{C\Delta z_1} \tag{6.20}$$

where T_1 is surface temperature and Δz_1 is the depth of the layer. Substituting for G from Eq. 6.11 and T_1 from Eq. 6.15 gives the amplitude and phase response as follows:

$$|A| = \sqrt{(\omega_1/2\omega)} \qquad = \sqrt{(P/2P_1)} \tag{6.21}$$

$$ARG(A) = -\pi/4 \tag{6.22}$$

where P is period of forcing flux. If we set $P_1 \equiv {}^1/_2$ day then for surface heat flux forcing of period 1 day, $|A| = 1$. However for P = 365 days $|A| = 19.1$. Therefore we might expect the MO model to amplify the annual cycle. In fact, the amplification is far smaller, as the surface heat flux is not independent of surface temperature; there is strong negative feedback due to turbulent fluxes and upward longwave emission. The implied temperature errors appear as errors in the turbulent fluxes especially during daytime and the maximum part of the annual cycle. This aspect will be dealt with in more detail in section 6.5.

$|A|$ and ARG(A) are shown as a function of period in figure 6.1.

6.3.3 The force restore models

Deardorff (1978) proposed Eqs. 6.23 and 6.24

$$\partial T_o/\partial t = 2\,G\,/C\delta_o - \omega_o(T_o - T_m) \tag{6.23}$$

$$\partial T_m/\partial t = G\,/C\delta_m \tag{6.24}$$

where T_o is taken as the surface temperature, T_m is the time mean of surface temperature over a period greater than one day, G is the flux directed downwards at the surface and ω_o is the angular equivalent to a period of 1 day. δ_o and δ_m are the e-folding depths for the daily cycle and another cycle longer than one day. The amplitude and phase response of the model is shown (after Jacobsen and Heise (1982)) in figure 6.1. Carson (1982, unpublished) suggested that a third equation be introduced so that the system becomes Eq. 6.23 plus Eqs. 6.25 and 6.26.

$$\partial T_m/\partial t = 2G\,/C\delta_m - \omega_m(T_m - T_k) \tag{6.25}$$

$$\partial T_k/\partial t = G\,/C\delta_k \tag{6.26}$$

where T_m is the mean over at least one day and ω_m, δ_m corresponds to the annual cycle and T_k the temperature of some slowly varying deeper layer with associated δ_k.

Substitution of G, T_o, T_m, T_k in terms of Eqs. 6.12 and 6.15 lead to the following:

$$i\omega\Delta T_o' e^{i\omega t} = \frac{2\Delta G\, e^{i\omega t}}{C\delta_o} - \omega_o(\Delta T_o' - \Delta T_m')e^{i\omega t} \tag{6.27}$$

$$i\omega\Delta T_m' e^{i\omega t} = \frac{2\Delta G\, e^{i\omega t}}{C\delta_m} - \omega_m(\Delta T_m' - \Delta T_k')e^{i\omega t} \tag{6.28}$$

$$i\omega\Delta T_k' e^{i\omega t} = \frac{\Delta G\, e^{i\omega t}}{C\delta_k} \tag{6.29}$$

Elimination of $\Delta T_m'$ and $\Delta T_k'$ from Eqs. 6.27 to 6.29 and substitution of ΔG_o from Eq. 6.13 leads after lengthy algebra to an expression for $\Delta T_o'$ in terms of ΔT given in Eq. 6.30.

$$(\omega_o^2+\omega^2)(\omega_m^2+\omega^2)\Delta T_o'$$

$$= \Delta T \{[\sqrt{(\omega\omega_o)}(\omega^2+\omega_m^2)(\omega+\omega_o) + \sqrt{(\omega\omega_m)}\ \omega_o(\omega_o\omega_m-\omega^2+\omega(\omega_o+\omega_m))$$

$$+ \omega_o\omega_m \sqrt{(\omega_k/\omega)}(\omega_o\omega_m-\omega^2-\omega(\omega_o+\omega_m))/2]$$

$$+ i [\sqrt{(\omega\omega_o)}\ (\omega^2+\omega_m^2)(\omega_o-\omega)+\sqrt{(\omega\omega_m)}\ \omega_o(\omega_o\omega_m-\omega^2-\omega(\omega_o+\omega_m))$$

$$- \omega_o\omega_m \sqrt{(\omega_k/\omega)}\ (\omega_o\omega_m-\omega^2+\omega(\omega_o+\omega_m))/2]\} \qquad (6.30)$$

Setting ω_o appropriate to a period of 1 day, ω_m to one year and ω_k to 10 years the amplitude and phase response as a function of ω was computed and is also shown in figure 6.1. It would appear that the Carson scheme has very similar characteristics to the scheme proposed by Jacobsen and Heise (1982) (not shown), except at low frequencies where the former's response tends to infinity and the latter's to zero.

The force restore models have the obvious advantage that the amplitude and phase response are correct at preset, dominant forcing frequencies and there is an improvement over a wider range of frequencies. However there is still some attenuation at high and intermediate frequencies and amplification at low frequencies. Attenuation of high frequency forcing may be quite realistic since such forcing would be unlikely to be in phase and would cancel when averaged over an area the size of AGCM grid square. Attenuation at around 20 days may be a more significant shortcoming as this is related to fluctuations on a synoptic time scale. At low frequencies all models behave similarly and the temperature response is amplified theoretically. In fact the amplification is more likely to appear as an error in the turbulent fluxes, which for forcing of longer periods than one year, will be small unless very long integrations involving climatic change are involved. Jacobsen and Heise (1982) discuss long period forcing in more detail. In fact low frequency amplification is a characteristic of any finite model which has a zero heat flux at the lower boundary. The alternative is a fixed temperature at the lower boundary. This leads to complete attenuation at low frequencies, and is less acceptable in climate modelling as it effectively introduces an infinite source/sink of heat in the soil.

6.4 Parametrization of surface temperature using multilayer models

6.4.1 General equations

The model is defined in figure 6.2. It is convenient to express each layer as a fraction of the surface layer; ie

$$\Delta z_r = \alpha_r \Delta z_1 \qquad (6.31)$$

where α_r is effectively a normalised depth.
From Eqs. 6.1 and 6.2 we can write, putting the differential with respect to z in finite difference form:

$$\frac{\partial T_1}{\partial t} = A_1\ G + B_1(T_2-T_1)$$

$$\frac{\partial T_2}{\partial t} = A_2 (T_2 - T_1) + B_2(T_3 - T_2)$$

and $$\frac{\partial T_r}{\partial t} = A_r (T_r - T_{r-1}) + B_r(T_{r+1} - T_r) \qquad (6.32)$$

In general A_r and B_r are defined in Eq. 6.33.

$$A_r = -\frac{2\kappa}{\Delta z_r(\Delta z_r + \Delta z_{r-1})} \quad , 2 \leq r \leq n$$

$$B_r = \frac{2\kappa}{\Delta z_r(\Delta z_r + \Delta z_{r+1})} \quad , 1 \leq r \leq n \qquad (6.33)$$

and $A_1 = 1/C\Delta z_1$

where the diffusivity $\kappa = \lambda/C$.

Substituting for Δz_r from Eq. 6.31 and specifying Δz_1 in terms of a characteristic frequency ω_1, whose e-folding depth is Δz_1 (defined with reference to Eq. 6.9) then Eq. 6.33 can be rewritten as in Eq. 6.34.

$$A_r = -\frac{\omega_1}{\alpha_r(\alpha_r + \alpha_{r-1})} \quad , 2 \leq r \leq n$$

$$B_r = \frac{\omega_1}{\alpha_r(\alpha_r + \alpha_{r+1})} \quad , 1 \leq r \leq n \qquad (6.34)$$

and $$A_1 = \sqrt{(\omega_1/2)}/\Upsilon \qquad (6.35)$$

where Υ is the thermal inertia defined as

$$\Upsilon = \sqrt{(\lambda C)} \qquad (6.36)$$

There are two possibilities for T_n. If we assume a zero heat flux condition at the bottom of the soil layers, then $B_n = 0$ (class 1 model). Otherwise $B_n \neq 0$ and we must prescribe a bottom temperature T_{n+1} which may be constant or allowed to vary climatologically (class 2 model). For climate simulations it is more acceptable to set $B_n = 0$, otherwise the bottom level becomes an infinite source or sink of heat, as noted previously.

6.4.2 Amplitude phase response of a multi-layer model

The amplitude phase response can be derived by substituting for G and T_1 to T_n in Eq.6.32 using Eqs. 6.12 and 6.15.

$$i\omega\Delta T_1' = A_1\Delta G + B_1 (\Delta T_2' - \Delta T_1')$$

$$i\omega\Delta T_r' = A_r(\Delta T_r' - \Delta T_r'_{-1}) + B_r(\Delta T_r'_{+1} - \Delta T_r')$$

$$i\omega\Delta T_n'_{-1} = A_n(\Delta T_n' - \Delta T_n'_{-1}) + B_n(-\Delta T_n') \qquad (6.37)$$

assuming T_{n+1} to be constant.

Using Eq. 6.13 Eqs. 6.37 may be solved for $\Delta T_1'$ in terms of ΔT by eliminating $\Delta T_r'$ (where $2 \leq r \leq n$) and substituting for ΔG.

We define $\Omega_r = \Delta T_r'/\Delta T_{r-1}'$

$$= \frac{A_r}{\{A_r + B_r\,(\Omega_{r+1}-1) - i\omega\}} \qquad (6.38)$$

Substitution of A_r and B_r gives

$$\Omega_r = \frac{(\alpha_r + \alpha_{r+1})}{(\alpha_r+\alpha_{r+1}) - (\alpha_r+\alpha_{r-1})(\Omega_{r+1}-1)+i\zeta\alpha_r(\alpha_{r+}\alpha_{r+1})(\alpha_r+\alpha_{r-1})} \qquad (6.39)$$

where $\zeta = \omega/\omega_1$ is a normalised frequency.

We note that for class 2 models

$$\Omega_n = \frac{(\alpha_n + \alpha_{n+1})}{(\alpha_n+\alpha_{n+1})+(\alpha_n+\alpha_{n-1}) + i\zeta\alpha_n\,(\alpha_n+\alpha_{n+1})(\alpha_n+\alpha_{n-1})} \qquad (6.40)$$

and for class 1

$$\Omega_n = \frac{1}{1 + i\zeta\alpha_n(\alpha_n+\alpha_{n-1})} \qquad (6.41)$$

Now at the surface

$$\Delta T_1' = A_1\Delta G/(B_1(1-\Omega_2)+i\omega) \qquad (6.42)$$

which on substituting for ΔG, A_1, B_1, gives

$$A = \frac{\Delta T_1'}{\Delta T} = \frac{\sqrt{\zeta}(1+\alpha_2)}{(1-i)(1-\Omega_2 + i\zeta(1+\alpha_2))} \qquad (6.43)$$

and since Ω_2 is a function of all Ω_r; $3 \leq r \leq n$, (Eq. 6.39) A is defined.

Therefore A is a function of ζ and α_r; $2 \leq r \leq n$ and the amplitude and phase response of the multilayer scheme is independent of λ and C, or the actual depths of the layers. In fact, as will be seen in section 6.4.2 it is the normalised depths α_r which determine the shape of the response and the relative range of frequencies over which $|A| \sim 1$ and $ARG(A) \sim 0$; and ω_1 determines the absolute position of the response curves on the frequency axis. Also, by defining A_r, B_r as in Eq. 6.34, Eqs. 6.32 are independent of λ and C, except for A_1 which is dependent on the product of λ and C. This has the useful property that in AGCM modelling, the same set of equations may be used globally without using different depths and only the thermal inertia (Υ) needs to vary spatially, since only surface temperatures need to be predicted. If soil temperatures at a given level are required (eg for diagnostic purposes) these can be computed given λ, C and ω_1.

It should be noted at this point, that the amplitude phase response approach tells us the behaviour of a scheme relative to an analytical solution. Its actual behaviour in a modelling context depends on λ, C and other aspects of the model, eg boundary layer parametrizations, etc.

6.4.3 Particular models

Having derived the general equations for a multilayer homogeneous soil model and its response function, it is now necessary to find a suitable scheme with optimum response for predicting surface temperatures in an AGCM context. The a priori requirements are a "good" response in the frequency range between about $^1/_2$ day to 1 year, but using the least number of levels. Various models were tried but only a few of these will be presented here to give some idea of the behaviour of such models.

Owing to the exponential decay of surface temperature waves as they penetrate downwards a suitable class of models would possibly be those where

$$\alpha_r = \alpha_0^{r-1} \quad \text{where } \alpha_0 \text{ is a constant.}$$

The frequency response curves for such models for different numbers of levels, n, and various α_1 are given in figure 6.3 to figure 6.5.

It would appear that n=4 at least is required. It is interesting to note that increasing n does not change the response at higher frequencies. $\left|\frac{A}{A}\right| = 1$ slightly disappointing feature is the size of the oscillations about and the slow upward trend discernible from low to high periods. It was found possible to improve performance by ad hoc adjustment of the ratios of one level to the next such that the oscillations about $|A| = 1$ were reduced. Two 4-level schemes were derived with characteristics as given in Table 6.1 and response as given in figure 6.6. The MKI version has a smoother response than the MKII although it is acceptable over a shorter frequency range. These models have been used in ODM and AGCM studies (sections 6.5 and 6.6) and have performed satisfactorily. The MO single layer equivalent is also given in Table 6.1.

Table 6.1

Soil Temperature Parametrizations: model parameters

Scheme	P_1 (days)	ω_1 (s^{-1})	No. of Layers	1,, n	Δz_1,,Δz_n (m)	Other Remarks
MO Equivalent	0.5	1.4544×10^{-4}	1	1.0	0.106	λ=1.546 J $m^{-1}s^{-1}K^{-1}$ C=2.061x10^6J $m^{-3}K^{-1}$
MK I	0.1467	4.9572×10^{-4}	4	1.0	0.055	For
				3.89	0.214	experiment
				10.89	0.599	VSAS (section 6.6)
				25.05	1.378	λ=1.8 J $m^{-1}s^{-1}K^{-1}$ C=2.4 x 10^6J $m^{-3}K^{-1}$
MK II	0.2048	3.5509×10^{-4}	4	1.0	0.065	For experiment
				3.908	0.254	VSAT (section 6.6)
				14.05	0.913	λ=1.8 J $m^{-1}s^{-1}K^{-1}$
				44.65	2.902	C=2.4 x 10^6J $m^{-3}K^{-1}$

6.4.4 Initialisation

The amplitude and phase response shown in the previous section, assumes that the model has been correctly initialised. This is straightforward if surface forcing is regular but in any practical application there will be a period of adjustment. In this work it will be assumed that the diurnal and annual temperature waves are regular and by far the most important. For a regular sinusoidal forcing flux at the surface, from Eq. 6.8 we have for T_r at level r

$$T_r = \bar{T} + \Delta T_d \exp(-z_r/\delta_d)\exp(i(\omega_d t - z_r/\delta_d)) + \Delta T_a \exp(-z_r/\delta_a)\exp(i(\omega_a t - z_r/\delta_a)) \quad (6.44)$$

where subscripts a and d refer to the diurnal and annual cycles respectively. ΔT is the amplitude of the surface temperature at each frequency.

Introducing reference times h_o, d_o and taking the real parts of Eq. 6.44 and ignoring fractions of a day for the annual cycle we have

$$T_r = \bar{T} + \Delta T_d \exp(-z_r/\delta_d)\cos(2\pi(h-h_o)/h_d - z_r/\delta_d)$$

$$+ \Delta T_a \exp(-z_r/\delta_a)\cos(2\pi(d-d_o)/d_a - z_r/\delta_a) \quad (6.45)$$

where h and d are the local hour and day numbers and h_o and d_o are the times of the maxima of each cycle respectively. Note that d_o will vary globally and may not be well defined in some tropical regions. h_d is the number of hours per day and d_a is the number of days per year, being 365 in the ODM and 360 in the AGCM.

ΔT_a and $\bar{T}$ can be derived from climate statistics for simplicity and ΔT_d can be derived from statistics or the previous daily range in a weather forecasting application. Initialisation of the diurnal temperature is probably unnecessary in AGCM applications. For an initialisation to work well, it is necessary that appropriate values of λ and C are used.

Eq. 6.45 is defined in terms of soil depths, but as we wish to work in terms of non-dimensional, normalised depths (α_r) we can redefine Eq. 6.45 by substituting for z_1, δ_d and δ_a in terms of ω_1, ω_d and ω_a. Eq. 6.45 then becomes

$$T_r = \bar{T} + \Delta T_{dr} \exp(-\xi_{dr})\cos(2\pi(h-h_o)/h_d - \xi_{dr})$$

$$+\Delta T_{ar}\exp(-\xi_{ar})\cos(2\pi(d-d_o)/d_a - \xi_{ar}) \qquad (6.46)$$

where $\xi_{dr} = \sqrt{(\omega_d/\omega_1)}\ \{\sum_{i=1}^{r-1} \alpha_i + \alpha_r/2\}$

and $\xi_{ar} = \sqrt{(\omega_a/\omega_1)}\ \{\sum_{i=1}^{r-1} \alpha_i + \alpha_r/2\}$

6.5 One dimensional model studies

6.5.1 Introduction

Using the one dimensional model derived in section 2, a number of simulations for a point in southern England and in the Sahel at 15 N were carried out in order to test the soil temperature scheme. Comparisons were made between the MO model, MK I and MK II of the 4-layer model and between different thermal inertias used with the MK II model. Results are summarised in Table 6.2 for an annual cycle. It can be noted that differences between the MK I and MK II (Experiments 2 and 3) are negligible at the surface. Naturally the deeper levels are different as they apply to different layer thicknesses. In much of the following we will only consider the MK II model.

6.5.2 Results of experiments

Figure 6.7 shows the behaviour of surface temperature for one annual cycle for the ODM using the MO scheme (Experiment 1). Winter temperatures appear to be too low on average (~ -2°C compared to an observed January mean of 4.5°C) although we would expect surface temperatures to be lower than air temperatures. Certainly ground minima are lower than air minima and ground maxima exceed air maxima, especially on good radiation nights and sunny days respectively. It has not been possible to ascertain the bias between ground and air temperatures for the winter. The experiment was repeated using the same random number sequence so that atmospheric forcing was very similar but this time the 4 level temperature scheme was used. Results are

Table 6.2

Annual values from ODM integrations comparing soil temperature schemes

Location	Experiment Number	Scheme	Average Surface Temperature	Average Soil Moisture Capacity	Total Precip.	Average Net Surface Radiation	Average Sensible Heat Flux	Average Latent Heat Flux	Average Net Radiation at top of Atmos
Southern England	1	MO	8.56	10.20	673.6	54.86	12.75	42.00	-71.74
	2	MK I (γ=2078.5)	9.53	12.03	669.2	49.98	9.34	40.50	-73.38
	3	MK II (γ=2078.5)	9.49	12.09	668.3	50.51	9.43	40.37	-73.01
	4	MK II (γ=1385.6)	8.83	11.61	671.0	52.53	10.88	41.30	-73.12
Sahel	5	MO	32.00	0.43	346.0	100.54	77.42	23.11	16.06
	6	MK II (γ=1385.6)	32.30	0.44	347.8	99.60	74.48	23.49	15.64

shown in figure 6.8 (Experiment 3). It is apparent that the diurnal range is much reduced, and that mean winter temperatures have increased, mainly as a result of increased minima. Some of the difference comes from using a 4-layer model but a proportion must be due to the use of different thermal characteristics. The values for various thermal parameters used in these experiments are presented in Table 6.3. Υ was rather high in experiment 3 so another integration (Experiment 4) was carried out using a lower value thought to be more typical of northern Europe, based on some data by Van de Griend et al (1985) and Chang (1958) (see appendix 6). Results from experiment 4

Table 6.3

Thermal constants used in integrations

SOURCE	λ ($J\ m^{-1}s^{-1}K^{-1}$)	C ($J\ m^{-3}K^{-1}$)	κ ($m^2\ s^{-1}$)	Υ ($J\ m^{-2}K^{-1}s^{-1/2}$)
Louis (1984)	1.8	2.4×10^6	7.5×10^{-7}	2078.5
Appendix 6	1.2	1.6×10^6	7.5×10^{-7}	1385.6
Table 6.1	1.5386	2.0514×10^6	7.5×10^{-7}	1776.6

are shown in figure 6.9. Decreasing thermal inertia, Υ clearly leads to an increase in the diurnal range, again mainly through the minima and so generally reducing mean temperatures. The imbalance between maxima and minima occurs because there is a difference in the feedback due to turbulent fluxes. During the day the evaporative and sensible heat fluxes depend strongly on surface temperature so that any increase due to changes in λ and C will tend to be damped and appear mainly as increases in evaporation and sensible heat flux. At night, however, under radiation conditions, the turbulent fluxes become very low and do not 'restrain' the minima. Evaporation is particularly effective in damping daytime maxima as can be seen from an integration of a Sahel climate (Experiment 5, figures 6.10 to 6.12), although temperatures are also depressed due to a reduction in net radiation following increased cloudiness. The relationship between soil moisture and maximum temperatures is clear. Minima are affected much less. As an example, the behaviour of the other temperature levels is shown in figure 6.13 for the southern England location (Experiment 3), showing clearly attenuation of the surface waves with depth and increasing phase difference from the surface forcing.

The effect on the soil heat flux of adding deeper soil temperature layers can be seen in figure 6.14. The annual cycle in surface soil heat flux can be seen clearly with a net downward flow of heat in the spring and a net upward flow in the autumn. Interestingly the variance of soil heat flux also increases throughout the year. Changes in net radiative, evaporative and sensible heat fluxes are harder to see from diagrams and so the annual means are summarised in Table 6.2. The differences are rather small for this location but might be expected to be larger for locations with a larger diurnal or annual range in temperature.

It has been noted that daily minimum temperatures increased in the four layer model (by an amount depending on the value of thermal inertia) and that maxima also show a slight increase. It might have been expected that changes in the seasonal soil heat flux would have led to a cooling of the surface in spring and summer and a warming in autumn and winter. However, spring and summer cooling was not observed in these ODM experiments. It was found that the sensible and latent heat fluxes at the surface decrease in total by about 9 Wm^{-2} over the summer thereby reducing the heat exchanged to the atmosphere. This shortfall was partly compensated for by increased horizontal advection of heat and moisture (in order to maintain the reference profiles) such that there was little change in the downward longwave radiation and a small decrease in the net downward shortwave radiation at the surface. It would appear that in the ODM the decrease in turbulent fluxes was partly balanced at the surface by a increase in upward longwave radiation following the rise in surface temperatures. The difference between net radiation and turbulent fluxes then appeared as an increase in the soil heat flux. In an AGCM overall compensation of reduced turbulent fluxes by horizontal advection would not be expected to be so great and so summer cooling is likely to be observed.

6.5.3 Conclusions

Inclusion of further soil layers appears to have a substantial impact on surface temperatures particularly in correcting excessively low minima. Thermal inertia is an important parameter and to some extent determines the annual and diurnal range of temperature. A relatively small impact is made on surface fluxes for the year as a whole, although turbulent fluxes are reduced by about 9 Wm^{-2} in total during the summer.

6.6 AGCM studies of soil temperature

6.6.1 Introduction

Two AGCM studies were carried out using the MK I and MK II versions of the 4-level soil temperature scheme and with $\lambda = 1.8$ J $m^{-1}s^{-1}k^{-1}$ and $C = 2.4 \times 10^6$ J $m^{-3}K^{-1}$. The MK I version was run for 15 months (Experiment VSAS) and the MK II for 3 months (Experiment VSAT). Early versions of the soil schemes based directly on depths were used (Eqs. 6.32 and 6.33) so that it was not easy to vary λ and C. Both integrations commenced at the end of February of year 3 of a long parallel control integration whose surface temperature was calculated using a single slab with heat capacity equivalent to 5 cm of water (see section 6.3.2). Initial temperatures were given by Eq. 6.45 using only the correction for the annual cycle (which in the AGCM is 360 days in length). Unfortunately, the annual range rather than amplitude was used erroneously in experiments VSAS and VSAT, initialising the Northern Hemisphere too cold and the Southern Hemisphere too warm. However this error does not substantially affect the results of the experiments or the conclusions drawn from them. The annual temperature means and amplitudes were derived from the control integration. In the descriptions of the experiments seasonal references apply to the northern hemisphere. VSAT turned out to be very similar to VSAS and is not mentioned further.

6.6.2 Results of experiments

Figures 6.15 and 6.16 show the mean seasonal surface temperatures for summer and winter for VSAS. Differences with the control are shown in figures 6.17 and 6.18. As expected but in contrast to the ODM results, there is a reduction in summer land surface temperatures of order 1 or 2K and an increase in winter temperatures as the deeper layers are heated and cooled respectively. Siberian winter temperatures have increased markedly for reasons discussed later. Spring and autumn temperatures (not shown) were consistently cooler and warmer respectively over the Northern Hemisphere land masses. The surface flux, G, for spring and autumn is shown in figures 6.19 and 6.20 respectively and show net heating of the land in spring and release of heat in the autumn. There are interesting departures from the broad trend in temperatures. The tropics generally appear to be slightly warmer on average throughout the year and Canada appears to be colder except in the Autumn.

An increase in tropical temperatures may be due to a change in the diurnal cycle. From the ODM studies we have seen that night minima are generally higher but maxima change little or increase slightly, thereby leading to an overall increase in average temperatures. However as we have noted a high value of γ was used and use of a more appropriate lower value should offset this tendency. Overall the simulation of tropical temperatures was good.

Figures 6.21 and 6.22 show the annual range of mean monthly temperatures for the experiment and control respectively. Comparison with the observed range (Figure 6.23, Manabe et al (1979)) shows that over the tropics the simulation is fairly good but that at high latitudes there are some problems. Generally speaking the larger range over Canada is an improvement but the reduction in range over Siberia has now made the annual range too small by about 5K locally, although the position of the maximum range is better. There is also an improvement over Antarctica. The low range of annual temperatures found over Siberia may be due to a shortcoming in the AGCM's climatology; in particular the tendency for strong persistent westerlies to develop at mid-latitudes in winter with blocking occurring far less than observed. Recent work in the Meteorological Office has had some success in correcting this bias through parametrization of gravity wave drag (Slingo and Pearson (to be published)). A reduction in thermal inertia might also serve to improve the annual range of temperature.

Figure 6.24 shows the diurnal range meaned over the summer; it is much smaller than observed (Fullard and Darby (1978)); this may be due to the use of climatological cloud and too large a thermal inertia as discussed in section 6.5. The discrepancy is likely to be greatest in areas with coarse dry soils.

The effect on other model fields is generally small and systematic differences tend to be obscured by larger random differences between experiment and control, especially in the precipitation field. There are however small but detectable decreases in evaporation and sensible heat fluxes in spring and summer over the Northern Hemisphere continents and a less consistent increase in the autumn.

Figure 6.1 Amplitude/phase response of single layer and 'force restore' models.

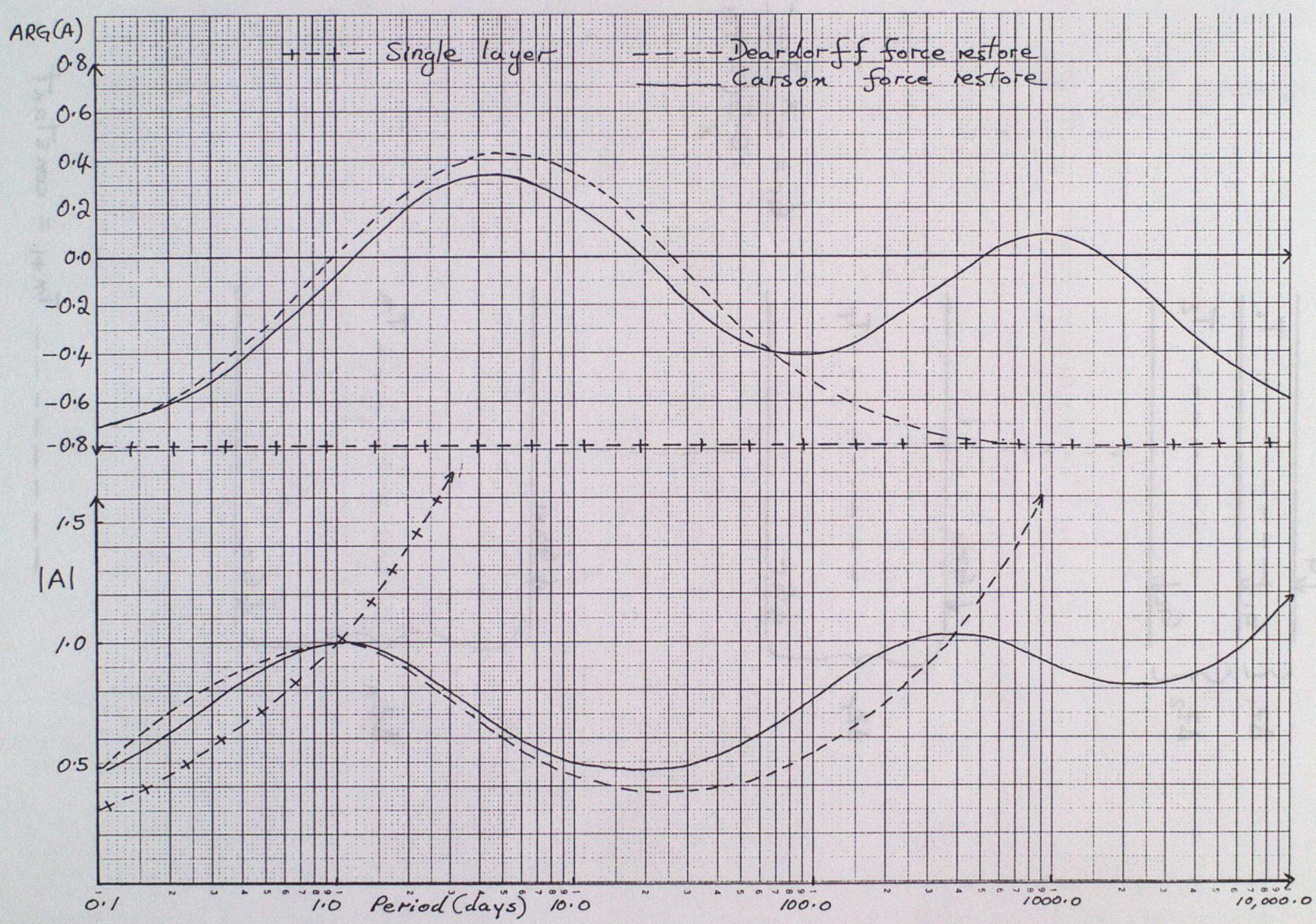

Figure 6.2 General n-layer soil temperature model (not to scale).

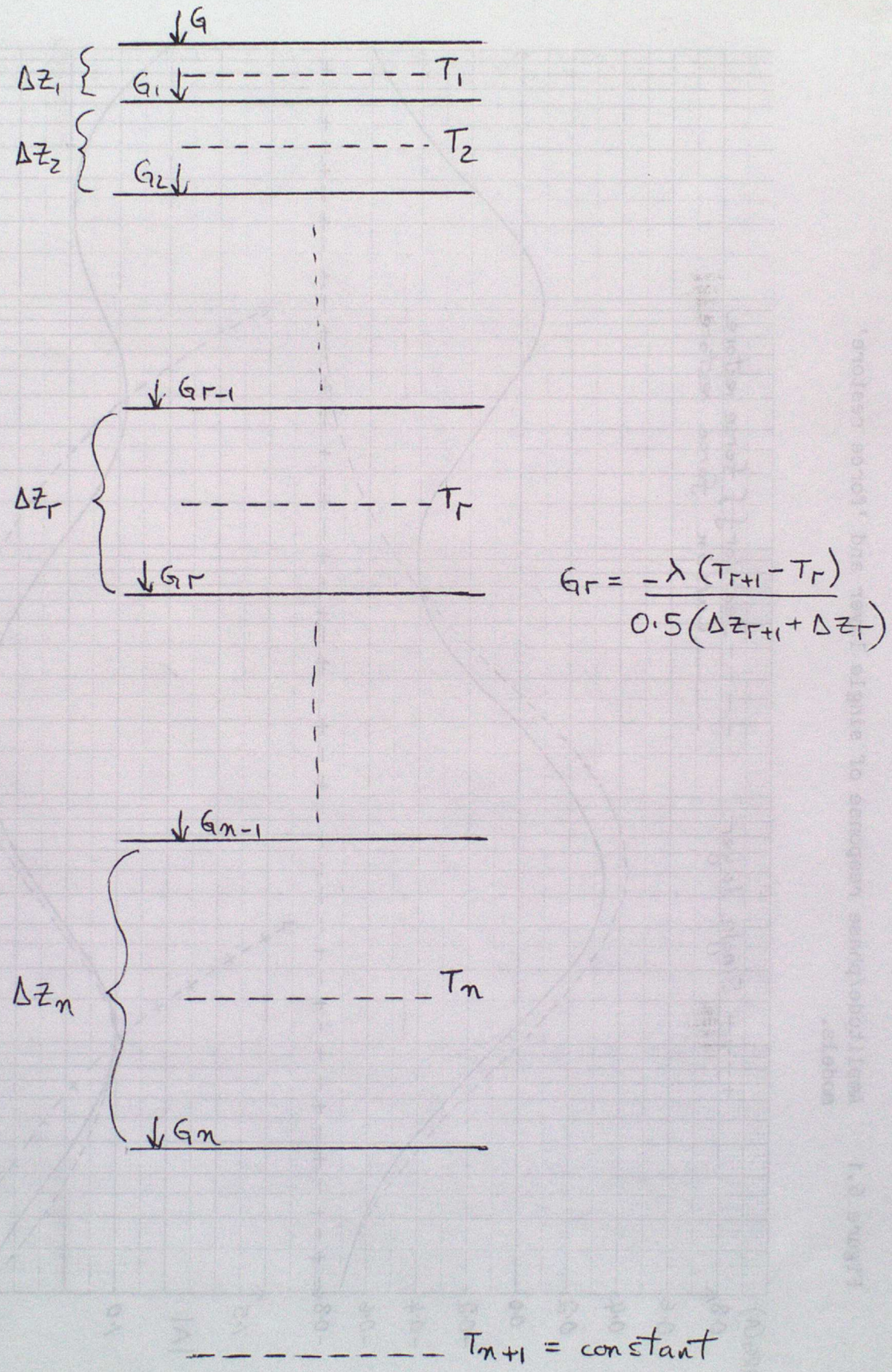

$$G_r = \frac{-\lambda (T_{r+1} - T_r)}{0.5(\Delta z_{r+1} + \Delta z_r)}$$

Figure 6.3 Amplitude/phase response of n-layer soil temperature model, $\alpha_o = 2$.

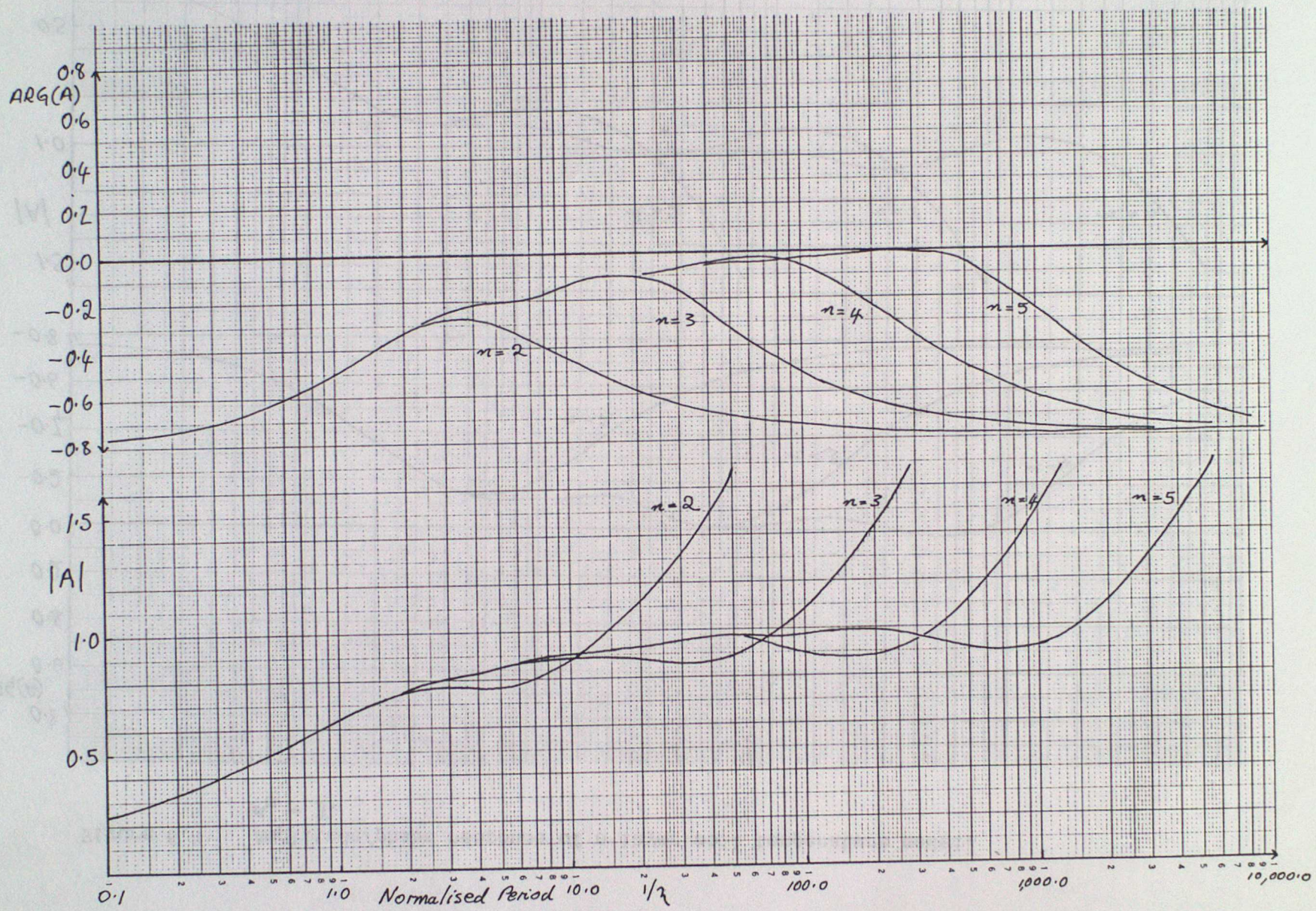

Figure 6.4 Amplitude/phase response of n-layer soil temperature model, $\alpha_0 = 3$.

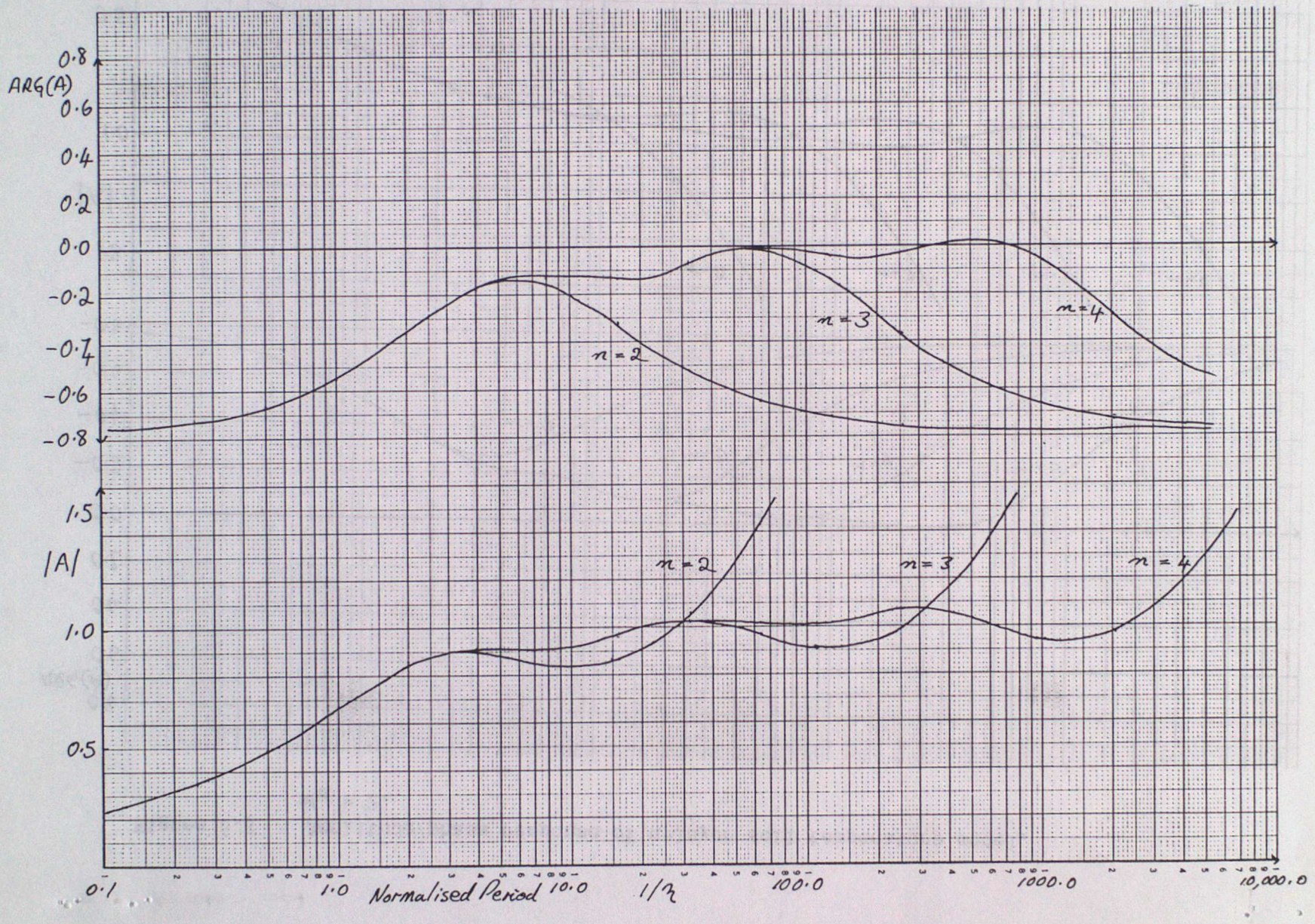

Figure 6.5 Amplitude/phase response of n-layer soil temperature model, $\alpha_0 = 4$.

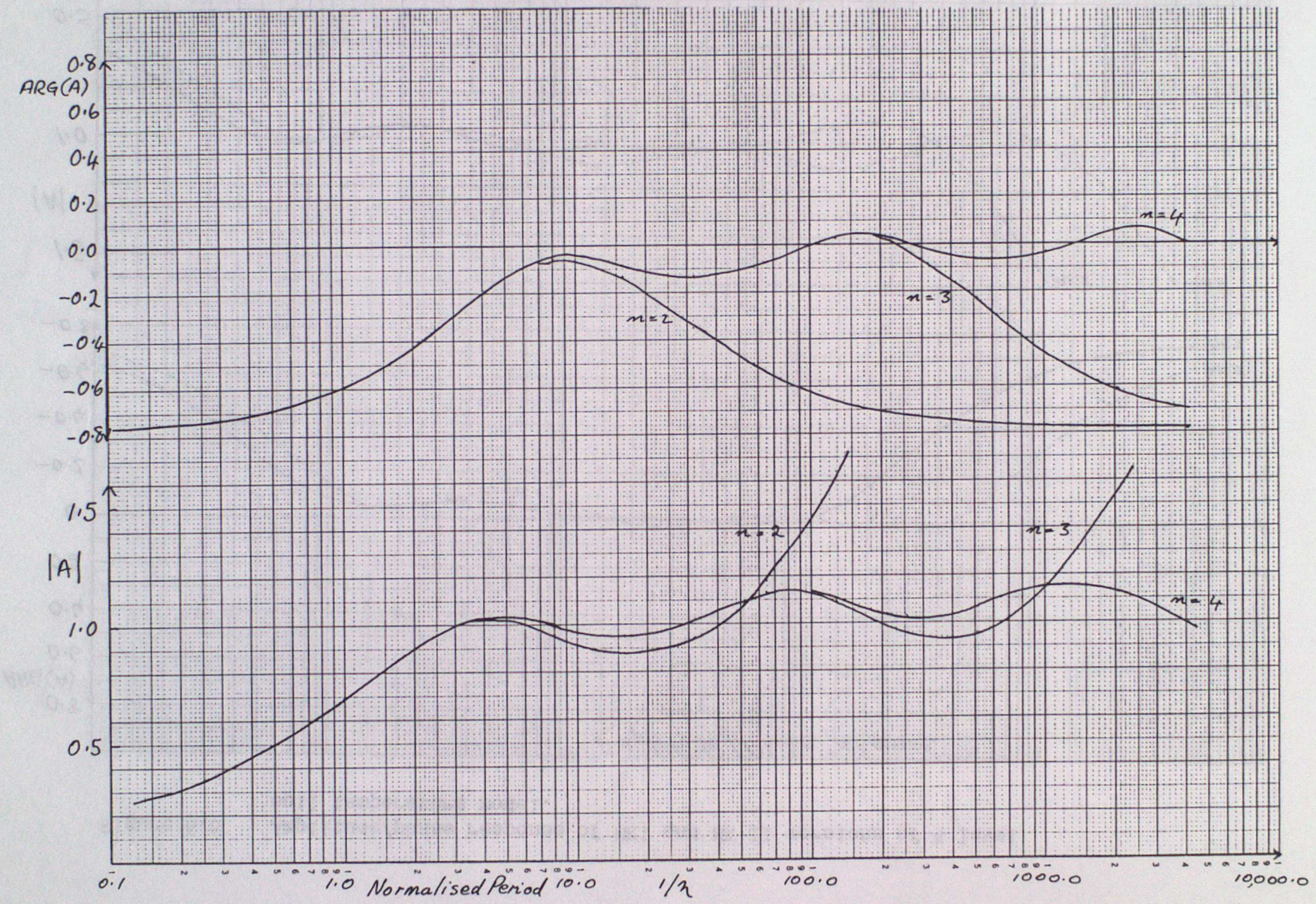

Figure 6.6 Amplitude/phase response of MKI and MK II versions of 4 level soil temperature model.

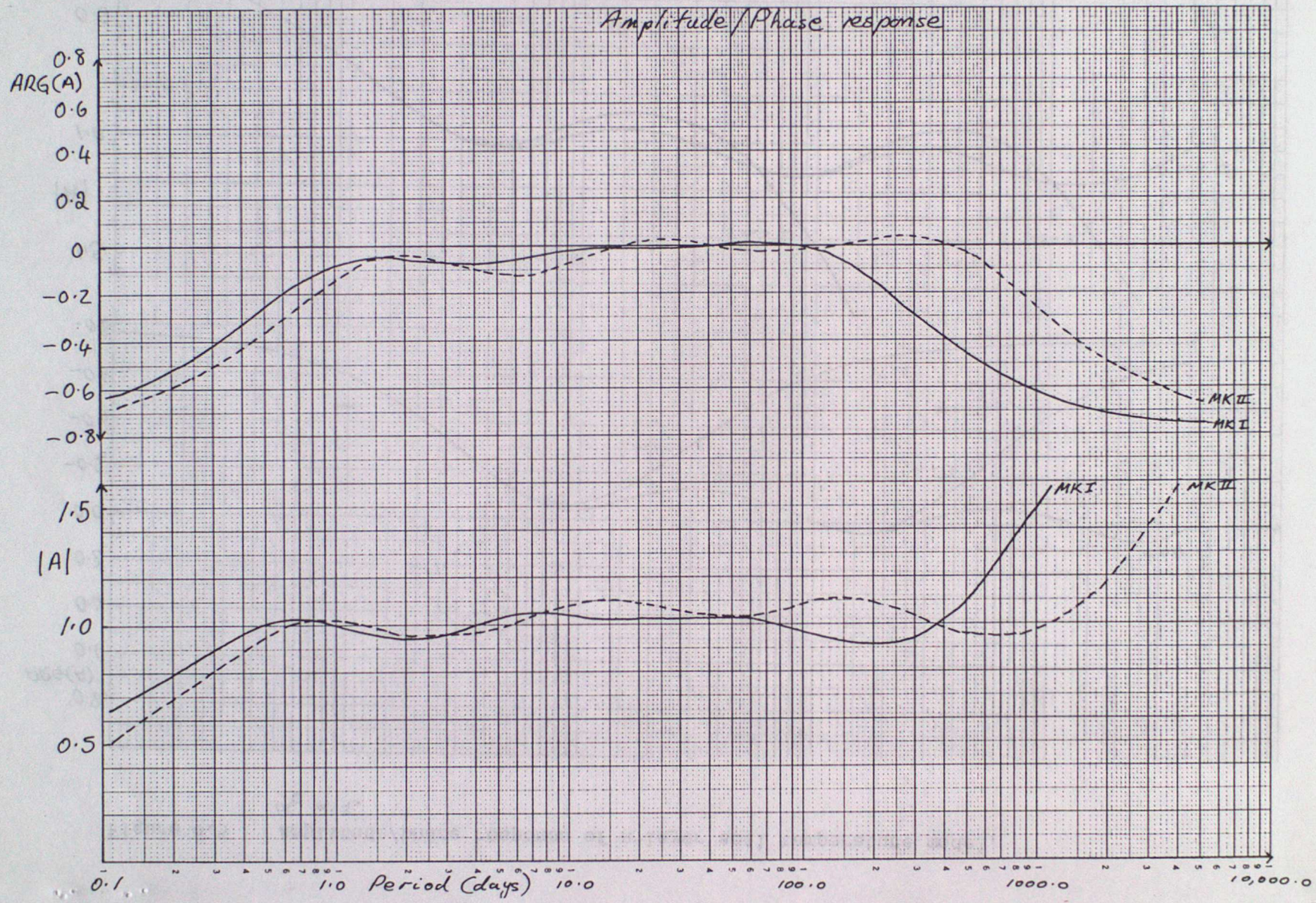

FIGURE 6.7

EXP 1 ANNUAL CYCLE SOUTHERN ENGLAND

MEDIUM SOIL. TALL GRASS, MO MODEL

—— TMEAN --- TMAX.TMIN

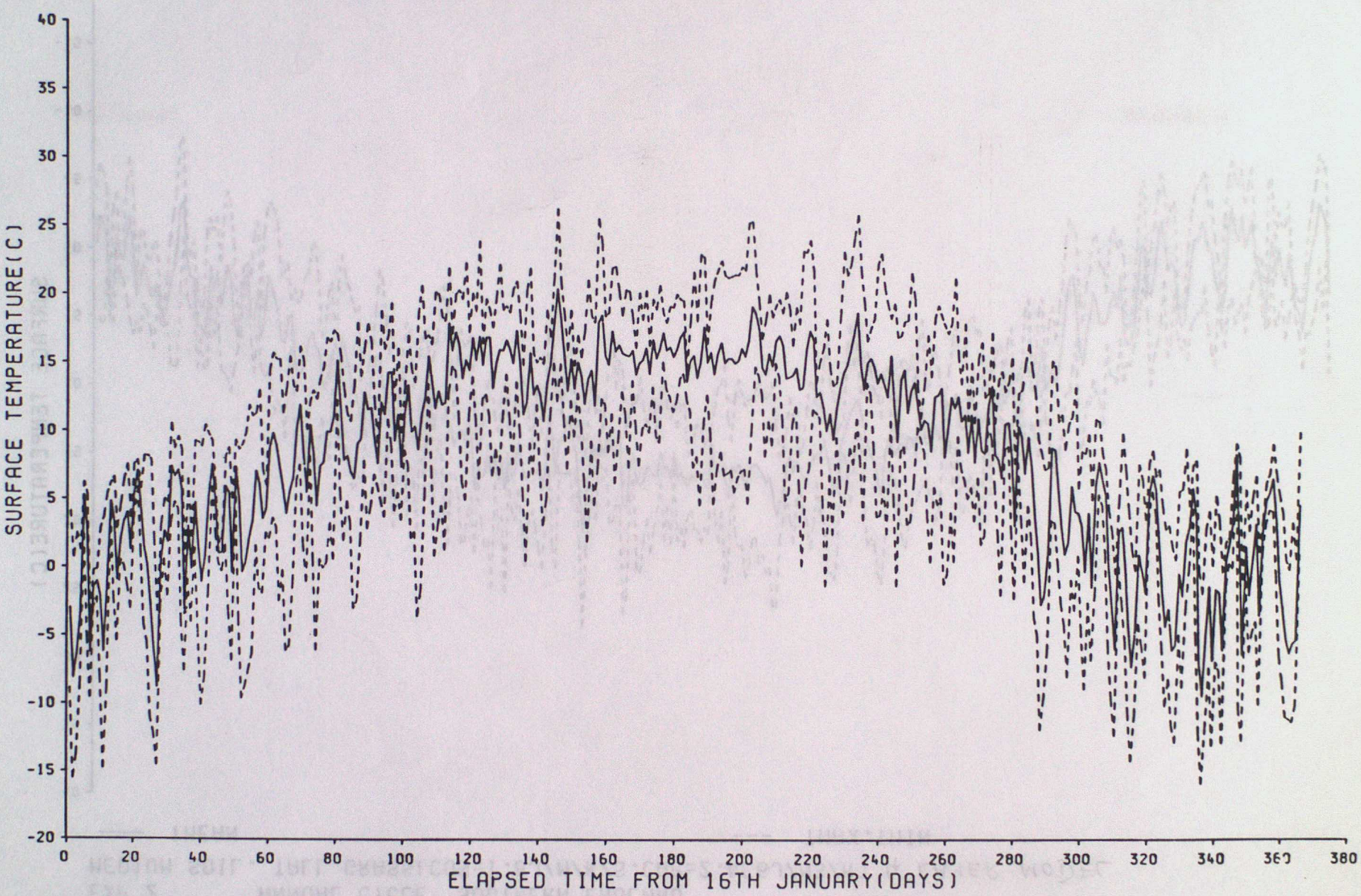

FIGURE 6.8

EXP 2 ANNUAL CYCLE SOUTHERN ENGLAND

MEDIUM SOIL. TALL GRASS(CON=1.8J/M/K/S.CAP=2.4E6J/M3/K) 4 LAYER MODEL

—— TMEAN --- TMAX.TMIN

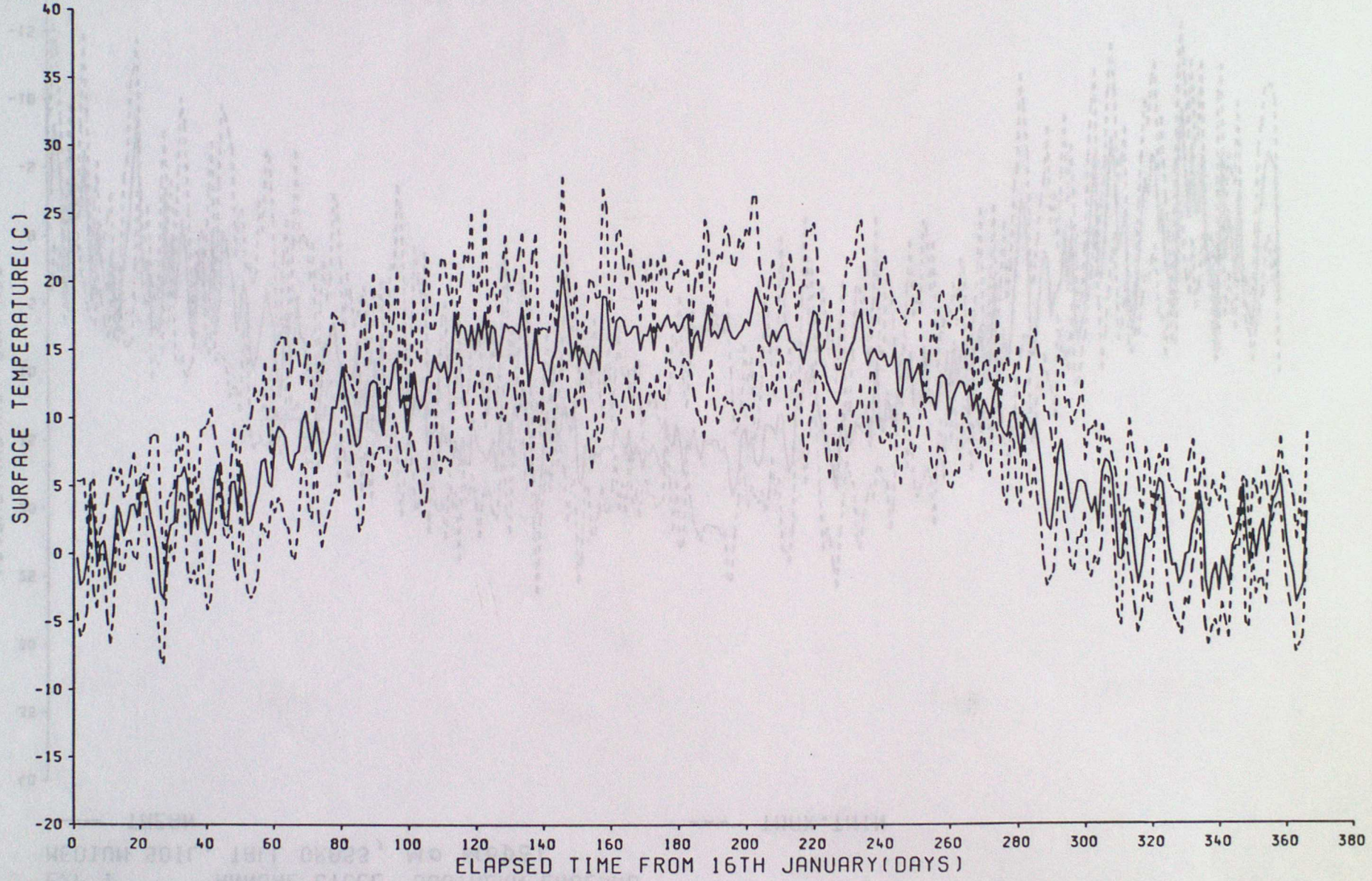

FIGURE 6.9

EXP 3 ANNUAL CYCLE SOUTHERN ENGLAND

MEDIUM SOIL. TALL GRASS(CON=1.2J/M/K/S.CAP=1.6E6J/M3/K) 4 LAYER MODEL

—— TMEAN --- TMAX.TMIN

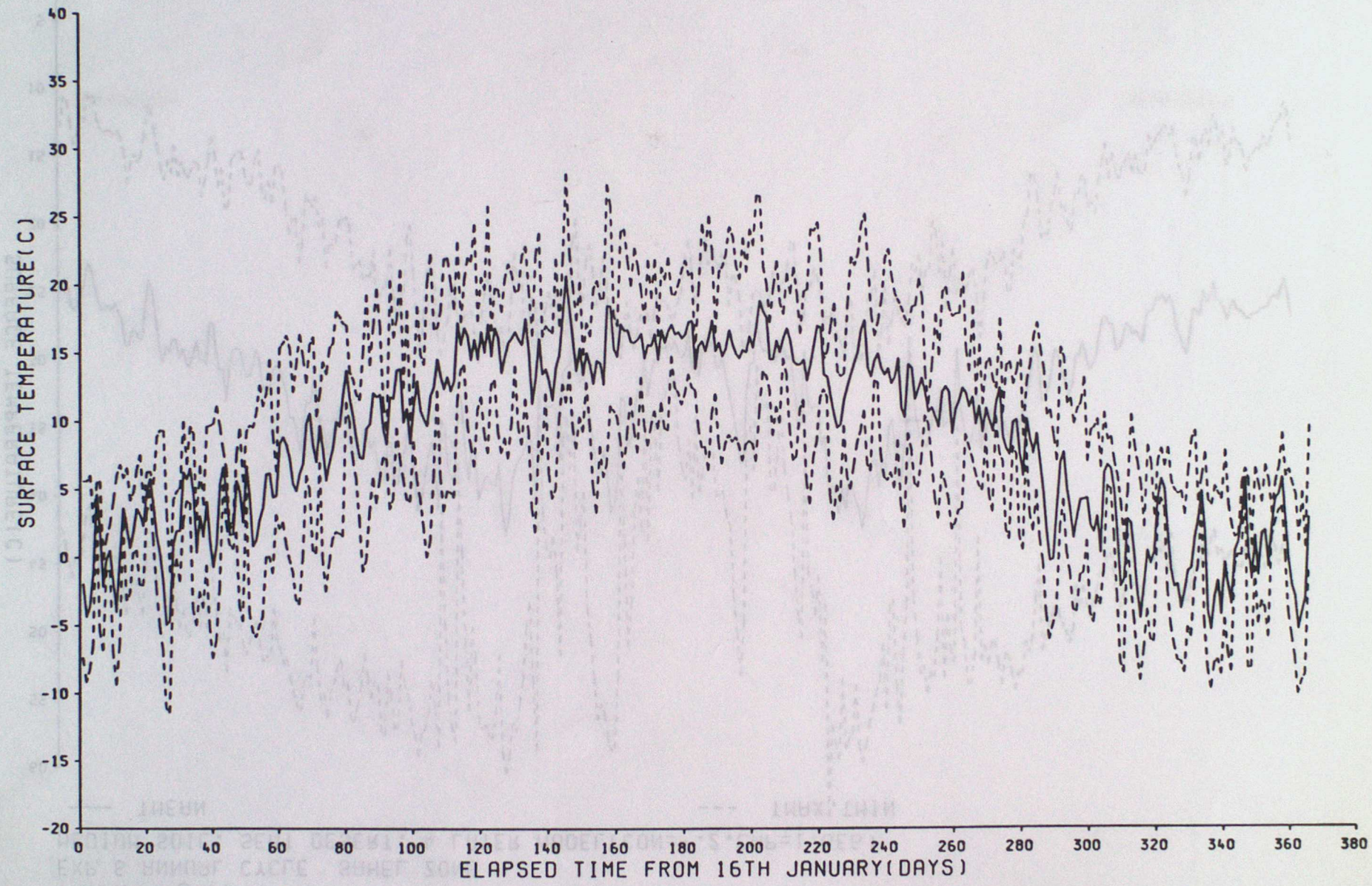

FIGURE 6.10

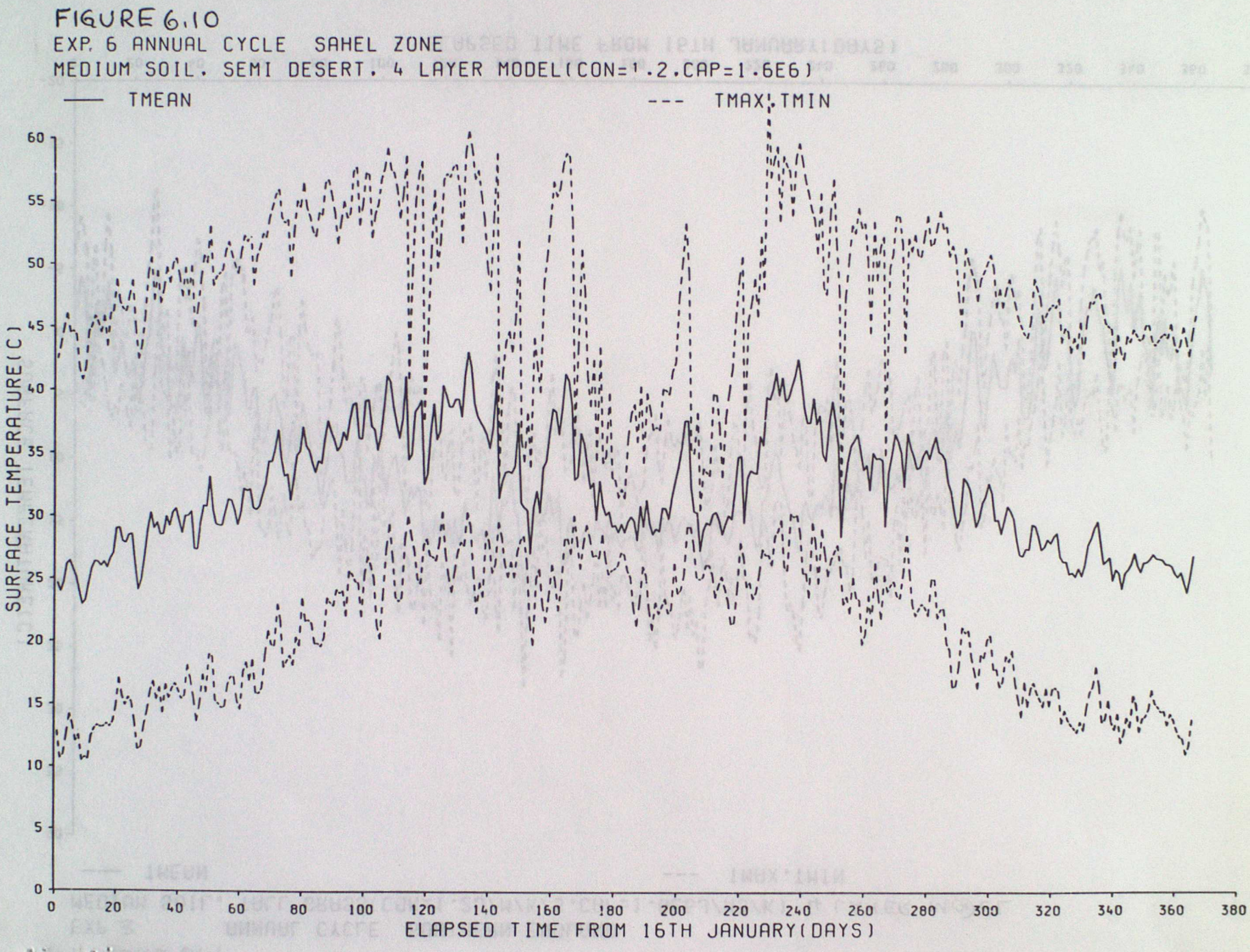
EXP. 6 ANNUAL CYCLE SAHEL ZONE
MEDIUM SOIL. SEMI DESERT. 4 LAYER MODEL(CON=1.2,CAP=1.6E6)
TMEAN
TMAX,TMIN
SURFACE TEMPERATURE(C)
0
5
10
15
20
25
30
35
40
45
50
55
60
0
20
40
60
80
100
120
140
160
180
200
220
240
260
280
300
320
340
360
380
ELAPSED TIME FROM 16TH JANUARY(DAYS)

FIGURE 6.11

EXP. 6 ANNUAL CYCLE SAHEL ZONE

MEDIUM SOIL. SEMI DESERT. 4 LAYER MODEL(CON=1.2.CAP=1.6E6)

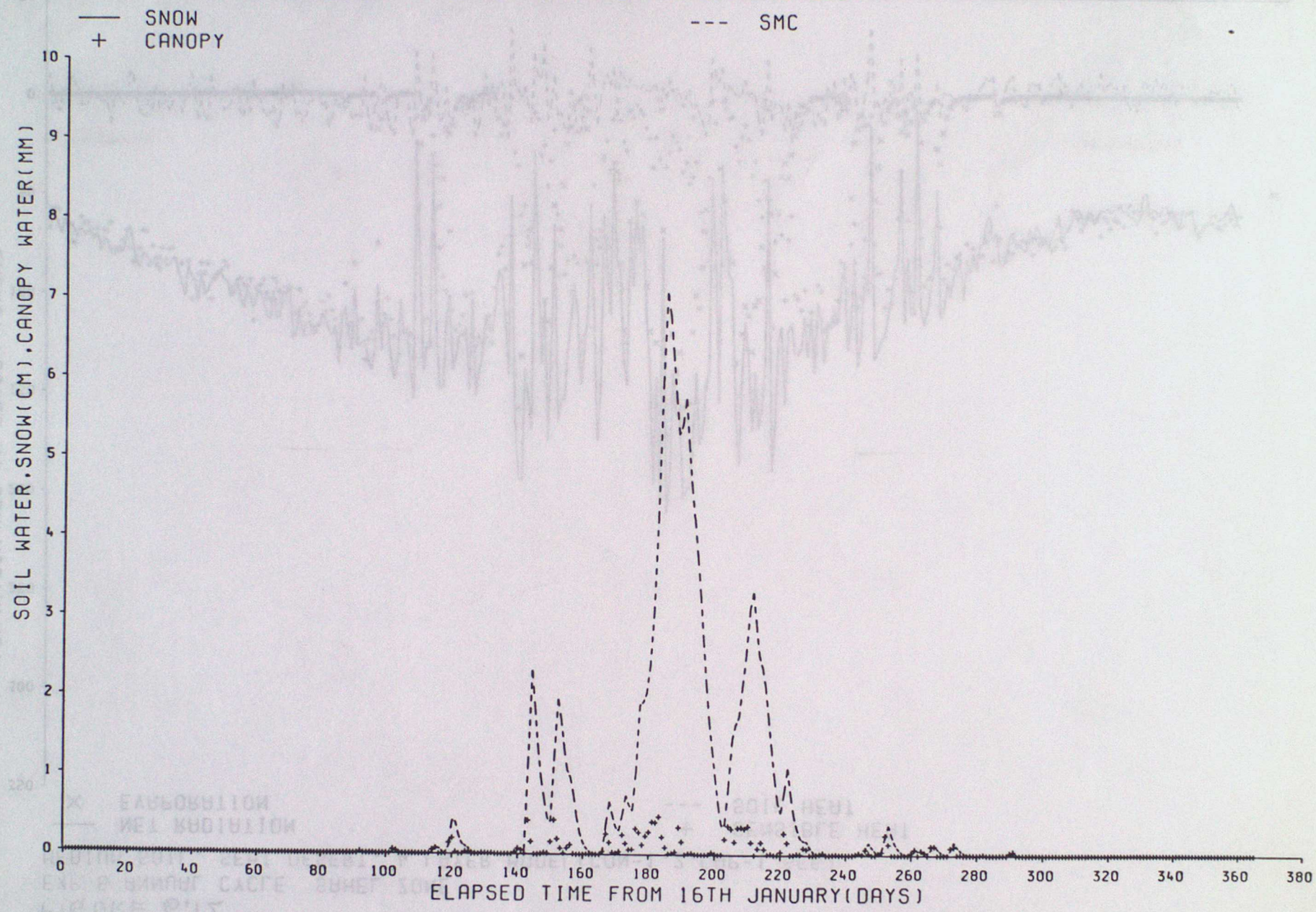

FIGURE 6.12

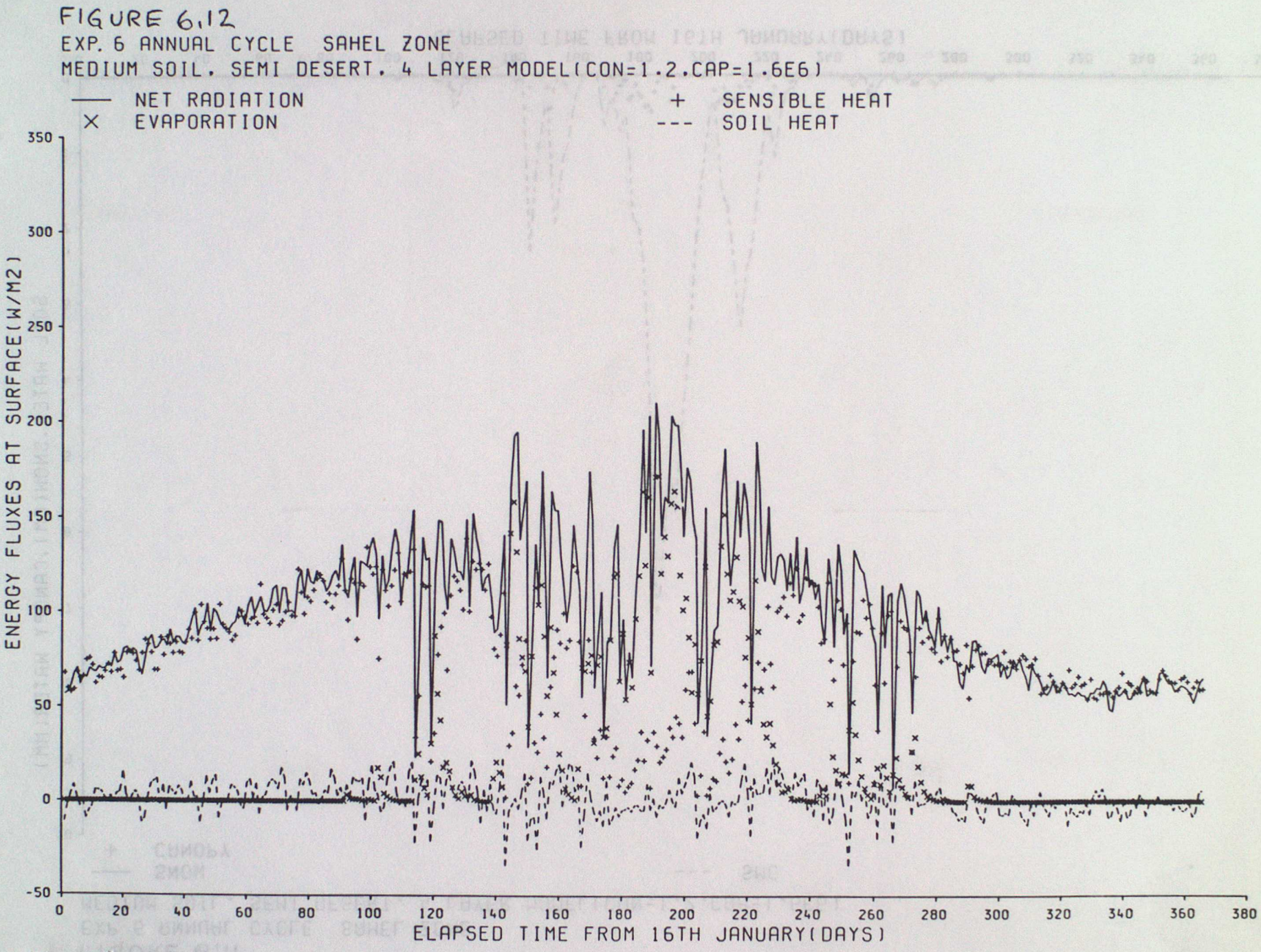
EXP. 6 ANNUAL CYCLE SAHEL ZONE
MEDIUM SOIL. SEMI DESERT. 4 LAYER MODEL(CON=1.2.CAP=1.6E6)
NET RADIATION
EVAPORATION
SENSIBLE HEAT
SOIL HEAT
ENERGY FLUXES AT SURFACE(W/M2)
350
300
250
200
150
100
50
0
-50
0
20
40
60
80
100
120
140
160
180
200
220
240
260
280
300
320
340
360
380
ELAPSED TIME FROM 16TH JANUARY(DAYS)

FIGURE 6.13

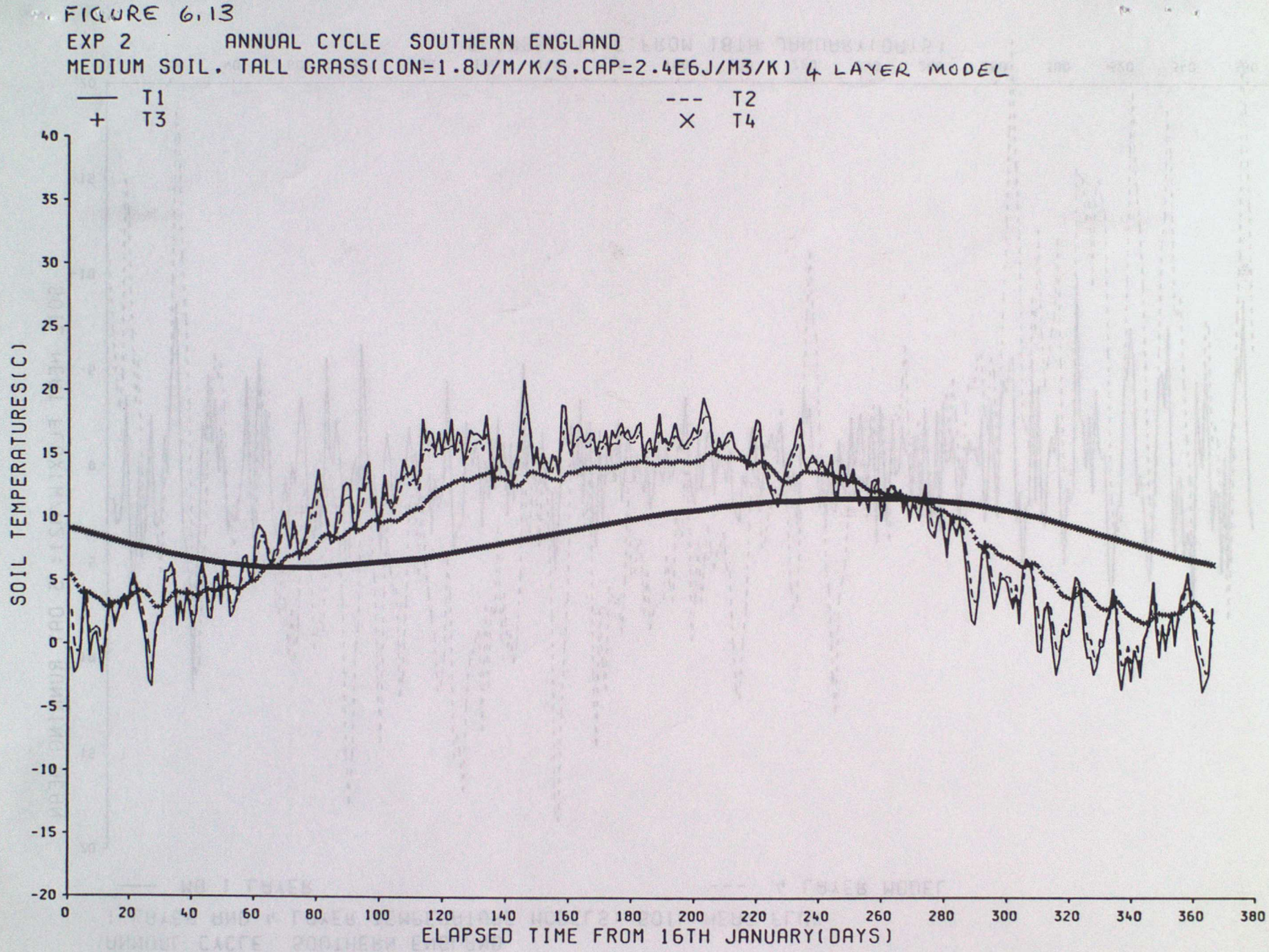
EXP 2 ANNUAL CYCLE SOUTHERN ENGLAND
MEDIUM SOIL. TALL GRASS(CON=1.8J/M/K/S.CAP=2.4E6J/M3/K) 4 LAYER MODEL
T1
T2
T3
T4
SOIL TEMPERATURES(C)
40
35
30
25
20
15
10
5
0
-5
-10
-15
-20
0
20
40
60
80
100
120
140
160
180
200
220
240
260
280
300
320
340
360
380
ELAPSED TIME FROM 16TH JANUARY(DAYS)

FIGURE 6.14

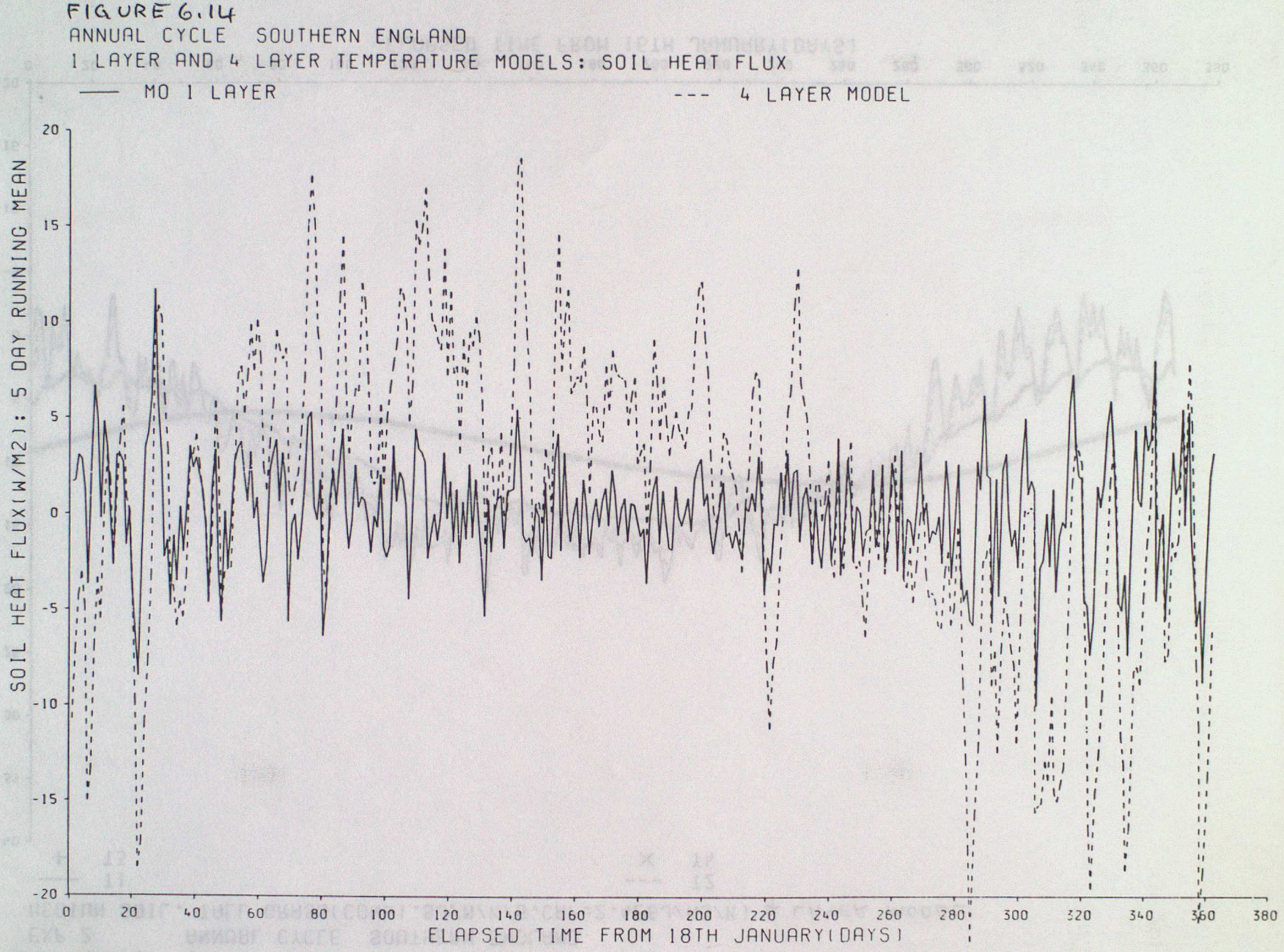
ANNUAL CYCLE SOUTHERN ENGLAND
1 LAYER AND 4 LAYER TEMPERATURE MODELS: SOIL HEAT FLUX
MO 1 LAYER
4 LAYER MODEL
SOIL HEAT FLUX(W/M2): 5 DAY RUNNING MEAN
20
15
10
5
0
-5
-10
-15
-20
0
20
40
60
80
100
120
140
160
180
200
220
240
260
280
300
320
340
360
380
ELAPSED TIME FROM 18TH JANUARY(DAYS)

Figure 6.15 Average surface temperature from June, July and August of AGCM experiment VSAS. Contours every 5°C.

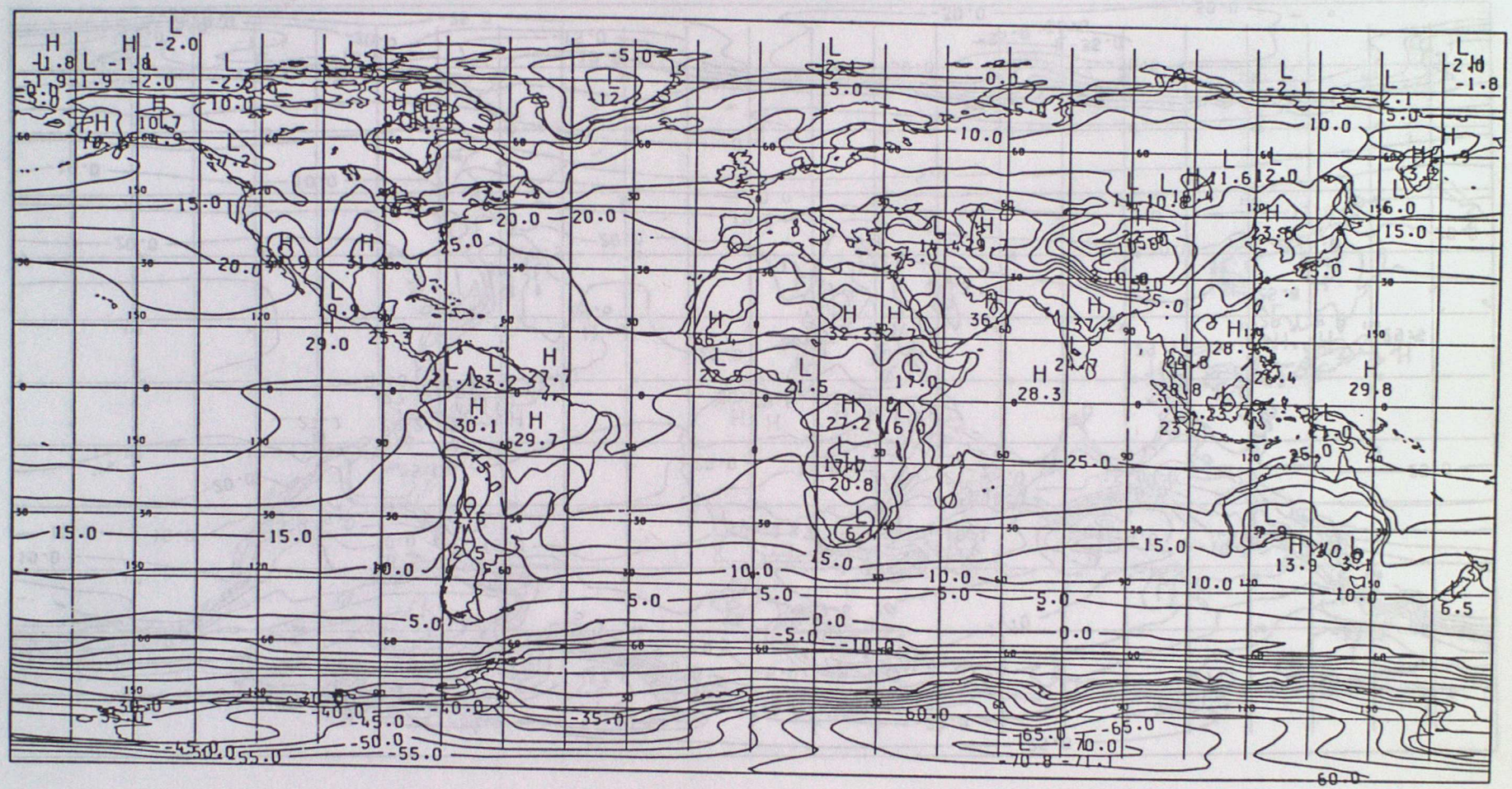

Figure 6.16 Average surface temperatures from December, January and February of AGCM experiment VSAS. Contours every 5°C.

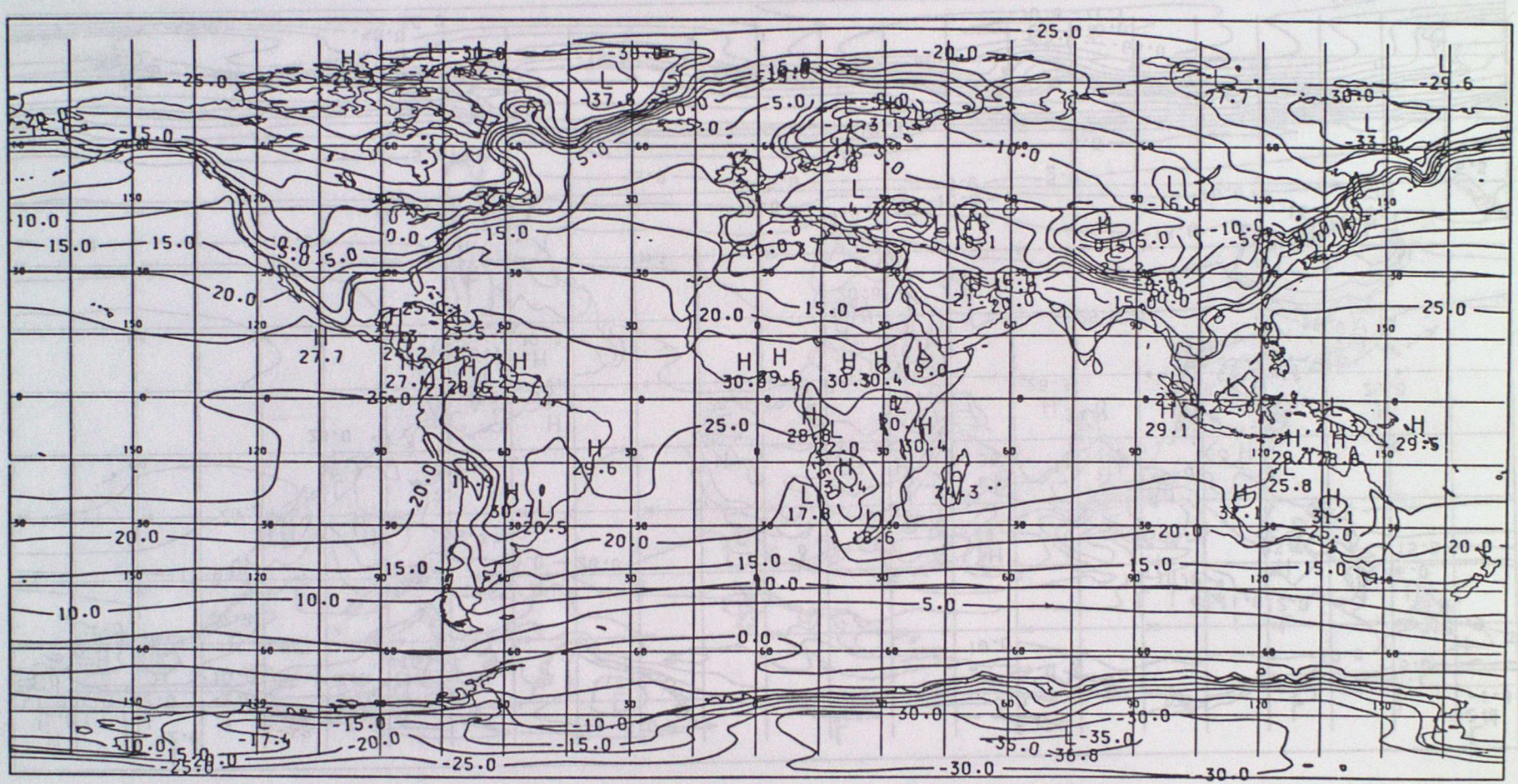

Figure 6.17 Difference in average surface temperature for June, July and August between AGCM experiment VSAS and single soil temperature layer control integration. Contours every 2K and negative areas shaded.

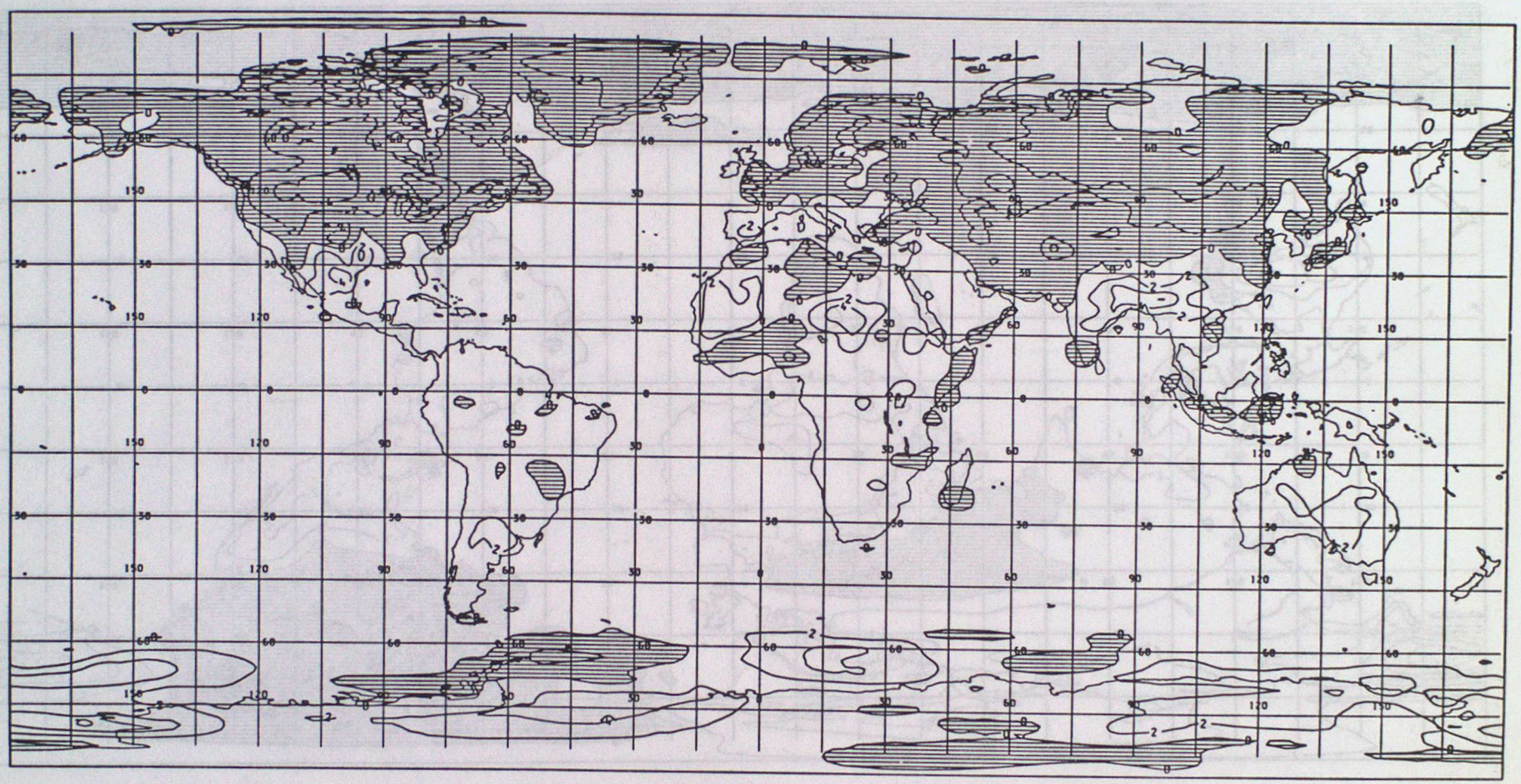

Figure 6.18 Difference in average surface temperature for December, January and February between AGCM experiment VSAS and single soil temperature layer control integration. Contours every 2K and negative areas shaded.

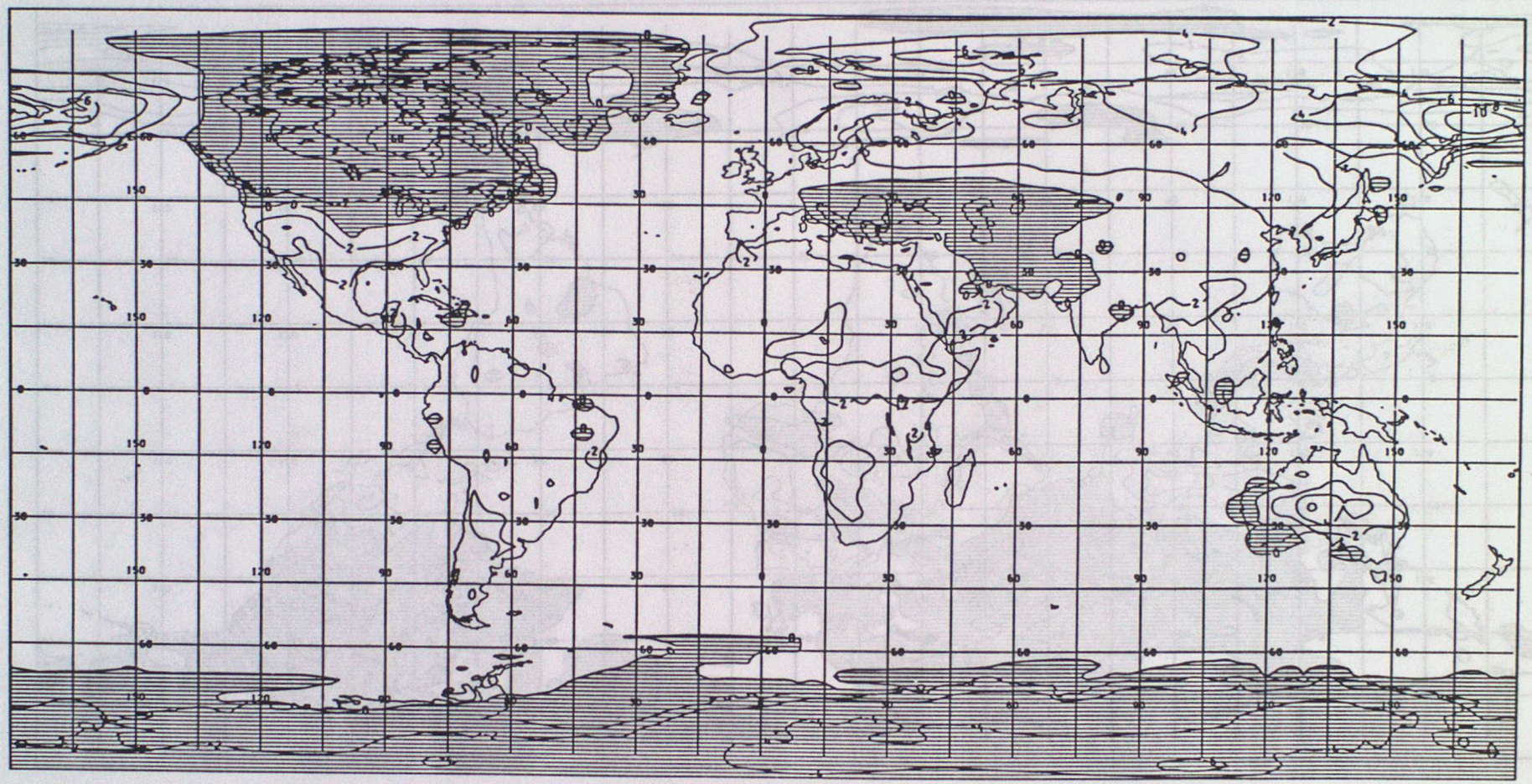

Figure 6.19 Average surface heat flux into soil from March, April and May of first year of AGCM experiment VSAS. Contours every 5 Wm^{-2} and negative areas shaded.

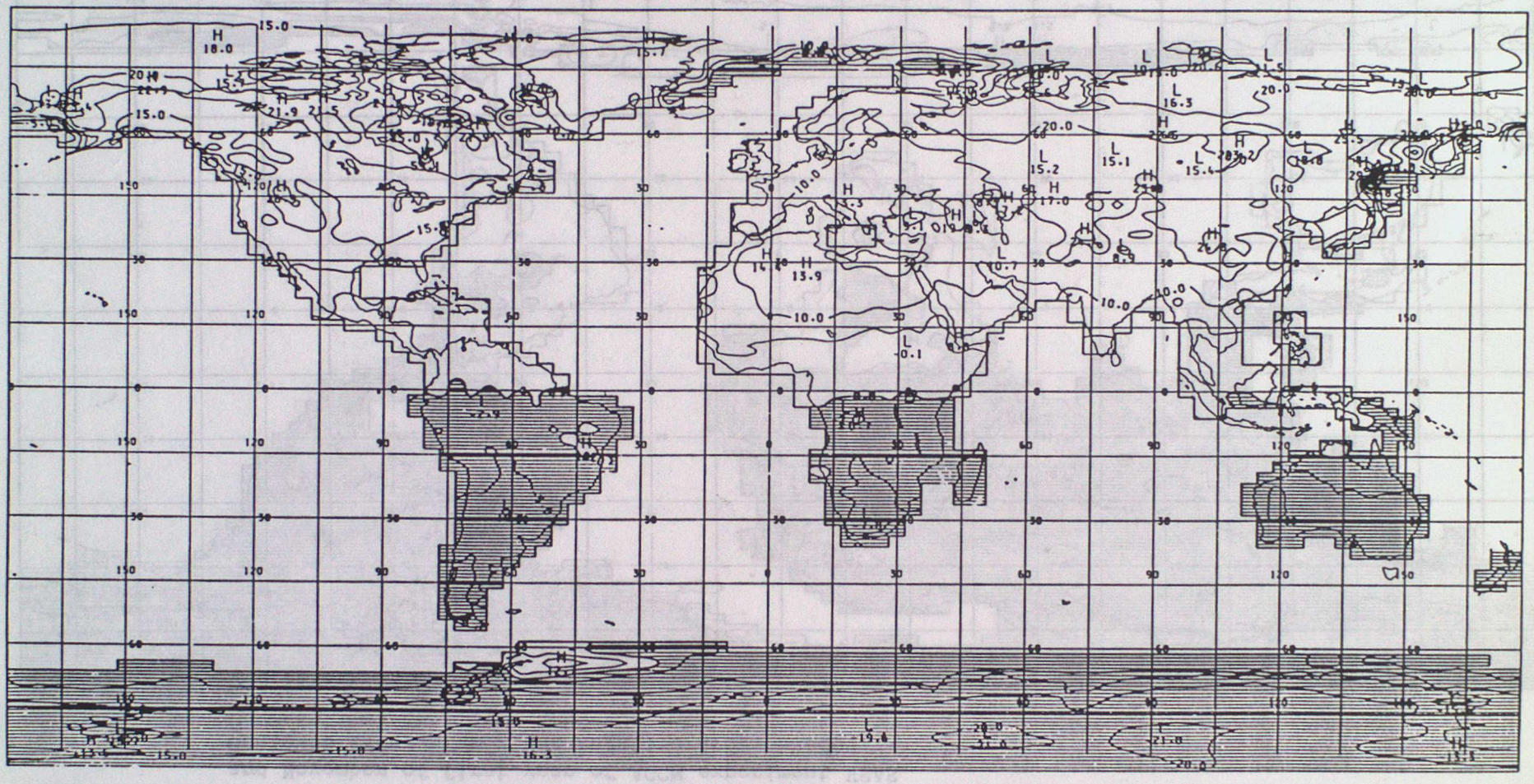

Figure 6.20 Average surface heat flux into soil from September, October and November of first year of AGCM experiment VSAS. Contours every 5 Wm^{-2} and negative areas shaded.

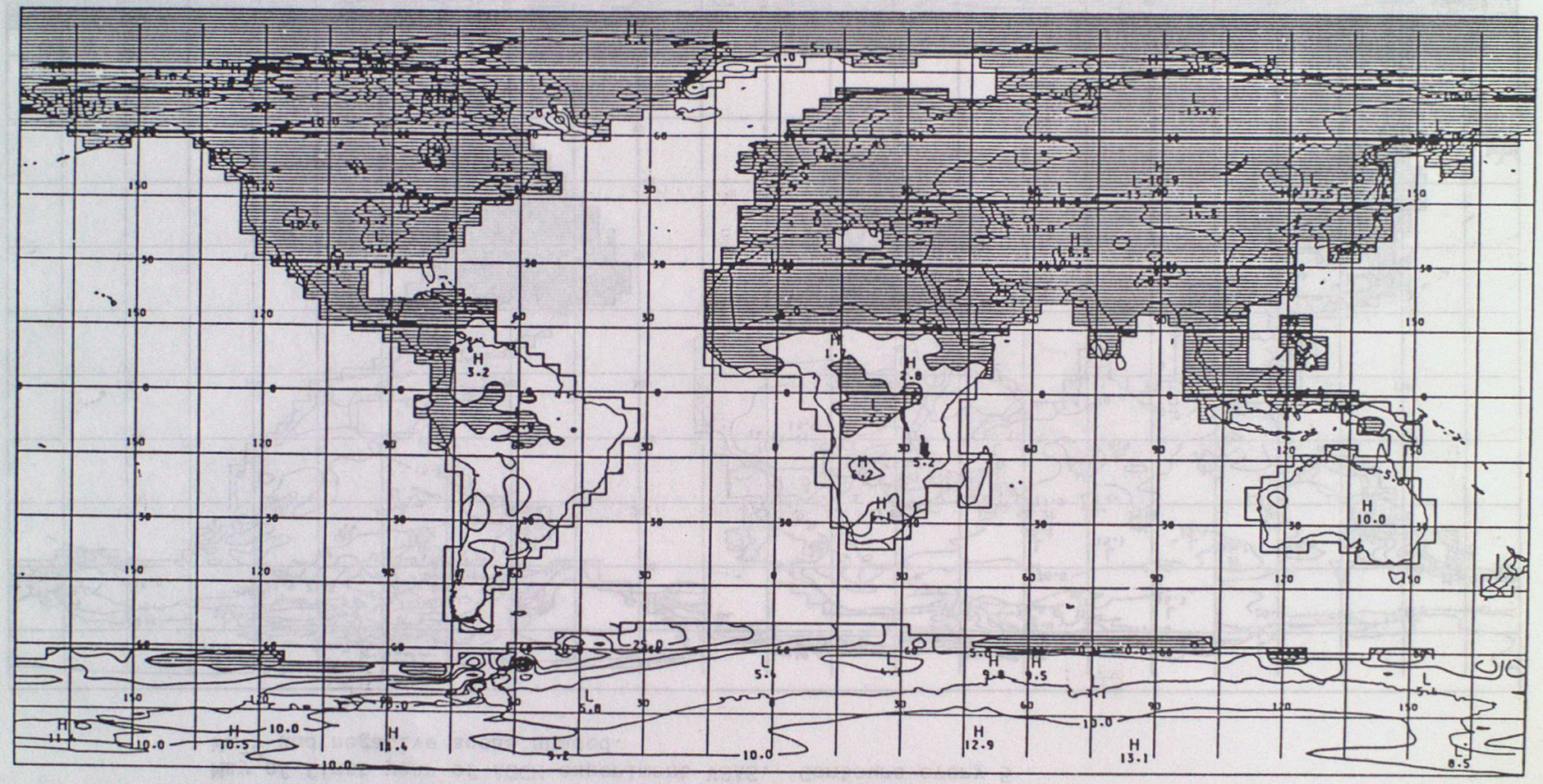

Figure 6.21 Annual range of monthly mean surface temperatures from AGCM experiment VSAS. Contours at 0, 1, 2 and every 5K.

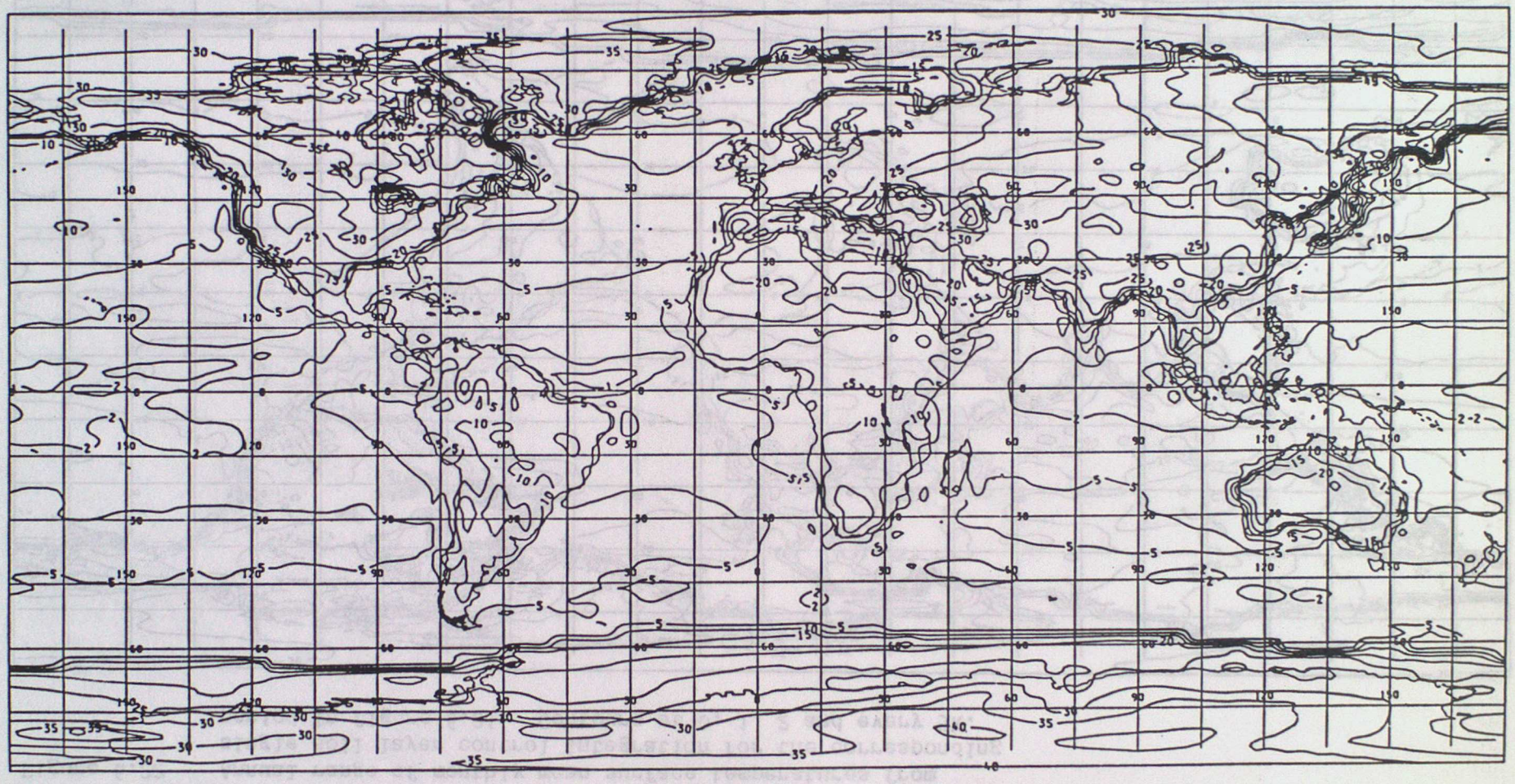

Figure 6.22 Annual range of monthly mean surface temperatures from single soil layer control integration for the corresponding period in figure 6.21. Contours at 0, 1, 2 and every 5K.

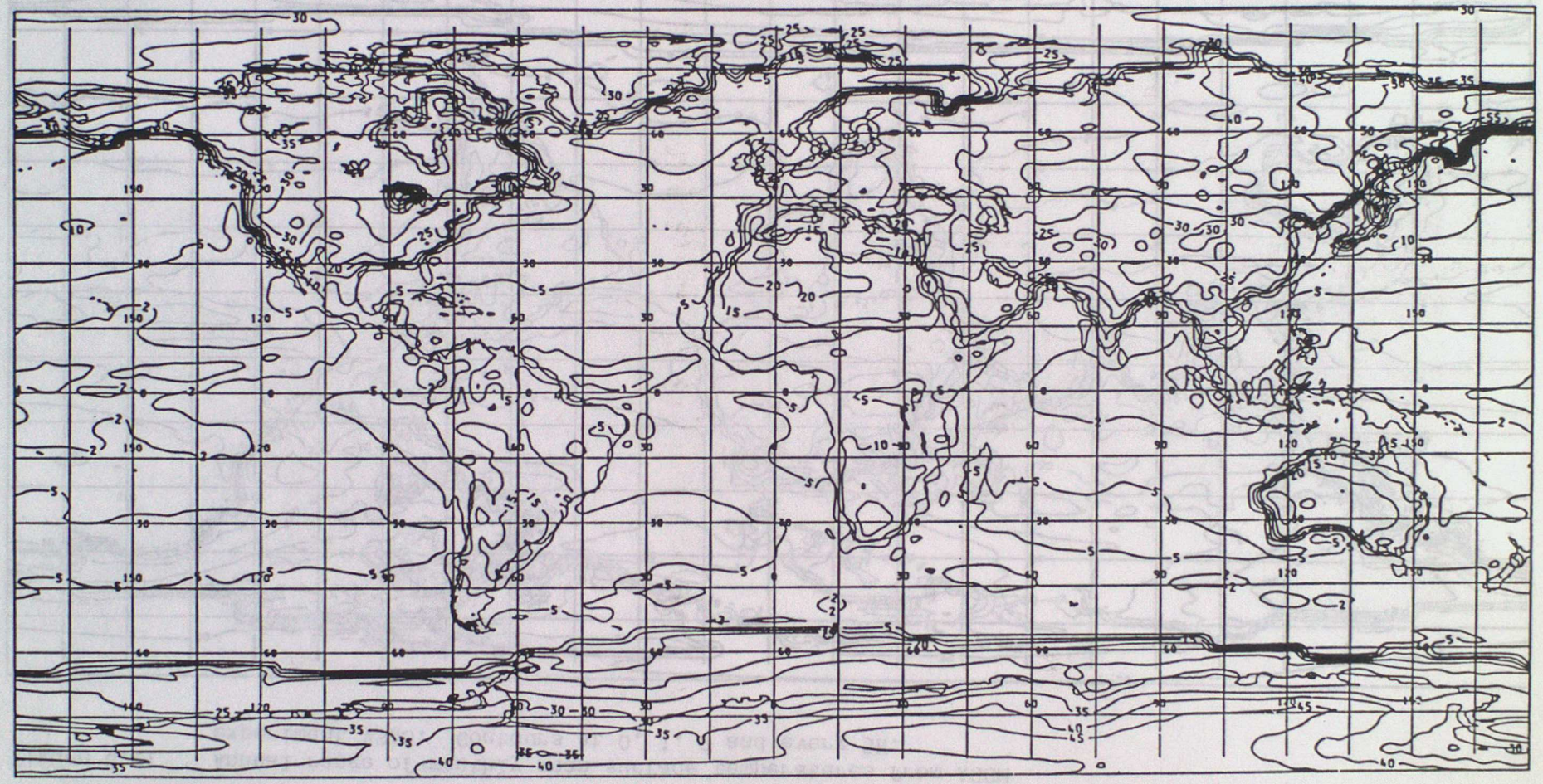

Figure 6.23 Observed seasonal range of surface ambient temperatures (August - February) from Manabe et al (1979). Contours every 2K between -10K and 10K and every 10K otherwise.

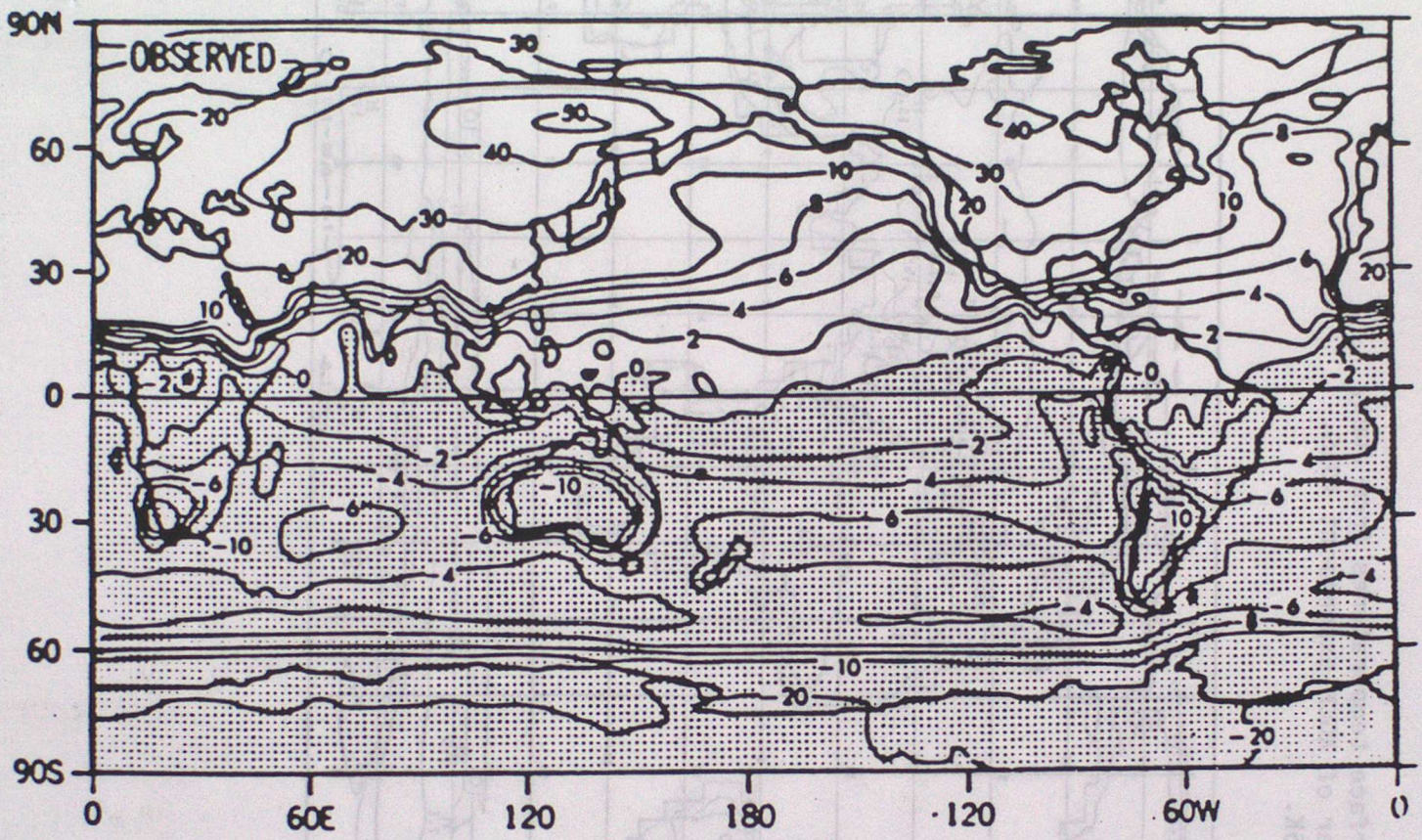

Figure 6.24 Average diurnal range of surface temperatures from June, July and August of first year of AGCM experiment VSAS. Contours at 1, 2 and every 5K.

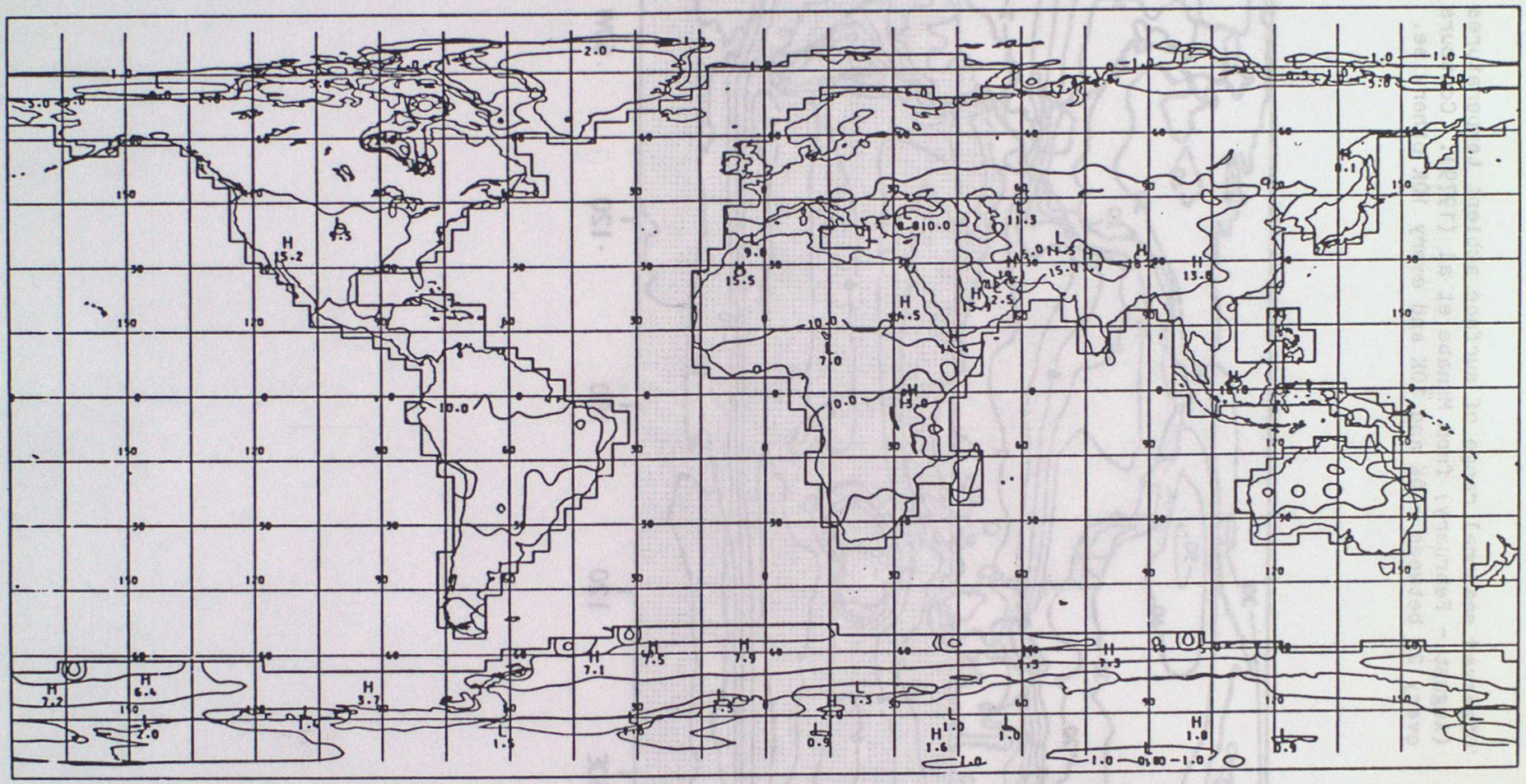

Figure 6.25 Variation of amplitude of annual temperature wave with soil depth for selected stations. Three theoretical solutions are also given for specific e-folding depths.

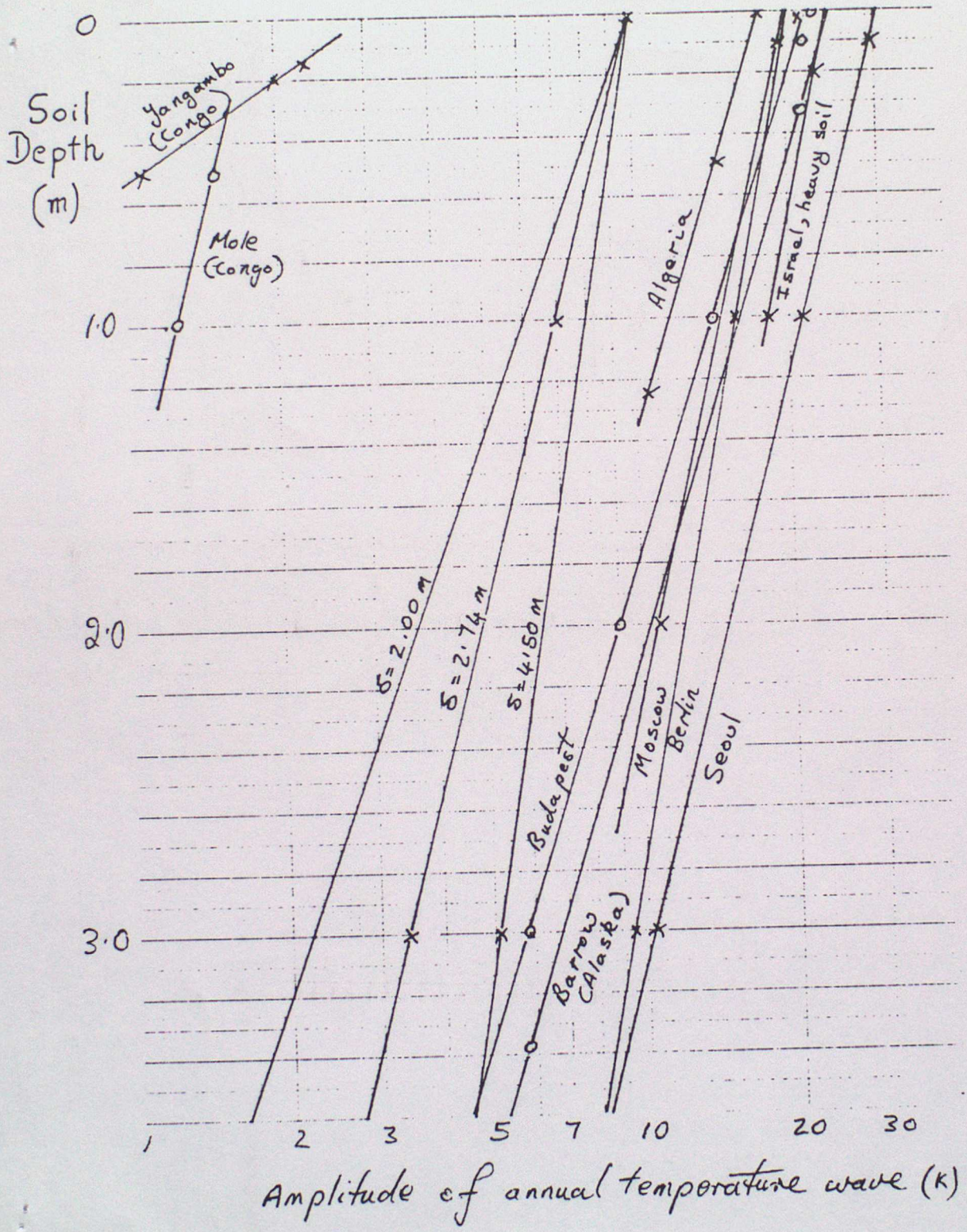

6.6.3 Conclusions

The simulation of surface temperatures is good overall. However, temperatures were notably warmer than climatology over Siberia in winter. This may have been due to the strong winter westerlies generated by the model. Neglect of the thermal properties of snow and use of a high value for the thermal inertia may have contributed also. The diurnal range of temperature was much lower than observed, due probably to the use of a high thermal inertia and of climatological cloud in the radiation routines.

Verification of surface temperature is difficult to make as surface temperatures are not measured routinely. However the development of satellite observing techniques may yield useful information in this regard. Satellites may also be used in the future to derive the spatial distribution of soil thermal properties.

6.7 Discussion and conclusions

A soil temperature parametrization has been derived and tested. Its amplitude and phase response relative to an analytical solution of the diffusion equation is good over a range of frequencies considered to be important on the AGCM timescale. However a number of simplifying assumptions were made which may introduce errors. The primary assumption was that of homogeneity of λ and C. In reality λ and C will not be spatially homogeneous due to their dependence on both soil type and moisture; they will also vary with time because of changes in soil moisture. Phase changes of soil water are ignored; these may be important in some regions where there is considerable melting and freezing of soil water. To deal with these aspects properly would require a more detailed soil model with account taken of changes in heat content due to rainfall, evaporation and runoff. One major omission is a correct treatment of the thermal characteristics of snow whose thermal inertia is considerably lower than that of soil. Benoit (1976) has proposed a soil temperature model which incorporates snow by allowing the temperature levels to move with the top of the snow layer. However such a model would involve the use of a greater number of levels. It is interesting to note that Geiger (1961) quotes values of λ and C for old snow which are very similar to those of wet clay (and those which we propose) so that perhaps the problem really only becomes important where there is frequent snowfall. Spatial variation of λ and C would be relatively easy to incorporate and might possibly be a first step towards solving problems related to the diurnal range and winter temperatures noted in section 6.6.2 although correction of high Siberian winter temperatures probably requires a marked improvement in the winter circulation. The effect of a vegetation canopy on soil temperatures is probably small due to its low thermal capacity, but perhaps the shading from solar radiation needs to be modelled explicitly.

Suggested improvements in order of importance are inclusion of spatially variable λ, C, explicit treatment of snow, soil moisture dependence of λ and C, thermal effects of phase changes of water, and thermal effects of a vegetation canopy. It would seem possible to simulate surface temperatures quite well using the scheme proposed in this section, given a judicious choice of λ and C. However the fact that it is possible to simulate temperatures correctly does not automatically mean that the turbulent fluxes will be correct as these depend on λ and C as well as the soil

moisture state. The scheme proposed in this section only increases computing time by about 6%. Before a more complex and computationally expensive scheme were introduced, it would have to be shown that it could lead to substantial improvement in the regions where the 4 level scheme described above is inadequate.

6.8 References

Benoit, R. 1976 A comprehensive parametrization of the Atmosphere Boundary Layer for GCM's. NCAR/CT - 39, National Centre for Atmospheric Research, Boulder, Colorado.

Bhumralkar, C. M. 1975 Numerical Experiments on the Computation of Ground Surface Temperature in an Atmospheric General Circulation Model. Journal of Applied Meteorology, 14, 1246-1258.

Carson, D. J. 1982 Current parametrizations of land-surface processes in atmospheric general circulation models. Land surface processes in atmospheric general circulation models. Edt. by P. S. Eagleson. 67-108 Cambridge, Massachusetts.

Chang, J. H. 1958 Ground Temperature Vol I, Blue Hill Met. Observatory. Harvard University, Milton, Mass.

Deardorff, J. W. 1978 Efficient prediction of ground surface temperature and moisture, with inclusion of a layer of vegetation. Journal of Geophysical Research, 83, 1889-1903.

Dooge, J. C.I. 1982 Parametrization of hydrologic processes. Land Surface processes in atmospheric general circulation models. Edt. by P. S. Eagleson, 243-288, Cambridge, Massachusetts.

Fullard, H. and Darby, H.C. 1978 The University Atlas. George Philip and Son Ltd. London.

Geiger, R. 1961 The Climate near the Ground, Harvard University Press, Cambridge, Massachusetts.

Jacobsen, I. and Heise, E. 1982 A new economic method for the computation of the surface temperature in Numerical Models. Beitr. Phys. Atmosph, 55, 128-141.

Lettau, H.	1954	Improved Models of Thermal Diffusion in the Soil. Trans. Amer. Geophysical Union, Vol. 35, 121-131.
Louis, J. F.	1984	ECMWF Forecast Model Physical Parametrisation. Research Manual 3, CH6, European Centre for Medium Range Weather Forecasts, Reading.
Manabe, S., Bryan, K. and Spelman, M. J.	1979	A global ocean-atmosphere climate model with seasonal variation for future studies of climate sensitivity, Dynamics of Atmospheres and Oceans, 3, 393-426.
Mintz, Y., Sellers, P. J. and Wilmott, C. F.	1983	On the design of an interactive biosphere for the GLAS General Circulation Model. NASA Technical Memorandum 84973.
Slingo, A. and Pearson, D.W.		A comparison of the impact of an envelope orography and of a parametrization of orographic gravity-wave drag on model simulations. To be published.
Van de Griend, A. A., Camillo, P. J. and Gumey, R. J.	1985	Discrimination of soil physical parameters, thermal inertia, and soil moisture from diurnal surface temperature fluctuations. Water Res. Res., 21, 997-1009.

Appendix 6 Derivation of λ and C

The AGCM experiments were carried out using values for λ and C quoted by Louis (1984). The resulting thermal inertia (Υ) appears to be too high and another global value was sought. Diffusivity (λ/C) determines the e-folding depth δ_a of the annual cycle and this was estimated from data by Chang (1958). The amplitude of the annual temperature wave at several locations were plotted as a function of depth and gradients calculated to find δ_a. (Figure 6.25) A value of δ_a = 2.7 m seems to be fairly typical. From Van de Griend (1985), $\Upsilon \sim 1400$ $Jm^{-2}K^{-1}s^{-1/2}$, was deduced as being typical.

Then since $\Upsilon = \sqrt{(\lambda C)}$

and $\delta_a = \sqrt{(2\lambda/C\omega_a)}$

we can find λ and C as follows:

$$\lambda = \sqrt{(\omega_a/2)}\ \Upsilon\delta_a$$

$$C = \Upsilon^2/\lambda$$

giving $C = 1.64 \times 10^6$ J m^{-3} K^{-1} and $\lambda = 1.19$ J m^{-1} s^{-1} K^{-1}

7. Sensitivity of European climate to land surface variations.

7.1 Introduction

7.2 One dimensional model results

7.2.1 Introduction to model integrations
7.2.2 Sensitivity to soil type
7.2.3 Sensitivity to land type
7.2.4 Sensitivity to canopy storage
7.2.5 Sensitivity to surface resistance
7.2.6 Sensitivity to root depth
7.2.7 Sensitivity to surface roughness

7.3 Conclusions

7.4 References

7. Sensitivity of European climate to land surface variations

7.1 Introduction

A number of AGCM experiments have been reported which have looked at the response of the atmosphere to changes in the land surface. Most experiments have considered the effect of varying albedo or soil moisture (eg Mintz (1984)). Both may change as a result of changes in land use and soil moisture will vary with external atmospheric conditions. Apart from changing albedo, changes in vegetation can lead to variations in a number of parameters which affect the soil moisture content of the soil. The primary way in which soil moisture may affect the climate is through evaporation. As we have seen from sections 3 and 4, evaporation becomes soil moisture controlled once the soil moisture content falls below a critical level and evaporation begins to decrease below the so-called potential rate.

For much of Northern Europe, potential evaporation occurs for much of the year but in the summer, soil moisture generally exerts a variable controlling influence. The importance of this for generation of precipitation has been demonstrated by Rowntree and Bolton (1983).

Because Europe is situated in a region of variable precipitation and soil moisture, there is a need to model correctly actual evaporation and the controlling influence of soil moisture. Sensitivity to various vegetation parameters affecting evaporation is therefore of interest.

In this section the results of some ODM integrations which have been discussed by Warrilow (1986) have been summarised and give an indication of the sensitivity of local climate in a European context to changes in land surface parameters without the complications of large scale feedback.

The ODM was described in section 2 and uses the land surface parametrization of hydrology discussed in section 3 and of interception in section 4. Surface temperatures are calculated for a single layer (see section 6).

7.2 One dimensional model results

7.2.1 Introduction to model integrations

Eleven annual cycle integrations were carried out in which either the soil or land types were varied or individual parameters such as surface resistance were changed. An estimate of the sensitivity of the climate to each parameter or soil or land type could then be made. Some of these experiments have been referred to in preceding sections but are presented here for completeness.

The various integrations are summarised in table 7.1. Annual values are given although sensitivity to evaporation is greatest in the summer. Three soil types and 3 vegetation types are compared along with changes to individual parameters. The control was taken to be an integration with long grass and medium soil (run 4).

Before looking at the sensitivity studies in detail it is worth reviewing the overall performance of the ODM. Table 7.2 compares the average of the annual mean values of all the integrations with the climate statistics given by Lockwood (1985) and the Met Office (1952). Agreement is quite good except for winter temperatures which are on the low side and it would appear that a surface albedo of 0.2 (grass) is more appropriate than 0.14 (forest).

KW

Table 7.1

Summary of results for ODM integrations over one annual cycle for a location in Southern England.

Run No	Particular Land surface characteristics	Mean LE (Wm^{-2})	Mean H (Wm^{-2})	Bowen Ratio	Mean R_{NTOP} (Wm^{-2})	Mean $R_{NBOTTOM}$ (Wm^{-2})	Mean SMC (cm)	Mean CANOPY (m)	Total Precipitation (mm)	Mean T* (°C)
2	Fine soil, tall grass	40.39	14.27	0.35	-71.41	54.77	9.52	0.56	671.0	8.70
3	Coarse soil, tall grass	37.39	17.40	0.47	-70.53	54.90	5.39	0.56	664.0	8.90
4	Medium soil, tall grass (r_s=60sm^{-1}, D=1.0m, z_o=.06m)	42.00	12.75	0.30	-71.74	54.86	10.20	0.57	673.6	8.56
5	Forest (r_s=150sm^{-1},D=1.5m,z_o=2.0m)	41.22	23.50	0.57	-61.94	64.86	14.58	0.74	681.5	8.92
6	Short grass (r_s=50sm^{-1}, D=0.6m, z_o=.02m)	37.90	15.77	0.42	-71.17	53.78	6.32	0.38	665.8	8.99
7	Forest, Canopy = 0	32.76	30.82	0.94	-61.28	63.71	17.60	0.00	635.1	9.32
8	As 4 with r_s = 120sm^{-1}	38.32	17.73	0.46	-69.52	56.17	11.87	0.55	662.2	8.88
9	As 4 with r_s = 0sm^{-1}	45.93	8.61	0.19	-72.84	54.65	8.30	0.62	693.8	8.30
10	As 4 with D = 0.10m	29.41	27.34	0.93	-67.06	56.87	1.06	0.55	652.6	9.50
11	As 4 with D = 0.50m	36.92	17.74	0.48	-70.58	54.77	5.32	0.56	662.2	8.94
12	As 4 with z_o = 0.60m	44.04	11.32	0.26	-72.14	55.49	9.95	0.51	687.66	8.38

Table 7.2 ODM performance. Simulation of the climate of Southern England. One years integration (meaned over all runs) compared with observations.

	Model results	Observations
Net downward radiation at top of atmosphere (Wm^{-2})		
grass, albedo = 0.2	-70.8 ± 1.8	-70*
forest albedo = 0.14	-61.6 ± 0.5	
Net downward radiation at surface (Wm^{-2})		
grass, albedo = 0.2	55.1 ± 0.9	53*
forest, albedo = 0.14	64.3 ± 0.8	
Upward turbulent fluxes		
Sensible heat (Wm^{-2})	18 ± 7	16*
Latent heat (Wm^{-2})	39 ± 5	37*
Annual precipitation (mm)	668.1 ± 16.4	700*
Annual runoff (mm)	135.8 ± 67.4	-
Annual evaporation (mm)	490.6 ± 60.4	465+
Annual average surface temperature (°C)	8.85 ± 0.4	10+
Estimated average monthly temperature (°C)		
July	17 ± 1	16.5+
January	-2 ± 1	4.5+

* Lockwood (1985)
\+ Meteorological Office (1952)

The low winter temperatures may be due to the following causes (1) insufficient exchange of heat between the atmosphere and surface when there is a strong inversion, possibly due to too low a vertical resolution (it was noted that on a number of cold days the lowest atmospheric level was considerably warmer than the surface) and (2) lack of a compensating heat flux from deeper soil layers. Fortunately the sensitivity of annual evaporation and sensible heat fluxes to winter temperatures is relatively small.

The primary effect of changing land surface parameters in these experiments was to alter the partitioning between sensible and latent heat fluxes. Two types are noted: (1) those experiments in which evaporation was changed directly, eg by changing surface resistance and (2) those in which evaporation varied due to soil moisture dropping below the critical level ($\beta < 1$) for differing periods of time. The range of variation in turbulent heat flux partition can be seen in figure 7.1 showing that the land surface can exert quite a large influence on the surface turbulent fluxes.

An important consequence of the variation in evaporation is the correlation between precipitation and evaporation. This was already noted in section 4 but it would appear to be a general result, regardless of cause as seen from figure 7.2, although the slope of the relationship does depend on the mechanism whereby evaporation is increased. Most of the enhancement of precipitation comes from the convective component. For large scale rainfall over these experiments the range is only 3% of the total whereas for convective rain it is 14%. It could be deduced that for larger areas and climates more dependent on convective rain the controlling influence of the land surface would be stronger. To keep this in perspective however, even for the canopy storage experiments a 5% increase in evaporation leads to only a 1.5% increase in annual rainfall.

7.2.2 Sensitivity to soil type

Experiment runs 2, 3 and 4 compare soil types (fine, coarse and medium soils respectively). The relative effect on evaporation and sensible heating can be seen from figure 7.2 and table 7.1. These experiments have been discussed in more detail in section 3.4 where it was noted that as texture becomes finer, field capacity increases, reducing gravitational drainage, but infiltration capacity decreases, thereby increasing surface runoff. The balance of these two processes has resulted in the medium textured soil having the highest average soil moisture content and the coarse textured the lowest. From table 3.2 it can be observed that annual runoff varies from 101.6 mm to 192.7 mm and evaporation from 473.9 to 531.7 so that the variation in evaporation is less than the variation in runoff.

The sensitivity to soil type is comparable to that of various vegetation parameters and so it seems to be necessary to allow for some variation in soil type in climate simulation experiments.

7.2.3 Sensitivity to land type

Three land types (long grass, forest and short grass) are compared in runs 4, 5 and 6. A complete summary of land parameter values is given in table 5.2. Replacing long grass with forest would appear to have the greatest potential impact on climate and several parameters change by substantial

amounts. For example, albedo decreases from 0.2 to 0.14, surface resistance increases from 60 sm^{-1} to 150 sm^{-1}, root depth increases from 1m to 1.5m, roughness increases from 0.06m to 2.00m and canopy capacity increases from 1.8 mm to 2.8 mm. Table 7.1 and figure 7.1 show, however, that evaporation decreases only slightly over the year but the sensible heat flux increases on average by 11 Wm^{-2}. This change is probably in response to the change in albedo. Interestingly rainfall increases slightly over the year despite an overall drop in evaporation. It would appear that the net effect of all parameter differences on evaporation is to cancel each other. Increasing root zone depth and canopy capacity tend to increase evaporation but this is offset by an increase in dry canopy resistance. Replacing long grass with short increases the Bowen ratio largely as a result of reduced soil moisture during the summer following a reduction in root depth from 1.0 to 0.6m.

7.2.4 Sensitivity to canopy storage

Two runs were carried out to compare the effect of including canopy interception and evaporation (run 5) and excluding it (run 7). Results from 60 days during the summer of each run have already been discussed in some detail in section 4.3.5. Results for the year are given in table 7.1 and we can see that the effect on the Bowen ratio is quite marked. The increase in evaporation due to the inclusion of a canopy has also led to an increase in convective rainfall. Figure 7.2 suggests that the feedback of evaporation on rainfall is greatest for this mechanism presumably because evaporation is enhanced just when precipitation is falling or has just fallen.

From table 7.1 it may be noted that soil moisture decreases markedly in the presence of a canopy (generally seen in observational studies) and in a drier climate could feed back and lead to a reduction in evaporation in some seasons. However in these experiments we can note that a 0.7 mm increase in canopy storage results in a 5% increase in evaporation.

7.2.5 Sensitivity to surface resistance

An increasing surface resistance would be expected to reduce evaporation and increase the Bowen ratio. Runs 4 (60sm^{-1}), 8 (120 sm^{-1}) and 9 (0 sm^{-1}) confirm that this is the case. The results were discussed fully in section 4.2.3. Important aspects to note are that the high resistance, low evaporation case maintains a relatively wet soil whereas the low resistance, high evaporation case eventually allows soil moisture to control evaporation and to reduce it in the late summer. Over the year therefore, the differences in evaporation are not as large as would have occurred had potential evaporation been maintained throughout. It may be deduced that other factors will influence the relationship between evaporation and resistance, such as climate, in particular the rainfall sequence, root depth and canopy storage. In these experiments a 5% increase in evaporation followed a 30 sm^{-1} increase in resistance.

7.2.6 Sensitivity to root depth

Comparing runs 4 (1m), 10 (0.1m) and 11 (0.5m) in which the root depth is altered, it was noted in section 4.2.3 that root depth strongly controls the amount of moisture available for transpiration. These integrations

suggest that an approximately 14cm change in root depth leads to a 5% change in evaporation over one year. Root depth is intrinsically difficult to ascertain and in reality it is likely that there is as much variation within the same vegetation type as there is between types. Other factors such as water table height and geology, as well as availability of nutrients and climate play an important part in determining root depth.

7.2.7 Sensitivity to roughness

Only one example is given. Run 12 has a roughness value 10 times that of run 4 (z_o = 0.06m) and yet the effect on evaporation is not large. Rowntree (1984) has shown that for a surface resistance of 60 sm^{-1} evaporation is relatively insensitive to roughness.

7.3 Conclusions

Most of the land surface parameters have a comparable impact on turbulent fluxes for the range of values that might be expected within the European area. Table 7.3 summarises the change in 4 parameters which would lead to a 5% change in evaporation. We might consider these values to represent the relative accuracy to which the parameters need to be specified. They also give some indication of the sensitivity of climate to land use changes within the northern European area.

Table 7.3

Variation of a surface parameter leading to a 5% variation in evaporation (averaged over a year)

r_s	±	30 sm^{-1}
D	±	14 cm
S_m	±	0.7 mm
z_o	±	factor of 10

7.4 References

Lockwood, J.G. 1985 World Climate Systems, London, Edward Arnold.

Meteorological Office 1952 Climatological Atlas of the British Isles, MO488, London, Her Majesty's Stationary Office.

Mintz, Y. 1984 The sensitivity of numerically simulated climates to land-surface boundary conditions, The Global Climate, CH6 (Edt, J. Houghton), Cambridge, Cambridge University Press.

Rowntree, P.R. 1984 Review of general circulation models as a basis for predicting the effects of vegetation changes on climate, Met O 20 Technical note II/225, Bracknell, Meteorological Office, Met O 20 (Unpublished).

Rowntree, P.R. and Bolton, J.A. 1983 Simulation of the atmospheric response to soil moisture anomalies over Europe, Quart. J. of Roy. Met. Soc., 109, 501-526.

Warrilow, D.A. 1986 Indications of the sensitivity of European climate to land use variations using a one dimensional model. To appear in Proc. Conf. on Parametrization of Land Surface Characteristics, Use of Satellite data in Climate Models, and First Results of ISLSCP, Rome 2 - 6 December 1985.

Figure 7.1 Sensible heat flux against latent heat flux from ODM annual cycle experiments for Southern England. Numbers refer to experiments mentioned in the text.

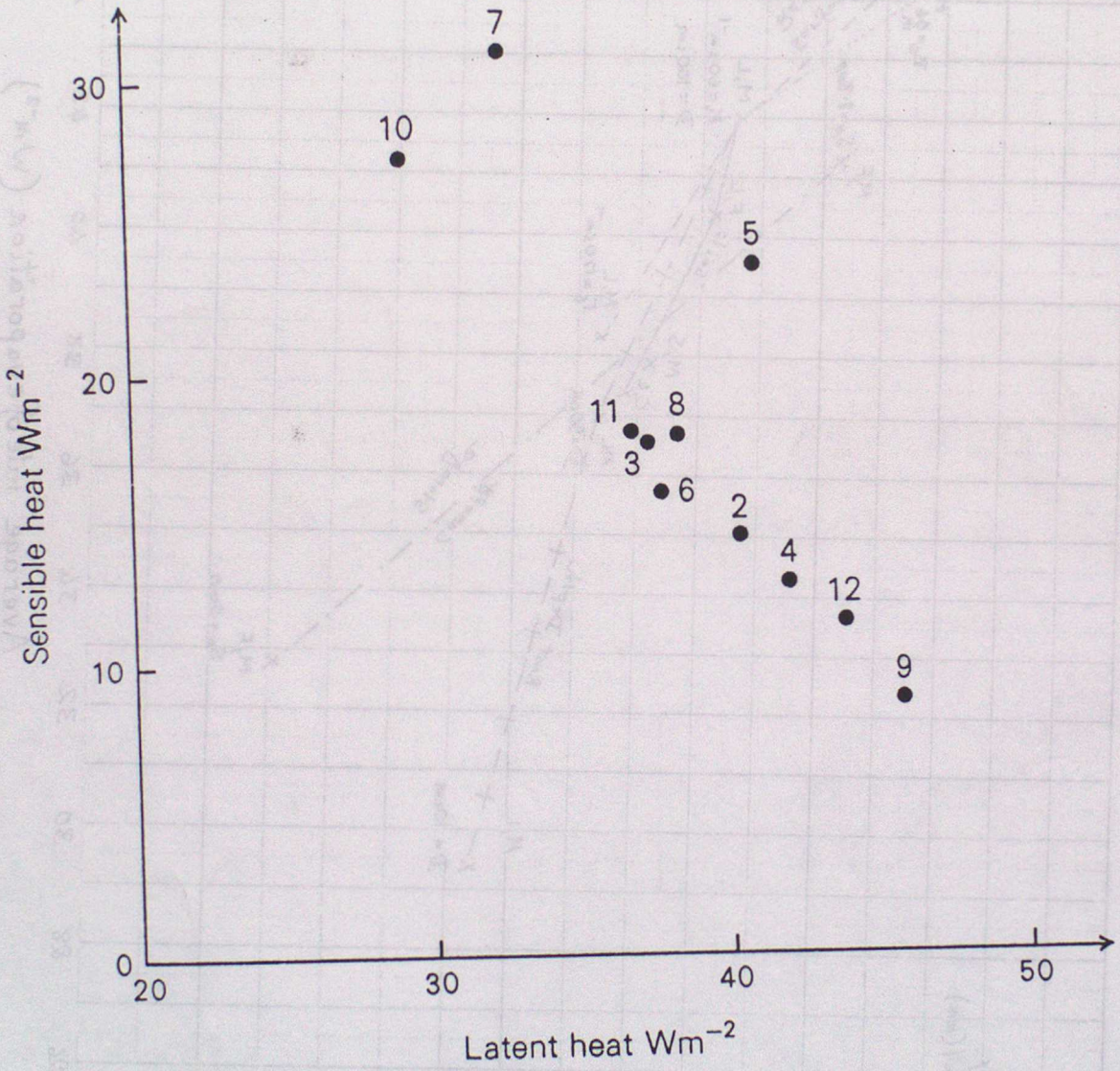

Figure 7.2 Precipitation and evaporation from ODM experiments for Southern England.

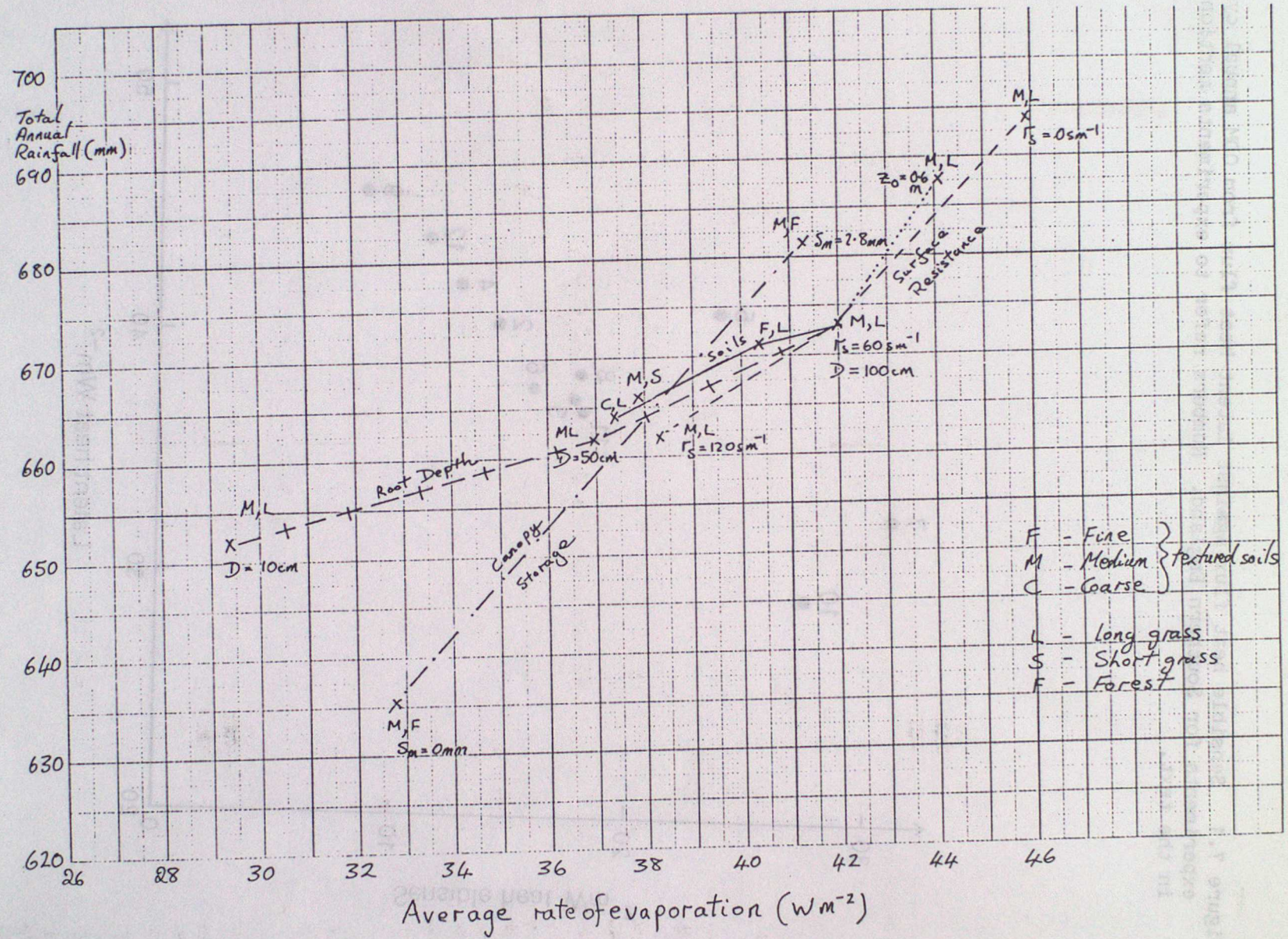

8. Conclusions and Summary

The climatic impact of land surface processes has been investigated using both AGCM and ODM experiments. The studies have been biased towards a more oceanic climate than is perhaps representative of Europe as a whole, nevertheless it has been shown that land surface processes do play an important part and would be expected to be even more important in more continental regions.

Each model is complementary. The ODM was developed further for the purposes of this report enabling a number of long integrations to be carried out without using excessive amounts of computer time. It had the added advantage that program changes could be made easily and quickly. The omission of large scale feedback allowed the direct effect of land perturbations to be studied without, say, the complications due to major changes in circulation and rainfall. The AGCM enables studies of global changes to be carried out, includes any feedback effects and can reveal large scale changes in pressure patterns and wind flow. The AGCM can in principle cope with large anomalies which are more difficult to treat in the ODM. The AGCM is naturally far more expensive to run, a point which needs to be borne in mind for land surface experiments when fairly long integrations are required to explore relatively slowly changing variables such as soil moisture and deep soil temperatures. Program changes are generally harder and more time consuming to implement.

Individual aspects of the land surface were looked at in detail and the broad conclusions are summarised below.

A detailed study of hydrological processes revealed that there is considerable complexity, stemming from the small spatial scale typical of the processes involved, the intrinsic variability and number of different soil moisture and runoff processes and the complexity of the boundary conditions. Problems are encountered in describing essentially local physical mechanisms on the scale of an AGCM grid square; data are sparse and a major component of the hydrological cycle, rainfall, is also spatially variable. In deriving a hydrological parametrization runoff was divided into two components: surface runoff and gravitational drainage through the lower boundary of a nominal 'active' root zone. The former requires that allowance for subgrid scale variations in rainfall should be made. This was attempted although it is suspected that the effect of spatial variability is still underestimated. Variations in surface infiltration capacity and soil characteristics were ignored but ought to be investigated in the future. The effect of vegetation on infiltration was accounted for in a simple manner although little is known about this subject. Other potentially important factors affecting runoff, such as underlying geology, slope and water table height were not treated. Nevertheless using the AGCM it was found that annual runoff totals compared fairly well with observations and differed surprisingly little from the results obtained using a 'bucket' model.

A review of recent literature shows that vegetation can exert a considerable controlling influence on transpiration by means of leaf stomata which can vary in size thereby controlling the flux of moisture from leaf to atmosphere. The integrated effect of stomatal control is referred to as surface resistance in this report. Originally the AGCM did

not take surface resistance into account, but some experiments were carried out which showed the beneficial effect of including a surface resistance of 60 sm^{-1}. Over the moist continents both evaporation and rainfall were observed to decrease by fairly substantial amounts. Further studies with the ODM gave indications of the sensitivity of evaporation to surface resistance. The response of stomata to other environmental factors was not modelled but should be considered in the future. Bare soil evaporation is not explicitly treated and probably needs to be modelled separately.

A parametrization of canopy interception of rainfall was developed and studied. It was observed in ODM experiments that the presence of a canopy led to an increase in evaporation during rainfall events and a corresponding enhancement of convective rainfall. It is also suggested that canopy interception should be included in the AGCM as it affects, evaporation, soil moisture and hence runoff.

A 4 level soil temperature parametrization was developed in which the response of surface temperatures to the soil heat flux was unbiassed for forcing frequencies of less than one day to more than one year. Appropriate values of heat capacity and conductivity needed to be defined and the response of the model to different values was considered. Initial values resulted in a thermal inertia which appeared to be too high leading to a diurnal range in temperature that was much less than observed. Although mean temperatures were well simulated continental winter temperatures were higher than observed, particularly over Siberia. Shortcomings in the simulation of the winter circulation were probably responsible for this.

Future work should consider the variation of heat capacity and conductivity with soil moisture content, the freezing and melting of soil water and the thermal effects of snowcover.

The ODM experiments reveal that the local European climate can respond significantly to varations in land surface parameters and show the need to ascertain parameter values to a precision suggested by an acceptable level of error in evaporation. They also show that it is necessary to distinguish between vegetation and soil types. However, as was noted in section 5 the relationship between parameter values and particular soil and vegetation types is not necessarily unique or simply defined and achieving a global distribution of parameters is not an easy matter. The advent of satellite observation of the surface may give new information in this respect.

Acknowledgements

The authors wish to thank Drs. P R Rowntree and H Cattle for their helpful comments on the preparation of this report and S Brentnall for the preparation of some diagrams. Finally the authors would like to thank the CEC for their contribution to the funding of this work under contract CL.113.UK(H).

DYNAMICAL CLIMATOLOGY TECHNICAL NOTES

DCTN 1	June 1984	A scheme for incorporating the thermodynamic sea-ice model into a coupled ocean-atmosphere model. C Gordon and M Bottomley
DCTN 2	Sept 1984	The parametrization of the upper ocean mixed layer in coupled ocean/atmosphere models. C Gordon and M Bottomley
DCTN 3	Sept 1984	The response of a simple thermodynamic sea-ice model to CCM forcing appropriate for perennial sea-ice. M Bottomley
DCTN 4	Sept 1984	Potential vorticity in the stratosphere derived using data from satellites. S A Clough, N E Grahame and A O'Neill
DCTN 5	Sept 1984	Simulation of the seasonal cycle of SST using globally specified climatological data to force simple ocean models. N E Grahame
DCTN 6	Sept 1984	Development of an improved CCM radiation scheme. A Slingo and R C Wilderspin
DCTN 7	Sept 1984	On the specification of surface fluxes in coupled atmosphere/ocean general circulation models. J F B Mitchell, C A Wilson and C M Price
DCTN 8	Sept 1984	A survey of possible repercussions of the Soviet river reversal programme on Arctic sea-ice. M Cattle
DCTN 9	Oct 1984	A study of a strong stratospheric warming during January 1982 T D A Fairlie
DCTN 10	Nov 1984	An intercomparison of the Met O 11 M45 model and the Met O 20 11-level model on the Cyber 205 J P Dyson
DCTN 11	Nov 1984	Simulation of observed time series of temperature and precipitation over eastern England. D M Reed
DCTN 12	Nov 1984	Forecasts and analyses of the onset of the Southwest monsoon. R Kershaw
DCTN 13	Nov 1984	On modelling the effects of CO_2 on climate. J F B Mitchell
DCTN 14	Dec 1984	Development of a revised longwave radiation scheme for an atmospheric general circulation model. A Slingo and R C Wilderspin
DCTN 15	Jan 1985	Rossby wavetrains in the stratosphere forced by localised disturbances in the troposphere. C J Marks (Oxford), A O'Neill and V D Pope

DYNAMICAL CLIMATOLOGY TECHNICAL NOTES

DCTN 16	Jan 1985	Observing system experiments using the Meteorological Office's 15-level model. R A Bromley
DCTN 17	Feb 1985	Atmospheric general circulation simulation of the climate of the Mediterranean region. M Cattle
DCTN 18	Feb 1985	Diurnal variation and cloud in a general circulation model. C A Wilson and J F B Mitchell
DCTN 19	Feb 1985	The sensitivity of the Saharan region in a general circulation model. W M Cunnington and P R Rowntree
DCTN 20	Mar 1985	The impact of aircraft observations on analyses and forecasts from the operational 15-level model. R E Barwell
DCTN 21	Mar 1985	Non-linear effects on heat-induced circulation of the tropical atmosphere. A E Gill and P J Phlips
DCTN 22	Apr 1985	Simulation of cloudiness with the U.K. Meteorological Office 11-layer AGCM. A Slingo and R C Wilderspin
DCTN 23	Apr 1985	An integrated approach to the representation of cloud processes. R E B Smith
DCTN 24	May 1985	Nuclear Winter: Calculations of the shortwave radiative effects of soot aerosols. A Slingo and P Goldsmith
DCTN 25	Jul 1985	Sea ice and the Antarctic winter circulation: a numerical experiment. J F B Mitchell and T S Hills
DCTN 26	Jul 1985	A Budyko-Sellers model for study of ocean-atmosphere interaction. W J Ingram
DCTN 27	Aug 1985	The effect of a shoaling thermocline on equatorially-trapped Kelvin waves. A E Gill and B A King
DCTN 28	Sept 1985	CO_2 climate sensitivity and model dependence of results. J F B Mitchell, C A Wilson and W M Cunnington
DCTN 29	Sept 1985	Handbook of the Meteorological Office 11-layer atmospheric general circulation model. Volume 1 : Model Description Edited by A Slingo
DCTN 30	Sept 1985	Impact of land surface variations on African rainfall in general circulation models. P R Rowntree, K F Wilson and A B Sangster

DYNAMICAL CLIMATOLOGY TECHNICAL NOTES

DCTN 31 Nov 1985 The annual cycle of sea level in the eastern tropical Pacific.
G R Bigg and A E Gill

DCTN 32 Nov 1985 An analytic model of the heat-induced tropical circulation in the presence of a mean wind.
P J Phlips and A E Gill

DCTN 33 Nov 1985 The effect of resolution and diffusion on the simulated climate.
J F Dyson

DCTN 34 Jan 1986 Rossby adjustment over a step.
M K Davey, A E Gill, E R Johnson and P F Linden

DCTN 35 Jan 1986 Issues concerning the evaluation of effective surface roughness of heterogeneous terrain.
D J Carson

DCTN 36 Mar 1986 Climate sensitivity and past climates : evidence from numerical studies
J F B Mitchell

DCTN 37 Mar 1986 Parametrizations of land-surface processes in Meteorological Office numerical weather prediction and climate models
D J Carson

DCTN 38 Apr 1986 Modelling of land-surface processes and their influence on European Climate
D A Warrilow

DCTN 39 Apr 1986 Simulation of climatic change due to increased CO_2
J F B Mitchell